

AMBIENT VIBRATION ASSESSMENT OF RUSKIN DAM

DYNAMIC PROPERTIES

by

BRADLEY GARY KEMP

B.A.Sc., University of Waterloo, 1982

A THESIS SUBMITTED IN PARTIAL FULFILLMENT OF

THE REQUIREMENTS FOR THE DEGREE OF

MASTER OF APPLIED SCIENCE

in

THE FACULTY OF GRADUATE STUDIES

Department Of Civil Engineering

We accept this thesis as conforming
to the required standard

THE UNIVERSITY OF BRITISH COLUMBIA

February 1996

© Bradley Gary Kemp, 1996

In presenting this thesis in partial fulfilment of the requirements for an advanced degree at the University of British Columbia, I agree that the Library shall make it freely available for reference and study. I further agree that permission for extensive copying of this thesis for scholarly purposes may be granted by the head of my department or by his or her representatives. It is understood that copying or publication of this thesis for financial gain shall not be allowed without my written permission.

Department of Civil Engineering
The University of British Columbia
Vancouver, Canada

Date 28 January 1996

ABSTRACT

Concrete gravity dams are significant civil engineering structures whose failure can produce catastrophic results. Field appraisal of their dynamic properties would be useful to validate numerical models used for structural analysis to determine, for instance, seismic resistance.

The suitability of ambient vibration testing and analysis to provide meaningful dynamic properties of a concrete gravity dam has been studied. Tests were conducted at B.C. Hydro's Ruskin Dam, located near Mission, B.C. Tests were completed at two reservoir levels to permit calibration of a numerical model. Two distinct methods of frequency domain based analysis were used to determine dynamic properties.

The first method used proven ambient vibration techniques, based on a "relative" single input-single output system, with no quantification of excitation. Relative transfer function relationships were constructed between a reference location on the dam and all other points on the dam at which measurements were taken. The selection of potential natural frequencies was completed by consideration of the power in the signals recorded. Final selection of natural frequencies and associated mode shapes was based on the resulting gain, phase and coherence values of the relative transfer functions.

In the second method, the field measurements were considered to represent a single input-single output system with output noise, as the bedrock signal was shown to represent the majority of input. For this approach, natural frequencies were indicated as peaks in cross-spectral density functions with high coherence and corresponding transfer functions having

phase factors equal to 90 degrees.

Two natural frequencies and corresponding mode shapes were identified. Confidence of prediction was found to be highest for the first of these. Although this was concluded to be a meaningful result, there is clearly a need for developing additional ambient vibration theory which can be implemented to identify dynamic properties.

To demonstrate the usefulness of the dynamic properties obtained through the ambient vibration testing and analysis, a numerical model of the dam utilizing the finite element method was subjected to modal analysis with which to complete calibration/parametric studies. Calibration was found successful only for the first natural frequency, probably because the numerical model failed to include the effects of water compressibility, which were shown through rudimentary calculations to be significant. Calibration to the first natural frequency is, however, considered meaningful as concrete gravity dam response is attributed mainly to the fundamental mode.

AMBIENT VIBRATION ASSESSMENT OF RUSKIN DAM
DYNAMIC PROPERTIES

TABLE OF CONTENTS

Abstract	ii
Table of Contents	iv
List of Tables	ix
List of Figures	x
List of Symbols	xii
List of Abbreviations	xiii
Conversion Table	xiv
Acknowledgements	xv

<u>Chapter</u>	<u>Subject</u>	<u>Page</u>
1	Introduction	1
	1.1 Why Conduct Ambient Vibration Tests of Structures?	1
	1.2 Objective	4
	1.3 Scope	4
	1.4 Funding	5
2	Concrete Gravity Dams: Perspectives	6

AMBIENT VIBRATION ASSESSMENT OF RUSKIN DAM

DYNAMIC PROPERTIES

TABLE OF CONTENTS Continued

<u>Chapter</u>	<u>Subject</u>	<u>Page</u>
	2.1 Dynamic Analysis	6
	2.2 Vibration Testing and Analysis	10
3	Dynamic Analysis Methodology	20
	3.1 Linear Elastic Modal Analysis	20
	3.2 Hydrodynamic Effects	23
	3.3 Calibration to Ambient Vibration Testing and Analysis	30
4	Ambient Vibration Analysis Methodology	32
	4.1 Two Ambient Analysis Techniques Used in this Thesis	32
	4.2 Theoretical Considerations	33
	4.3 Hybrid Bridge Evaluation System (HBES)	58
	4.4 Complementary Analysis	63
5	Signal Processing and Ambient Vibration Testing Methodology	67
	5.1 Sampling Time Domain Records	67
	5.2 Error Calculation	74
	5.3 HBES Data Acquisition	78
	5.4 Test Design Considerations	81

AMBIENT VIBRATION ASSESSMENT OF RUSKIN DAM
DYNAMIC PROPERTIES

TABLE OF CONTENTS Continued

<u>Chapter</u>	<u>Subject</u>	<u>Page</u>
6	Ambient Vibration Testing and Analysis Program	85
	6.1 Dam Selection	86
	6.2 Description of Ruskin Dam and Generating Station	87
	6.3 Field Testing Program	91
7	Trial Test	93
	7.1 Objectives	93
	7.2 Test Design	94
	7.3 HBES Results	96
	7.4 Complementary Analysis Results	99
	7.5 Discussion	100
	7.6 Conclusions	101
	7.7 Recommendations	102
8	Low/High Reservoir Tests	104
	8.1 Objectives	104
	8.2 Test Design	105
	8.3 Low Reservoir	107

AMBIENT VIBRATION ASSESSMENT OF RUSKIN DAM

DYNAMIC PROPERTIES

TABLE OF CONTENTS Continued

<u>Chapter</u>	<u>Subject</u>	<u>Page</u>
	8.3.1 HBES Results	107
	8.3.2 Complementary Analysis Results	111
8.4	High Reservoir	116
	8.4.1 HBES Results	117
	8.4.2 Complementary Analysis Results	120
8.5	Discussion	126
8.6	Conclusions	130
8.7	Recommendations	132
9	Dynamic Analysis	133
	9.1 Numerical Modelling Considerations	133
	9.2 Description of Base Model	135
	9.3 Calibration Studies	144
	9.4 Parametric Studies	151
	9.5 Conclusions	154
	9.6 Recommendations	156

AMBIENT VIBRATION ASSESSMENT OF RUSKIN DAM
DYNAMIC PROPERTIES

TABLE OF CONTENTS Continued

<u>Chapter</u>	<u>Subject</u>	<u>Page</u>
10	Conclusions	157
11	Recommendations	160
	Bibliography	163
Appendix A	Equipment Used, Field Tests and Photographs	170
Appendix B	Analysis of Trial Test, 23 January 1994	197
Appendix C	Analysis of Low Reservoir Test, 30 April & 1 May 1994	215
Appendix D	Analysis of High Reservoir Test, 7 & 8 May 1994	267
Appendix E	Numerical Modelling Studies	314

AMBIENT VIBRATION ASSESSMENT OF RUSKIN DAM

DYNAMIC PROPERTIES

LIST OF TABLES

Table 5.1	Single Input-Single Output Problem Random Errors, ϵ_r	76
Table 5.2	Standard Deviation of Phase Factor, $\sigma\Phi_{xy}(f)$ (degrees)	78
Table 7.1	Trial Test: Data Acquisition Parameters	97
Table 8.1	Low/High Reservoir Tests: Data Acquisition Parameters	106
Table 8.2	Low Reservoir Results-HBES Analysis Summary	111
Table 8.3	Low Reservoir Results-Complementary Analysis Summary	116
Table 8.4	High Reservoir Results-HBES Analysis Summary	121
Table 8.5	High Reservoir Results-Complementary Analysis Summary	125
Table 8.6	Summary of All Test Results	127
Table 9.1	Summary of ANSYS© Elements in FEM Base Model	138
Table 9.2	Summary of FEM Base Model Material Properties	140
Table 9.3	Selection of Master Degrees of Freedom	143
Table 9.4	Low/High Reservoir Calibration: Comparison of Natural Frequencies Obtained from the FEM Base Model and the Ambient Analysis	147
Table 9.5	Low/High Reservoir Calibration: Frequency Shift Comparison	148

AMBIENT VIBRATION ASSESSMENT OF RUSKIN DAM

DYNAMIC PROPERTIES

LIST OF FIGURES

Figure 4.1	Idealized Single Degree of Freedom System, Force Input	43
Figure 4.2	Idealized Single Input-Single Output System	45
Figure 4.3	Example of an Idealized Two Degree of Freedom System Modeled as a Relative Single Input-Single Output System for Ambient Vibration Analysis	50
Figure 4.4	Idealized Single Degree of Freedom System, Foundation Displacement Input	53
Figure 4.5	Example of Idealized Two Degree of Freedom System Modeled as a Single Input-Single Output with Noise System for Ambient Vibration Analysis . . .	55
Figure 4.6	Idealized Multiple Input-Single Output System (Uncorrelated Inputs)	57
Figure 5.1	Discrete Fourier Transform of a Time Domain Signal, Using Fast Fourier Transform Algorithm	68
Figure 5.2	Example of Aliasing	71
Figure 5.3	Example of Signal Leakage	72
Figure 5.4	The Effect of Windowing Signals	73
Figure 5.5	The Effect of the Hanning Window	74
Figure 6.1	Location of Ruskin Dam	86

AMBIENT VIBRATION ASSESSMENT OF RUSKIN DAM

DYNAMIC PROPERTIES

LIST OF FIGURES Continued

Figure 6.2	Plan of Ruskin Dam and Generating Station	88
Figure 6.3	Photograph of Ruskin Dam from Atop Ruskin Generating Station	89
Figure 6.4	Ruskin Dam: Details of Vertical Contraction Joint	90
Figure 8.1	Low Reservoir ANPSD Functions	108
Figure 8.2	Low Reservoir: Phase Factor, Vertical Direction, Input: Nodes 32-35 (East Bedrock), Output: Node 13 (Ogee)	113
Figure 8.3	Low Reservoir: Transfer Function Gain, Phase Factor and Coherence, Vertical Direction, Input: Nodes 33 (East Bedrock), Output: Node 13 (Ogee) . . .	116
Figure 8.4	High Reservoir ANPSD Functions	118
Figure 8.5	High Reservoir: Phase Factor, Vertical Direction, Input: Nodes 31-34 (East Bedrock), Output: Node 13 (Ogee)	122
Figure 8.6	High Reservoir: Transfer Function Gain, Phase Factor and Coherence, Vertical Direction, Input: Nodes 33 (East Bedrock), Output: Node 13 (Ogee) . . .	123
Figure 8.7	Low/High Reservoir Ambient Mode Shapes	127
Figure 9.1	FEM Base Model	136
Figure 9.2	Detail of Bedrock Zonation in FEM Base Model	141
Figure 9.3	Mode Shape Comparison: Ambient vs. FEM Base Model	146
Figure 9.4	Low/High Reservoir Calibration: Frequency Shift Comparison	149

AMBIENT VIBRATION ASSESSMENT OF RUSKIN DAM

DYNAMIC PROPERTIES

LIST OF SYMBOLS

The following is a list of the most commonly used symbols in this thesis.

$x(t), y(t)$	Time Domain Signals
$G_{xx}(f)$	One sided Power Spectral Density Function for $x(t)$
$G_{xy}(f)$	Two sided Cross-spectral Density Function for $x(t)$ and $y(t)$
$H(f)$	Transfer Function
$ H(f) $	Transfer Function Gain
$\Phi_{xy}(f)$	Phase Factor of Transfer Function for $x(t)$ and $y(t)$
$\gamma_{xy}^2(f)$	Coherence Function between $x(t)$ and $y(t)$
f_{wl}	Fundamental Frequency of Reservoir (Hz)
f_{dl}	Fundamental Frequency of Dam without Reservoir (Hz)
Ω	Ratio, = f_{wl} / f_{dl}
Δt	Time Domain Signal Sampling Interval (seconds)
N	Number of Points Sampled Per Segment
n_d	Number of Segments
T	Time Length of Segment (seconds)
f_c	Nyquist Frequency (Hz)
Δf	Frequency Resolution (Hz)

AMBIENT VIBRATION ASSESSMENT OF RUSKIN DAM

DYNAMIC PROPERTIES

LIST OF ABBREVIATIONS

The following is a list of the most commonly used abbreviations in this thesis.

BCH:	British Columbia Hydro
UBC:	University of British Columbia
USBR:	United States Bureau of Reclamation
MAC:	Modal Assurance Criteria
DOF:	Degree of Freedom
SDOF:	Single Degree of Freedom
MDOF:	Multi Degree of Freedom
HBES:	Hybrid Bridge Evaluation System
ANPSD:	Average Normalized Power Spectral Density
PSD:	Power Spectral Density Function
XSD:	Cross-spectral Density Function
FFT:	Fast Fourier Transform
DFT:	Discrete Fourier Transform
FEM:	Finite Element Method

AMBIENT VIBRATION ASSESSMENT OF RUSKIN DAM

DYNAMIC PROPERTIES

CONVERSION TABLE

Work in this thesis is presented in Imperial units of measure (except temperature). The following are conversion formulas to metric (SI) units.

$$1 \text{ ft} = 0.305 \text{ m}$$

$$1 \text{ lb} = 4.448 \text{ N}$$

$$1 \text{ slug} = 14.59 \text{ kg}$$

$$1 \text{ lbm} = 0.454 \text{ kg}$$

$$1 \text{ psi} = 6.895 \text{ kPa}$$

$$1 \text{ psf} = 47.88 \text{ Pa}$$

$$1 \text{ lb/ft}^3 = 16.019 \text{ kg/m}^3$$

ACKNOWLEDGEMENTS

This thesis was completed under the supervision of Dr. C.E. Ventura and Dr. D.J. Anderson of the University of British Columbia (UBC).

The author wishes to acknowledge the opportunity granted to himself by his supervisor, Mr. Tibor Pataky of B.C. Hydro (BCH) and the UBC Faculty of Civil Engineering, to complete this thesis while enrolled in the UBC/BCH Professional Partnership Program. In addition, the author wishes to acknowledge the funding and co-operation received from BCH to conduct the field testing. In particular, gratitude is extended to the Director of Dam Safety, Mr. G.M. Salmon and to the Ruskin Dam Production Supervisor, Mr. L.E. Pope.

To complete the field work presented in this thesis required assistance from numerous people. Appreciation is expressed in this regard for the following Ruskin Dam personnel; Mr. J. Hocking, Mr. C. Scott, Mr. R. Matheson and Mr. L. Stott. Appreciation also is expressed in this regard for the following UBC graduate and undergraduate students; Ms. I. Villemure, Dr. A. Felber, Mr. V. Latendresse, Mr. M. Rezai, Mr. N. Shuster, Ms. L. Pan, Mr. R. Hui and Mr. M. Baraka. Most of these people had to work long hours on weekends to complete the field work.

Appreciation is expressed to Dr. A. Felber of Experimental Dynamic Investigations Ltd. (EDI), Vancouver, B.C., for allowing the use of EDI software in the analysis of ambient data presented in this thesis.

The numerical model of Ruskin Dam used in this thesis was originally developed at BCH by Mr. E. Arguilar under the direction of Mr. C.K. Wong and Mr. R. Hui. Mr. B.H. Fan of BCH provided useful comments on some of the text in this thesis.

CHAPTER 1

INTRODUCTION

1.1 Why Conduct Ambient Vibration Tests of Structures?

As structural analysis techniques continually evolve and become increasingly sophisticated, awareness grows of potential shortcomings in their representation of structural behaviour. This is prevalent in the field of structural dynamics. Each occurrence of a large earthquake in a populated area together with the accompanying survey of structural response and damage results in re-evaluation of the state-of-the-art in structural dynamics analysis methods. Any means which can be used to increase confidence in structural dynamics analysis techniques is clearly welcome.

Large civil engineering structures are usually too complex for accurate dynamic analysis by hand. It is typical to use matrix algebra based solution methods, using the finite element method of structural modelling and analysis, on digital computers. All linear models have dynamic properties which can be evaluated using techniques of dynamic analysis, such as modal analysis. The modal analysis technique can provide the natural frequencies and corresponding mode shapes for a numerical model of a structure (Clough & Penzien 1975, 176-181, Humar 1990, 420-426). For an existing structure, the accuracy of such a linear finite element method model can be validated

through comparison of these dynamic properties with those obtained from testing of the actual structure. *Vibration testing and analysis of an existing structure can provide quantitative evaluation of its dynamic properties.*

The theories of vibration testing and analysis are well advanced. Common applications for its theories are found in mechanical engineering, where it is used to study industrial machinery noise and vibration problems. Mechanical/electrical engineering journals dedicated to the dissemination of research include the Journal of Sound and Vibration, published in the London, England by Academic Press Ltd. and the Journal of Vibration and Acoustics, published by the American Society of Mechanical Engineers, Fairfield, NJ, USA. Mechanical/civil engineering conferences dedicated to the topic include the International Modal Analysis Conference (IMAC), sponsored by the Society for Experimental Mechanics, Bethel, CT, USA. As well, civil engineering and seismic engineering conferences attract interest in the subject. Seismic engineering conferences of note include the World Conference on Earthquake Engineering, sponsored by the International Association of Earthquake Engineers (IAEE), the U.S. National Conference on Earthquake Engineering, sponsored by the Earthquake Engineering Research Institute (EERI) and the Canadian Conference on Earthquake Engineering, sponsored by the Canadian Association for Earthquake Engineering (CAEE). In the US, a standard for vibration testing of buildings is available from the Acoustical Society of America and is numbered: ANSI S2.47-1990 (ANSI 1990).

Vibration testing and analysis techniques commonly use some device whose express

purpose is to artificially induce a force or displacement to excite the structure.

Usually a controlled periodic, random, transient or impact force is used. This is relatively expensive and with very long massive structures, such as dams, it may be necessary to use more than one exciting device, thereby increasing the costs for testing.

Ambient vibration analysis (Luz 1992) is a vibration testing and analysis technique targeted for large civil engineering structures. The method requires no artificial excitation to be imparted to the structure being tested. It relies on the naturally occurring ambient vibrations which the structure undergoes. This provides a distinct cost advantage over the other methods which require a costly artificially induced means to excite the structure.

Also of interest, dynamic properties of a structure may vary over time, as a result of changing material properties due to weathering or as a result of response to the load history. Determination of dynamic properties before and after an extreme load event, such as an earthquake, may indicate changed conditions not evident by conventional means of evaluation, such as visual inspection or standardized material non-destructive testing. *Vibration testing can therefore be considered for use as a monitoring tool, for providing dynamic properties over time, which can be studied to identify structural changes.*

The justification and technology exists for vibration testing and analysis of large civil engineering structures. The ambient vibration method presents a potentially

inexpensive form of this work.

1.2 Objective

The objective of the research described herein is to determine the usefulness of ambient vibration testing and analysis techniques for obtaining dynamic properties of concrete gravity dams, through conducting such work at a suitable B.C. Hydro dam.

1.3 Scope

The scope of this thesis is itemized, as follows:

- *Conduct a literature review to determine the state of the art of vibration testing and analysis of concrete gravity dams and of dynamic analysis of concrete gravity dams.*
- *Select an appropriate B.C. Hydro dam for vibration testing and analysis.*
- *Design an ambient vibration testing program for the selected dam.*
- *Use an appropriate numerical model of the selected dam to investigate whether*

it can be demonstrated to calibrate the model to the test results.

- *If possible, provide recommendations for future research in the area of ambient vibration testing and analysis of concrete gravity dams.*

1.4 Funding

B.C. Hydro (BCH) provided \$25000 funding for the field tests. Of this total, \$10000 was used by the University of British Columbia (UBC) to purchase a new field analysis computer and 2 new sets of accelerometers and signal conditioning equipment. The remaining \$15000 was spent on labour, equipment rental and expenses. In addition, the author received a stipend through the BCH/UBC Professional Partnership Program while attending UBC full time.

All data acquisition equipment was supplied by UBC. Funding for this equipment was originally obtained from the Ministry of Transportation and Highways for the Province of British Columbia and the Natural Sciences and Engineering Research Council of Canada (NSERC).

CHAPTER 2

CONCRETE GRAVITY DAMS: PERSPECTIVES

2.1 Dynamic Analysis

Dams are important civil engineering structures, due to the vast extent of property damage and loss of life which would result from their failure and their high replacement cost. Hydroelectric utilities with plant in seismically active regions, such as BCH, have embarked on safety assessment programs of their dams. BCH's Guidelines for Selecting and Applying Seismic Criteria for Dams (BCH 1988) outlines a strategy for selection of the appropriate analysis method for completing a seismic assessment of their dams and notably, their concrete gravity dams. Briefly, the rigor of the method to be used depends on the consequences of failure of the dam being studied, the height of the dam and the 475 year return period estimate of ground motion at the site. The least rigorous approach is the *pseudo-static* analysis method and the most rigorous approach is the *dynamic* analysis method.

In the not too distant past, earthquake loading of gravity dams was only analyzed using pseudo-static analysis methods. Pseudo-static methods are based on simplistic representations of the earthquake response of gravity dams, which are easy to understand, can be analyzed using hand calculations and provide a perceived

conservative approach. The classic example of a pseudo-static method is described in the United States Bureau of Reclamation's (USBR) Monograph 19 (USBR 1977). This method assumes that the dam behaves as an infinitely rigid structure (hence no dynamic amplification of ground motion) and that the reservoir water is incompressible. Hydrodynamic effects are realized by an additional upstream face pressure using theory contained in the USBR's Monograph 11, by Zangar (Zangar 1953). Zangar had improved/extended the original work of Westergaard (Westergaard 1931).

The introduction of digital computers and the finite element method has allowed for the use of more complex dynamic analysis methods. These are of two main forms: *response spectrum* and *time history* analysis (ANSYS 1992, I:3-53 and I:3-83).

Response spectrum analysis is the most popular method of dynamic analysis as it is relatively more efficient than time history analysis, requiring less computing power and time. To conduct this type of analysis, a *modal* analysis is first needed to obtain the natural frequencies and mode shapes of the model of the dam. The maximum response of the dam model for each mode is then obtained for a pre-selected response spectrum. The response of a pre-selected number of modes are then superimposed to obtain the total response of the dam model.

With the advent of less costly computing power, the time history method of dynamic analysis is becoming more popular. Time history analysis can handle material and geometric non-linearities, which cannot be dealt with in response spectrum analysis.

This method of analysis subjects the finite element method model of the dam to a loading time history. The load may be of many types, such as displacement, force, temperature, etc. The history is broken into a series of linear analyses at each time increment or time step of the total time history. A time history of the model response results. A modal analysis is not required, yet can be performed if the time history model is linear.

A complete discussion of the assumptions inherent in either response spectrum or time history analysis is beyond the scope of this thesis. Modal analysis is however of interest to this thesis as the dynamic properties provided by it may be confirmed through field testing of the structure which it represents. Theoretical considerations for a modal analysis are discussed in Section 3.1. Both material and geometric linearity is assumed. The former implies elastic material properties. Classical damping is also an inherent assumption. As well, with large complex problems, solution algorithms typically utilize simplifying routines such as mass condensation or Guyan reduction (Cook et al 1989, 387-391) to shorten the length of computer run time while maintaining an acceptable reduction in solution accuracy. Proper validation of a finite element method model used to complete a modal analysis through calibration of its dynamic properties will require careful consideration of such assumptions.

The USBR currently uses several commercially available finite element based computer programs to carry out response spectrum analyses of their concrete gravity dams using both response spectrum and time history methods (Nuss 1991). These

programs include SAPIV (Wilson et al 1974), which is a general purpose finite element based program and the specialized EAGD-84 developed at the University of California (Fenves and Chopra 1984). EAGD-84 completes 2 dimensional time history analysis and is further discussed in Section 3.2.

The state-of-the-art in gravity dam dynamic analysis is in constant flux, as practitioners absorb the availability of greater computer power and researchers attempt to incorporate more rational representations of the actual dams (Chopra 1987, Singhal 1991, Pataky 1994). For the foreseeable future, finite element method models will continue to be used for either response spectrum or time history dynamic analyses of gravity dams. For general interest, areas of current research into gravity dam behaviour include:

- *dam-reservoir interaction* (Darbre 1993, Fok et al 1986, Hall and Chopra 1980, Kuo 1982)
- *dam-reservoir bottom interaction* (Bougach and Tassoulos 1991, Fenves and Chopra 1984)
- *dam-foundation interaction* (Danay & Adeghe 1993, Chopra & Zhang 1991)
- *simplified seismic or dynamic analysis* (Selvam et al 1993, Rashed and Iwan 1985, Ghobarah et al 1994, Fenves and Chopra 1986)

- *non-linear behaviour* (Bhattacharjee & Leger 1992)
- *fracture mechanics in dams* (Dungar et al 1991)
- *hydrodynamic pressures in cracks* (Dewey et al 1994)
- *three dimensional effects* (Ghobarah et al 1994)

As well, current research into related areas includes:

- *size effects of material properties* (Saouma et al 1991, Bazant 1992)
- *effect of vertical contraction joints (arch dams)* (Fenves et al 1992)

2.2 Vibration Testing and Analysis

A chronological summary will follow of related vibration testing and analysis of concrete dams. Many of these are arch dams and although the structural behaviour of arch dams is not at all similar to gravity dams, these tests are included as they are considered of benefit for gaining the proper historical perspective of the development of vibration testing and how it relates to gravity dams. An excellent paper summarizing vibration testing and analysis of concrete arch and gravity dams to 1988, is by Hall (Hall 1988).

The method of exciting a dam is grouped into 2 general categories: forced (being any of periodic, random or transient) and ambient. Forced methods all impart a controlled excitation from a device constructed expressly for this purpose . Periodic and random are similar in that the load is imparted continuously over time and the steady-state response of the structure is measured. A transient test may involve repeated load applications. With transient, the load application may be repeated after the structure has stopped responding to it. Ambient testing imparts no controlled load to the structure. The assumed steady-state response of the structure is measured during ambient testing.

The literature indicates that research into vibration testing and analysis of concrete dams was ongoing in the early 1960's in Japan (Takahashi 1964). The reference paper presents comprehensive research. Forced vibration tests were completed on gravity and arch dams. Measurements of hydrodynamic pressures were made. Measurements of dam response during seismic events are presented and analyzed. Dynamic properties obtained from the field work were compared to results for lab vibration testing on scale models and to numerical models calculated by hand using Rayleigh-Ritz techniques. Water was treated as an additional mass in the hand calculations. The paper concluded that water compressibility is unimportant in assessing the seismic response of dams. However today, water compressibility is still considered to be important in this regard (as following discussion will illustrate). This early paper indicates the value of field vibration tests to study dam behaviour. It concludes with (Takahashi 1964, 259):

"... the vibration we studied are all small in their scale. Therefore, our

important task in the future is to explore the limit of large vibrations ..."

This conclusion is still valid. Vibration testing typically subjects a dam to much lower amplitudes of motion than would be expected in a design earthquake. Dynamic properties may vary with the amplitude of the motion, due to non-linear material or geometric behaviours. This must always be borne in mind when the results of vibration testing are used to predict the dynamic response of a structure to strong shaking.

In the U.S., the first instance of vibration testing found in the literature was conducted on the Monticello Dam, a concrete arch dam, in California (Rouse and Bouwkamp 1967). The first concrete gravity dam tested in the U.S. was the Pine Flat Dam in California (Rea et al 1975). These early tests excited the dams via forced vibration generators mounted on the dam crest. The generators were of the eccentric mass type, which yield a force which varies sinusoidally over time. The Monticello Dam tests utilized two exciters which were located either side of the dam centre and operated in phase to excite symmetric responses and out of phase to excite anti-symmetric responses. In all of these tests, dam responses were measured using accelerometers. The latter report also describes measurement of the hydrodynamic pressures, using piezo-electric pressure transducers. In all tests, natural frequencies, mode shapes and the damping associated with each natural frequency were obtained.

Since the late 1970's, the number of references in the literature to vibration testing and analysis of concrete dams is found to increase significantly.

An extensive vibration testing and analysis program of concrete arch dams was completed by ANCO Engineers Inc. of California in 1982 (ANCO 1982). Three different California arch dams were tested: Pacoima Dam, Big Dalton Dam and Monticello Dam. Forced vibration tests were completed using eccentric mass shakers. Transient vibration tests were completed using a gas expansion transient popper in the reservoir. Measurements were made of dam accelerations and hydrodynamic pressures in the reservoir. Test data was used to calibrate a finite element model of Pacoima Dam. The salient conclusions from this work were (ANCO 1982, 9-1):

"... Forced vibration testing and parameter estimation is necessary for model verification and accurate safety analysis. ...

... Forced vibration testing is necessary to complement finite element dynamic analysis for an improved understanding of dam dynamics. ...

... Forced vibration testing for model verification and/or monitoring of dynamic properties for damage detection is not inexpensive but is appropriate and necessary for critical, high-risk dams. ..."

It is noted that the ANCO results are reasonably close to the previously reported Rouse & Bouwkamp results for the Monticello dam. Disappointingly, no utilization of the hydrodynamic pressure measurements is indicated in the ANCO report.

The U.S. Army Engineer Waterways Experiment Station (part of the U.S. Army Corps of Engineers) completed testing of the Richard B. Russell Dam, a gravity dam located on the Savannah R. between Georgia and South Carolina, before impoundment of the reservoir (Chiarito & Mlakar 1984). A single forced vibration generator, supplying a sinusoidal varying time history of force, was used. The excitor was operated at three separate positions on the dam to facilitate construction of mode shapes. The results

were compared to dynamic properties obtained from finite element models of the dam. It was found that foundation flexibility needed to be included for proper calibration of dynamic properties.

The Vieux Emosson arch dam in Switzerland has been the subject of several vibration tests. A joint Swiss, British and French effort was reported in 1982 (Deinum et al 1982), in which eccentric mass vibrators were used to excite the dam. More recently, the Swiss Federal Laboratories for Materials Testing and Research (EMPA) has reported on further testing. Two reports were issued by EMPA (Deger et al 1993, Pietrzko 1993). The first paper describes the testing and the results which were used to calibrate a finite element method model of the dam. A single random vibration generator was used. The calibration is facilitated with a software package called LINK. LINK uses the experimental results with a Modal Assurance Criterion (MAC) software package to identify what stiffness/mass parameters in the finite element model should be modified to best match a selected number of natural frequencies/mode shapes. The second paper describes a study into the influence of the vibrator placement on the test results. It was concluded that (Pietrzko 1993, 251):

"... For single input, modal testing, as presented, the exciter can be mounted at any point and in any arbitrary direction and does not have to be oriented in accordance with any of the coordinate axes used for the orientation of roving transducers. The only criterion of placement is the efficient excitation (maximising) of contributions of all modes of interest to the measured driving point FRF. ..."

This conclusion can be considered of interest for ambient vibration measurement when quantification of excitation is attempted (which this thesis will include). Normally quantification of the ambient excitation is an impossible task. For instance, it is not

feasible to measure the traffic and wind loading supplying the majority of ambient excitation for a bridge. However, a gravity dam with power tunnels in the nearby bedrock is probably being subjected to significant vibration as a result of this power generation activity. It is possible to measure this signal, and treat it as an input excitation. *The above conclusion for a random force generator is significant as it suggests that as long as the ambient excitation (power generation activity) supplies a reasonably random signal, with its frequency content able to excite all modes of interest, the direction and location of its action is not important.*

There are published results of ambient and transient vibration testing on the Ban Xia arch dam, located in China (Xuehai et al 1987). Transient excitation of the dam was achieved by pulses of 5-10 thousandths of a second duration, from groups of small rockets attached to the crest or in a gallery. Ambient excitation was achieved by detonation of explosives in the reservoir. For the transient tests, rockets were exploded either in or out of phase. Mode shapes were defined along the crest and an internal gallery. Damping was estimated to be 2-3% for each natural frequency. Reasonable agreement is demonstrated between natural frequencies/mode shapes/damping obtained from the tests to those obtained from a modal analysis of a finite element model of the dam. The finite element model did not include the foundation and lumped masses were used to represent the reservoir.

The Italian firm ISMES has been conducting a unique type of vibration testing and analysis on the Talvacchia Dam, an arch dam in Italy (Fanelli et al 1988, Fanelli et al 1992). The dam has a fully automated and permanent instrumentation package,

consisting of plumb lines, joint movement transducers, thermometers, reservoir level indicators and transducers/exciters to affect vibration testing. This includes a forced vibration generator which subjects the dam to twice daily tests through the frequency range 3-11 Hz. The instrumentation is also programmed to record any seismic events and the dam's response to them. The data obtained is used to calibrate a finite element model of the dam. As well, correlations between the variables being measured is being studied. The paper indicates that the values of the natural frequencies of the dam vary with the condition of the joints, temperature and reservoir elevation.

Testing on the Morrow Point Dam, an arch dam in Colorado, was used to calibrate a finite element model of it (Duron 1987, Duron & Hall 1988) and to investigate the hydrodynamic effects of dam-reservoir interaction. Testing was completed with a pair of forced vibration exciters which generated sinusoidal varying time histories of force. Both dam and reservoir response was measured. The former with accelerometers and the latter with hydrophones. Water compressibility was studied for its role in the calibration. It was found that the symmetric and antisymmetric mode shapes of the finite element method model were affected differently by the inclusion of water compressibility. The symmetric mode shapes were found to be significantly affected by the inclusion of water compressibility whereas the opposite was true for the antisymmetric modes shapes. A later paper describes further testing on the Morrow Point Dam (Duron et al 1992), intended to capture hydrodynamic effects. Detailed descriptions of the instrumentation used is provided. In this instance, a single forced vibration excitor, generating sinusoidal varying time histories of force, was used. It is concluded possible to obtain reliable hydrodynamic data which can be used for

determining the importance of water compressibility. Evaluation of reservoir-dam interaction is indicated as being in progress.

Duron and Hall also report on testing of the Santa Anita Dam, an arch dam located in California (Duron & Hall 1991). The paper describes the results of a successful test to record both the dam and the surrounding foundation response. Here a single vibration forced generator was used. The dam is unsymmetrical and it is shown that due to this, orientation of the exciter determined whether symmetric or antisymmetric responses would be excited. It was summarized that (Duron and Hall 1991, 208):

"... Since dam-rock interface motions are on the order of 1% of the crest motions, precise modelling of the rock mass in a mathematical model of the dam-rock system is probably not necessary to capture the major features of the dam response. ..."

This finding is of interest as finite element models of dams generally include a significant portion of the foundation bedrock.

Testing of Outardes 3 Dam, a gravity dam located in Quebec, is reported by University of Sherbrooke researchers and others (Paultre et al 1992). Here a single forced vibration generator of the eccentric mass type was used, yielding the sinusoidal varying time history of force. Accelerometers measured dam response and hydrophones measured reservoir response. Two separate tests, by different researchers, are presented and analyzed in the paper. The intend was to study reservoir-dam interaction and to provide data sufficient for calibration of a finite element model of the dam. The exciter was located in turn at 3 different locations on the dam crest. Conclusions were as follows (Paultre et al 1992, 3576):

"... The forced vibration tests conducted on Outardes 3 dam have successfully demonstrated the applicability of newly developed techniques to the testing of large concrete gravity dams. The good agreement shown between both the magnitude and the phase of the acceleration responses obtained by both research teams suggests that the differences in accelerometer characteristics (10 Volts/g and 300 Hz cutoff for the QA-700 versus 50 Volts/g and 50 Hz for the SA-102) do not significantly affect data quality. The use of a single vibrator placed at different locations along the crest of a long gravity dam appears to yield satisfactory measurements. ..."

The University of Sherbrooke has conducted subsequent tests on Outardes 3, to study, amongst other things, the thermal affects on the dams dynamic properties. No papers have been published yet describing the results of these tests.

Preliminary results of a comparison study of vibration testing and results from periodic and ambient excitation methods has been reported (Duron et al 1994). The tests were conducted on the Shaver Lake Dam, a gravity dam, the Big Creek No. 4 Dam, an arch dam and the Florence Lake Dam, a multiple arch dam, all in California. The Big Creek No. 4 Dam was subjected to all 3 types of test, with the specific intent of (Duron et al 1994, 60):

"... to investigate the dam-foundation and dam-water interactions; to compare the measured response characteristics from forced-vibration [periodic], ambient, and transient responses; and to evaluate simplified test procedures based on ambient and transient measurements. ..."

For this dam, a single excitation devise was used in the periodic vibration test. The article finishes by concluding (Duron et al 1994, 62):

"... ambient and transient responses found on a small dam are very comparable to those produced by more elaborate forced-vibration testing. ..."

In summary, the literature indicates that vibration testing and analysis of concrete dams, including gravity dams, has been ongoing for over 30 years. Most of these

revolve around applying an artificially induced and controlled excitation to the dam. Results are found to be useful for analyzing dam behaviour and validating numerical (usually finite element method based) models of the dam. Relevant aspects of dam behaviour being studied through vibration testing and analysis include:

- *dam-reservoir interaction*
- *dam-foundation interaction*
- *effect of joints and temperature on dynamic properties*

Ambient vibration testing and analysis is not well represented in the literature.

CHAPTER 3

DYNAMIC ANALYSIS and NUMERICAL MODEL CALIBRATION METHODOLOGY

The Scope of Work (Section 1.3) stipulates that a numerical model of the selected BCH dam will be built and a calibration to the ambient analysis results undertaken. This chapter describes the key concepts needed for an understanding of this calibration work.

3.1 Linear Elastic Modal Analysis

Response Spectrum Analysis

As described in Section 2.1, dams are usually analyzed dynamically by one of two methods: *time history* analysis, or, *response spectrum* analysis. A *modal* analysis is a required step in the response spectrum analysis (it can also be completed on a *linear* numerical model constructed for the time history analysis). It is the modal analysis which determines the natural frequencies and mode shapes of the numerical model. The modal analysis is of importance to this thesis as its results are used in the calibration procedure. To place the modal analysis in its proper context, a brief description of the steps in a response spectrum analysis is given as follows:

1. *Choose Numerical Model:* To complete a response spectrum analysis it is necessary to have a model of the structure. With the finite element method, the structure is modelled as a multi-degree of freedom (MDOF) system, which is a discrete idealization of the structures stiffness and mass. Dynamic analysis will be based on the dynamic equations of motion using matrix algebra.
2. *Modal Analysis (Linearized Eigenvalue Problem Analysis):* The dynamic equation of motion, in matrix form, is solved for its undamped formulation, to yield the eigenvalues (which are numerically equal to the square of the natural frequencies) and corresponding eigenvectors (mode shapes) of the model.
3. *Obtain Response Spectrum:* A response spectrum is selected. In words, a response spectrum is a graphical representation in the frequency domain, of the numerical relationship between the maximum response of a family of single degree of freedom systems and a prescribed selected input motion. The response can be in terms of displacement, velocity or acceleration. The input motion may be a recorded or synthetically generated earthquake. The damping of the family of single degree of freedom systems must be specified.
4. *Spectrum Analysis:* Using the results of the modal analysis and the chosen response spectrum, the contribution of each mode to the total response is evaluated and combined using a *method of superposition*. Methods of superposition do not add the individual modal responses algebraically as they do not typically occur at the same point in time. One suggested method of

superposition involves the calculation of the square root of the sum of the squares of the individual modal responses to obtain the total response (Clough and Penzien 1975, 561-564).

The theoretical development for a modal analysis will now be briefly described.

Modal Analysis

The following development is paraphrased from the Clough and Penzien textbook (Clough and Penzien 1975, 176-177).

The dynamic equation of motion for an undamped MDOF system is:

$$[M]\{\ddot{u}\} + [K]\{\dot{u}\} = \{0\} \quad (3.1)$$

Where:

$[M]$ = the matrix of discrete masses

$[K]$ = the matrix of discrete stiffnesses

$\{u\}$ = vector of displacements

$\{\ddot{u}\}$ = vector of accelerations

For a linear system, a solution for $\{u\}$ exists for the case of free vibrations:

$$\{u\} = \{A\} \sin (\omega t + \theta) \quad (3.2)$$

Where:

$\{A\}$ = arbitrary shape function

θ = phase angle (radians)

t = time

ω = frequency of vibration (radians/second)

The second derivative of this solution is:

$$\{\ddot{u}\} = -\omega^2 \{u\} \quad (3.3)$$

Substituting eq's. (3.2) and (3.3) into eq. (3.1) yields:

$$\{[K] - \omega^2[M]\}\{A\} = 0 \quad (3.4)$$

This represents a *linearized eigenvalue problem*. The non-trivial solution for eq. (3.4) is found from solving the following determinant:

$$|[K] - \omega^2[M]| = 0 \quad (3.5)$$

Solving the resulting coefficient matrix determinant (or *characteristic equation*) yields a series of *eigenvalues*, ω_i^2 , with each ω_i defined as a *natural frequency* of the numerical model. Each eigenvalue is back substituted into eq. (3.4) to solve for the corresponding *eigenvector*, $\{A_i\}$, also known as the corresponding *mode shape*.

The total number, i , of natural frequencies and corresponding mode shapes obtained will equal the number of degrees of freedom in the MDOF model.

3.2 Hydrodynamic Effects

A key feature of any numerical model of a dam used for dynamic analysis is its

representation of the reservoir behaviour. Literature review found that in the last 15 years much research has concerned itself with how best to represent this behaviour, particularly in papers being published by the Earthquake Engineering Research Centre (EERC) at the University Of California (Berkeley) (Hall and Chopra 1980, Kuo 1982, Fenves and Chopra 1984, Fok et al 1986, Fenves et al 1989).

The two methods represented in the literature are:

- *Incompressible Water (Lumped Mass)*
- *Compressible Water*

Each of these will now be briefly described.

Incompressible Water (Lumped Mass)

For simplicity, many analyses are completed assuming that the reservoir acts as an *incompressible* fluid during dynamic excitation. To represent an incompressible fluid, it is necessary to calculate an effective *added mass* to represent the fluid, which is then added to the numerical models mass, usually lumped at the discrete points already comprising the model (hence termed a *lumped mass*). This lumped mass will therefore affect the resulting inertia loads. The net effect will depend on the change in response amplification caused by adding the mass. One thing is certain though, the

magnitude of the lumped mass is frequency independent and will therefore affect all natural frequencies of the model proportionately, as from the characteristic equation obtained from the linearized eigenvalue problem in the preceding section, the eigenvalues of the model, ω_i^2 , will vary directly with stiffness and inversely with mass (Humar 1990, 420-424). Therefore, the act of adding a lumped mass representing the reservoir will be to decrease the natural frequencies of the dam.

The simplest method of obtaining the magnitude of the lumped masses is by consideration of the total hydrodynamic pressure calculated from pseudo-static analysis methods. The USBR's pseudo-static methodology (USBR 1977) uses its own Monograph 11 in which is detailed how to calculate the hydrodynamic pressure, P , which treats the dam as infinitely rigid and the reservoir as an incompressible fluid (Zangar 1953), as follows:

$$P = C \alpha \gamma z \quad (3.6)$$

Where:

C = dimensionless pressure coefficient

α = normalized horizontal earthquake acceleration

γ = unit weight of water

z = total reservoir depth at section being analyzed

The normalized horizontal earthquake acceleration, α , is the earthquake horizontal earthquake acceleration, a_h , normalized with respect to the acceleration of gravity, g , or:

$$\alpha = a_h / g \quad (3.7)$$

The dimensionless pressure coefficient, C , has a parabolic distribution with a maximum value, C_m , at the base of the dam and is obtained from:

$$C = (C_m/2)[(h/z)(2-h/z) + \sqrt{\{h/z(2-h/z)\}}] \quad (3.8)$$

With:

h = depth of water

C_m = dimensionless maximum value of C for a given upstream face slope

The value of C_m varies from a maximum value of 0.735 for dams with a vertical upstream face, to 0.41 for dams with an upstream face sloped at an angle of 45 degrees to the horizontal.

The lumped mass at a point i , m_l^i , can be found by integrating the hydrodynamic pressure over the tributary area, a , to the point i and then dividing through by the horizontal earthquake acceleration, a_h , or:

$$m_l^i = (1/a_h) \int_a P da \quad (3.9)$$

As a refinement to the above approach, the USBR is currently starting to use *incompressible fluid elements* in some of their finite element method numerical modelling (Nuss 1991). This method calculates added masses by a method different from the USBR pseudo-static approach, by utilizing the acoustic wave equation:

$$(1/C_w^2)(\partial^2 P / \partial t^2) - \nabla \cdot \nabla P = 0 \quad (3.10)$$

Where:

P = acoustic pressure (= $P(x, y, z, t)$)

$\nabla ()$ = divergence matrix operator on ()

$\nabla \cdot ()$ = gradient matrix operator ($\delta x/\delta t \delta y/\delta t \delta z/\delta t$) on ()

C_w = sonic wave velocity in water (normally taken as 4760 ft/sec)

By using the acoustic wave formulation, the method is able to consider the shape and flexibility of the dam and foundation. However, the resulting lumped mass is still frequency independent. The method is based on doctoral work by Kuo (Kuo, 1982).

Compressible Water

An advanced representation of hydrodynamic effects would consider the frequency dependent dynamic characteristics of the dam-foundation-reservoir interaction. This is possible by including in the numerical model, a discretization of the reservoirs mass and stiffness, hence, its *compressibility*. To do this requires a more direct inclusion of the hydrodynamic effect utilizing the acoustic wave equation for water given above in the analysis of the numerical model. The following describes a number of computer programs which do this.

A two dimensional analysis program developed at EERC is called EAGD-84, which uses the two dimensional form of the wave equation (Fenves and Chopra 1984). The foundation may also be modelled with stiffness and mass. The program completes a modal analysis and calculates the natural frequencies and mode shapes of the dam-

foundation. The dam-reservoir interaction is not included in a modal analysis and hence no provision is made in the program to obtain the dynamic properties of the dam-foundation-reservoir system. The reservoir effects are included only in a time history analysis, which yields displacements and stresses at the specified time increment. The reservoir is modelled as a fluid domain which is of constant depth and of infinite length in the upstream direction. Researchers have found that the shape of the reservoir does impact on the frequency variation of the hydrodynamic force (Hall and Chopra, 1980, 70) so EAGD-84's reservoir representation must be considered carefully. Of interest, the program considers the energy absorbing capability of the reservoir bottom. This feature is found to have a significant impact on dam response, its inclusion generally acting to decrease the dam response (Fenves and Chopra, 1984, 179-182). In addition, with respect to the programs foundation modelling capability, it is reported that consideration of the dam-foundation interaction decreases the response of a dam (Chopra 1987, 44).

A three dimensional analysis program developed also at EERC, called EACD-3D completes analysis of arch dams or gravity dams (Fok et al 1986). The EERC report on the dam suggests that it only be considered for gravity dams for which three dimensional effects are considered important, i.e., those located in narrow valleys (Fok et al 1986, 1). Similar to EAGD-84, the program allows for modelling of the foundation and completes a modal analysis only of the dam-foundation and includes reservoir interaction only in time history analyses. As well, the energy absorbing capability of the reservoir bottom can be considered. Reportedly, a new version of EACD-3D will be available in the near future.

As discussed in Section 9.1, the finite element method computer program used for this thesis is ANSYS©. This program allows for the inclusion of water compressibility in two or three dimensional analysis, through use of acoustic fluid elements. The resulting fluid-structure coupling yields unsymmetric matrices for which an *unsymmetric matrix modal* analysis is required, using the Lanczos unsymmetric eigensolver algorithm. (ANSYS 1982, IV:15-42 to 15-43). An alternate method is also detailed by ANSYS© in which a model with the acoustic elements is subjected to a *harmonic response* analysis, in which the response of the model is obtained at discrete frequency increments through a specified frequency range (ANSYS 1992, IV:17-18 to 17-25). Maximas in plots of the response will indicate natural frequencies.

The above discussion demonstrates that inclusion of water compressibility complicates the modelling and analysis. Is water compressibility important? It has been reported in the literature by researchers familiar with the modelling of dam-reservoir interaction, that the key parameter to evaluate is the ratio, Ω , of the fundamental frequency of the reservoir water, f_{wl} , to the fundamental frequency of the dam without reservoir, f_{dl} , or:

$$\Omega = f_{wl} / f_{dl} \quad (3.11)$$

If the dam is flexible enough in relation to the reservoir, the effect of water compressibility is insignificant. Hence the value of Ω below which consideration of water compressibility is significant is reportedly 1.5 (Hall 1988, 59) or 2 (Chopra 1987, 45).

Normally, the value of f_{dl} is obtained either from a numerical model of the dam or from vibration testing. The value of f_{wl} can be obtained either from vibration testing or from formulas derived for fluid domains of certain geometries, e.g., for a fluid domain of semi-circular cross-section and infinite length (normally acceptable for a dam reservoir):

$$f_{wl} = C_w / (3.41H) \quad (3.12)$$

Where:

H = maximum depth of reservoir (ft)

3.3 Calibration to Ambient Vibration Testing and Analysis

Naturally, much of the literature concerning vibration testing and analysis of structures includes comparison of the dynamic properties obtained to those obtained from a numerical model. Calibration of numerical models to vibration test results is an area of research interest, particularly in the hope of arriving at an automated procedure (Guo and Hemingway 1991, Felber 1993 71-75, Deger et al 1993 262, Ewins 1984 226-233). Most efforts are directed at developing algorithms to identify errors in the mass and stiffness matrices in the numerical models which can then be corrected.

This thesis will not attempt automated calibration procedures. Calibration will be completed by comparing from the numerical modal analysis and the vibration test analysis:

- *the magnitudes of natural frequencies*
- *a least squares calculation of the deviance from a purely scalar relationship between mode shapes (eigenvectors)*

It is noted that several orthogonality calculations can be made to compare mode shapes (eigenvectors) (SEM 1993, 1.9) which are not used in this thesis.

Mode Shape Comparison Criteria

Consider a mode shape (eigenvector) for a given structure, defined at n points. If one plotted the experimental vs. numerical model mode shape normalized magnitude at the n points, a perfect correlation would yield a line with a 45 degree angle (a slope equal to 1). The Modal Assurance Criteria (MAC) calculates the least squares deviation of the points from such a line (Ewins 1984, 225). The MAC between the vectors representing the two mode shapes; experimental, $\{A_e\}$, and numerical model, $\{A_m\}$, is defined as:

$$MAC = \frac{|\{A_e\}^T \{A_m\}|^2}{[\{A_e\}^T \{A_e\}][\{A_m\}^T \{A_m\}]} \quad (3.13)$$

The MAC calculation will be used to compare mode shapes.

CHAPTER 4

AMBIENT VIBRATION ANALYSIS METHODOLOGY

The bulk of work in this thesis involves analysis of ambient signals. This chapter describes the theoretical background for the ambient analysis methods.

4.1 Two Ambient Vibration Analysis Techniques Used in this Thesis

A structure, when subjected to excitation, has a response. Both the excitation and response can be measured and represented as signals varying in time. The excitation signal is termed an *input* signal and the response signal is termed an *output* signal. Traditionally, ambient vibration testing and analysis only uses the output signal to deduce dynamic properties. This traditional approach forms the basis for the first analysis technique used in this thesis. However, it was recognized that certain concrete gravity dams, such as the one chosen as the subject for this thesis, have power generation activities located nearby which may generate a significant proportion of the ambient excitation. Successfully capturing the ambient input signal exciting the dam would provide a non-traditional means to analyze ambient data. In this thesis a second analysis technique is developed by quantifying this input signal and using it to identify dynamic properties.

The ambient analysis techniques used in this thesis can be characterized by the *input-output system* they use:

1. *Hybrid Bridge Evaluation System (HBES): relative single input-single output system*
2. *Complementary Analyses:* uses both the *relative single input-single output system* for performing detailed checking of the HBES results and other studies and also utilizes *single input-single output system with output noise* to study the excitation signal captured in the foundation.

The two systems will be described in due course as part of the following development of the fundamental principles behind both ambient analysis techniques.

4.2 Theoretical Considerations

As introduced in Sections 1.0 and 2.2, ambient vibration testing does not rely on any artificial device whose express purpose is to excite the structure. It is dependent on using the existing ambient vibrations, which may be man-made nonetheless, to supply sufficient excitation to allow for identification of dynamic properties. How those signals are analyzed to obtain the dynamic properties is the subject of this Section.

First, the fundamental concepts of stationary and ergodic processes and Fourier

transformation are discussed.

Stationary and Ergodic Processes

Ambient vibrations are measured in the time domain. The process which they represent is considered both a *stochastic* process, i.e., occurring over time and a *random* process, i.e., from Bendat and Piersol (Bendat and Piersol 1993, 2):

"... a physical phenomenon and the data representing it are considered random when a future time history record from an experiment cannot be predicted within reasonable experimental error. ..."

The analysis of the ambient vibrations in this thesis treats the random stochastic processes which they represent as both *stationary* and *ergodic*. To understand what stationary and ergodic processes are, consider a group or *ensemble* of independent measurements of that process. At any time, t , the statistical *averaging* properties, such as mean value, can be calculated over the ensemble. If these averaging properties do not change over time, the process is considered stationary. If one considers a single recording from the ensemble, if the averaging properties calculated over the length of the recording are equivalent to those calculated over the ensemble, then the process is considered ergodic. A stationary process may or may not be ergodic, whereas an ergodic process is by definition also a stationary process. The importance of these concepts to ambient vibration testing and analysis is that the ambient tests will yield a single recording of an underlying physical process (vibration of the concrete gravity dam at a point). The recording will be used in ambient analysis to calculate statistical

averaging properties which in turn are used to determine the dynamic properties of the dam. Therefore, the process must be stationary and ergodic for the dynamic properties determined to be considered accurate representations of the dams physical characteristics.

Fourier Transformation

The ambient vibration analysis in this thesis is completed in the frequency domain, using frequency domain functions, although signals are measured in the time domain. To convert the recorded time domain information to the frequency domain, Fourier transformation is necessary.

Given a continuous time domain function, $x(t)$, which could represent either a continuous recording of response at a point on a structure being excited or a continuous time domain function calculated to represent such a recording, its representation in the frequency domain, $S_x(f)$, can be calculated using the *continuous Fourier transform*, notated as:

$$S_x(f) = \int_{-\infty}^{\infty} x(t) e^{-j2\pi ft} dt \quad (4.1)$$

Where:

f = frequency (Hz)

$j = \sqrt{-1}$

$S_x(f)$ is also known as the *spectrum* of $x(t)$.

Fourier transformation essentially represents any time domain signal in the frequency domain as a combination of sine waves.

As described earlier, ambient data represents a random process and it is not described by mathematical function. Therefore, to convert ambient time domain data to the frequency domain, a discretization of the time domain data is required, using a *discrete Fourier transform*. This process of discretization is described briefly as follows:

Given a continuous time domain function $x(t)$, a discretized representation is obtained by sampling $x(t)$, a total of N times, at a Δt time interval. The new discretized function is notated as $x(N\Delta t)$.

The discrete Fourier transform of $x(N\Delta t)$ is $S_x(m\Delta f)$, calculated using:

$$S_x(m\Delta f) = \Delta t \sum_{i=0}^{i=(N-1)} x(i\Delta t) e^{j2\pi m i / N} \quad (4.2)$$

Where:

Δf = discrete frequency interval defining $S_x(m\Delta f)$, $m = 0, \pm 1, 2, 3, \dots$

Calculation of the above discrete Fourier transform is made more efficient by the *fast Fourier transform* (FFT) algorithm. The classical fast Fourier transform algorithm assumes that the number of samples, N , is a multiple of 2, thereby allowing certain symmetries to occur reducing the number of calculations. This algorithm is used in

this thesis. The fast Fourier transform was developed by J.W. Cooley and J.W. Tukey (Cooley and Tukey 1965).

With the concepts of stationary and ergodic processes and Fourier transformation, attention can now be directed towards identification of dynamic properties from the ambient signals.

Spectral Density Functions

We can transform time domain data to frequency domain. Once in the frequency domain, what are the frequency domain functions needed to identify dynamic properties?

The basic frequency domain function required is the *spectral density function*.

Spectral density functions can be derived in several ways. The following is a brief description of their derivation from correlation functions as paraphrased from Bendat and Piersol and Ewins (Bendat and Piersol 1993 50-54, Ewins 1984 79-80):

Given 2 time domain signals $x(t)$ and $y(t)$, one can calculate the time domain *cross-correlation function* of these two signals, $R_{xy}(\tau)$, which is: the expected value (or "average" and hence is based on calculation of statistical averaging properties) of the product of $x(t)$ and $y(t + \tau)$, notated as:

$$R_{xy}(\tau) = E[x(t), y(t + \tau)] \quad (4.3)$$

With:

τ = time delay (seconds)

$E[]$ = expected value of $[]$

The Fourier transformation of the correlation function yields the *cross-spectral density function* or *cross-spectrum*, $S_{xy}(f)$. If $x(t) = y(t)$, the cross-spectral density function becomes the *power spectral density function*, *auto spectral density function* or *auto-spectrum*, $S_{xx}(f)$. The power spectral density function, with a time delay equal to zero (there is none with identical signals) can be interpreted as the frequency distribution of the mean square value of $x(t)$. The general cross-spectral density function, is defined as:

$$S_{xy}(f) = \int_{-\infty}^{\infty} R_{xy}(\tau) e^{j2\pi f\tau} d\tau \quad (4.4)$$

Of note, general Fourier transforms such as that shown for $S_{xy}(f)$ above provide "two-sided" functions, in that both positive and negative values of f are defined. In practise, it is convenient to work with the positive values only, or so-called "one-sided" functions. The one-sided cross-spectrum is indicated as $G_{xy}(f)$, and the one-sided auto-spectrum is indicated as $G_{xx}(f)$. $G_{xy}(f)$ is defined as:

$$G_{xy}(f) = 2S_{xy}(f) = 2 \int_{-\infty}^{\infty} R_{xy}(\tau) e^{j2\pi f\tau} d\tau, \text{ for: } f > 0 \quad (4.5)$$

$$G_{xy}(f) = S_{xy}(f) = \int_{-\infty}^{\infty} R_{xy}(\tau) e^{j2\pi f\tau} d\tau, \text{ for: } f = 0 \quad (4.6)$$

$$G_{xy}(f) = 0, \text{ for: } f < 0 \quad (4.7)$$

Expressions for $G_{xx}(f)$ are similar.

Spectral density functions can also be obtained via direct Fourier transformation of the original time domain signals. See the textbook by J.S. Bendat and A.G. Piersol (Bendat and Piersol 1993, 54-56) for details.

The value of spectral density functions is that they can be used to indicate natural frequencies of systems. We define $x(t)$ as the input signal and $y(t)$ as the output signal for a single degree of freedom (SDOF) system. If the input signal is wide band random noise, $G_{xx}(f)$ would appear of uniform magnitude across the entire frequency range of zero to infinity. $G_{xy}(f)$ will show a peak at the natural frequency of the system reflecting the systems large amplitude response at resonance. The peak should theoretically be of infinite magnitude, but for reasons of data discretization during measurement (sampling interval), the peak will be of a finite magnitude.

With extension to multi-degree of freedom (MDOF) systems representing actual structures, it would seem a simple matter to calculate spectral density functions to identify the system natural frequencies. This is true when both input and output signals can be accurately measured, such as with forced vibration testing and analysis. However, traditional ambient testing and analysis uses the output signal only. Maxima of output spectral density functions may also represent large amplitude/duration responses caused by strengths in the input. Further criteria is needed to ascertain whether the frequencies corresponding to localized maxima in output spectral density functions are due to resonance of the system.

Transfer Function, Transfer Function Gain and Phase Factor

The *transfer function* or *frequency response function*, $H(f)$, (transfer function is the chosen term in this thesis as opposed to frequency response function) for a physical system represents a frequency domain description of the systems dynamic response properties. These properties are used in determining whether frequencies identified through spectral density function analysis are in fact probable natural frequencies. As a result, calculating the transfer function is of utmost importance and will be described in due course, but what is a transfer function and what are the properties it has of interest? To answer this requires illustration with a common type of transfer function using elementary structural dynamics principles and a SDOF system.

First, consideration is given to a very simplistic but analytically powerful type of function, known as the *delta function*, $\delta(t)$. The delta function is a function of infinite magnitude acting over an infinitely small period of time, or in other words, a "spike". The Fourier transform of $\delta(t)$ is 1 over all frequencies.

The delta function may be used in determining a special type of excitation, known as the *unit impulse*, as follows. Let:

$$F(t) = F \delta(t) \quad (4.8)$$

If F is numerically equal to unity, then $F(t)$ becomes the unit impulse.

The response of any physical system in the time domain, to the unit impulse, is termed the *unit impulse response function*, $h(t)$. The Fourier transform of the unit impulse

response function is the *transfer function*, $H(f)$, for that system.

Now, the properties of interest of the transfer function must be derived. Consider a viscously damped SDOF system, as shown in Figure 4.1 (Bendat and Piersol 1993, 18 and 20).

The linear differential equation of motion for the SDOF system is:

$$F(t) = m\ddot{x} + c\dot{x} + kx \quad (4.9)$$

Now let $F(t)$ = the unit impulse. The response of the SDOF system, $x(t)$, is now equal to the unit impulse response function, $h(t)$.

Substituting eq. (4.8) into eq. (4.9):

$$\delta(t) = m\ddot{h} + c\dot{h} + kh \quad (4.10)$$

The Fourier transform is denoted by \Rightarrow . Therefore, remembering:

$$h(t) \Rightarrow H(f) \quad (4.11)$$

The derivatives of the response are then:

$$\dot{h} \Rightarrow j2\pi f H(f) \quad (4.12)$$

$$\ddot{h} \Rightarrow -(2\pi f)^2 H(f) \quad (4.13)$$

Therefore, taking the Fourier transformation of both sides of the differential equation of motion, yields:

$$1 = H(f)\{- (2\pi f)^2 m + j2\pi f c + k\} \quad (4.14)$$

Or:

$$H(f) = 1/[-(2\pi f)^2 m + j2\pi f c + k] \quad (4.15)$$

Define the *damping ratio* of the SDOF system as ζ and the *ratio of frequency to the undamped natural frequency of the SDOF system* as β . These are equal to:

$$\zeta = c/\{2\sqrt{k/m}\} \quad (4.16)$$

$$\beta = f/\{1/(2\pi)\}\sqrt{k/m} \quad (4.17)$$

With f in Hz in the above equations. Substituting eqs. (4.16) and (4.17) into eq.

(4.15) yields:

$$H(f) = 1/\{k(1 - \beta^2 + j 2\zeta\beta)\} \quad (4.18)$$

Now from eq. (4.18), the transfer function is a complex number and therefore it has a *gain*, $|H(f)|$, and *phase factor*, $\Phi(f)$. It is the transfer function gain and phase factor which comprise the information in the transfer function which can be used to determine natural frequencies, described as follows.

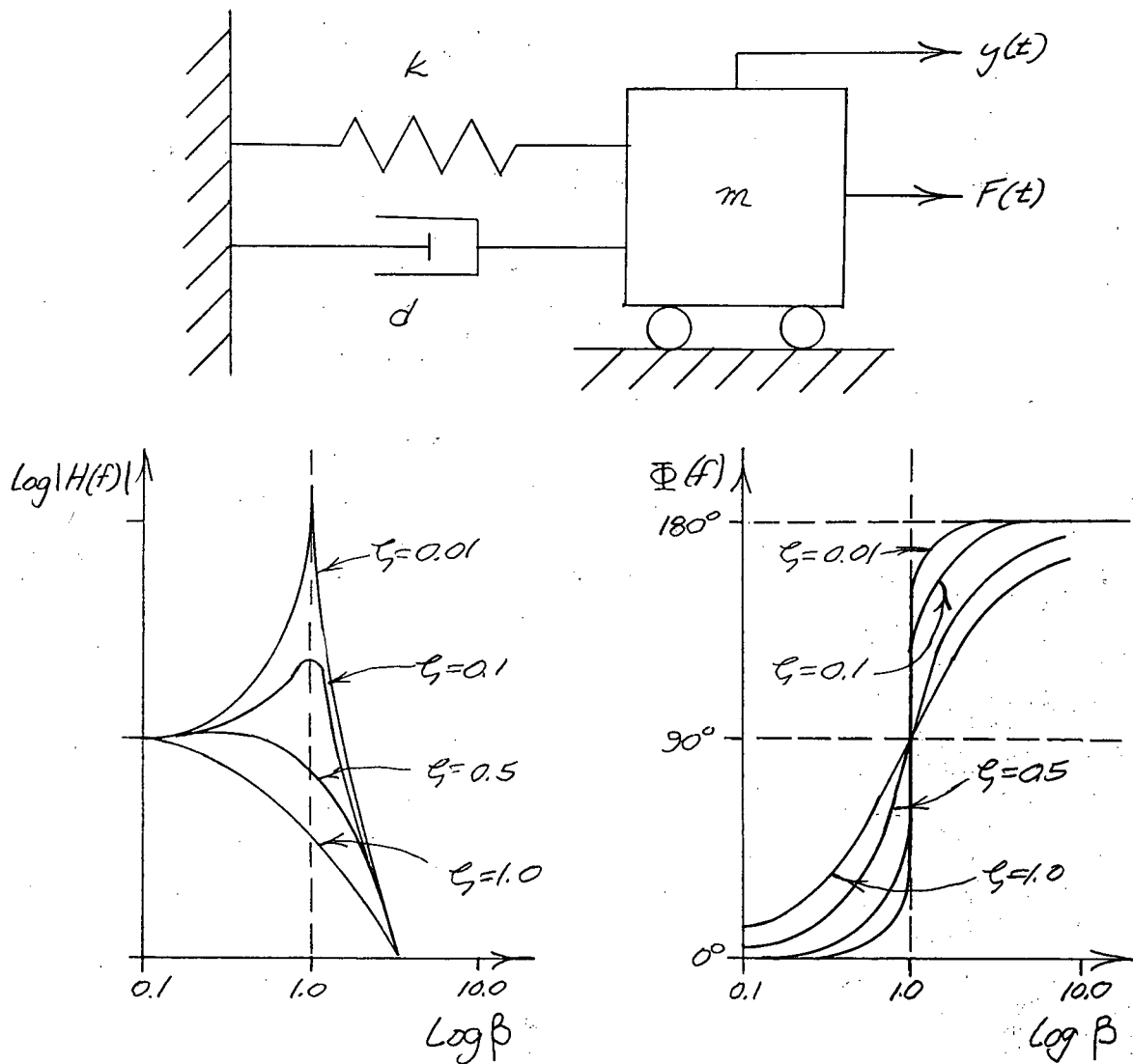
Plots of the transfer function gain and phase factor for the SDOF system are also depicted in Figure 4.1. The equations for these are:

$$|H(f)| = 1/[k\sqrt{(1 - \beta^2)^2 + (2\zeta\beta)^2}] \quad (4.19)$$

$$\Phi(f) = \tan^{-1}\{2\zeta\beta/(1 - \beta^2)\} \quad (4.20)$$

Note from Figure 4.1 that the gain, $|H(f)|$, peaks at $\beta = 1$, i.e., at the natural frequency for the SDOF system and that the corresponding phase factor, $\Phi(f)$, = 90

degrees. These features of the gain and phase factor are particular to the type of transfer function represented, which is a *force input-displacement output transfer function* (force is the input and displacement is the output).



m = Mass	$ H(f) $ = Transfer Function Gain
k = Stiffness	$\Phi(f)$ = Phase Factor
d = Damping	ζ = Damping Ratio
$F(t)$ = Force Input	β = Ratio of Natural Frequency to Undamped Natural Frequency
$y(t)$ = Displacement Output	

Figure 4.1 Idealized Single Degree of Freedom System, Force Input

The above derivation is based on the premise that the damping, stiffness and mass are known for the system. However, vibration analysis makes use of the input and output signals only to calculate the transfer function, which for the SDOF force input-displacement output system are $F(t)$ and $x(t)$ respectively. Traditional ambient vibration analysis techniques use the output signal $x(t)$ alone.

Before detailing the traditional ambient analysis technique, it is first necessary to describe how it is that transfer functions are calculated from input and output signals using spectral density functions calculated from them and also to define one further criteria used for identifying natural frequencies.

Transfer Functions from Spectral Density Functions

The manipulation of the spectral density functions to obtain the transfer functions, is paraphrased from Bendat and Piersol (Bendat and Piersol 1993, 78-81) and Ewins (Ewins 1984, 79-82), as follows:

An idealization of a *single-input single-output system* is shown in Figure 4.2 (Bendat and Piersol 93, 79). The input is $x(t)$ and the output is $y(t)$.

Defining the *output-output autocorrelation relation*, $R'_{xx}(\tau)$, and the *input-output cross-correlation relation*, $R'_{xy}(\tau)$, as:

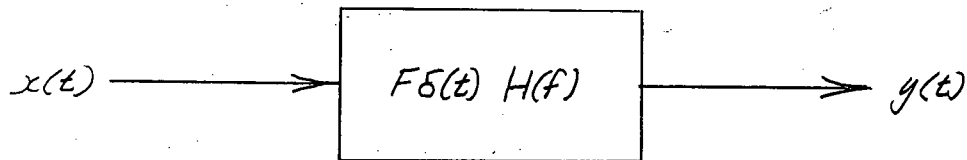
$$R'_{xx}(\tau) = E[x(t), x(t + \tau)] \quad (4.21)$$

$$R'_{xy}(\tau) = E[x(t), y(t + \tau)] \quad (4.22)$$

The Fourier transforms of $R'_{xx}(\tau)$ and $R'_{xy}(\tau)$ yields the *input-output auto spectrum relation* and the *input-output cross-spectrum relation* respectively. The one-sided form for these is:

$$G_{yy}(f) = |H(f)|^2 G_{xx}(f) \quad (4.23)$$

$$G_{xy}(f) = H(f) G_{xx}(f) \quad (4.24)$$



$x(t)$ = Input Signal
 $y(t)$ = Output Signal
 $H(f)$ = Transfer Function
 $F\delta(t)$ = Unit Impulse Function

Figure 4.2 Idealized Single Input-Single Output System

Both eqs. (4.23) and (4.24) contain the needed transfer function. The transfer function obtained from the input-output cross-spectrum relation is superior in accuracy, as from Bendat and Piersol (Bendat and Piersol 1993, 313):

" ... This result again shows the superiority of the cross-spectrum method to the autospectrum method in giving a lower random error by the factor $1/|\gamma_{xy}(f)|$ "

The input-output cross-spectrum relation method is used to obtain transfer functions in

this thesis. Using polar notation:

$$G_{xy}(f) = |G_{xy}(f)| e^{j\theta_{xy}(f)} \quad (4.25)$$

$$H(f) = |H(f)| e^{j\theta(f)} \quad (4.26)$$

Therefore substituting eqs. (4.25) and (4.26) into eq. (4.24):

$$|G_{xy}(f)| = |H(f)| |G_{xx}(f)| \quad (4.27)$$

Or:

$$|H(f)| = |G_{xy}(f)| / |G_{xx}(f)| \quad (4.28)$$

And:

$$\theta_{xy}(f) = \theta(f) \quad (4.29)$$

As all of the frequency domain functions are complex, the transfer function, $H(f)$, may be expressed differently. First express the cross-spectral density as a complex number:

$$G_{xy}(f) = C_{xy}(f) - jQ_{xy}(f) \quad (4.30)$$

With:

$$C_{xy}(f) = \text{the real part}$$

$$Q_{xy}(f) = \text{the imaginary part}$$

Now substituting eq. (4.30) into eq. (4.28):

$$|H(f)| = \sqrt{\{C_{xy}^2(f) - jQ_{xy}^2(f)\}} / |G_{xx}(f)| \quad (4.31)$$

As noted above, the phase of the transfer function is equal to the phase of the cross-spectral density function, therefore:

$$\theta(f) = \theta_{xy}(f) = \tan^{-1}\{Q_{xy}(f)/C_{xy}(f)\} \quad (4.32)$$

The above derivation shows how to obtain the transfer function with its needed gain and phase factor information, from spectral density functions calculated from input and output signals.

Coherence Function

The *cross-spectrum inequality* is defined as (Bendat and Piersol, 1993, 53):

$$|G_{xy}(f)|^2 \leq G_{xx}(f) G_{yy}(f) \quad (4.33)$$

Re-arranging eq. (4.33), the *coherence function* is defined as follows:

$$\gamma_{xy}^2(f) = \{|G_{xy}(f)|^2\} / G_{xx}(f) G_{yy}(f) \quad (4.34)$$

With:

$$0 \leq \gamma_{xy}^2(f) \leq 1 \quad (4.35)$$

From Bendat and Piersol 1993 (Bendat and Piersol 1993, 84):

"... when the coherence function is greater than zero but less than unity, one or more of the following four main conditions exist:

1. *Extraneous noise is present in the measurements.*
2. *Resolution bias errors are present in the spectral estimates.*
3. *The system relating $x(t)$ to $y(t)$ is not linear.*
4. *The output $y(t)$ is due to other inputs besides $x(t)$"*

At a natural frequency, linearity is expected and extraneous noise is expected to be minimized, therefore the coherence function should be very close to 1. This property of the coherence function comprises the other criteria for identifying natural

frequencies.

It is useful to summarize the main concepts developed to this point. With stationary and ergodic input and output signals representing a structural systems excitation and response, Fourier transformation of correlation functions can be used to obtain spectral density functions which will show maxima at potential natural frequencies of the system. The spectral density functions can in turn be used to calculate coherence functions and transfer functions. The coherence function and the gain and phase factor of the transfer function have properties which can be used to assist in determining which spectral density function maximas represent true natural frequencies. Now having developed the theoretical background it is now appropriate to detail the two ambient analysis techniques used in this thesis.

Relative Single Input-Single Output Systems

The first technique of ambient analysis used provides both natural frequencies and mode shapes. To understand how it does this, the theory presented so far must be extrapolated to MDOF systems, using only output signals.

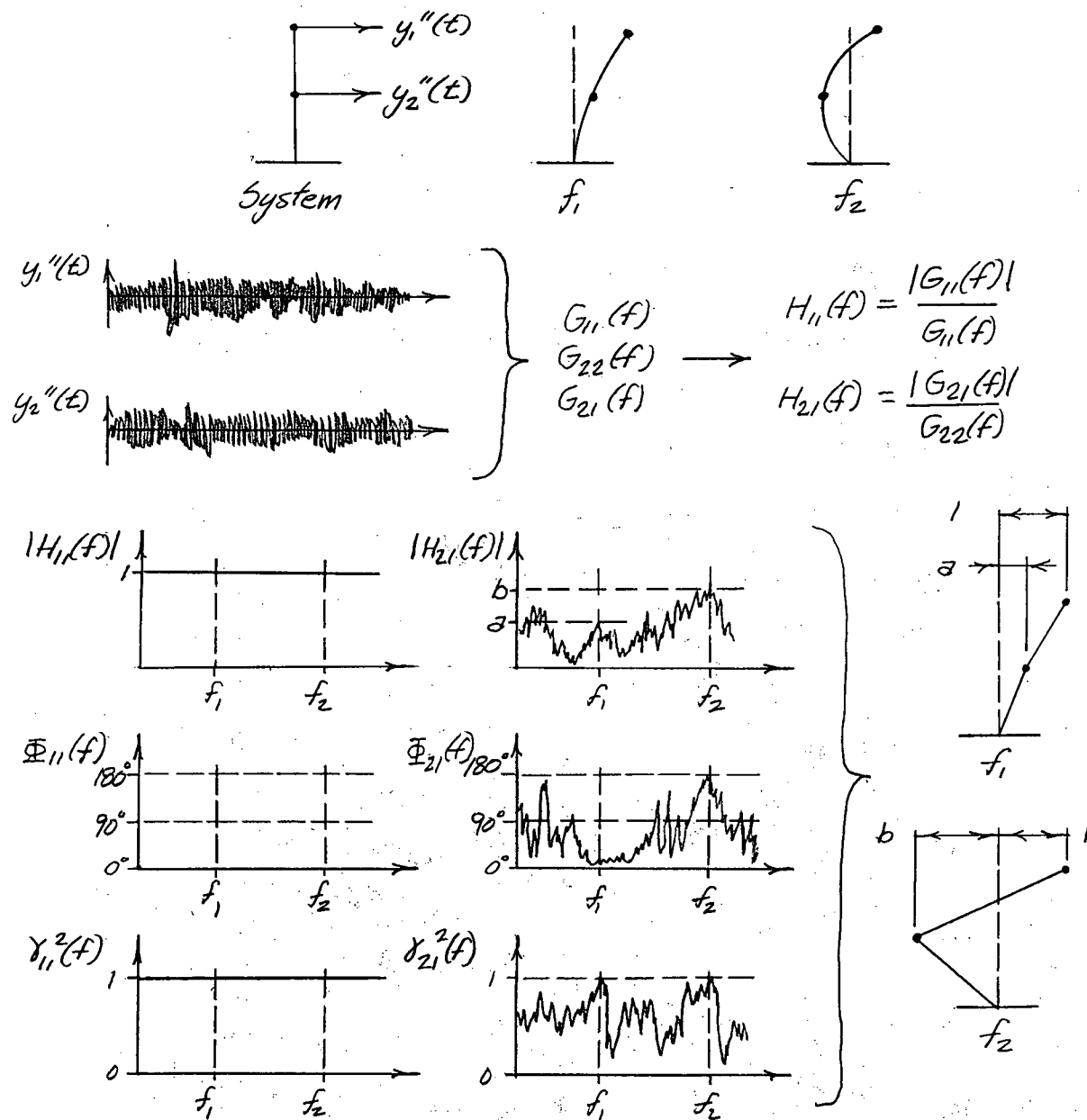
The key theoretical consideration concerns the phase at resonance of the MDOF system. From Felber (Felber 1993, 22):

"... If the structure is classically damped ... and, therefore, only has real valued modes, then at resonance the signals from [any] two degrees of freedom are either perfectly in phase or out of phase. ..."

Paraphrasing from Felber (Felber 1993, 14): classical damping is a term which applies to the solution of the differential equation of motion and means that the solution to the undamped equation (i.e., the modal analysis, representing free vibration of the undamped system) is identical to the solution of the damped equation and that it yields only real valued modes (non-complex). Ambient analysis in this thesis also assumes that the structure behaves with classical damping (as following discussion will indicate). Consideration of non-classical damping would entail a significant change to both the ambient analysis techniques used in this thesis and the numerical modelling technique. Literature review does not indicate any use of non-classical damping in the vibration testing and analysis of dams and therefore its use is concluded outside the scope of work in this thesis.

The preceeding discussion indicates that with a classically damped system, considering any two degrees of freedom, if one constructs a transfer function treating one signal as the input signal and the other signal as the output signal, the phase factor will be equal to 0 or 180 degrees at resonance. This forms the basis for the first technique. With an ambient test, one point is designated as the "reference" point, and treated as an input signal for construction of transfer functions with all other points.

This concept is illustrated in Figure 4.3 where a two degree of freedom system is depicted with typical gain and phase factor relationships which might be obtained from actual measurements. The plots are not drawn as smooth lines to indicate that the measurements would include error and be of a finite frequency resolution. To identify



$y_1''(t), y_2''(t)$ = Time Histories of Ambient Vibration Measurement
 $G_{11}(f), G_{22}(f), G_{21}(f)$ = One Sided Auto-spectrum
 $H_{11}(f), H_{21}(f)$ = Transfer Functions
 $|H_{11}(f)|, |H_{21}(f)|$ = Transfer Function Gains
 $\Phi_{11}(f), \Phi_{21}(f)$ = Phase Factors
 $\gamma_{11}^2(f), \gamma_{12}^2(f)$ = Coherence Functions
 f_1, f_2 = Natural Frequencies

Figure 4.3 Example of an Idealized Two Degree of Freedom System Modelled as a Relative Single Input-Single Output System for Ambient Vibration Analysis

the natural frequencies, one considers the gain and phase factor of the transfer functions and the coherence. Here, the gain is shown to exhibit maxima at the two natural frequencies, where the corresponding phase factor is appropriately very close to either 0 or 180 degrees and the corresponding coherence function is very close to 1.

To determine mode shapes, one considers the gain and phase factor information. Considering the two degrees of freedom in Figure 4.3, the ratio of responses defines the mode shape. Paraphrasing Felber (Felber 1993, 23-27): at a natural frequency, the response magnitude is equivalent to the gain of the transfer function. Therefore, the ratio of responses can be approximated by the ratio of the gains and to construct the mode shape, the ratio of gains is calculated for each point with respect to the reference point. This process is illustrated in Figure 4.3.

For the two degree of freedom system in Figure 4.3, there are two *single input-single output systems* represented. Each of these systems has an output "relative" to the reference point, therefore each is termed a *relative single input-single output system* and each produces a *relative transfer function* from which the gain and phase factors are calculated. This method of signal analysis is the basis of the Hybrid Bridge Evaluation System developed at UBC and further described in Section 4.3.

Single Input-Single Output with Output Noise System

The second technique is used to identify natural frequencies only, although a method to construct mode shapes is felt possible. For theoretical support, further derivation considering an SDOF subjected to foundation excitation, use of a different *displacement input-displacement output transfer function*, is required.

Theory is paraphrased from Bendat and Piersol (Bendat and Piersol 1986). Shown in Figure 4.4 is the conceptual SDOF system.

The SDOF in Figure 4.4 has the differential equation of motion:

$$kx + c\dot{x} = m\ddot{y} + c\dot{y} + ky \quad (4.36)$$

Again let the excitation, $x(t)$ = the unit impulse, $F\delta(t)$, then the response of the SDOF system, $y(t)$, is again equal to the unit impulse response function, $h(t)$.

The differential equation of motion becomes:

$$k\delta(t) + c\dot{\delta}(t) = m\ddot{h} + c\dot{h} + kh \quad (4.37)$$

Noting that:

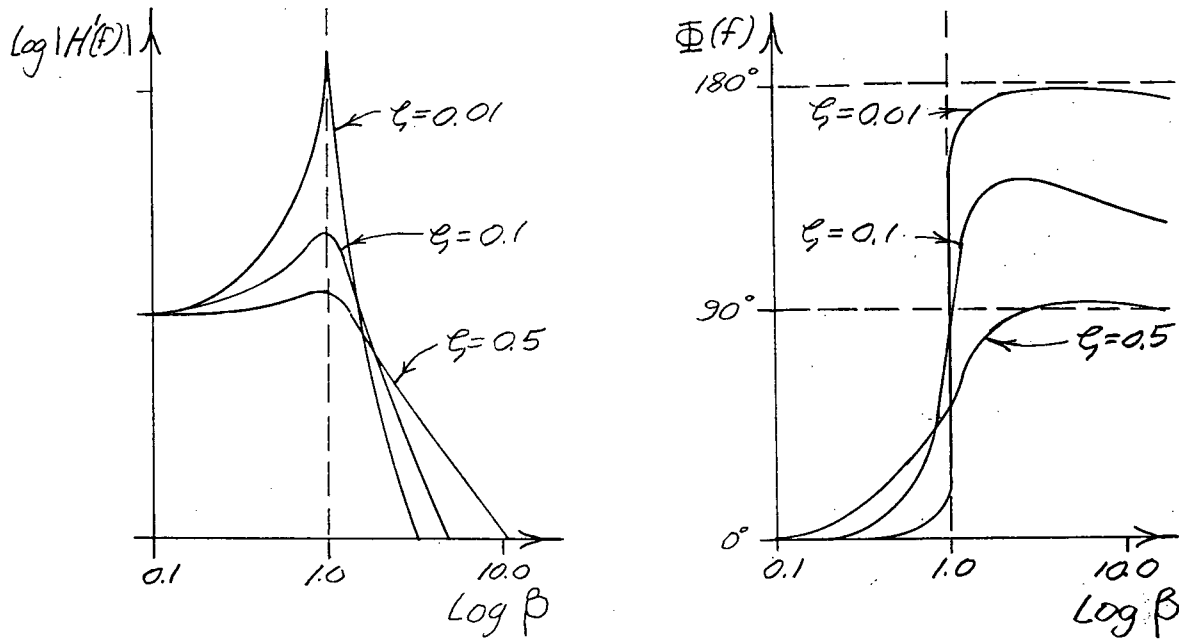
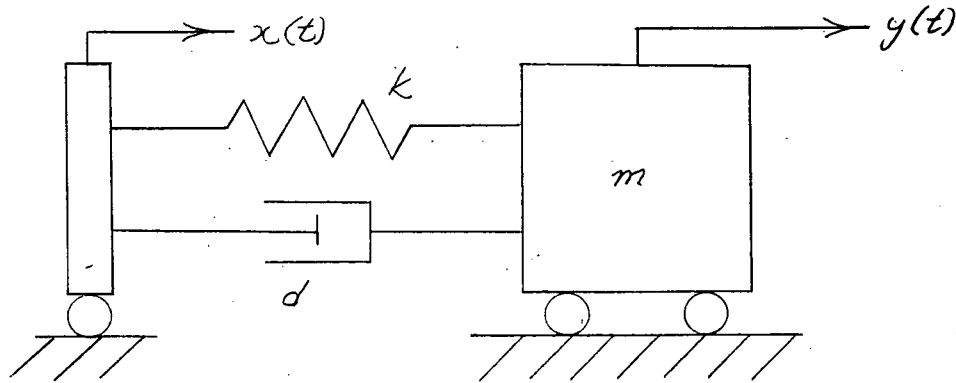
$$\delta(t) \Rightarrow j2\pi f \quad (4.38)$$

Taking the Fourier transformation of both sides of the differential equation of motion yields:

$$(k + j2\pi f c) = H'(f) \{ -(2\pi f)^2 m + j2\pi f c + k \} \quad (4.39)$$

Or:

$$H'(f) = (k + j2\pi f c) / \{ -(2\pi f)^2 m + j2\pi f c + k \} \quad (4.40)$$



m = Mass
 k = Stiffness
 d = Damping
 $x(t)$ = Displacement Input
 $y(t)$ = Displacement Output
 $|H'(f)|$ = Transfer Function Gain
 $\Phi(f)$ = Phase Factor
 ζ = Damping Ratio
 β = Ratio of Natural Frequency to Undamped Natural Frequency

Figure 4.4 Idealized Single Degree of Freedom System, Foundation Displacement Input

Note that the transfer function is notated as $H'(f)$ and not $H(f)$, to distinguish it from the force input-displacement output transfer function derived previously for the force excited SDOF system. The system gain, $|H'(f)|$, and the system phase, $\Phi(f)$, are also depicted in Figure 4.4. The equations for these are:

$$|H'(f)| = \sqrt{\{1 + (2\zeta\beta)^2\} / \{(1 - \beta^2)^2 + (2\zeta\beta)^2\}} \quad (4.41)$$

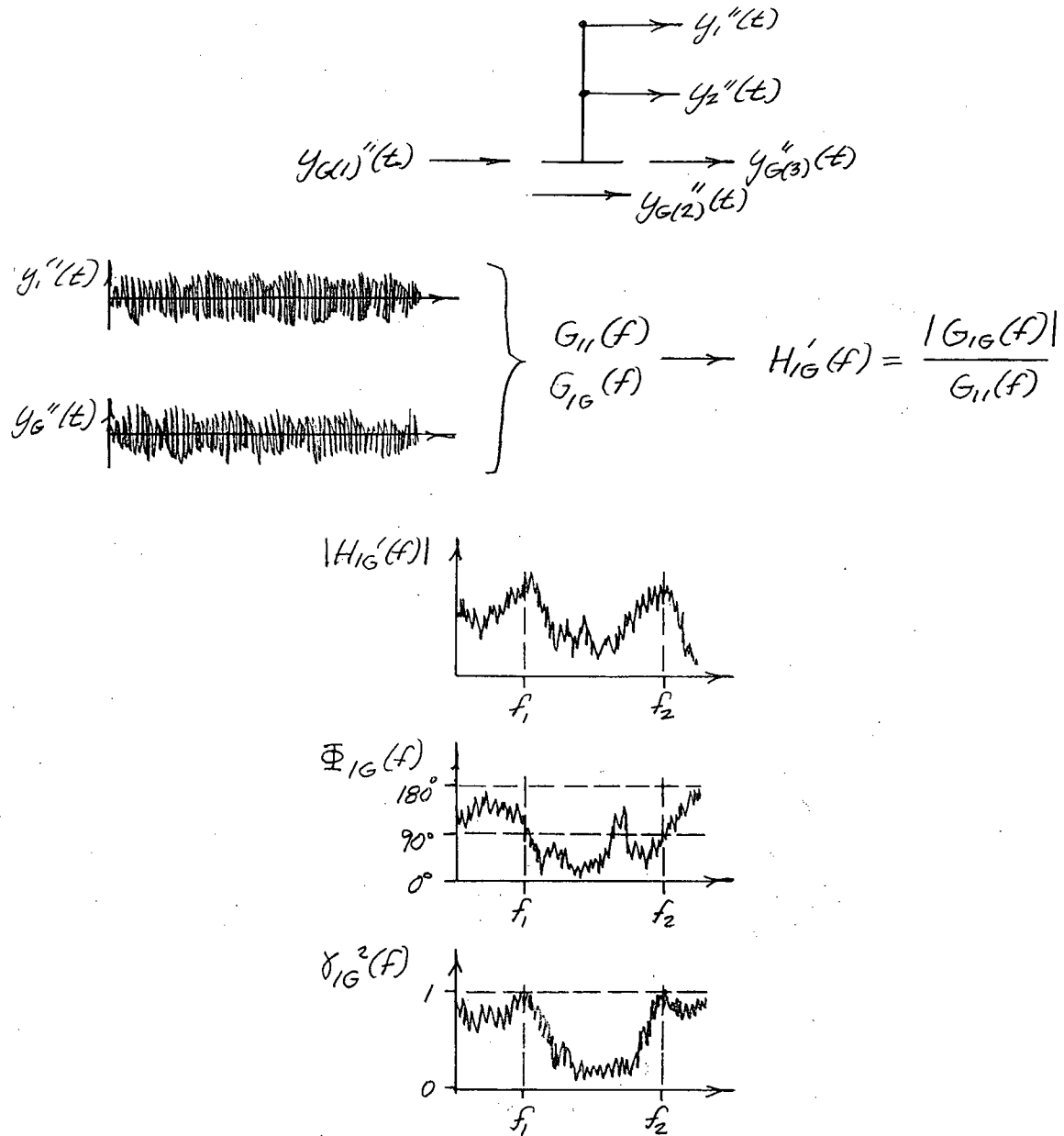
$$\Phi(f) = \tan^{-1}\{2\zeta\beta^3 / (1 - \beta^2 + 4\zeta^2\beta^2)\} \quad (4.42)$$

Of note, usually a transfer function derived with a foundation input and structural output (or vice versa) is termed a *transmissibility function*. In this thesis the term "transmissibility function" will not be used.

The important feature to note in Figure 4.4 is that at the natural frequency of the SDOF system, or at $\beta = 1$, the phase, $\Phi(f)$, is nearly 90 degrees for very low values of damping, ζ .

Figure 4.5 shows the identical two degree of freedom system shown previously in Figure 4.3, but with measurements made of the foundation displacement.

As shown in Figure 4.5, there are multiple measurements made of the foundation displacement. Any of these can be used as the input signal to construct a single input-single output system with either of the two output measurements. Transfer functions calculated will have phase factors exhibiting crossings through 90 degrees at the natural frequencies for very low damping. The difference in the phase factor value at a natural frequency is the key theoretical difference between the two methods used.



$y_1''(t)$ = Time History Of Ambient Vibration Measurement
 $y_{G(1)}''(t), y_{G(2)}''(t), y_{G(3)}''(t), y_G''(t)$ = Time Histories of Ambient Vibration Measurement
 $H_{IG}'(f)$ = Transfer Function
 $|H_{IG}'(f)|$ = Transfer Function Gain
 $\Phi_{IG}(f)$ = Phase Factor
 $\gamma_{IG}^2(f)$ = Coherence Function
 f_1, f_2 = Natural Frequencies

Figure 4.5 Example of Idealized Two Degree of Freedom System Modelled as a Single Input-Single Output with Noise System for Ambient Vibration Analysis

A concrete gravity dam system, i.e., the dam-foundation-reservoir system, is a multiple input-single output system as there are many ambient excitations acting coincident.

The second method will be shown to work because:

- Damping for dams is sufficiently low. Vibrations testing shows damping for natural frequencies to be generally less than 4 % (Hall 1988, 115)
- Excitation originating in the foundation is significant, so significant that consideration of coherence will show that the other excitations can be considered output noise.

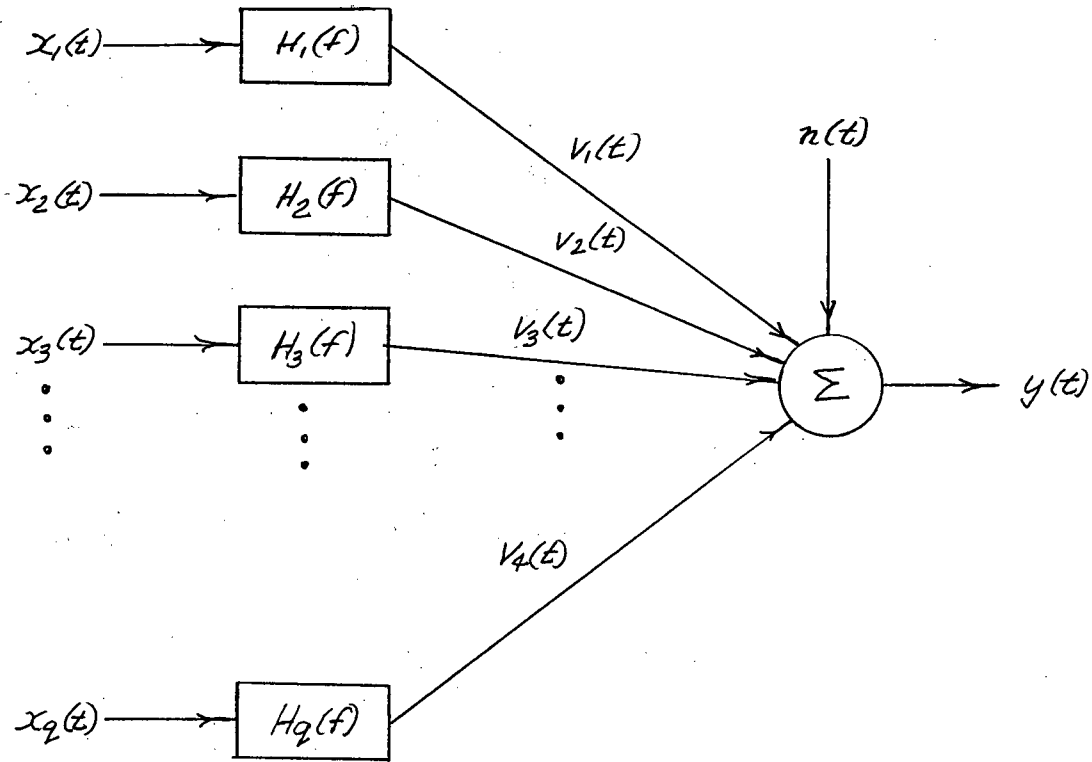
Justification for the second point above is derived as follows, considering theory from Bendat and Piersol (Bendat and Piersol 1975, 211-214).

Shown in Figure 4.6 (Bendat and Piersol 1993, 205), is a multiple input-single output system. Assuming that each of the inputs are mutually uncorrelated, a reasonable assumption in the case of concrete gravity dams where the wind, foundation vibration, wave action from the reservoir and deck traffic are such, then the multiple coherence function, $\gamma_{y:x(\Sigma q)}^2(f)$, is equal to the summation of coherence functions between each input and the output:

$$\gamma_{y:x(\Sigma q)}^2(f) = \gamma_{y:x(1)}^2(f) + \gamma_{y:x(2)}^2(f) + \dots + \gamma_{y:x(q)}^2(f) \quad (4.43)$$

And:

$$0 \leq \gamma_{y:x(\Sigma q)}^2(f) \leq 1 \quad (4.44)$$



$x_1(t), x_2(t) \dots x_q(t)$ = Input Signals
 $v_1(t), v_2(t) \dots v_q(t)$ = Output Signals Without Noise
 $H_1(t), H_2(t) \dots H_q(t)$ = Transfer Functions
 $y(t)$ = Actual Output Signal
 $n(t)$ = Noise Signal

Figure 4.6 Idealized Multiple Input-Single Output System (Uncorrelated Inputs)

If one is capturing the input which represents the majority of excitation, $\gamma_{y:x(*)}^2(f)$,

then:

$$\gamma_{y:x(\Sigma q)}^2(f) \approx \gamma_{y:x(*)}^2(f) \quad (4.45)$$

And:

$$0 \leq \gamma_{y:x(*)}^2(f) \leq 1 \quad (4.46)$$

If at a probable natural frequency, $\gamma_{y,x(*)}^2(f)$ is shown to be close to 1, then, the majority of excitation is being provided by that input and all other inputs are insignificant and can be considered to represent output noise. The estimate of the natural frequency is shown to be reliable.

The second technique only records the single most significant input. Therefore, it is a *single input-single output system with output noise system*

4.3 Hybrid Bridge Evaluation System (HBES)

All ambient tests for this thesis utilized the Hybrid Bridge Evaluation System (HBES) for analysis of the measured data. HBES was developed mostly by Dr. Andreas Felber for his Ph.D. thesis for UBC (Felber 1993). HBES, as the name implies, was developed originally for the evaluation of bridge dynamic properties from ambient data. Conceptually, HBES is a system utilizing several computer programs, in which measured ambient time history data from numerous degrees of freedom is transformed to the frequency domain using fast Fourier transform algorithms, where it is then organized and reduced into manageable form. *HBES then allows for testing the frequency domain data with the principles detailed in Section 4.2 for relative single input-single output systems in order to determine natural frequencies and mode shapes.*

HBES as described by Felber has three main steps, however, only the first two were utilized for this thesis. These first two steps are named herein as:

- *STEP 1: Average Normalized Power Spectral Densities (ANPSDs)*
- STEP 2: ULTRA and VISUAL

Step 1 can be completed with computer program P2, available from Experimental Dynamic Investigations Ltd., in Vancouver, B.C. Step 2 uses computer programs ULTRA and VISUAL. ULTRA and VISUAL were developed at UBC as part of the Felber Ph.D. thesis (Felber 1993).

The third step of HBES is the interactive construction of a finite element model of the bridge tested, using the commercially available computer program such as SAP90®.

The following details the two steps of HBES defined and utilized:

STEP 1: Average Normalized Power Spectral Densities (ANPSDs)

The first step is identification of *potential* natural frequencies by calculation and evaluation of Average Normalized Power Spectral Density (ANPSD) functions.

ANPSDs are calculated using the P2 computer program. ANPSDs are a calculated average of power spectral density (PSD) functions

ANPSDs are calculated as follows (Felber 1993, 53):

$$ANPSD(f_k) = (1/l) \sum_{i=1}^{i=l} NPSD_i(f_k) \quad (4.47)$$

$$NPSD_i(f_k) = PSD(f_k) / \sum_{k=0}^{k=n} PSD(f_k) \quad (4.48)$$

Where:

$NPSD$ = normalized power spectral density

PSD = power spectral density

f_k = k th discrete frequency

n = number of discrete frequencies

l = number of PSDs

As discussed in Section 4.2, the peaks of PSDs indicate natural frequencies or other phenomena. Similarly, the composite spectral density ANPSD peaks also indicate natural frequencies or other phenomena. The ANPSD is intended to be a better indicator than individual PSDs normally used for this purpose because, according to Felber (Felber 1993, 53):

"...You can not assume that all of the structure's natural frequencies are represented in an averaged PSD of a single measurement location because this location may coincide with a node of a vibration node. You need to consider the average PSDs of all measured locations to ensure all of the natural frequencies of a structure are identified. ..."

The ANPSD provides for a quick appraisal of potential natural frequencies from the aggregate PSD information available. Weakly indicated natural frequencies may not necessarily have distinctive ANPSD peaks as a result of the averaging process and so review of individual PSDs remains a valid complementary analysis technique.

STEP 2: ULTRA and VISUAL

After ANPSDs are calculated and potential natural frequencies are identified, the identification of *probable* natural frequencies is performed. Conceptually, HBES completes this by first assembling the set of gains from the *relative transfer functions* (remember that these are calculated from the input-output cross-spectral relation corresponding to the relative single input-single output system representing the structure). The set of gains is herein termed the *operating deflected shape*. The operating deflected shape is calculated at each frequency increment over the frequency range of interest. Next, this set of operating deflected shapes is subject to user controlled testing with coherence and phase factor principles described in Section 4.2. The coherence is calculated from the cross-spectral relation and the phase factors are obtained from the relative transfer functions. Finally, the set of operating deflected shapes are animated. The frequency or frequency ranges which correspond to potential natural frequencies or frequency ranges identified with the ANPSDs, and at which the tested operating deflected shapes produce the most sensible animated shapes, are then considered to correspond to probable natural frequency or frequency ranges.

To test an operating deflected shape at a potential natural frequency, the user selects both a phase and coherence window. The window allows only those points which are within the specified phase or coherence tolerance to remain animated. Next, after specifying the windows, the user can quickly surf through the frequency range of interest and frequency ranges over which the majority of measured points remain

animated are easily found. If these match potential natural frequencies identified with the ANPSDs, most likely a probable natural frequency range has been found. The great achievement of HBES is that all of this can be done fairly quickly.

ULTRA is used to calculate various frequency domain functions, such as spectral density functions, transfer functions, phase factor and coherence functions. ULTRA also allows for calculation of windowed *potential modal ratio* functions (PMR), which represents the set of transfer function gains for a given measured point, with gains set to zero which do not meet either of the phase factor or coherence windows (contained in the points *.MOD* file). For instance, one could select windows of phase factor equal to 10 degrees and coherence equal to 0.9. Only gains corresponding to measured points within the set which have a phase between 0-10 degrees or 170-180 degrees and a coherence of at least 0.9 will be left by ULTRA available to be animated, whereas other gains will be set to zero and will not animate. The lack of animation for critical points at a potential natural frequency will result in a non-sensible operating deflected shape and the conclusion that a probable natural frequency is not represented. The animation is completed with the program VISUAL.

A key consideration with ambient techniques is that signals obtained at natural frequencies will be contaminated and not yield phases of exactly 0 or 180 degrees or coherence of near 1. This allows for the possible acceptance of mode frequencies/shapes with relaxed phase and coherence factors.

Analysis with HBES was found inconclusive in some instances. Therefore other

complementary analyses to "unbundle" the HBES results and to provide a second technique of ambient vibration analysis were used.

4.4 Complementary Analyses

Complementary analyses are intended to provide additional detailed research which HBES does not strictly do. Complementary analyses devised are:

- *Coincident Time Histories*
- *Detailed Phase Change*
- *Power Spectral Densities (PSDs), Cross Spectral Densities (XSDs), Phase and Coherence*
- *Transfer Function (second ambient analysis technique)*

Coincident Time Histories

These analyses are unique in that they were intended to address specifically the connectivity details of the gravity blocks in the numerical model of Ruskin Dam.

To complete this analysis, time histories were obtained on gravity blocks, immediately adjacent to vertical construction joints. The time histories were then hard copied and reviewed for their similarity. Time histories showing identical plots would suggest that the gravity blocks were moving monolithically. The coherence and phase functions of the transfer functions calculated between coincident signals were also calculated and hard copies reviewed to provide further evidence as to the behaviour of the gravity blocks.

Detailed Phase Change

Using VISUAL with .MOD files calculated from ULTRA with open phase factor and coherence windows allows for insight into the relationship between operating deflected shape and frequency. If modes are well spaced in the frequency domain and noise in the signal is not too high, interference should be at a minimum and frequency ranges where the majority of nodes have a consistent phase factor should coincide with a frequency range containing a probable natural frequency. However, it was found that when scanning a large VISUAL model, such as that constructed for Ruskin Dam, it was difficult to discern over what ranges the phase factor was consistent for all nodes. It was felt that detailed scrutiny of a hard copy of the changing phase factor data would be useful in reviewing the HBES results.

The error in the phase factor calculation is dependent on the coherence. The error is shown in Table 5.2 in Section 5.2. Coherence needs to be considered when reviewing

detailed phase change data. Where phase instability exists, the coherence should be very low.

To complete this, an *open windowed* analysis with ULTRA is performed, i.e., the phase factor window is 0-90 degrees and the coherence window is 0-1 (thereby letting all points participate).

To complete the work, a select number of nodes was chosen, intended to define the operating deflected shapes. A hard copy of the calculations performed by ULTRA was then produced and frequency ranges of stability identified. For a frequency range to be considered, stability had to exist in both of the vertical and upstream-downstream directions. These ranges would then be compared to the HBES results for discrepancies.

Power Spectral Densities (PSDs), Cross Spectral Densities (XSDs), Phase Factor and Coherence

ULTRA was used to calculate power spectral density functions (PSDs), cross-spectral density functions (XSDs) and the phase factor and coherence functions. These functions were studied to:

- *"Unbundle" the HBES work*

- *Study the bedrock signals*

Essentially then, this analysis involved review of hard copies of the PSDs, XSDs, phase factor and coherence functions.

Transfer Function

This analysis was devised to determine whether a single input-single output with output noise system could be used to represent the dam being excited by the ambient foundation vibrations. As discussed in Sections 4.1 and 4.2, if this was so, an alternative method for determining the natural frequencies would be available. The key theoretical consideration is that the phase factor of the transfer functions calculated from such a system is not near 0 or 180 degrees at a natural frequency, as it is with the relative transfer functions calculated for points on the dam using HBES. Instead, it is near 90 degrees. Of importance, the coherence needs to indicate a corresponding high value to indicate that the majority of excitation is due to the foundation vibrations and has been successfully captured. Other sources of excitation would be treated as output noise and act to lower the coherence.

CHAPTER 5

SIGNAL PROCESSING and AMBIENT VIBRATION TESTING METHODOLOGY

The theoretical basis for ambient vibration analysis in this thesis was described in Chapter 4. In Chapter 5 is described signal sampling/processing, including significant concerns and errors resulting from conversion of the time domain data to the frequency domain using the discrete Fourier transform. Also described is how HBES is operated during ambient testing and signal processing and the resulting main considerations for test design.

5.1 Sampling Time Domain Records

General

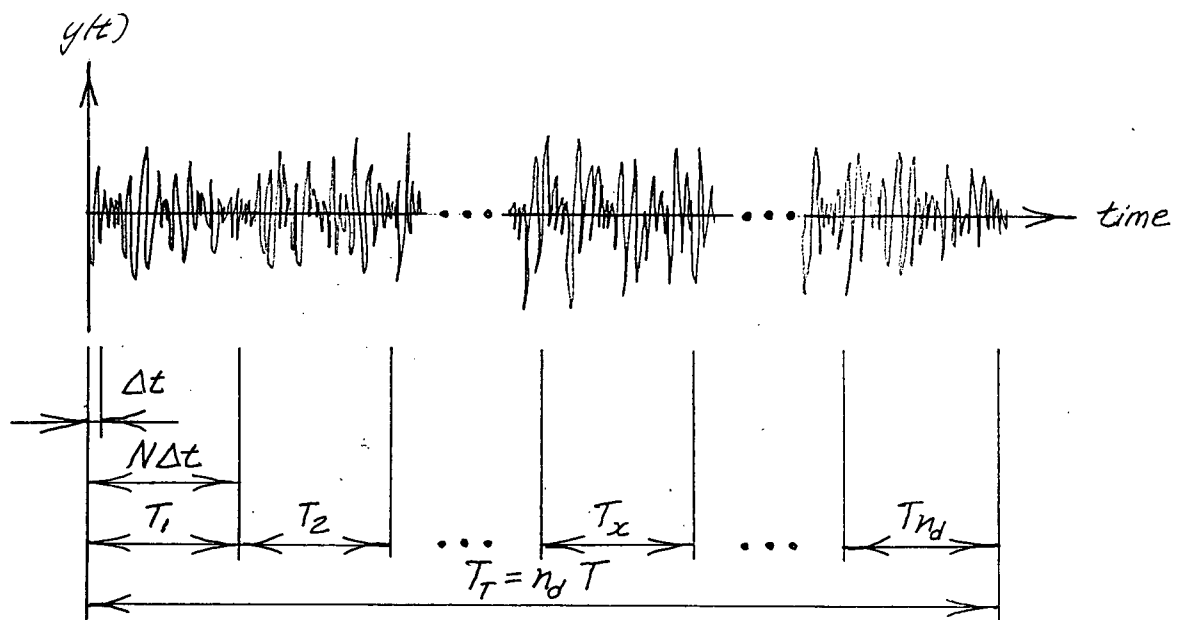
Shown in Figure 5.1 is a representation of a signal record in the time domain being measured (sampled) with the record divided into a number of segments.

If:

Δt = sampling interval (seconds)

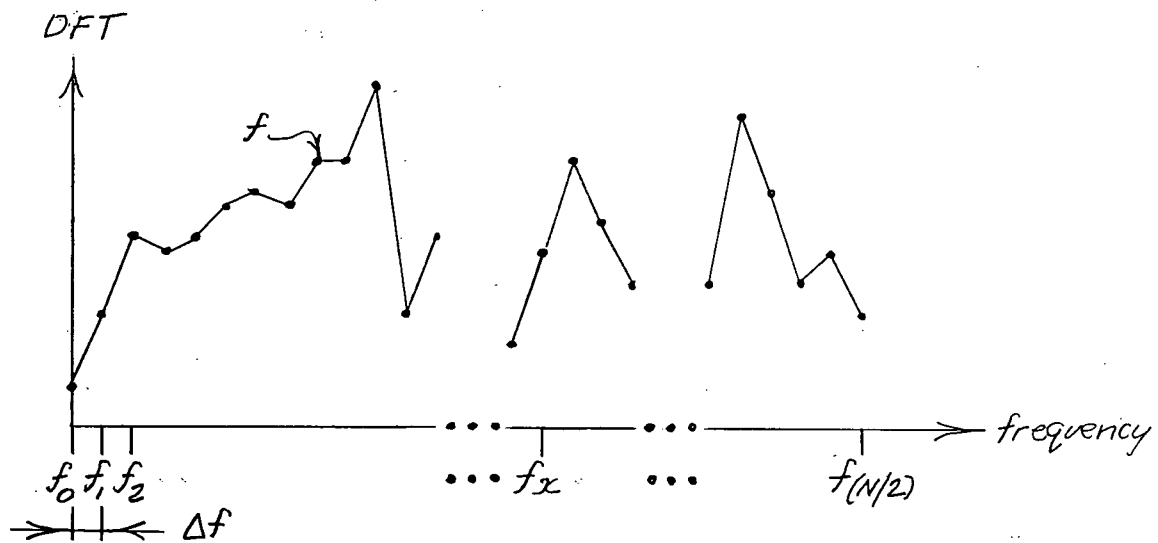
Therefore:

$1/\Delta t$ = the sampling frequency (Hz)



$y(t)$ = Time Domain Signal
 Δt = Sampling Interval
 T = Segment Length
 N = Number of Points Sampled Per Segment

T_T = Record Length
 T_x = Segment Length "x"
 n_d = Number of Segments



DFT = Discrete Fourier Transform of $y(t)$
 f = Frequency Point
 f_x = Frequency Point "x"
 Δf = Frequency Resolution

Figure 5.1 Discrete Fourier Transform of a Time Domain Signal, Using Fast Fourier Transform Algorithm

Also:

T = segment length (seconds)

N = number of points sampled per segment

Then:

$$T = N\Delta f \quad (5.1)$$

If:

n_d = number of segments

Then the total record length, T_t , is:

$$T_t = n_d T \quad (5.2)$$

As discussed in Chapter 4, the analysis of ambient time domain signals in this thesis uses the fast Fourier transform (FFT) algorithm. Also shown in Figure 5.1 is a discrete Fourier transform (DFT) obtained from the FFT, where:

f_x = frequency point "x"

Δf = frequency interval or frequency resolution (Hz)

A significant property of the FFT is that the total number of frequency points which are defined by it is equal to $N/2$. The corresponding frequency, equal to the highest frequency point, or $f_{(N/2)}$, is the highest frequency which can be resolved from the FFT and is termed the *Nyquist Frequency*, f_c , which is found, in Hz, by:

$$f_c = (N/2)\Delta f \quad (5.3)$$

The Nyquist frequency can be shown to be numerically equal to one half the sampling

frequency, as follows. For a given segment, x , the frequency resolution, Δf , is given by:

$$\Delta f = 1/T \quad (5.4)$$

Substituting eqs. (5.2) and (5.4) into eq (5.3) yields:

$$f_c = 1/(2\Delta t) \quad (5.5)$$

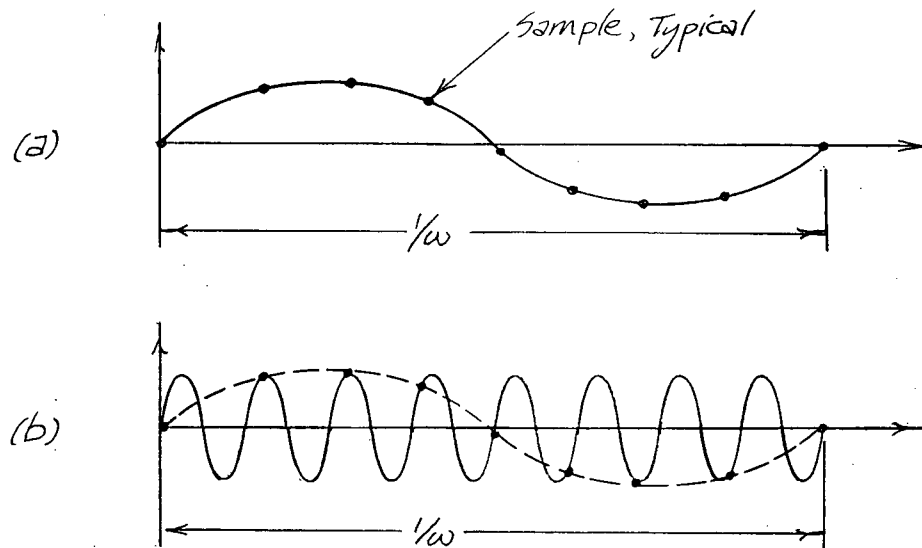
The above relationships, involving f_c , N , Δf and Δt will be used when setting data acquisition parameters.

Aliasing

A major source of error in DFTs is the appearance of *aliased* frequencies. A simple example of aliasing is shown in Figure 5.2 (Ewins 1984, 118), showing two different signals, being sampled at the same rate. The resulting DFT would indicate a spike at the frequency of the signal shown in Figure 5.2 (a) , although the original signals contain two very distinct frequencies (one higher and aliased with the lower).

To reduce the effect of aliasing, one uses a *low pass filter* during sampling, to artificially cut out frequencies higher than the highest frequency of interest, which may alias themselves with lower frequencies due to the sampling and DFT calculation process.

The selection of a low pass filter must be made prior to sampling data and becomes one of the data acquisition parameters.

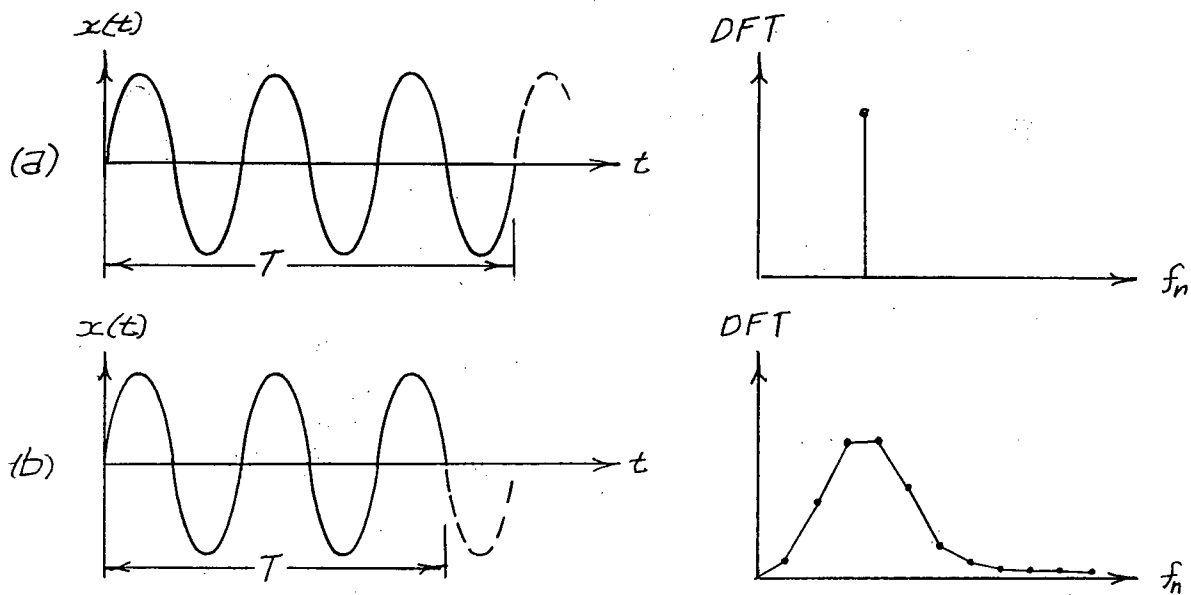


- Case (a): Periodic Time Domain Signal Of Frequency, ω , Sampled At Frequency Higher Than ω
- Case (b): Periodic Time Domain Signal Of Frequency, ω , Sampled At Frequency Slightly Higher Than ω

Figure 5.2 Example of Aliasing

Leakage

Leakage is a problem which results from the fact that only a finite sample of a system is being taken. Shown in Figure 5.3 (Ewins 1984, 120) is an example of two DFTs calculated from different sample lengths of the same signal. In the second case, due to the non-periodicity of the sample length recorded, the DFT is incorrect due to *leakage* of energy to adjacent frequencies.



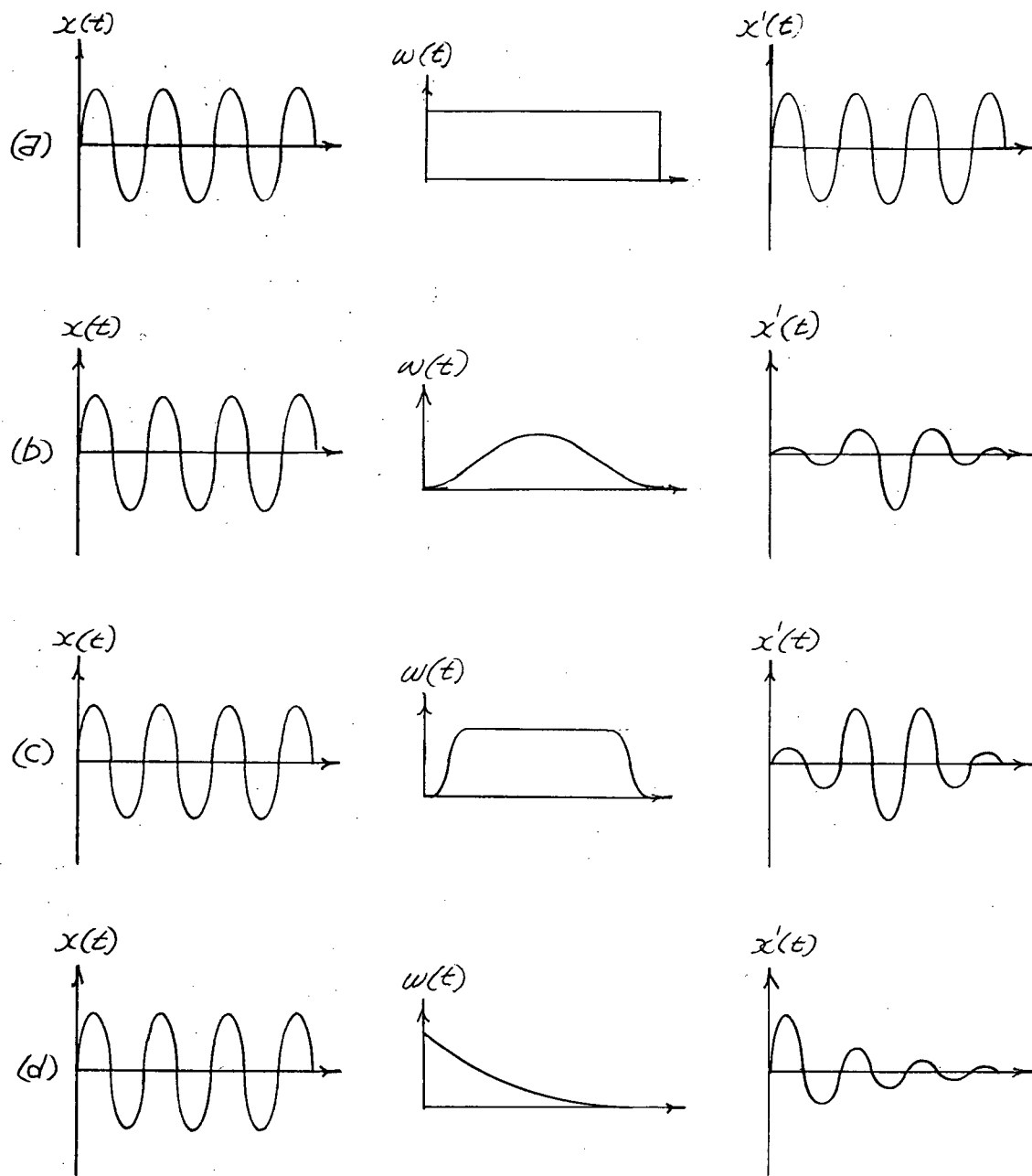
- Case (a): Periodic Signal With Periodic Sampling
 Case (b): Periodic Signal With Non-periodic Sampling

$x(t)$ = Continuous Time Domain Signal
 DFT = Discrete Fourier Transform of $x(t)$
 T = Segment Length
 f_n = Discretized Frequencies
 t = Time

Figure 5.3 Example of Signal Leakage

To enhance accuracy of the calculated DFTs, the sampled record can be subjected to the *windowing* process, described from Ewins as follows (Ewins 1984, 121):

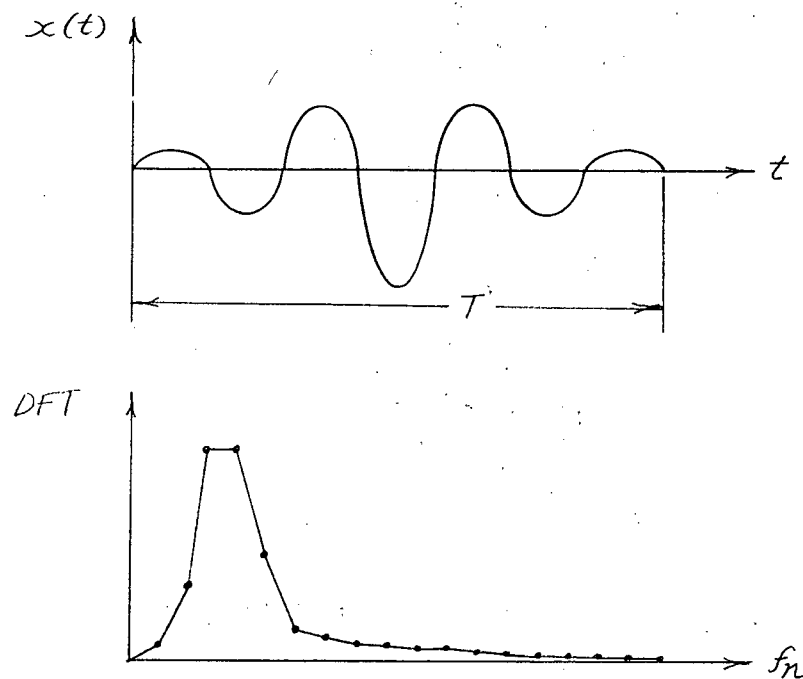
"... Windowing involves the imposition of a prescribed profile on the time signal prior to performing the Fourier Transform and the profiles or 'windows' are generally depicted as a time function, $\omega(t)$, as shown in [Figure 5.4]. The analyzed signal is $x'(t) = x(t)\omega(t)$. The result of using a Hanning or Cosine Taper window is seen in the third column of [Figure 5.4] and this in turn produces the improved spectrum shown in [Figure 5.5]. The Hanning (b) or Cosine Taper (c) windows are typically used for continuous signals, such as produced by steady periodic or random vibration, while the Exponential window (d) is used for transient vibration applications where much of the important information is concentrated in the initial part of the time record ..."



- Case (a): Rectangular Window
 Case (b): Hanning Window
 Case (c): Cosine Taper Window
 Case (d): Exponential Window

$x(t)$ = Time Domain Signal
 $w(t)$ = Window Function in Time Domain
 $x'(t)$ = Windowed Time Domain Signal ($= x(t) w(t)$)

Figure 5.4 The Effect of Windowing Signals



$x(t)$ = Continuous Time Domain Signal
 T = Segment Length
 t = Time
 DFT = Discrete Fourier Transform of $x(t)$
 f_n = Discretized Frequencies

Figure 5.5 The Effect of the Hanning Window

Windowing then is a process which can be completed "after-the-fact", during signal processing of the recorded signals in the time domain but prior to calculation of DFTs. ULTRA subroutines allow for the imposition of such windows on the recorded signals.

5.2 Error Calculation

Error calculation is not a subject which is treated comprehensively in this thesis. It is

however, felt to be of importance to mention error and some of the basic formulas.

There are two types of measurement error: *random* and *bias* (Bendat and Piersol 1993, 38):

"... The errors that occur in the analysis of random data may be divided into two classes. The first is a haphazard scatter in the results from one analysis to the next of different samples of the same random data, and is called the random error. Random errors are a direct result of the fact that averaging operations must be performed over a finite number N of sample records or over a single sample record of finite length T. It follows that all analyses will involve a random error. The second type of error is a systematic error that will appear with the same magnitude and in the same direction from one analysis to the next, and is called the bias error. ..."

Further (Bendat and Piersol 1993, 114 and 115):

"... Random errors in estimates of frequency response functions are due to the following sources:

- 1. Measurement noise in the transducers and instrumentation, and computational noise in the digital calculations.*
- 2. Other unmeasured inputs that contribute to the output and are uncorrelated with the measured input....*

... Bias errors can arise in estimates of frequency response functions from four primary sources as follow:

- 1. Extraneous noise in the input measurement that does not pass through the system.*
- 2. Resolution bias errors in the spectral density estimates.*
- 3. Nonlinear system parameters.*
- 2. Other unmeasured inputs that contribute to the output and are uncorrelated with the measured input...."*

The resolution bias errors, ϵ_{br} , for $G_{xx}(f)$ and $|G_{xy}(f)|$ are calculated from:

$$\epsilon_{br} = (-1/3)(\Delta f / B_r)^2 \quad (5.6)$$

Where:

B_r = half-power bandwidth of spectral peak (Hz)

Well defined spectral peaks are required to determine the half-power point bandwidth. Typically, ambient data in this thesis did not provide sharply defined spectral peaks. Other bias errors are not addressed in any detail in this thesis.

For single input-single output problems, which can be either relative single input-single output systems as in HBES or single input-single output with output noise as in the complementary analyses, the formulas for the random error of the *estimates* of auto-spectrum, cross-spectrum, coherence and the gain of the transfer function are shown in Table 5.1 (Bendat and Piersol 1993, 303):

Table 5.1
Single Input-Single Output Problem Random Errors, ε_r

ESTIMATED QUANTITY	RANDOM ERROR, ε_r
$G_{xx}(f), G_{yy}(f)$	$1/\sqrt{n_d}$
$ G_{xy}(f) $	$1/(\gamma_{xy}(f)\sqrt{n_d})$
$\gamma_{xy}^2(f)$	$\sqrt{2(1-\gamma_{xy}^2(f))}/(\gamma_{xy}(f)\sqrt{n_d})$
$ H(f) $	$\sqrt{(1-\gamma_{xy}^2(f))}/(\gamma_{xy}(f)\sqrt{2n_d})$

Bendat and Piersol also describe that the standard deviation in the phase factor estimate, $\sigma\Phi_{xy}(f)$, is approximately equal to the random error of the gain of the

transfer function, $\epsilon_n |H(f)|$, if the latter is sufficiently small (Bendat and Piersol 1993, 309-310). Or:

$$\sigma\Phi_{xy}(f) \approx \epsilon_n |H(f)| \quad (5.7)$$

Or:

$$\sigma\Phi_{xy}(f) \approx \sqrt{\{1 - \gamma_{xy}^2(f)\} / (\gamma_{xy}^2(f) \sqrt{2n_d})} \quad (5.8)$$

Shown in Table 5.2 is a summary of $\sigma\Phi_{xy}(f)$ for various coherence values.

Of importance, in Table 5.2 note that all of these errors are dependent on the number of segments, n_d , and the coherence, $\gamma_{xy}^2(f)$. The dependence on n_d reflects that these formulas are derived from consideration of statistical averaging principles. Obviously then, increasing the number of segments and/or attaining high coherence between the signals measured will act to lower the random error in the estimate of each of these functions and the standard deviation of the phase factor. The coherence between recorded signals is dependent of the system being measured, the quality of the equipment being used and the use of proper recording procedures. As a result, once signals are recorded, the coherence cannot be altered. However, ULTRA has the ability to re-sample recorded signals to produce a higher number of segments which can result in an increase in the accuracy of each of the estimated functions. However, as the frequency resolution, Δf , is inversely proportional to the segment length, T , by subdividing T_T into shorter segments T , will result in a reduction in frequency resolution in the data. As a general rule, analysis in this thesis used the data as recorded to maximize frequency resolution.

Table 5.2
Standard Deviation of Phase Factor, $\sigma\Phi_{xy}(f)$ (degrees)

COHERENCE, $\gamma_{xy}^2(f)$	NUMBER OF SEGMENTS, n_d			
	8	16	32	64
0.5	14.32	10.13	7.16	5.06
0.55	12.96	9.16	6.48	4.58
0.6	11.70	8.27	5.85	4.14
0.65	10.51	7.43	5.26	3.72
0.7	9.38	6.63	4.69	3.32
0.75	8.27	5.85	4.14	2.92
0.8	7.16	5.06	3.58	2.53
0.85	6.02	4.25	3.01	2.13
0.9	4.77	3.38	2.39	1.69

Error analysis of frequency domain functions calculated from the recorded signals in this thesis was restricted to random checks. Any future review of the work contained in this thesis would be enhanced considerably by a thorough treatment of the possible errors in the analysis.

5.3 HBES Data Acquisition

The program used to control data acquisition equipment is called AVDA. AVDA is an upgrade of a prior program entitled AVTEST, which was developed as part of HBES by Dr. Andreas Felber for his Ph.D. thesis for UBC (Felber 1993).

The data acquisition equipment used is described in Appendix A. The sensors, cabling, data acquisition and storage equipment and spectral analyzer are all available at UBC. Further details of this equipment is found in Felber (Felber 1993).

AVDA operates on the data storage computer. To run AVDA, the user first selects a number of data acquisition parameters. Felber and Schuster theses (Felber 1993, Schuster 1994) contain details on these selections, however, they will be briefly described herein. At the time of the field testing for this thesis, to run AVDA, at the command line the user specified:

- Nyquist Frequency, f_c
- Number Of Points Per Channel (an index number)
- Number Of Channels Being Recorded
- Global Gain
- Sensor Calibration Option
- Filename
- Site Identifier

- Setup Description

The *Nyquist Frequency*, f_c has been described. The *Number Of Points Per Channel* is the number of sampled points per segment, N . *Number Of Channels* had to be selected between 1-8.

The *Global Gain* is an important parameter which if selected incorrectly will result in clipping of the recorded signals (if selected too high) or in poor resolution (if selected too low). The threshold of recorded signals is equal to the product of the sensor output voltage and the global gain. This threshold cannot exceed 10 volts. The sensors being utilized have a sensitivity of 5 volts/g. Therefore, a global gain of 2 can be specified although 5 was commonly used to reflect the low strength in the ambient signals being recorded (a further manual "amplification" of each individual signal may be performed, described below).

The *Sensor Calibration* is an option for AVDA to perform a routine check to ensure that the sensors are connected and are functioning. The *Filename* refers to the 8 character name given to the recorded files to be storage, each with a "bbb" extension. *Site Identifier* and *Setup Description* are used as identifiers which will be stored with the data stored.

The signal conditioning equipment allows for manual setting of signal amplification, low pass filter and high pass filter, for each of the eight channels being recorded. These must be recorded separately by the user as they are not included in the stored

data files. The signal amplification acts similar to the global gain, except that it may be applied to individual channels. The amplification can be set between 1 and 2000. To confirm whether the gain/amplification level is correct, AVDA allows for real time display of signals, with amplitude in defined as the signal threshold of 10. This allows for field modification of the signal amplification prior to actually recording a signal. Low pass filters could be set at 2.5, 5.0, 12.5, 25.0 or 50.0 Hz. The high pass filters could be set at 0.1 or 5.0 Hz. Low pass filters are used to prevent aliasing as previously discussed. High pass filters are used to eliminate amplifier drifting effects (see Felber 1993).

5.4 Test Design Considerations

Test design is influenced by the limitations of the UBC equipment and data acquisition software. For instance, the number of channels which could be recorded during a test is 8. If more than 8 measurements are desired, they had to be completed in a sequence of tests. To construct mode shapes with HBES requires selection of at least one reference location. The reference location must remain stationary throughout the test. Usually, more than one reference location is chosen. Therefore, the number of measurements available for each test is 8 minus the number of references.

With respect to the selection of reference sensor locations. For a given mode shape, if the reference sensor is located at an anti-node (where no motion is occurring), there is danger of not identifying the mode shape as the set of relative transfer functions

needed to construct the mode shapes (i.e., the gains of these functions) will not be well defined with a poor input signal at the associated natural frequency.

Of prime importance for planning is the time required to complete the sequence of tests. To determine the time, one needs to determine for each test in the sequence:

- total time history length
- total time to set up the sensors.

Total time history length, T , is dependent on the number of segments to be recorded, n_d , the number of points recorded per segment, N , and the sampling interval, Δt . The number of segments will affect the error in the measurement, as described in Section 5.1. The resulting error is not possible to predict before a test, one simply selects the number of segments to be reasonably high, bearing in mind that ULTRA can allow for re-sampling. The number of segments and the sampling interval are interrelated and also affect the error in the measurement and the frequency resolution, Δf , as described in Section 5.1. One must therefore have some notion as to a reasonable frequency resolution to work with.

After appraisal of the objectives of the test, a grid of measurements is chosen (a "wish list"). The sequence of tests is then determined which will complete the chosen grid. The time to complete the sequence is estimated and the manpower required is estimated. After consideration of the available budget, the grid is inevitably revised

until a *Preliminary Test Plan* is formed. A meeting with B.C. Hydro Production staff at the selected site is then required to determine the operational/safety considerations which will affect the Preliminary Test Plan. After this meeting, a *Final Test Plan* is formed. At this stage the other data acquisition parameters, for low pass and high pass filters and global gain are selected.

In summary, the Final Test Plan will include:

- A finalized grid of measurement locations
- A sequence of tests to complete the grid
- An organized plan for manpower to complete the tests
- Safety and dam operational considerations
- Data acquisition parameters:
 - Sampling frequency
 - Number of segments per test
 - Number of points per segment

- Low pass and high pass filters
- Global gain

CHAPTER 6

AMBIENT VIBRATION TESTING AND ANALYSIS PROGRAM

6.1 Dam Selection

In order to select an appropriate concrete gravity dam, exploratory discussions were held between the thesis author, BCHs Director Of Dam Safety, members of BCHs Structural Department and the UBC advisors for this thesis. Most of BCHs concrete gravity dams were reviewed for their viability to be used for the field work in this thesis. Eventually, the following criteria were used in selection of the appropriate dam:

- *Location:* If possible, the selected dam should be located close to UBC, so that transportation costs for equipment and test personnel would be reduced and the potential for excessive lodging costs would be minimized.
- *Practicality:* The selected dam should be of current interest to BCH, preferably being studied coincident, so that the test results could be of some practical use. As well, accounting instruments would be in place for funding.

Ruskin Dam is a concrete gravity dam located near Maple Ridge, in the greater

Vancouver metropolitan area and therefore relatively close to UBC. Its location is shown in Figure 6.1.

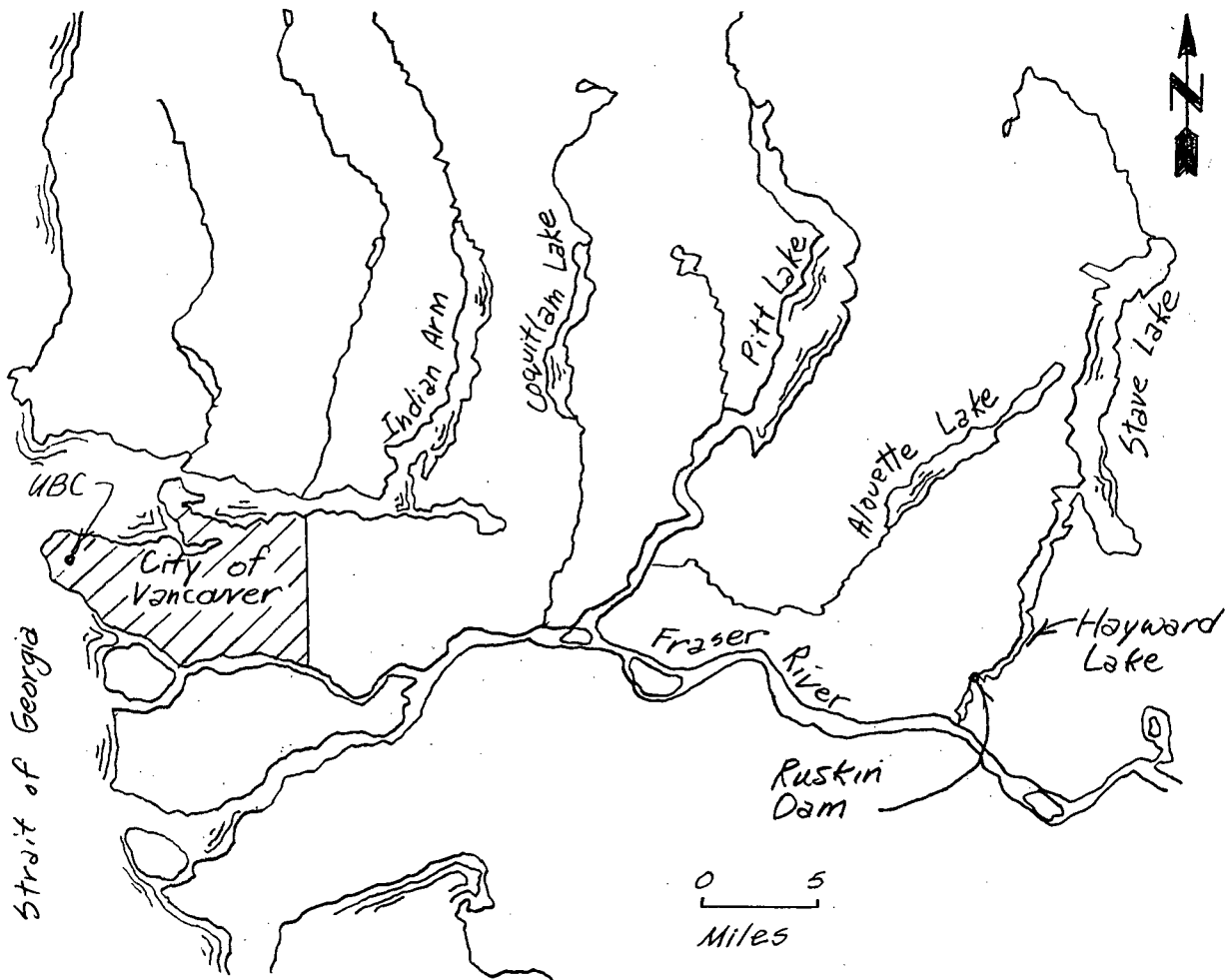


Figure 6.1 Location of Ruskin Dam

Ruskin Dam was currently being studied by B.C. Hydro under its Dam Safety Program, for any deficiencies. The work had indicated that the consequences of failure of Ruskin Dam were high (i.e., significant property damage and loss of life) and that dynamic analysis to evaluate seismic response was justified. Dynamic

analysis of the dam was underway with a numerical model of the dam, using the finite element method. It was apparent that the accuracy of the dynamic analyses would benefit if the ambient vibration testing and analysis could provide useful information for calibration of the numerical model. As a result, Ruskin Dam became the favoured candidate and was eventually selected for study. Results were made available to the Dam Safety team studying the dam as soon as they were available.

6.2 Description of Ruskin Dam and Generating Station

Ruskin Dam is a concrete gravity dam built in 1930. Three power intakes on the left (east) side lead via tunnels through the bedrock, to a generating station located immediately downstream. The station houses 3 units, each with a generating capacity of 35.2 MW. The dam was originally built with only two power intakes. The third was added in 1950, 60 ft to the east of the first two. See Figure 6.2 for a plan of the site and Figure 6.3 for a photo of the dam.

The dam has a straight axis over the majority of its length and is approximately 420 ft long, including the structure for power intakes 1 and 2. It has an overflow section 273 ft long and a non-overflow section on the right (west) side approximately 80 ft long. There is an approx. 12 degree bend in the upstream face of the overflow section (not visible for the road deck in Figure 6.2), at the vertical contraction joint 41 ft from its west end. The bend continues to the west end of the overflow section, where it straightens once again to parallel with the longitudinal axis.

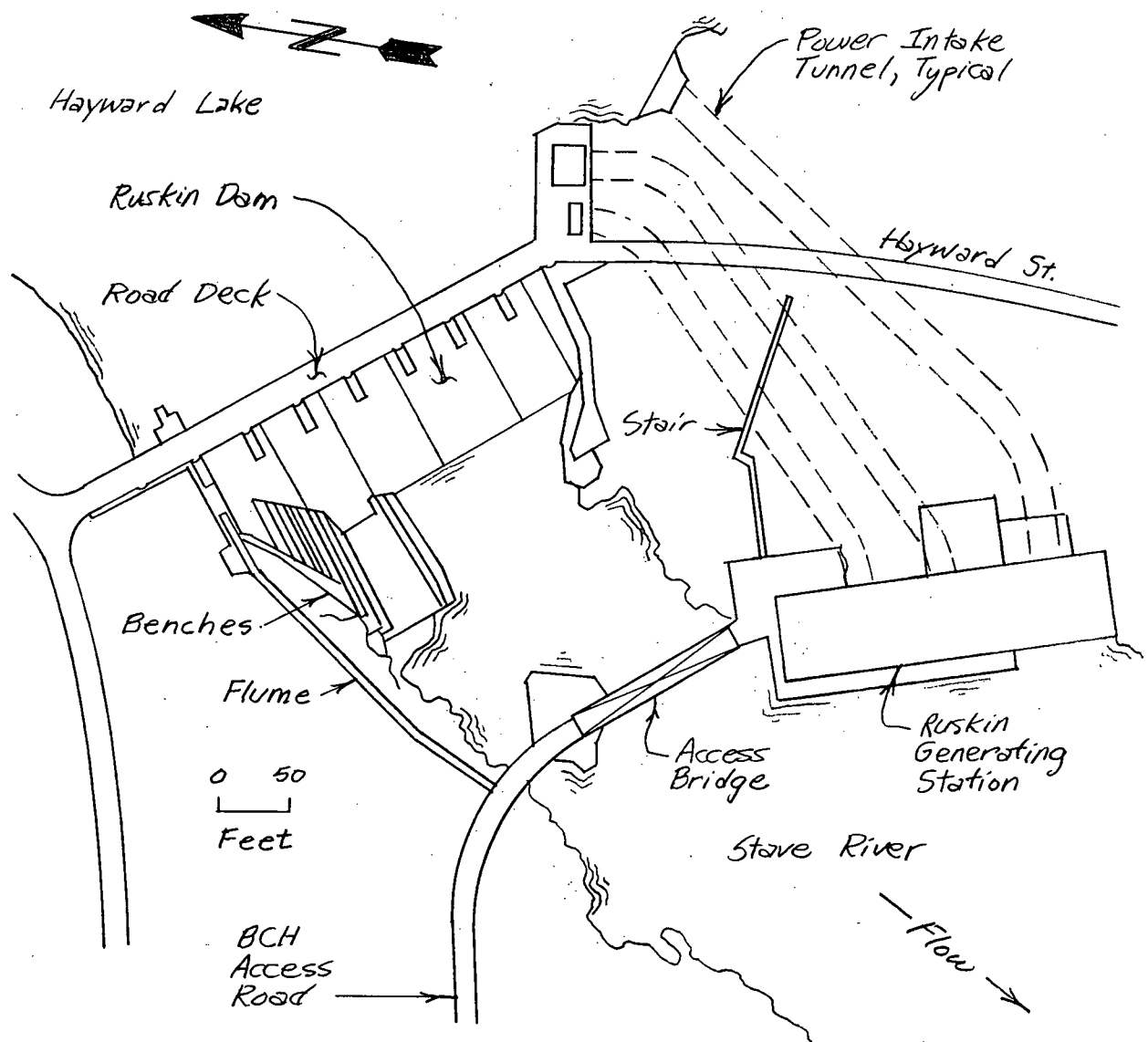


Figure 6.2 Plan of Ruskin Dam and Generating Station

Built atop the entire length of the dam is a road deck of continuously reinforced concrete. Across the overflow section are located seven radial gates. The piers housing the gates also support the road deck and affix it to the top of the gravity blocks. The maximum height from the concrete/bedrock interface to the top of deck is approximately 190 ft. The maximum height of the tallest gravity block is

approximately 155 ft width. The extreme left side block is about 26 ft wide.

The vertical contraction joints between gravity blocks are constructed with vertical keys with two vertical pipes for grouting. Grouting was completed two winters after reservoir impoundment.

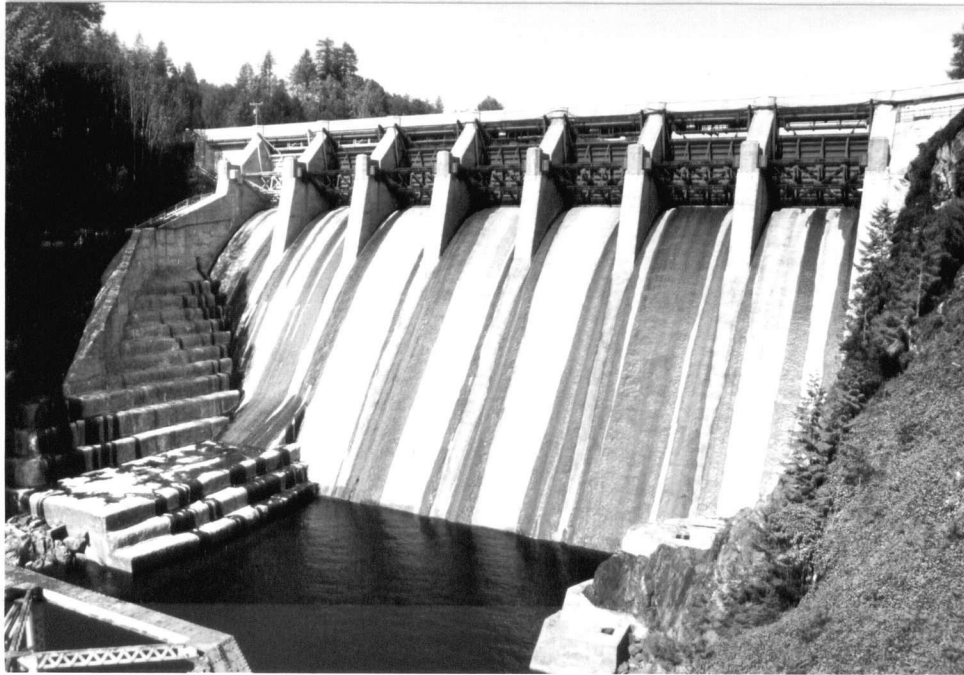


Figure 6.3 Photograph of Ruskin Dam from Atop Ruskin Generating Station

See Figure 6.4 for a section through one of the vertical contraction joints.

The gravity blocks and the intake structure are founded on bedrock. The extreme right abutment of the non-overflow section is against fill.

Each of the 3 power tunnels leading from the power intakes traverse a different route

through the bedrock. All are concrete lined except over their extreme downstream end which is steel lined. All three have square cross-sectioned entrances, which transition to a circular cross-section. All concrete lined inside diameters (I.D.s) are 21 ft and

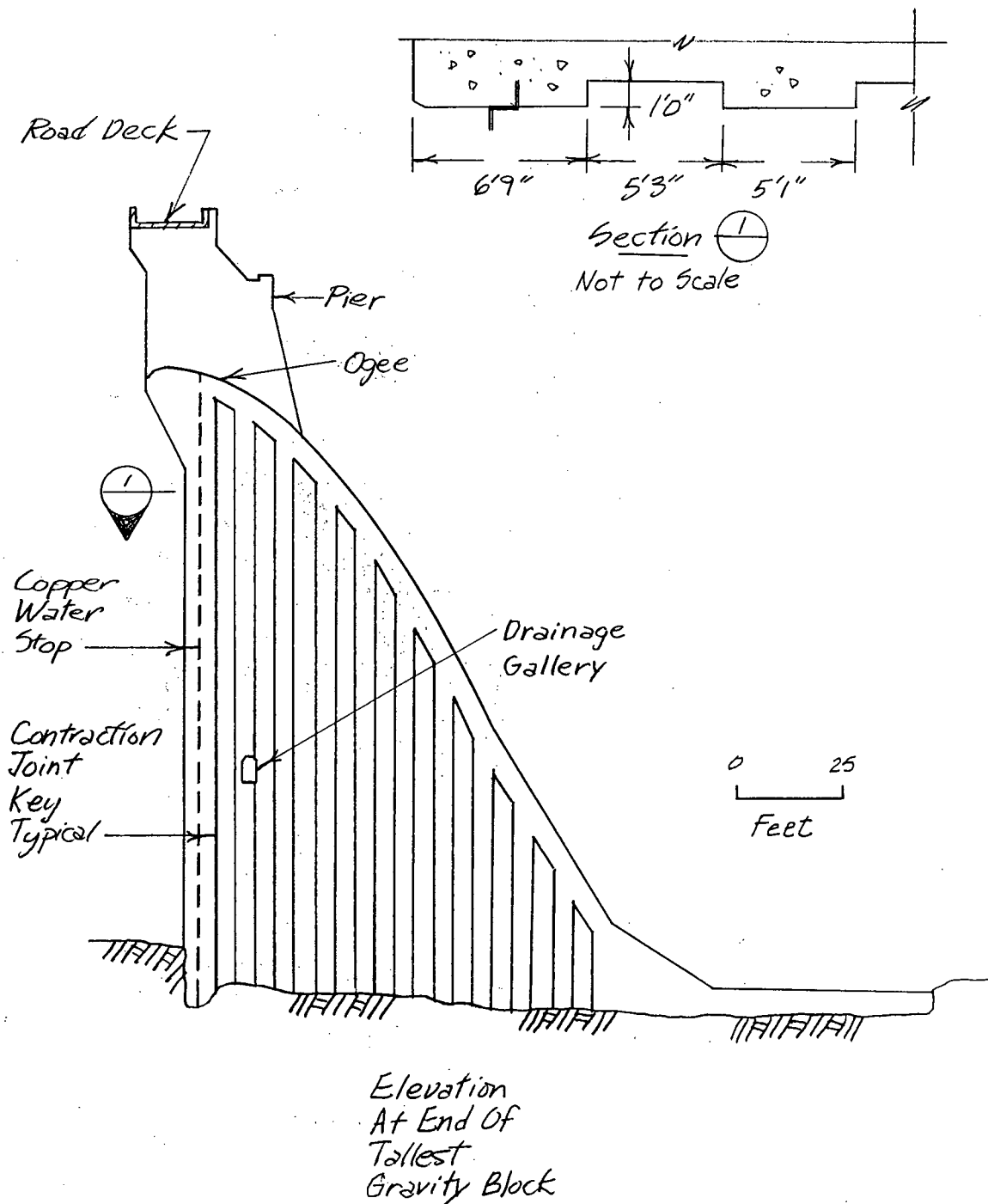


Figure 6.4 Ruskin Dam: Details of Vertical Contraction Joint

steel lined I.D.s are 19 ft. Power tunnel 1 has a 32 % grade over its concrete lined length. Power intake 2 has a 25 % grade over its concrete lined length. Both of these have a 6.2 % grade over their steel lined length. Power intake 3 drops vertically from its entrance for about 100 ft. Thereafter, it continues at a 2 % grade in both the concrete and steel lined lengths. The varied design of the power intakes/tunnels should result in considerable turbulence in the water flow.

Generators/turbines in the powerhouse spin at 120 rpm or 2 Hz. The listed head for the site is 123 ft.

Ambient excitation at Ruskin Dam originates from wind, waves, deck traffic and vibrations from the foundation. The majority of ambient excitation was expected to come from the left abutment bedrock, where the power intake tunnels are located.

6.3 Field Testing Program

Field testing was completed in 2 phases, as follows:

- Phase 1: Trial Test
- Phase 2: Low/High Reservoir Tests

Trial Test

The trial test was designed to be of limited scope. Its purpose was mainly to determine the viability of proceeding with more comprehensive testing.

Low/High Reservoir Tests

The comprehensive tests, i.e., the low/high reservoir tests, were to be used for meeting the thesis objective of providing data for study to demonstrate the usefulness of the ambient technique (see Section 1.2). The scope of this thesis demanded that the usefulness be demonstrated by calibration of a numerical model of the dam (see Section 1.3). It was apparent that testing at two reservoir elevations would provide a parametric set of calibration data for the numerical model.

CHAPTER 7

TRIAL TEST

7.1 Objectives

To determine the viability of proceeding with more comprehensive testing, the objectives for the trial test were:

- *Objective 1, Determine Suitability of Ambient Vibration Signal Strength:* The fundamental question was: would the amplitude of ambient vibrations on the dam be sufficient to permit analysis? Therefore, the first objective was to appraise the ambient vibration signal strength.
- *Objective 2, Cursory Determination of Dynamic Properties of Dam:* The signal content was to be investigated for its suitability for determining dynamic properties of the dam, i.e., natural frequencies and corresponding mode shapes.
- *Objective 3, Determine Whether Gravity Blocks Exhibit Monolithic or Independent Dynamic Behaviour:* Original construction details indicate the dam had been constructed with grouted vertical contraction joints, probably to achieve monolithic structural behaviour. To determine whether monolithic or

independent action was occurring at the ambient vibration level of excitation was considered a suitable problem to investigate as part of the trial test.

- *Objective 4, Cursory Analysis Of Bedrock Signals:* It was presumed that significant excitation of the dam would be through the foundation bedrock due to the power generation activity. A preliminary analysis of captured bedrock signals was therefore deemed to be suitable to study as part of the trial test.

7.2 Test Design

To fit within a limited budget, the test needed to be completed in one day. The time of the year was January (1994), and so with daylight hours short, only a limited number of measurements could be made. In addition, no control of the reservoir was planned.

To meet objective 1, measurements would first be taken atop the easily accessible road deck, to check whether sufficient ambient vibration was occurring. This was considered the most flexible part of the structure. Negative results would put a stop to the trial test. Positive results would result in its continuation. Measurements would be made along lines paralleling the dams longitudinal axis, from abutment to abutment, atop piers supporting the road deck.

With positive results for objective 1, objectives 2 and 3 would be met by taking a

series of measurements atop the ogee of the dam. Again points would be measured along a line parallel to the dams longitudinal axis. Gravity block interaction would be investigated by obtaining coincident acceleration time histories from pairs of sensors located on either side of a vertical joint. In this case, measurements were made in the upstream-downstream, vertical and cross-canyon directions.

To meet objective 4, if time permitted, measurements would be made on the east abutment, where bedrock outcrops were present and the generation activity was located (no bedrock outcrops were visible on the west abutment).

The measurement locations for the trial test are shown in Figure A1 in Appendix A. The VISUAL model resulting from the test is shown in Figure A2. Most measurements are in the upstream-downstream direction of the dam, where the amplitude of motion was expected to be largest. The two reference locations (nodes 5 and 7) were chosen at the approximate third points in the critical upstream-downstream direction, to minimize the risk of missing mode shapes.

Critical data acquisition parameters needed to be determined before the field testing. For concrete gravity dams, the first and most significant natural frequency is generally less than 10 Hz. For the majority of concrete gravity dams the dynamic response in the critical upstream-downstream direction will be at frequencies below 20 Hz. Therefore, the highest frequency of interest was felt to be about 20 Hz and the Nyquist frequency, f_c , only needed to be equal to this value. However, to allow for possible analysis of higher frequencies (which was never undertaken) an f_c of 40 Hz was

selected. The number of points for each segment, N , was selected to be 4096. From eq. (5.3) this yields a frequency resolution, Δf , equal to $2 f_c/N$, or 0.0195 Hz. From eq. (5.4) the segment length, T , is then $1/\Delta f$ or 51.2 seconds. Generally 16 segments were recorded for a total duration of $16(51.2) = 819$ seconds or 13.5 minutes for each test.

From eq (5.5), the sampling frequency, $1/\Delta t$, is equal to twice Δf , or 80 Hz.

Signal filters needed to be determined as well. As the highest frequency of interest was considered to be 20 Hz, a low pass filter of 12.5 Hz was selected. A high pass filter of 0.1 Hz was selected. In retrospect, a low pass filter of 25 Hz may have been a better choice as identification of dynamic properties above 12.5 Hz has been hampered.

A summary of pertinent data acquisition parameters used is shown in Table 7.1.

Further details of the trial test, including the ambient conditions recorded, are contained in Appendix A.

7.3 HBES Results

Refer to Appendix B for details of the analysis.

General

Typically, accelerations measured varied between 50 and 1000 micro-g's, comparing favourably to the accelerometer resolution of 0.2 micro-g's. Testing proceeded quickly from the deck to the ogee as a result. As well, time permitted measurement at two locations on the east abutment bedrock. At each of these locations, sensors were placed atop existing concrete structure which was cast against the bedrock.

Table 7.1
Trial Test: Data Acquisition Parameters

DATA ACQUISITION PARAMETER	VALUE
Nyquist Frequency, f_c	40 Hz
Low Pass Filter	0.1 Hz
High Pass Filter	12.5 Hz
No. Of Segments, n_d	16
Points Per Segments, N	4096
Global Gain	5 db
Gain	6-18 db

Step 1: Average Normalized Power Spectral Densities

Review of the ANPSDs contained in Appendix B indicated potential natural frequency ranges as follows:

- Dam acting independently: 7.0-8.0 and 12.8-14.1 Hz where the ogee ANPSD exhibited significant maximas and the east abutment bedrock ANPSD did not, thereby suggesting independent amplified action.
- Dam acting jointly with bedrock: 8.5-9.2, 11.9-12.8, 15.8-16.7 and 17.9-18.1 Hz, all of which had significant ANPSD maximas for both the ogee and east abutment bedrock, suggesting either a natural frequency of both or of a frequency component of the excitation in the bedrock causing large amplitude motion of the dam.

Step 2: ULTRA and VISUAL

Operating deflected shapes corresponding to the frequencies mentioned above were viewed using VISUAL and subjected to phase and coherence windows. This analysis showed that the 8.5-9.2, 15.8-16.7 and 17.9-18.1 Hz frequency ranges did not exhibit good phase factors or coherence at the deck and ogee nodes, indicating that these were not natural frequencies. The other potential natural frequency ranges showed reasonable phase factors and coherence. These were then deemed to contain probable natural frequencies of the dam. The median frequency judged to have the highest phase factor and coherence for the majority of measured points was selected. The final selection, with mode shapes as described along the upstream-downstream direction of the ogee is:

- 7.3 +/- 0.1 Hz, single curvature
- 12.1 +/- 0.2 Hz, one inflection point
- 13.4 +/- 0.2 Hz, one inflection point

The mode shapes are shown in Figures B2 and B3 in Appendix B.

7.4 Complementary Analyses Results

Refer to Appendix B for detail of the analysis.

Coincident Time Histories

Shotcrete had been applied in the past to the downstream side of the ogee. The shotcrete effectively covered the vertical contraction joints. Cracks were found in this shotcrete suggesting differential movement of at least the outer downstream skin of the gravity blocks due most likely to thermal loads. On the day of the test, 23 January 1994, the average temperature of the outer thickness of the dam concrete (and shotcrete) is expected to have been close to its annual minimum temperature and thermal contraction effects would be near their most influential. If differential movement between blocks were to be detected, it would be most probable when

conditions were as on the day of the test.

Coincident time histories of acceleration measured on either side of the vertical contraction joints showed nearly identical traces in each of the upstream-downstream, vertical and cross-canyon directions. Coherence functions between like directional measurements in each of the vertical and upstream-downstream directions were shown equal to unity over most of the 5-20 Hz frequency range. The lone cross-canyon pair measured showed a similar trend, with coherence equal to slightly less than unity. Below 5 Hz, the phase was very unstable. It was concluded that the evidence was sufficient to indicate monolithic behaviour of the gravity blocks at the ambient level of excitation. Note that careful consideration is required before extrapolation of the monolithic assumption is made to larger amplitude excitations. This would involve quantifying stresses and strains on the vertical contraction joints and comparing these to the available resistance.

7.5 Discussion

Insufficient east bedrock points were measured to draw significant conclusions about the significance of the signals from there.

The strong excitation provided by the power tunnels at Ruskin Dam has no doubt contributed to the success of the work described herein. Storage dams, or dams with penstocks may not have such favourable excitation. If ambient vibration testing and

analysis is considered for other sites, it would be advisable to conduct a quick trial test, with minimal manpower and measurement, to indicate the viability of proceeding with more comprehensive tests.

7.6 Conclusions

1. *Objective 1, Determine Suitability Of Ambient Vibration Signal Strength:* The signal strength was concluded to be sufficiently strong to allow for ambient vibration signal analysis.
2. *Objective 2, Cursory Determination Of Dynamic Properties Of Dam:* The natural frequencies and mode shapes (as defined along the ogee) determined were:
 - 7.4 +/- 0.1 Hz, single curvature
 - 12.1 +/- 0.2 Hz, one inflection point. *A natural frequency close to this value with a similar mode shape will be indicated with the low/high reservoir tests, however will be concluded as not representing a natural frequency/mode shape of the dam.*
 - 13.4 +/- 0.2 Hz, one inflection point

It is recognized that the low pass filter used was equal to 12.5 Hz and as a result, identification of dynamic properties above this frequency has been hampered. Unfortunately, this filter value was not changed during the low/high reservoir tests.

3. *Objective 3, Determine Whether Gravity Blocks Exhibit Monolithic Or Independent Dynamic Behaviour:* It was concluded that at the ambient level of excitation, the gravity blocks indicated monolithic behaviour.
4. *Objective 4, Cursory Analysis Of Bedrock Signals:* It was concluded that insufficient measurements of the signals from the east bedrock had been made to complete understanding of their significance.

7.7 Recommendations

1. A trial test with a limited scope of measurement, is a worthwhile low cost measure which should be implemented to quickly ascertain the value of more comprehensive tests.
2. Additional comprehensive ambient vibration testing be completed on Ruskin Dam to further study the value of these techniques for determining dynamic properties of concrete gravity dams.

3. Comprehensive testing should include measurement of additional points on the dam to better define mode shapes and on the surrounding bedrock to enhance study of the excitation signals in the bedrock.
4. The monolithic behaviour indicated at the ambient level of excitation requires careful consideration for extrapolation to larger amplitude excitations, such as earthquakes.

CHAPTER 8

LOW/HIGH RESERVOIR TESTS

8.1 Objectives

Objective 1, Detailed Study of Ambient Vibration Testing and Analysis Techniques:

The analysis of the trial test was completed in a cursory manner. Detailed review of the HBES was warranted to confirm its ability to attain dynamic properties of concrete gravity dams. As well, mode shape definition was incomplete, particularly in the vertical and cross-canyon directions. Therefore, additional points needed to be measured on the dam to improve this definition.

Objective 2, Comprehensive Analysis of Bedrock Signals: The trial test only measured two points on the bedrock and these were only analyzed in a cursory manner. Therefore, additional points would be measured on the bedrock and a more thorough analysis of their significance in determining dynamic properties of the dam would be completed.

Objective 3, Analysis of the Effects of a Reservoir Drawdown: The hydrodynamic effect was considered of interest. To provide for parametric calibration of a numerical model of Ruskin Dam with respect to the reservoir elevation, tests would be completed

at two reservoir elevations.

8.2 Test Design

Considering the required manpower costs, budgetary constraints dictated that the testing needed to be completed in about 6 days. Safety concerns dictated that the work should be completed on weekend days, to minimize interference with traffic on the road deck (considered heavier during weekdays). Two test were required at different reservoir elevations, therefore, to minimize thermal effects on the dynamic properties, the two were to be scheduled as close as possible in time. As a result of these considerations, two coincident weekends in April/May (1994) were chosen for the tests.

To accommodate the objectives for a larger number of measurement points on the dam and bedrock, a new grid resulted, as shown in Figure A4 in Appendix A. This grid was formed at regular intervals across the road deck, the ogee and in a gallery through the overflow section. Bedrock outcrops were not located on the west side and so bedrock measurement was restricted to the east side. A single reference sensor location was selected at a point on the ogee where, from the trial test, no modal inflection point was located between 0-20 Hz. Three channels were dedicated to each of the following directions: upstream-downstream, vertical and cross-canyon. This would allow for input-output cross spectrum relations (and resulting transfer functions, phase factors and coherence functions) to be constructed between like directional

measurements or orthogonally directioned measurements. The majority of analysis is between like directional measurements. However, for mode shape construction, all measurements would be constructed using a single reference signal, to ensure that the relative magnitude in orthogonal directions would be correct.

The sequence of measurements were designed to complete the ogee and east side bedrock on one day and the road deck and gallery on the second day.

Data acquisition parameters are shown in Table 8.1. No significant changes were made from those selected for the trial test except that due to time constraints, some measurements only had 8 segments recorded.

Further details of planning to develop the Preliminary Test Plan and Final Test Plan for the low/high reservoir field testing are contained in Appendix A.

Table 8.1
Low/High Reservoir Tests: Data Acquisition Parameters

DATA ACQUISITION PARAMETER	VALUE
Nyquist Frequency, f_c	40 Hz
Low Pass Filter	0.1 Hz
High Pass Filter	12.5 Hz
No. Of Segments, n_d	16 or 8
Points Per Time History	4096
Global Gain	5

8.3 Low Reservoir

Refer to Appendix C for details of the low reservoir test analysis.

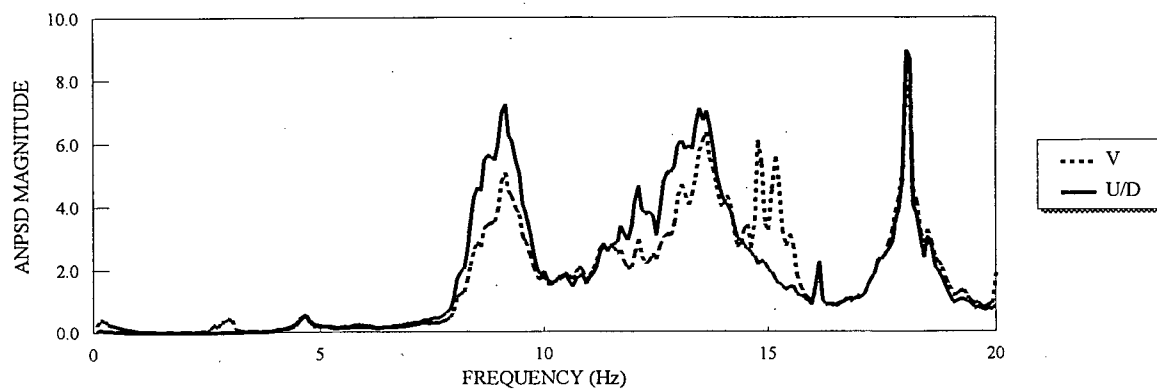
8.3.1 HBES Results

Step 1: Average Normalized Power Spectral Densities

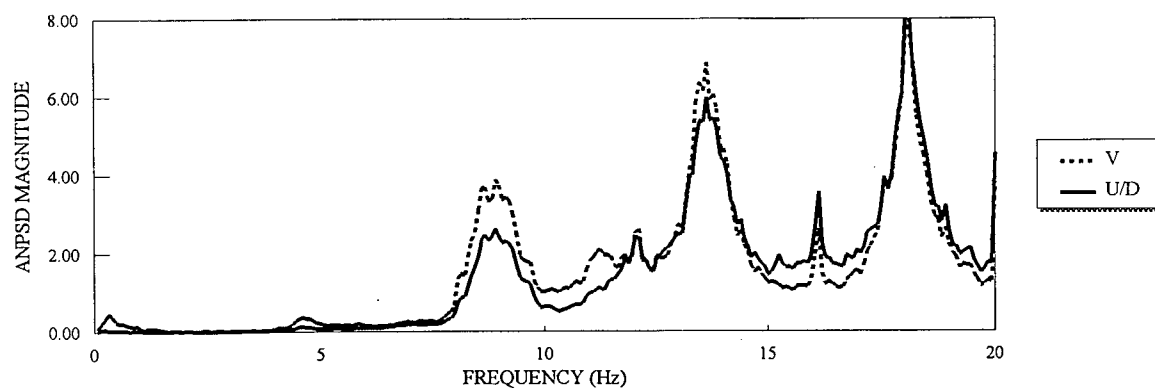
ANPSDs were plotted for nodes on the deck, ogee and east bedrock, in each of the upstream-downstream, vertical and cross-canyon directions. Shown in Figure 8.1 are the ANPSDs for the ogee, deck and east bedrock, in the upstream-downstream and vertical directions. The ogee/deck plots are quite similar, whereas the east bedrock is very different. These differences were used to infer the following potential natural frequencies:

- The east bedrock exhibits significant ANPSD maximas and the ogee/deck do not, over the ranges: 4.0-5.0 and 12.0-13.0 Hz. These ranges are considered to contain potential natural frequencies of the bedrock or frequency components of the excitation originating from within the bedrock.

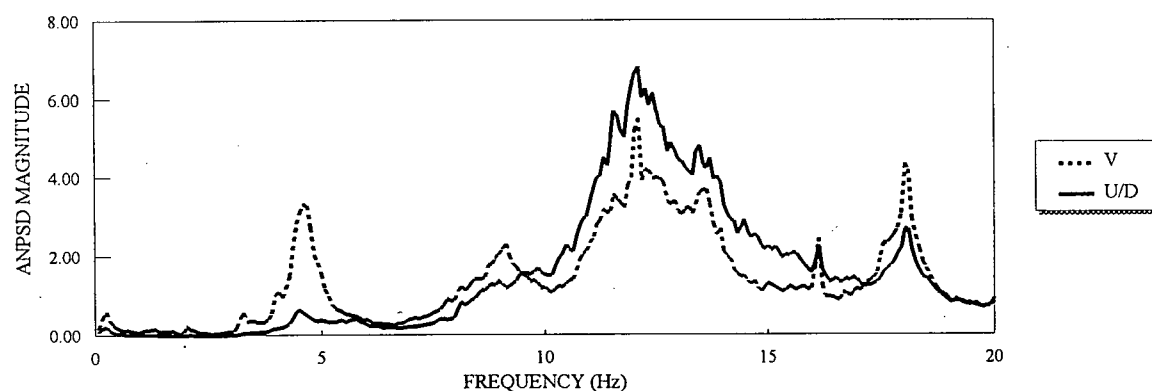
OGEE



DECK



EAST BEDROCK



Notes:

1. All plots are made with 64 segments with a resolution of 0.0781 Hz.
2. In legends shown: U/D = upstream-downstream, V = vertical

Figure 8.1 Low Reservoir ANPSD Functions

- The deck/ogee ANPSDs exhibit significant ANPSD maximas and the east bedrock does not, over the ranges: 8.0-10.0 and 13.0-15.0 Hz. This suggests independent amplified action of the dam and therefore these ranges are considered to contain potential natural frequencies of the dam.
- The east bedrock and deck/ogee jointly exhibit significant ANPSD maximas over the ranges: 16.0-16.1 and 17.0-19.0 Hz. These ranges are considered to contain potential natural frequencies encompassing the dam alone or both the dam and bedrock or they could be representative of frequency components of the excitation originating from within the east bedrock which are causing a large motion of the dam.

Step 2: ULTRA and VISUAL

The following summarizes the ULTRA and VISUAL work:

- Based on good phase factors for the bedrock measurements, there is strong evidence of a probable natural frequency of the bedrock at 4.6 \pm 0.3 Hz. The mode shape appears to be a rigid body resonance.
- Based on excellent phase factor, there is strong evidence of a probable natural frequency of the dam at 8.3 \pm 0.3 Hz. The large range is due

to the conflicting results between the ANPSD and VISUAL studies.

The ANPSD peaks do not coincide with the frequency range for best phase factor. The mode shape is a single curvature shape in both the upstream-downstream and vertical directions.

- Based on good phase factor, there is reasonable evidence of a probable natural frequency of the dam at 13.6 ± 0.3 Hz. The mode shape has one inflection point along the ogee in both the upstream-downstream and vertical directions.
- Based on fair-good phase factor, there is slight evidence of a potential natural frequencies at 18.0 ± 1.0 Hz and 12.1 ± 0.1 Hz.
- The 16.0-16.1 Hz range exhibited very poor phase factor and so it was concluded that this range did not contain a probable natural frequency.

HBES Summary

The final selection of probable natural frequencies and corresponding mode shapes from HBES is described in Table 8.2. Mode shapes are identical to the operating deflected shapes shown in Figures C3, C4, C6, C7 and C8 in Appendix C, at the corresponding frequency.

Table 8.2
Low Reservoir-HBES Analysis Summary

PROBABLE NATURAL FREQUENCY RANGE (Hz)	LOCATION OF ANPSD STRENGTH	MODE SHAPE DESCRIPTION (as defined along ogee)	PHASE FACTOR OF MAJORITY OF NODES
4.6 +/- 0.3	East Bedrock	Rigid body motion of bedrock	0-20, 160-180 degrees
8.3 +/- 0.3	Deck Ogee	Single curvature	0-10, 170-180 degrees
12.1 +/- 0.1	East Bedrock Deck Ogee	One inflection point near east end.	0-20, 160-180 degrees
13.6 +/- 0.3	Deck Ogee	One inflection point on the east side	0-20, 160-180 degrees
18.0 +/- 1.0	East Bedrock Deck Ogee	Two inflection points	40-140 degrees

8.3.2 Complementary Analysis Results

Detailed Phase Change

The detailed phase change analysis supported the HBES findings, except at the probable natural frequency predicted at 12.1 +/- 0.1 Hz where significant phase instability for most dam nodes was found.

Power Spectral Densities (PSDs), Cross Spectral Densities (XSDs), Phase Factor and Coherence

Detail scrutiny of PSDs, XSDs, Phase Factor and Coherence functions showed support for HBES results.

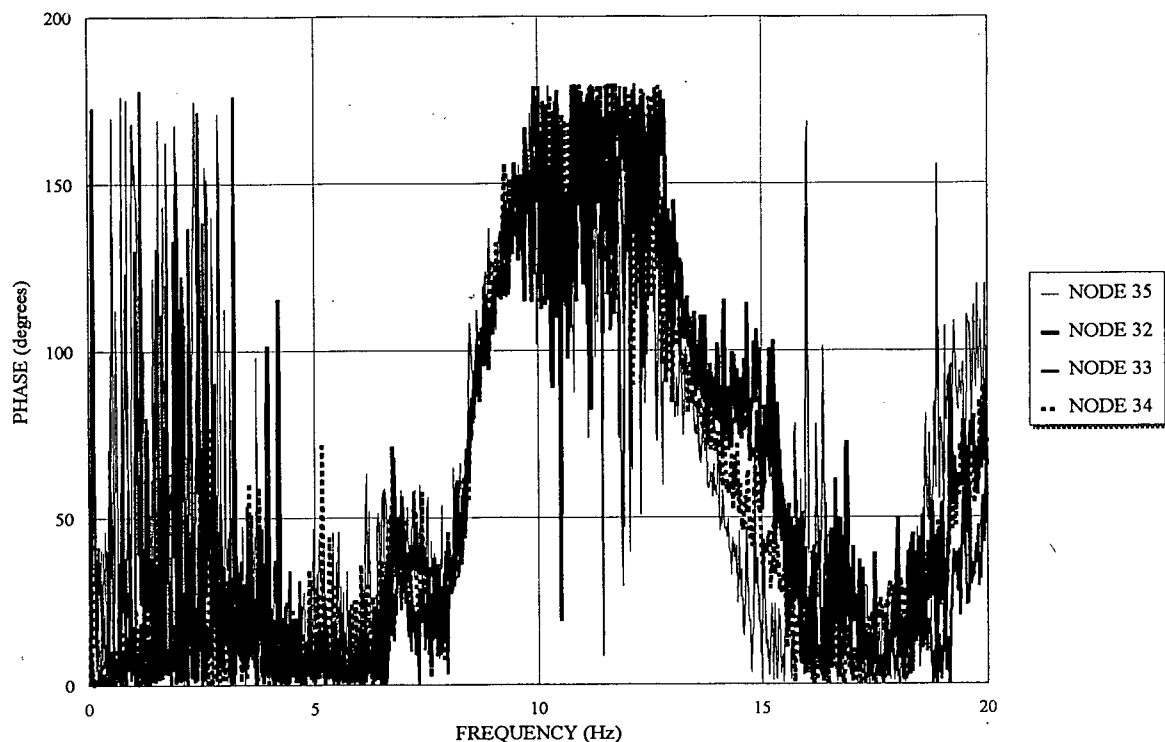
Transfer Function

It was found that the vertical signal recorded from the bedrock can be successfully used as input for transfer functions with the dam signals, based on reasonable correlation to the HBES results. The upstream-downstream signals, when used as input in a similar transfer function, were not found to be as reliable.

Shown in Figure 8.2 is the phase factor calculated using the vertical signal from four different locations on the bedrock. Two 90 degree crossing points are consistently shown.

To further illustrate the results, shown in Figure 8.3 are the transfer function gain, phase factor and coherence function plots using Node 33 alone as the input signal (see Figure A4 in Appendix A for location). Of interest:

- The first transfer function peak is located at 8.7 Hz, for which the



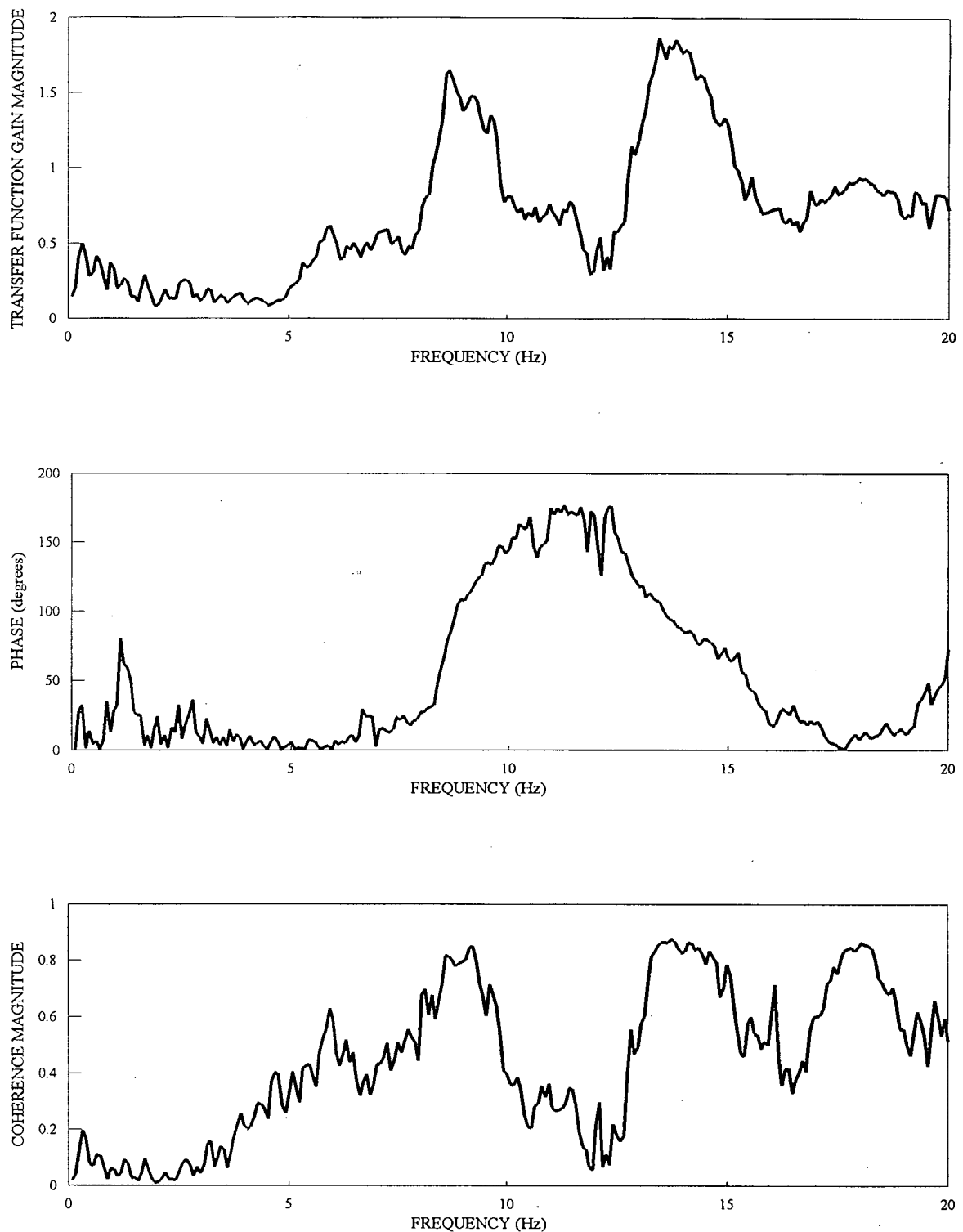
Notes:

1. All plots are made with 16 segments with a resolution of 0.0195 Hz.

Figure 8.2 Low Reservoir: Phase Factor, Vertical Direction, Input: Nodes 32-35 (East Bedrock), Output: Node 13 (Ogee)

corresponding phase factor is 85 degrees and the coherence function is 0.82. The coherence value is significantly high indicating that the vertical signal represents the majority of ambient excitation.

- The second transfer function peak is located at 13.4 Hz, for which the corresponding phase factor is 107 degrees and the coherence function is 0.86, once again, a significantly high value.



Notes:

1. All plots are made with 64 segments with a resolution of 0.0781 Hz.

Figure 8.3 Low Reservoir: Transfer Function Gain, Phase Factor and Coherence, Vertical Direction, Input: Node 33 (Bedrock), Output: Node 13 (Ogee)

Using the vertical signal based transfer function and all bedrock measurements considered, the following was concluded:

- The first natural frequency is predicted to be at 8.7 ± 0.1 Hz, yielding good correlation to the range of 8.6 ± 0.3 Hz found with the HBES system.
- The second natural frequency is predicted to be at 14.0 ± 1.0 Hz and is therein poorly correlated to the HBES prediction of 13.6 ± 0.3 Hz.
- Potential natural frequencies at 12.1 ± 0.1 Hz, 16.1 ± 0.1 Hz and 18.0 ± 1.0 Hz are not indicated.

Complementary Analysis Summary

All results from the complementary analyses are summarized in Table 8.3.

In summary the complementary analyses have provided further evidence for identifying natural frequencies. Of importance, the evidence for 2 of the 4 probable natural frequencies identified with HBES (at 12.1 ± 0.1 Hz and at 18.0 ± 1.0 Hz) is weakened to the point where they will not be considered as being natural frequencies. Work with the numerical model will provide further insight into this selection.

Table 8.3
Low Reservoir Results-Complementary Analysis Summary

HBES PROBABLE NATURAL FREQUENCY RANGE (Hz)	INDIVIDUAL STUDY RESULTS		
	DETAILED PHASE CHANGE	PSD, XSD, PHASE AND COHERENCE	TRANSFER FUNCTION
4.6 +/- 0.3	Similar to HBES	Similar to HBES, the bedrock XSDs, phase and coherence plots yield strong support for a natural frequency in the bedrock	Similar to HBES
8.3 +/- 0.3	Similar to HBES	Similar to HBES	Similar to HBES, with frequency range indicated as 8.7 +/- 0.1 Hz
12.1 +/- 0.1	Poor phase stability noted suggests no natural frequency	Similar to HBES	No evidence of natural frequency
13.6 +/- 0.3	Similar to HBES	Similar to HBES	Similar to HBES, with frequency range indicated at 14.0 +/- 1.0 Hz
18.0 +/- 1.0	Similar to HBES	Very poor phase coupled with good coherence suggests no natural frequency	No evidence of natural frequency

8.4 High Reservoir

Refer to Appendix D for details of the high reservoir test analysis.

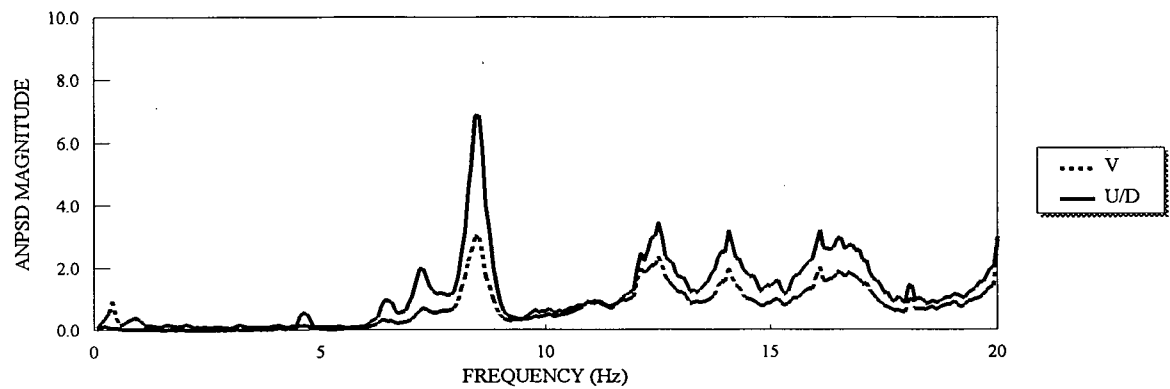
8.4.1 HBES Results

Step 1: Average Normalized Power Spectral Densities

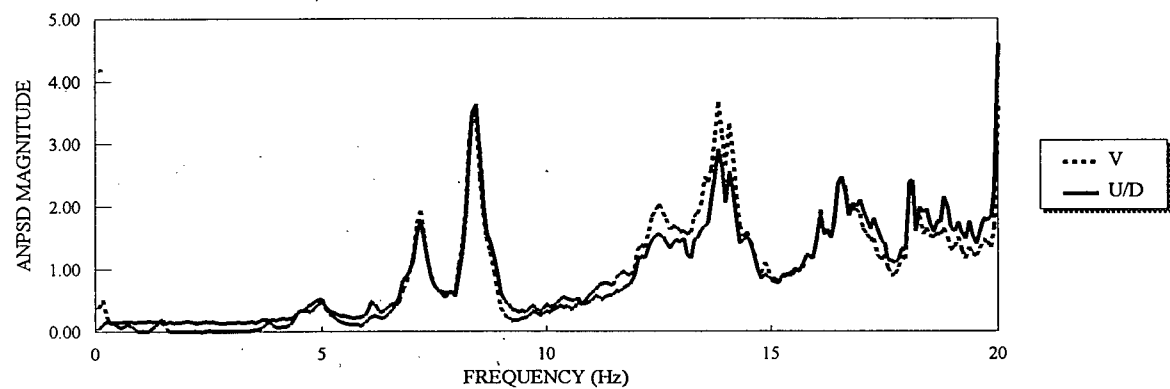
As with the low reservoir, ANPSDs were plotted for nodes on the deck, ogee and east bedrock, in each of the upstream-downstream, vertical and cross-canyon directions. Figure 8.4 contains ANPSDs for the ogee, deck and east bedrock, in the upstream-downstream and vertical directions. The following is found:

- The deck/ogee ANPSDs exhibit a significant ANPSD maxima between 6.8-8.0 Hz. This suggest independent amplified action of the dam and therefore this range is considered to contain a potential natural frequency of the dam.
- The east bedrock and deck/ogee jointly exhibit significant ANPSD maximas and the east bedrock does not at 4.0-5.0, 8.0-9.0, 11.8-13.5, 13.5-15.0 and 15.0-17.9 Hz. These ranges are considered to contain potential natural frequencies of the dam or both the dam and east bedrock or they could be representative of frequency components of the excitation from the bedrock which are causing large amplitude motion of the dam.

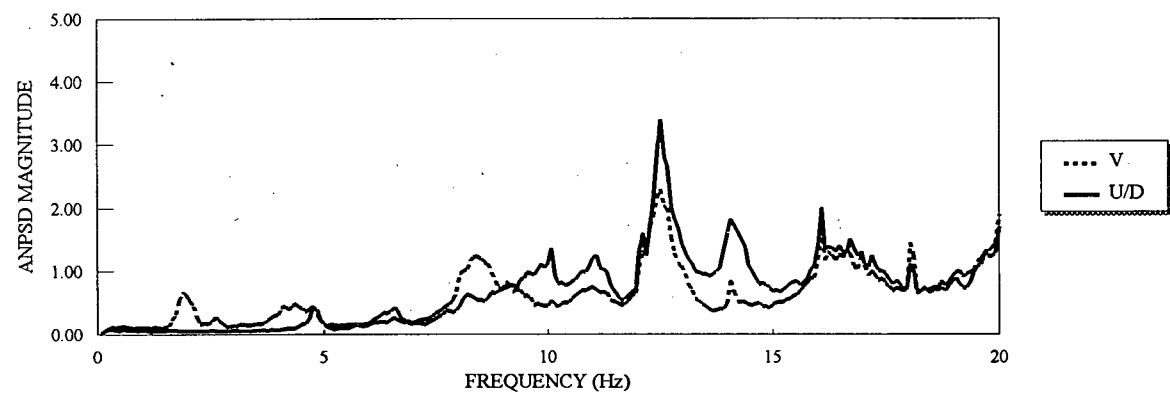
OGEE



DECK



EAST BEDROCK



Notes:

1. All plots are made with 64 segments with a resolution of 0.0781 Hz.
2. In legends shown: U/D = upstream-downstream, V = vertical

Figure 8.4 High Reservoir ANPSD Functions

Step 2: ULTRA and VISUAL

The following summarizes the ULTRA and VISUAL work:

- Based on fair phase factor, there is evidence of a probable natural frequency of the bedrock at 4.5 ± 0.1 Hz. The mode shape is a rigid body motion.
- Based on excellent phase factor, there is strong evidence of a probable natural frequency of the dam at 7.1 ± 0.1 Hz. The mode shape is a single curvature in both the upstream-downstream and vertical directions.
- Based on fair-good phase factor and ANPSD strength, there is slight evidence of other natural frequencies at 12.1 ± 0.1 , 12.5 ± 0.1 , 14.0 ± 0.2 , 16.8 ± 0.7 Hz..
- Based on good phase factor, the 13.2 ± 0.2 Hz range also provides evidence of a probable natural frequency. This range does not have corresponding significant ANPSD strength.
- ANPSD strength between 8.5 ± 0.5 Hz does not correspond to a probable natural frequency due to inadequate phase for the majority of dam nodes.

HBES Summary

The final selection of probable natural frequencies and corresponding mode shapes from HBES is described in Table 8.4. Mode shapes are identical to the operating deflected shapes shown in Figures D3 through D8 in Appendix D, at the corresponding frequency.

8.4.2 Complementary Analysis Results

Detailed Phase Change

The detailed phase change analysis supported the HBES findings, except at the probable natural frequency predicted at 12.1 ± 0.1 Hz where significant phase instability for most dam nodes was found.

Power Spectral Densities (PSDs), Cross Spectral Densities (XSDs), Phase Factor and Coherence

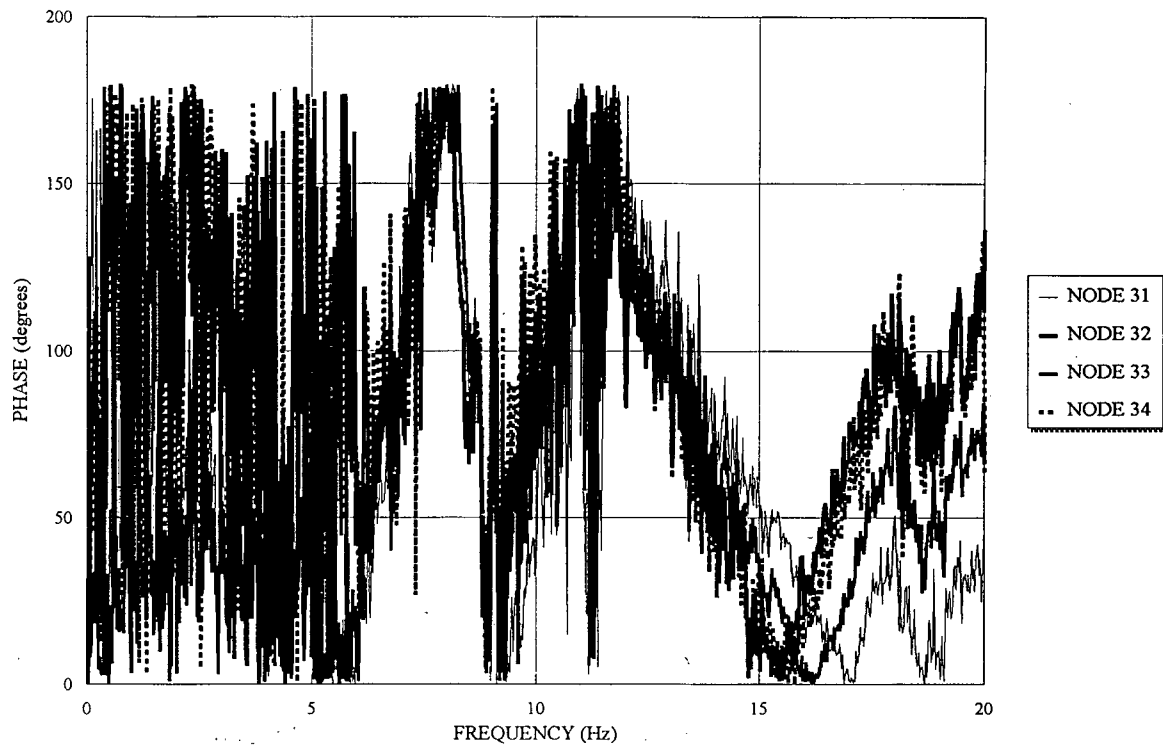
Detail scrutiny of PSDs, XSDs, Phase Factor and Coherence functions showed support for HBES results.

Table 8.4
High Reservoir-HBES Results Summary

PROBABLE NATURAL FREQUENCY RANGE (Hz)	LOCATION OF ANPSD STRENGTH	MODE SHAPE DESCRIPTION (as defined along ogee)	PHASE FACTOR OF MAJORITY OF NODES
4.5 +/- 0.1	East Bedrock Deck	Rigid body motion of bedrock	40-140 degrees
7.1 +/- 0.2	Deck Ogee	Single curvature	0-10, 170-180 degrees
12.1 +/- 0.1	East Bedrock Deck Ogee	One inflection point near east end	0-20, 160-180 degrees
12.5 +/- 0.1	East Bedrock Deck Ogee	One inflection point near east end	0-20, 160-180 degrees
13.2 +/- 0.2	none	One inflection point on east side	0-20, 160-180 degrees
14.0 +/- 0.4	East Bedrock Deck Ogee	One inflection point on east side	difficult to discern
16.8 +/- 0.7	East Bedrock Deck Ogee	Two inflection points	40-140 degrees

Transfer Function

As found for the low reservoir analysis, transfer function construction with the vertical signal based transfer function was again successful. Shown in Figure 8.5 is the phase factor calculated using the vertical signal from four different locations on the bedrock. Several 90 degree crossing points are noted.



Notes:

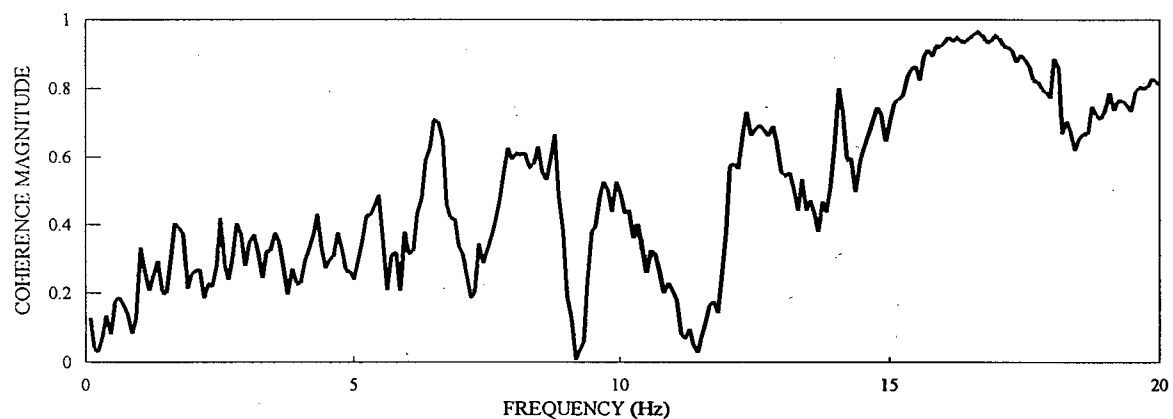
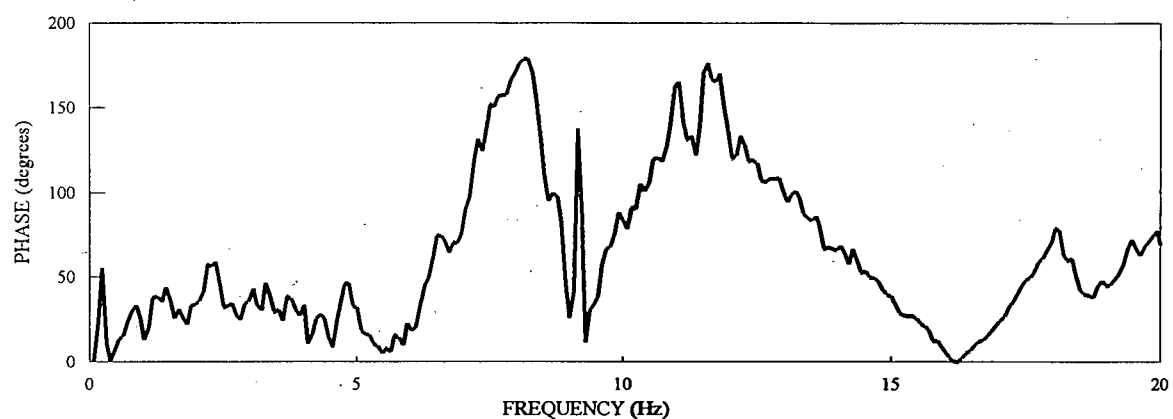
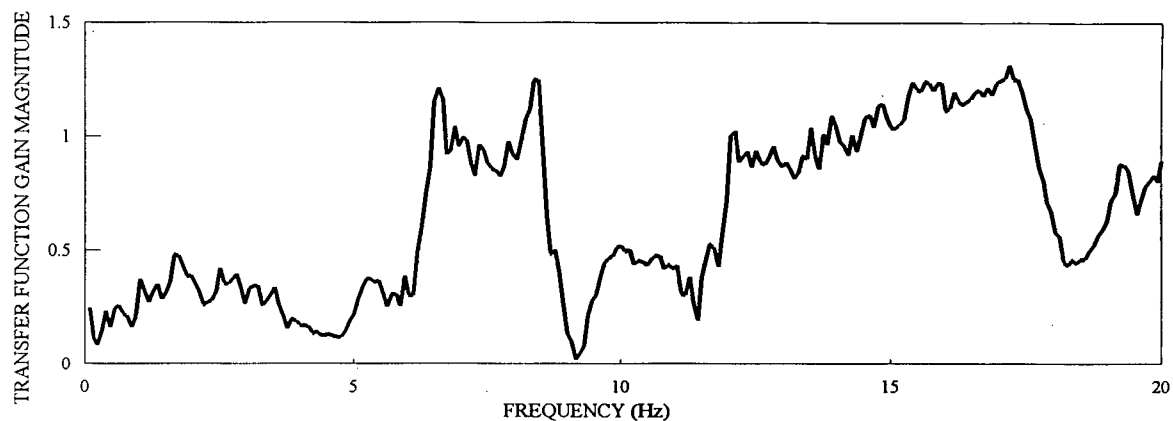
1. All plots are made with 16 segments with a resolution of 0.0195 Hz.

Figure 8.5 High Reservoir: Phase Factor, Vertical Direction, Input: Nodes 31-34 (East Bedrock), Output: Node 13 (Ogee)

Shown in Figure 8.6 is the transfer function gain, phase factor and coherence function plots for Node 33 in the vertical direction.

The following is noted in Figure 8.6:

- At 7.0 Hz there is a transfer function peak, the phase is 90 degrees and there is a coherence of 0.7. This coherence value is sufficiently high enough to support identification of a natural frequency.



Notes:

1. All plots are made with 64 segments with a resolution of 0.0781 Hz.

Figure 8.6 High Reservoir: Transfer Function Gain, Phase Factor and Coherence, Vertical Direction, Input: Node 33 (Bedrock), Output: Node 13 (Ogee)

- Two 90 degree crossings between 8.0-10.0 Hz are not natural frequencies, due to poor correlation to transfer function peaks and low coherence.
- At 13.4 Hz there is a small transfer function peak, the phase is 88 degrees and there is a coherence of 0.53.

As a result, the following conclusions are drawn:

- The first natural frequency is predicted to be at 7.0 ± 0.1 Hz, yielding very good correlation to the range of 7.1 ± 0.1 Hz found with the HBES system.
- The second natural frequency is predicted to be at 13.3 ± 0.3 Hz yielding reasonable correlation to the HBES prediction of 13.2 ± 0.2 Hz.
- Other potential natural frequencies found with HBES are not indicated.

Complementary Analysis Summary

All results from the complementary analyses are summarized in Table 8.5.

Table 8.5
High Reservoir Results-Complementary Analysis Summary

HBES PROBABLE NATURAL FREQUENCY RANGE (Hz)	INDIVIDUAL STUDY RESULTS		
	DETAILED PHASE CHANGE	PSD, XSD, PHASE AND COHERENCE	TRANSFER FUNCTION
4.5 +/- 0.1	Similar to HBES	Similar to HBES, the bedrock XSDs, phase and coherence plots yield strong support for a natural frequency in the bedrock	Similar to HBES
7.1 +/- 0.2	Similar to HBES	Similar to HBES	Similar to HBES
8.5 +/- 0.5	Poor phase stability which suggests no natural frequency	Poor phase coupled with reasonable coherence suggests no natural frequency	No evidence of a natural frequency
12.1 +/- 0.1	Poor phase stability suggests no natural frequency	Similar to HBES	No evidence of natural frequency
12.5 +/- 0.1	Similar to HBES	Similar to HBES	No evidence of natural frequency
13.2 +/- 0.2	Similar to HBES	Similar to HBES	Similar to HBES, with frequency range indicated at 13.3 +/- 0.3 Hz.
14.0 +/- 0.4	Similar to HBES	Similar to HBES	No evidence of a natural frequency
16.8 +/- 0.7	Similar to HBES	Similar to HBES	No evidence of natural frequency

As with the low reservoir work, the complementary analysis has provided further evidence for identification of natural frequencies. As such, the HBES predicted probable natural frequencies at 12.1 +/- 0.1, 12.5 +/- 0.1, 14.0 +/- 0.4 and 16.8 +/- 0.7 Hz are not found to be as strongly identified and will not be considered as representing natural frequencies of the dam.

8.5 Discussion

Results from both reservoir tests are summarized in Table 8.6. Mode shapes as defined along the ogee are shown in Figure 8.7.

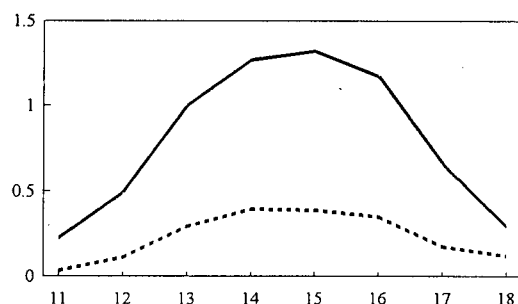
The following remarks are made concerning the results:

- Complementary analyses which "unbundled" the HBES analysis, i.e., the Detail Phase Change and PSD, XSD, Phase and Coherence studies and the complementary analyses which provided a new independent means for estimating natural frequencies, i.e. the Transfer Function study, provided valuable further evidence for identification of natural frequencies. In some cases the evidence was strengthened and in others, it was weakened. Only natural frequencies for which the evidence is most strong are included in Table 8.6.
- Best reliability of prediction, based on phase factor consideration and the Transfer Function study, is for the first natural frequency. This remains a meaningful result as the majority of concrete gravity dam dynamic response is associated with the first natural frequency.
- Mode shapes for both tests indicate significant components in both of the vertical and upstream-downstream directions.

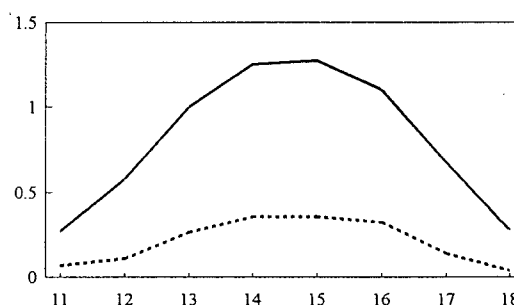
Table 8.6
Summary of All Test Results

RESERVOIR CONDITION	RESERVOIR ELEVATION (ft)	PROBABLE NATURAL FREQUENCY (Hz)	MODE SHAPE DESCRIPTION (as described along the ogee)
LOW	188.46-189.51	8.6 +/- 0.4	Single curvature of ogee (first natural frequency)
		13.6 +/- 0.3	One inflection point
HIGH	210.34-210.71	7.1 +/- 0.2	Single curvature of ogee (first natural frequency)
		13.3 +/- 0.3	One inflection point

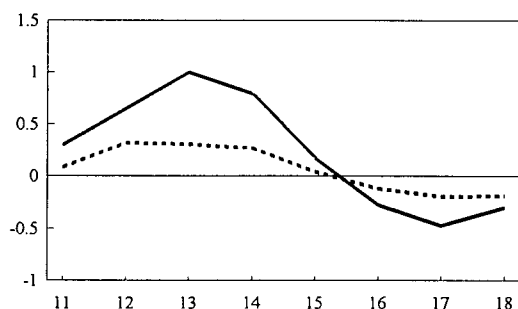
LOW RESERVOIR
8.6 +/- 0.4 Hz



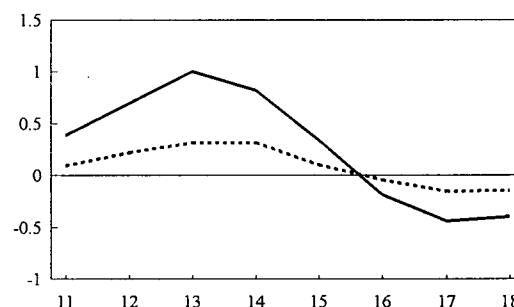
HIGH RESERVOIR
7.1 +/- 0.2 Hz



13.6 +/- 0.3 Hz



13.3 +/- 0.3 Hz



Notes:

1. Abscissa: amplitude normalized to the reference sensor location
2. Ordinate: ambient vibration measurement locations along the ogee, see Figure A4 in Appendix A
3. Solid line = upstream-downstream direction, dashed line = vertical direction
4. Positive Sense: downstream in upstream-downstream direction, up in vertical direction

Figure 8.7 Low/High Reservoir Ambient Mode Shapes

- The number of points measured on the dam during the comprehensive testing in April/May, is judged to have been sufficient to adequately construct mode shapes.
- The number of bedrock signals recorded was limited by the available bedrock outcrops, none of which were found on the right abutment. However, this did not present a problem as excitation originating from the bedrock was from the power generation in the left abutment. In addition, although low quality signals were recorded for some bedrock measurements during the high reservoir test (low coherence), there were enough of adequate quality to allow for meaningful analysis. It would have been of significant value to have completed some tests using a bedrock reference sensor, in order to illustrate whether it was possible to construct mode shapes using the gains of resulting transfer functions
- Referring to Table 8.6, it is apparent that the reservoir elevation has had an effect on the dynamic properties of the dam. Two similar mode shapes were identified for both tests, one of near single curvature (first natural frequency) and one with a single inflection point. The corresponding estimates of their natural frequencies are affected by the reservoir elevation. The most reliably estimated (and important) first natural frequency is shown to increase 21% with a drop of 14% of the maximum reservoir depth (as measured along the upstream side of the dam). Two reliable data points are now available to perform a parametric calibration with reservoir elevation of the numerical

model of Ruskin Dam.

- The primary factor used for determining natural frequencies is the magnitude of the phase factor. There was a great emphasis placed on its value in both the HBES (relative single input-single output system) and the complementary analyses, particularly the transfer function analysis (single input-single output system with output noise). As discussed in Chapter 4, the phase criteria used herein is based on classical damping. Consideration of non-classical damping theory would yield complex phases which may result in acceptance of some of the potential natural frequencies which have been rejected (i.e., the ANPSD strength at 8.5 ± 0.5 Hz for the high reservoir test). It seems reasonable then to suggest that further development of ambient analysis theory incorporating non-classical damping is required.
- The success of the transfer function analysis suggests that if ambient techniques are considered for other concrete gravity dams, a trial test should investigate whether there are any measurable excitation sources suitable for use as input signals.
- Of interest would be forced vibration testing at Ruskin Dam, to provide further proof of the accuracy of the dynamic properties obtained via ambient vibration testing and analysis.
- The use of the 12.5 Hz low pass filter has probably hampered identification of

dynamic properties above this value. Any future ambient testing should utilize a higher low pass filter frequency cut-off.

- As a result of this work, ambient techniques are considered acceptable for consideration at other gravity dams to determine dynamic properties.

8.6 Conclusions

1. *Objective 1, Detailed Study of Ambient Vibration Testing and Analysis*

Techniques:

- Ambient vibration techniques have successfully estimated two natural frequencies and corresponding mode shapes of Ruskin Dam and therefore should also be useful for estimating similar dynamic properties of other concrete gravity dams in BCH's system.
- The reliability and accuracy of estimation varies for each of the natural frequencies identified. The most reliable estimate is for the first natural frequency.
- The Hybrid Bridge Evaluation System (HBES) and the complementary analyses used herein were suitable for estimating natural frequencies and corresponding mode shapes of Ruskin Dam and therefore could also

be useful for estimating similar dynamic properties of other concrete gravity dams in BCH's system.

- There is a need for additional ambient analysis theory incorporating non-classical damping considerations, which can be used to identify other natural frequencies.

2. *Objective 2, Comprehensive Analysis Of Bedrock Signals:*

- A transfer function, constructed with the vertical bedrock signal measured near the power tunnel intakes as input, has been shown to provide an independent means for identifying natural frequencies, with equal or higher accuracy than HBES.
- A natural frequency of the bedrock was identified at 4.3-4.9 Hz.

3. *Objective 3, Analysis Of The Effects Of A Reservoir Drawdown:* The reservoir drawdown was shown to have a significant effect on the natural frequencies identified, with the first natural frequency increasing 21% with a 14% drop in reservoir elevation.

8.7 Recommendations

1. A trial test should investigate whether there are any measurable excitation sources suitable for use as input signals for transfer functions, which can be used to estimate natural frequencies and mode shapes.
2. To facilitate calibration of finite element models with ambient results, a reservoir drawdown during testing is advised, so that a parametric calibration of the natural frequencies estimated with reservoir elevation is possible.
3. To provide further proof of the accuracy of the dynamic properties of Ruskin Dam obtained via the ambient vibration testing and analysis presented herein, the dam should be subjected to forced vibration testing and analysis, at corresponding high/low reservoir levels and at the same time of the year.
4. Future ambient vibration testing and analysis of Ruskin Dam should attempt to construct mode shapes using the gain of single input-single output with output noise transfer functions, with bedrock signal as input.
5. Further ambient vibration analysis theory needs to be developed which implements non-classical damping considerations.
6. Future ambient vibration testing of Ruskin Dam should utilize a low pass filter cut-off frequency higher than the 12.5 Hz utilized for the work in this thesis.

CHAPTER 9

DYNAMIC ANALYSIS

9.1 Numerical Modelling Considerations

As discussed in Section 6.1, BCH had found that should its Ruskin Dam fail during a seismic event it would result in high consequences. Under BCHs guidelines for seismic analysis of dams (BCH 1988) this justified dynamic analysis to study the dams behaviour under seismic loading. To this end it was appropriate to construct a numerical model of Ruskin Dam using the finite element method (FEM). BCH had recent experience with using the ANSYS® computer program for FEM analysis and so this was selected for the Ruskin Dam FEM model (ANSYS® is available from Swanson Analysis System, Inc., Houston, Pennsylvania, USA). Considerations for the FEM model included:

- Previous studies completed under BCHs Dam Safety program (BCH 1985) had found that traditional two dimensional slice analyses of the dams stability yielded less than acceptable factors of safety against sliding for seismic loading. The geometry of Ruskin Dam yielded a length to height ratio of about 1.8, which suggested that three dimensional behaviour might be realized which would prove beneficial. Therefore, these previous studies recommended that

three dimensional stress and stability analysis be completed.

- The vertical contraction joints between monoliths of the dam were constructed with keys (see Section 6.2) which had been grouted. Nonetheless, these were considered to represent vertical planes of weakness in the dam which would have to maintain their integrity if three dimensional behaviour was to be realized. Therefore, a three dimensional model of the dam should discretize these joints in order to quantify their behaviour accurately.
- The pier/deck overtop of Ruskin Dam was suspected of being weak. Therefore, a three dimensional model should include a reasonably accurate representation of these structures.

As a result of the above considerations, BCH engineers determined it was prudent to construct a three dimensional FEM model of the dam. The model would discretely model the vertical contraction joints and the decks/piers. In addition, research has shown that inclusion of the dam-foundation interaction is significant (Chopra 1987, 44). Therefore, the bedrock would also be discretely modelled. However, the bedrock would be modeled without mass as it was intended only to model the stiffness feature of the dam-foundation interaction. In other works, the foundation modeled was intended to represent the support conditions for the dam and make no attempt at representing joint dam-foundation modal behaviour

The type of analysis to subject the FEM model to could be of two main types:

response spectrum or time history (see Section 2.1). Time history analysis becomes extremely time consuming with a large model. Therefore, the three dimensional model of Ruskin Dam would be subjected to response spectrum type analysis. The calibration/parametric studies described herein are only concerned with the modal analysis step in the response spectrum analysis.

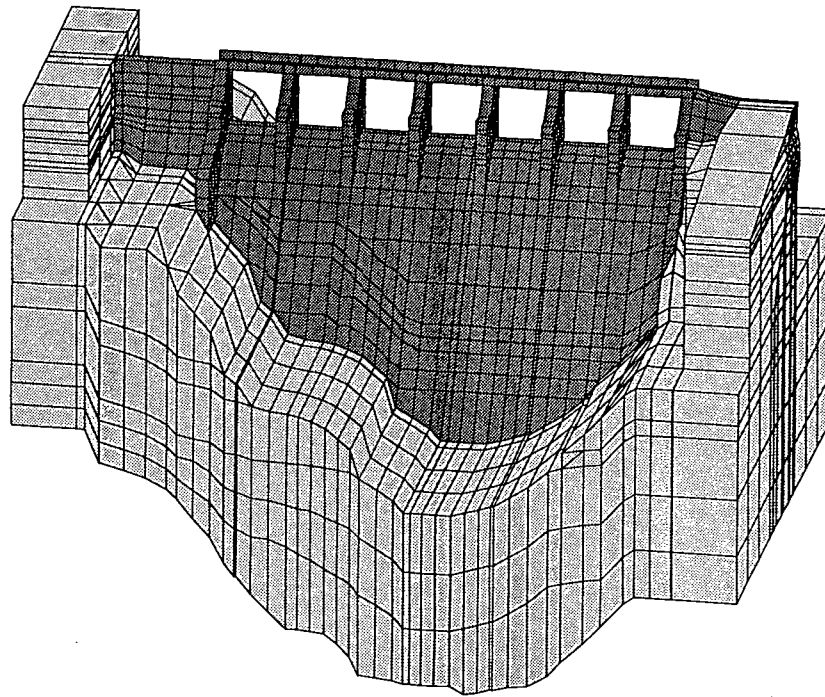
Further, the following was of significance for detailing the model:

- During the 1980s, there had been ongoing upgrading of the drainage system and existing piezometer installations for Ruskin Dam. A significant number of cores had been removed in this work which were available for detailed evaluation to determine bedrock material properties.
- BCH had records of testing conducted on the concrete during the dams construction which indicated a unit weight of 155.6 lbs/ft³. Since that time, there had been no further testing to confirm the concretes in-situ properties.

9.2 Description of Base Model

Elements and Grid

The FEM *base model* of Ruskin Dam is shown in Figure 9.1. The dam and



Notes:

1. View of FEM base model of dam is from downstream side, east abutment

Figure 9.1 FEM Base Model

foundation are constructed of linear 8 noded solid elements with 3 degrees of freedom (DOF) at each node, known as SOLID45 elements in the ANSYS® code. The dam is about 350 feet long across the overflow and non-overflow sections and is about 190 feet high at the deepest section to the top of the deck. The foundation modelled with the dam was taken 131 feet below the deepest section of the dam and a similar distance beyond the toe and heel of the dam at its deepest section and 40 feet beyond the ends of the dam. The power intake section was not included in the model. The vertical contraction joints are modelled with two planes of coincident nodes at each

joint.

The deck/piers were carefully modelled but the 7 radial gates between the piers were not modeled. The deck is constructed of quadratic 4 noded shell elements with 6 DOF at each node and linear 2 noded beam elements with 6 DOF at each node, or SHELL63 and BEAM44 elements respectively in the ANSYS® code.

Although ANSYS® has the ability to model water elements discretely and to include compressibility effects, BCH engineers decided to model the hydrodynamic effect of the reservoir by treating the water as incompressible with lumped masses attached to nodes of the upstream face of the dam. The lumped masses were calculated from theory by Zangar (Zangar 1953) and were configured to act in the upstream-downstream direction. Where the radial gates are located, the tributary reservoir lumped mass was applied at the trunnion support points for the gates. There was no consideration made of the relative stiffness of the gate structure to the dam stiffness and whether or not this would affect the value of the lumped mass.

Table 9.1 summarizes the elements used and their number. The final grid for the dam was considered sufficient for meaningful stress analysis of the joints and deck/piers.

Material Properties

The cores removed from the foundation were reviewed by BCH engineers, along with

other geotechnical/geological information available and an appraisal of bedrock material parameters was made (BCH 1995, Appendix D). Of significance, the bedrock was found to be of variable quality, with the central portion of the dam founded on material of generally softer material than the abutments. As a result, the bedrock was broken into two zones, with different stiffness properties for each, given as both a range and as a recommended single value. The range was given for consideration in

Table 9.1
Summary of ANSYS® Elements in FEM Base Model

PORTION OF RUSKIN DAM MODELLED	ANSYS® ELEMENT TYPE	ELEMENT DESCRIPTION	TOTAL NUMBER OF ELEMENTS IN MODEL
Dam Foundation	SOLID45	linear 8 noded solid	6563
Deck Slab	SHELL63	quadratic 4 noded shell	204
Deck Beams	BEAM44	2 noded beam	102
Reservoir	MASS21	point mass	544

parametric studies. The central portion was specified to have a modulus of 0.5×10^8 to 2.09×10^8 psf, with a single value of 1.09×10^8 psf and the abutments were specified to have a range of 4.18×10^8 to 8.36×10^8 psf, with a single value of 6.27×10^8 psf. For the FEM base model, the two zones were further subdivided into a total of 7 zones to affect a smooth gradation of the stiffness, as shown in Figure 9.2 and listed in Table 9.2.

The in-situ quality of the concrete in the dam was largely unknown. Therefore, the unit weight indicated in the construction records was used and the compressive strength was assumed to be 3000 psi. No consideration was given to the concrete having gained strength in-situ since construction. The dynamic modulus was obtained by first calculating the static modulus from the Canadian concrete design code formula (CSA 1984, 8.5.1), as follows (converted to Imperial units):

$$E_c = 61000 \sqrt{f_c} \quad (9.1)$$

Where:

E_c = static modulus of elasticity or stiffness in psi

f_c = compressive strength in psi

The stress-strain curve for concrete is known to be non-linear and the above relation yields a secant modulus. The dynamic modulus has been shown in research to be higher (Mindess 1981, 480). Therefore, to obtain the dynamic modulus, the static modulus, E_c , was increased arbitrarily increased by 50%.

Boundary Conditions/Supports

As discussed, the foundation is discretized in order to act as a realistic support for the dam. All nodes on the bottom of the foundation are restrained in each of the

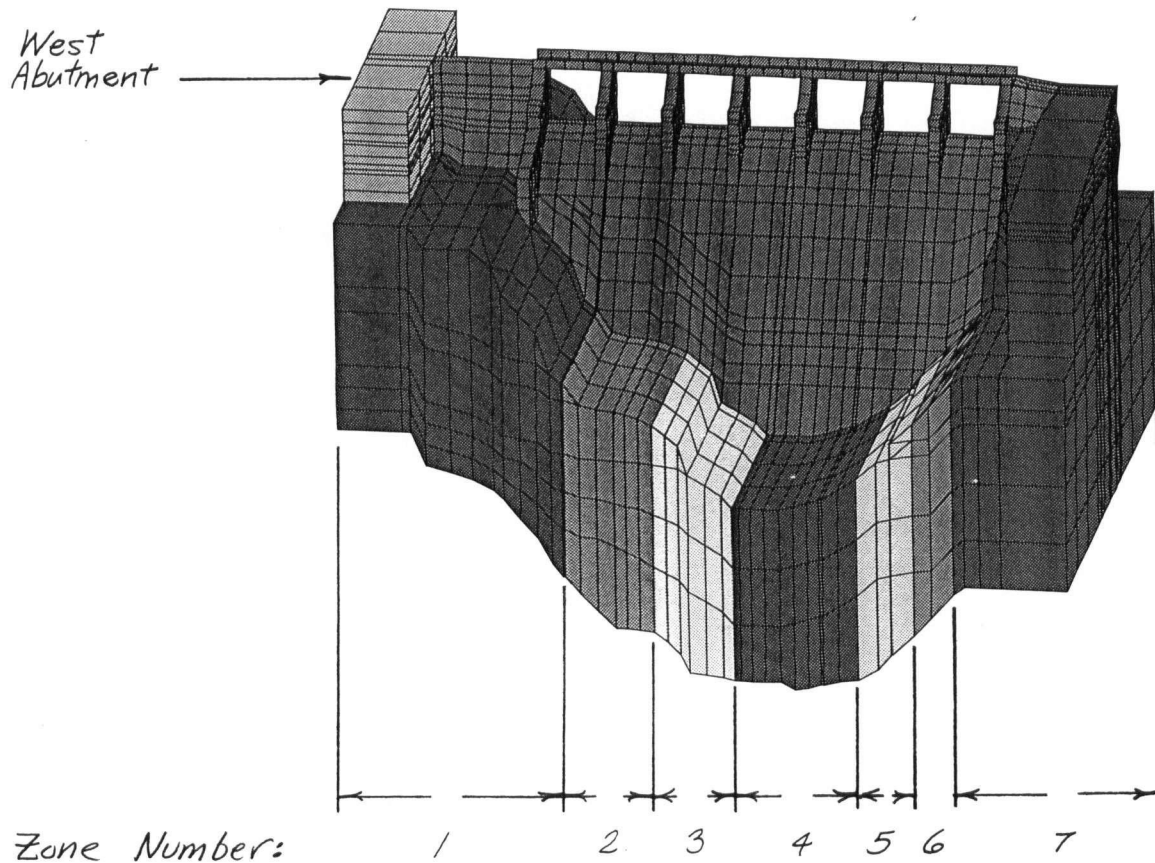
upstream-downstream, vertical and cross-canyon directions. The nodes on the sides of the foundation are restrained in the upstream-downstream and cross-canyon directions.

Table 9.2
Summary of FEM Base Model Material Properties

PORTION OF RUSKIN DAM MODELLED	MATERIAL PROPERTY	VALUE
Dam Deck Slab Deck Beam	Mass Density	4.66 slugs/ft ³
	Dynamic Modulus	7.20×10^8 psf
Foundation	Dynamic Modulus	Zones 1 and 7: 6.27×10^8 psf Zones 2 and 6: 4.18×10^8 psf Zones 3 and 5: 2.09×10^8 psf Zone 4: 1.04×10^8 psf West Abutment (fill): 4.32×10^6 psf
Reservoir	Mass Density	1.94 slugs/ft ³

Vertical Construction Joint Connectivity

The trial test showed strong evidence that at the ambient level of excitation, the gravity blocks were moving monolithically. This was especially true in the upstream-downstream and vertical directions. Although the model had the capability to have nodes at the joints coupled in any direction, the trial test results were used to justify coupling them in each of the upstream-downstream, vertical and cross-canyon directions.



Notes:

1. View of FEM base model of dam is from downstream side, east abutment

Figure 9.2 Detail of Bedrock Zonation in FEM Base Model

Master Degrees of Freedom

Analyses were completed on either an IBM compatible portable computer, with a 486 series CPU, containing 32 Mb of random access memory and 600 Mb of hard drive space, or a unix workstation, the SUN® SPARCstation LX, with a 6 Gb hard drive.

Both computers were of about the same speed in completing a modal analysis.

The base model had a total of 20828 nodes. With most having 3 DOF, there were over 60000 DOF. A modal analysis of this model would take an unreasonably long period of time to complete a modal analysis on the computers being used. Therefore, *Guyan reduction* was used to condense the mass matrix by the use of *master DOF*. All other DOF are removed and are termed *slave DOF*. The masses associated with the slave DOF are considered to move quasistatically with the master DOF. The problem for the analyst is deciding where and how many master DOF are required to obtain an acceptable simplification. ANSYS® suggests that the reduced mass, contained in the mass matrix of master DOF, be at least 85-90% of the total mass of the model (ANSYS 1992, I:3-31). The critical directions for analysis of a gravity dam is their upstream-downstream direction, and to a lesser extent, the vertical direction. Selection of master DOF was then completed in order to achieve this goal. To select master DOF (Cook et al 1989, 389):

"... Master d.o.f. should be those for which inertia is most important. Such d.o.f. have a large mass-to-stiffness ratio. ..."

ANSYS® has a routine which allows for automatic selection of master DOF (ANSYS 1992, I:3-29). However, it was found that use of this routine did not result in acceptable reduced masses. Therefore, some nodes were user selected, which were mainly nodes along the crest of the dam over its central portion, where stiffness in the model would be least. The remaining portion of master DOF selected by the automatic routine in ANSYS® would typically be located on the upstream face of the dam, where the lumped masses were located, as the mass/stiffness ratio was large.

The total mass of the model was 0.14×10^8 lbm. In the upstream downstream direction, all of this mass was acting and so for an acceptable selection of master DOF the reduced mass required is 85% of this value or 0.12×10^8 lbm. In the vertical direction, the lumped masses on the upstream face would not be acting and so the resulting mass was 0.1×10^8 lbm and therefore the required reduced mass was 0.85×10^7 lbm. It was found that 1250 master DOF were needed to achieve these figures. Approximately half of these were user selected. Shown in Table 9.3 is a summary of the reduced mass obtained for various computer runs.

Table 9.3
Selection of Master Degrees of Freedom

COMPUTER ANALYSIS NO.	TOTAL MASTER DEGREES OF FREEDOM	DIRECTION	REDUCED MASS (lbm x 10^6)	PERCENT OF TOTAL DIRECTIONAL MASS
1	750	Upstream-Downstream	12	86
		Vertical	2.0	20
		Cross-Canyon	0.78	8
2	1000	Upstream-Downstream	13	93
		Vertical	8.0	80
		Cross-Canyon	4.6	46
3	1250	Upstream-Downstream	13	93
		Vertical	8.6	86
		Cross-Canyon	7.0	70
4	1500	Upstream-Downstream	13	93
		Vertical	8.9	89
		Cross-Canyon	7.8	78

9.3 Calibration Studies

Objectives

Objective 1: Demonstrate Whether the Numerical Model can be Calibrated to the Ambient Vibration Testing and Analysis Dynamic Properties: This fundamental objective addresses one of the tasks of the Scope for this thesis in Chapter 1.

Objective 2: Study the Hydrodynamic Representation in the Numerical Model: Most vibration work on concrete gravity dams in the literature did not include tests at different reservoir elevations. Therefore, the opportunity for this type of calibration of the numerical model is somewhat unique. As discussed in Section 3.2, the lumped mass representation of hydrodynamic effects has limitations.

Essentially all of the calibration study is discussed in this Section, although some pertinent figures are contained in Appendix E.

Low/High Reservoir

The FEM base model was analyzed at both reservoir elevations, using 1250 master DOF. Shown in Table 9.4 is a summary of the first five natural frequencies obtained for modal analysis compared with those obtained from the ambient analysis. Visual

inspection of the corresponding mode shapes showed that the first two from the FEM base model matched the first two from the ambient analysis.

Shown in Figure 9.3 is a comparison of the first two mode shapes along the ogee. From Figure 9.3 it is immediately apparent that the ambient and FEM model have calibrated reasonably well for the first two mode shapes at both reservoir elevations.

To confirm mode shape correlation, computation of a Modal Assurance Criterion (MAC) value was completed in the upstream-downstream and vertical directions, for the nodes on the ogee and gallery using eq. (3.1). Results are shown in Figure E12, in Appendix E. MAC analysis found that the correlation of the first natural frequency/mode shape is excellent, with the MAC value almost equal to 1 in both the vertical and upstream-downstream directions. The second natural frequency/mode shape is not as well correlated, with MAC values of about 0.85 for the low reservoir and 0.65 for the high reservoir.

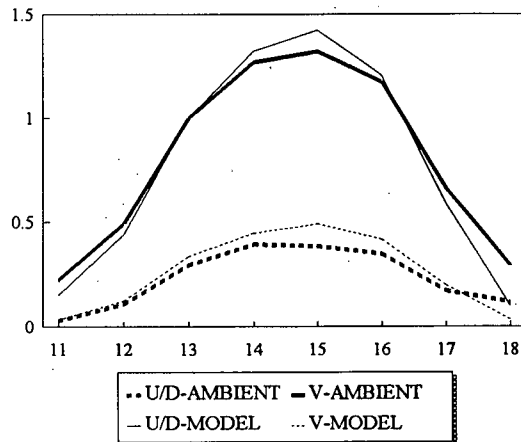
The MAC analysis confirmed that the model did not reproduce a mode shape matching the rigid body motion of the dam noted at 4.5-4.6 Hz for either reservoir elevation (ambient analysis concluded this was a natural frequency of the bedrock).

Hydrodynamic Effects

The numerical model has apparently reproduced the first two natural frequencies and

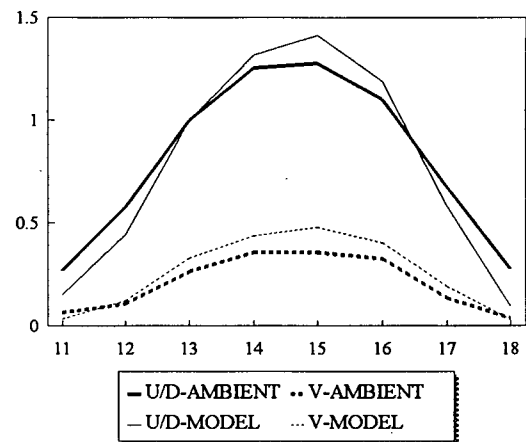
LOW RESERVOIR

AMBIENT: 7.1 +/- 0.2 Hz FEM BASE MODEL: 7.5 Hz

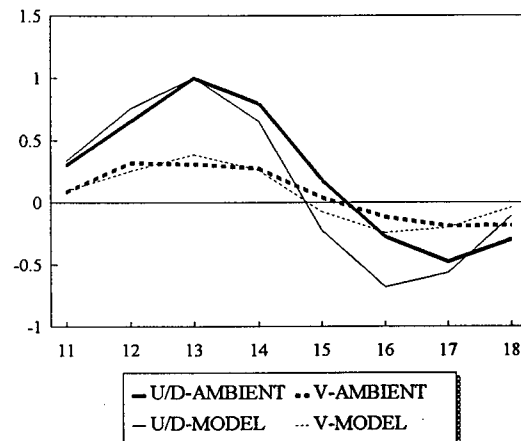


HIGH RESERVOIR

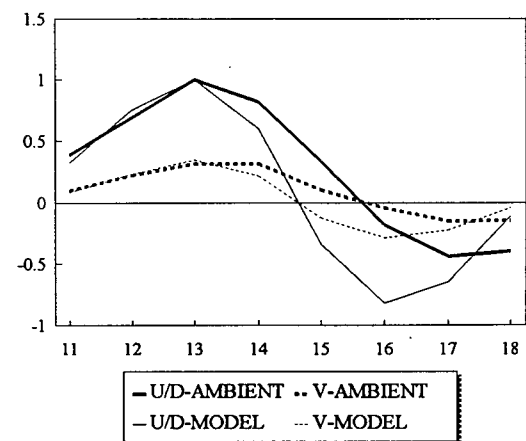
AMBIENT: 8.6 +/- 0.4 Hz FEM BASE MODEL: 8.6 Hz



AMBIENT: 13.3 +/- 0.3 Hz FEM BASE MODEL: 11.6 Hz



AMBIENT: 13.6 +/- 0.3 Hz FEM BASE MODEL: 13.9 Hz



Notes:

1. Abscissa: amplitude normalized to the reference sensor location
2. Ordinate: ambient vibration measurement locations along the ogee, see Figure A4 in Appendix A
3. In legends shown: U/D = upstream-downstream, V = vertical
3. Positive Sense: downstream in upstream-downstream direction, up in vertical direction

Figure 9.3 Mode Shape Comparison: Ambient vs. FEM Base Model

corresponding mode shapes identified in the ambient work. Examination of the natural frequency magnitudes was then undertaken.

As shown in Table 9.4 the numerical model results correlate well for the low reservoir results, with both natural frequencies falling within the natural frequency ranges given for the ambient results. The correlation is not as good with the high reservoir as both model natural frequencies fall outside of the ambient ranges.

Focusing on the first natural frequency, it is easily shown that a slight change of the material parameters would bring both high and low reservoir models within the ambient ranges. The natural frequencies of the dam, f_n , will vary with the model stiffness, k and model mass, m , which from elementary structural dynamics theory is:

$$f_n \propto \sqrt{(k/m)} \quad (9.2)$$

Table 9.4
Low/High Reservoir Calibration: Comparison of Natural Frequencies Obtained from the FEM Base Model and the Ambient Analysis

RESERVOIR ELEVATION	NATURAL FREQUENCY (Hz)	
	NUMERICAL MODEL	AMBIENT
Low	8.6 13.9 15.3 16.2 17.0	8.2-9.0 13.3-13.9
High	7.5 11.6 13.9 14.6 16.0	6.9-7.3 13.0-13.6

Therefore, a slight decrease in the model stiffness would cause all natural frequency magnitudes to drop. This could no doubt be accomplished within the bounds given for the material parameters. However, a problem exists for the second natural frequency. Here, a similar drop would occur. By inspection of Table 9.4, this is not a desired result as the magnitude for the second natural frequency is already too low for the high reservoir case. Clearly, a problem exists.

Comparing the shift in natural frequencies provides further insight. The shifts are summarized in Table 9.5 and shown graphically in Figure 9.4. For the fundamental mode, the model shows a shift of 1.1 Hz between the low and high reservoir cases, a value which falls within the envelope provided by the ambient frequency range of 0.9-2.1 Hz. For the second mode, the model shows a shift of 2.3 Hz, a value which falls outside the ambient frequency range envelope of 0.3-0.9 Hz. The only variable to have changed in the two analyses is the reservoir elevation. Therefore, the results indicate a weakness in representation of the hydrodynamic effects.

Table 9.5
Low/High Reservoir Calibration: Frequency Shift Comparison

	FREQUENCY SHIFT BETWEEN LOW AND HIGH RESERVOIRS (Hz)	
	FIRST NATURAL FREQUENCY	SECOND NATURAL FREQUENCY
NUMERICAL MODEL	1.1	2.3
AMBIENT RANGE	0.9-2.1	0.3-0.9

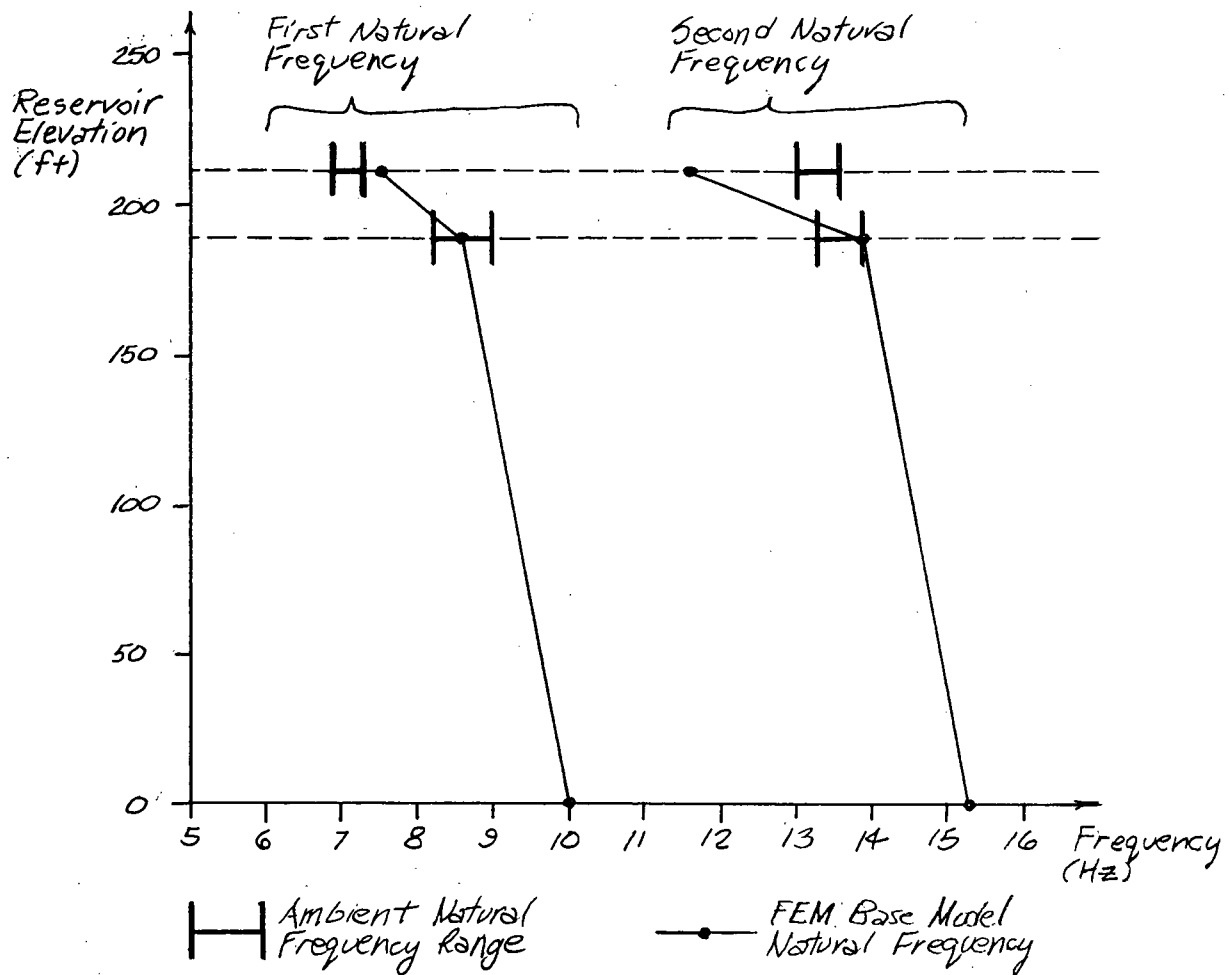


Figure 9.4 Low/High Reservoir Calibration: Frequency Shift Comparison

An indication the importance of water compressibility can be obtained by calculation of the value of Ω , equal to the ratio of the fundamental frequencies of the reservoir, f_{wl} , to the dam without reservoir, f_{dl} , as given by eq. (3.11). The base model was re-analyzed with no reservoir, which yielded $f_{dl} = 10.0$ Hz.

It is possible to experimentally measure the natural frequencies of an impounded reservoir (Duron 1987) however, lacking such a measurement for the Ruskin Dam

reservoir, the suggested formula given in eq. (3.12) is used.

At the high reservoir elevation, $f_{wl} = 8.7$ Hz and $\Omega = 0.9$. At the low reservoir elevation, $f_{wl} = 10.1$ Hz and $\Omega = 1.0$. The value of Ω below which consideration of water compressibility is significant is reportedly 1.5 (Hall 1988, 59) or 2 (Chopra 1987, 45). These calculations suggest that water compressibility is significant for Ruskin Dam.

Another factor for consideration is the effect of the gates on the response of the dam. The water acting against the gates is located at the top of the dam where it will have a significant effect on its response (Chopra, 1987, 43). Incorrect modelling of the hydrodynamic effect of the water acting against the gates could significantly effect the results. The low reservoir test had the water level essentially at the crest of the ogee (only 3' above it) where the hydrodynamic effect of the water on the gates would be insignificant and the model was shown to calibrate well for both natural frequencies. The lack of agreement for the second natural frequency for the high reservoir case could have due to an inaccurate representation of the hydrodynamic effect of water acting against the gates.

In summary, the lack of calibration to the second natural frequency for the high reservoir case is probably due to an inaccurate representation of the hydrodynamic effect acting on either the dam and/or the gates. Water compressibility is shown through rudimentary calculation to be important and so the lumped mass representation

used is most likely incorrect for the second natural frequency.

It is noted that although the base model has only been calibrated to the first natural frequency, this remains a meaningful result for concrete gravity dams in general, as from Chopra and Fenves (Chopra and Fenves 1984, 8):

"... The response of short vibration-period structures, such as concrete gravity dams, to earthquake ground motion is primarily due to the fundamental mode of vibration. ..."

9.4 Parametric Studies

Objectives

Parametric studies were undertaken to see what effect varying some of the base models parameters would have on the dynamic properties and whether an *improved model* could be obtained. Objectives of this work were:

Objective 1, Improve on the Ordering of Mode Shapes: The ambient work showed a succession of operating deflected shapes exhibiting an orderly progression of inflection points along the ogee. This behaviour was sought in the numerical model.

Objective 2, Improve on the Difference Between the First and Second Natural

Frequency Magnitudes: As indicated in the previous section, at the high reservoir, the difference in magnitude between the first and second natural frequencies of the base model did not match that obtained from the ambient results. It was deemed of interest to determine whether this difference could be matched.

Results

Parametric studies and results are detailed in Appendix E. The following summarizes each study and its findings:

Foundation Dynamic Modulus: The foundation dynamic modulus was made a uniform 2.09×10^8 , 4.18×10^8 and 6.27×10^8 psf in all zones (see Figure 9.2). No improvement in the difference between the first/second natural frequency magnitudes was indicated however, the mode shape order seemed to improve with the higher stiffnesses at 4.18×10^8 and 6.27×10^8 psf. Unfortunately, these values were higher than the upper bound given for the central portion of the foundation by BCH engineering recommendation.

Concrete Dynamic Modulus: The concrete dynamic modulus was increased 50%. Stiffening the dam concrete improved markedly on the difference between the first/second natural frequency magnitudes however their magnitudes were far too high. Mode shape ordering was not improved.

Modified Boundary Conditions: The power intake had not been discretely represented in the base model. This study modified support conditions where the power intake was located. This results did not indicate any improvements.

Enlarged Foundation: The foundation was enlarged by adding a 40 foot width to each abutment. This study did not indicate any improvements.

As a result of the parametric studies it was deduced that an improved model could not be constructed. Certainly, a slight uniform decrease in the foundation dynamic modulus would bring the first natural frequency of both low and high reservoir base models within both low and high reservoir ambient results. However, only the low reservoir base model second natural frequency would be similarly accommodated. The high reservoir base model second natural frequency would simply be shifted farther away from the ambient result. This modelling problem, although not solved, would nonetheless have not been recognized without the ambient work. Consequently, the ambient work can be conclusively said to have proved valuable in the calibration/parametric studies of the numerical model.

It is noted that the parametric studies were completed at the high reservoir elevation. This implicitly includes the unknown hydrodynamic effect of the reservoir acting on the radial gates. Future parametric studies should be completed with the reservoir level at the ogee to eliminate the need for consideration of this effect.

9.5 Conclusions

1. Calibration Studies:

1.1 *Objective 1: Demonstrate Whether the Numerical Model can be Calibrated to the Ambient Vibration Testing and Analysis Dynamic Properties:*

- The numerical model was successfully calibrated to the first natural frequency and corresponding mode shape.

1.2 *Objective 2: Study aspects of the hydrodynamic representation in the numerical model:*

- Rudimentary calculation shows that water compressibility is significant for Ruskin Dam.
- The numerical models representation of the hydrodynamic effect by lumped mass is probably incorrect for the second natural frequency.
- Understanding of hydrodynamic effects on Ruskin Dam was greatly facilitated by obtaining ambient results at two different reservoir elevations.

2. Parametric Studies:

2.1 *Objective 1, Improve On The Ordering Of Mode Shapes.*

- This was shown feasible only with a uniform foundation modulus higher than BCH engineering recommendations.

2.2 *Objective 2, Improve On The Difference Between The First and Second Natural Frequency Magnitudes.*

- This was shown feasible by increasing the magnitude of the concrete dynamic modulus of the base model, however was not meaningful as the magnitudes of natural frequencies became too high.

3. A rational way of improving on the base model by shifting its parameters was not identified.
4. The size of the base model meant that significant computing time was required for modal analysis and that modifications required to affect calibration/parametric studies also required significant time, which inhibited the efficiency of these studies.
5. Dynamic properties identified with ambient vibration testing and analysis have

proven useful in calibration/parametric studies of the numerical model of the dam.

6. Future parametric studies should be undertaken with the reservoir level at the ogee to eliminate the consideration of the hydrodynamic effect on the radial gates.

9.6 Recommendations

1. Future numerical modelling of Ruskin Dam should consider modelling of water compressibility.
2. Future numerical modelling of Ruskin Dam should include a review of the hydrodynamic effect of the reservoir acting on the radial gates.
3. Vibration testing for the purpose of numerical model calibration should include testing at differing reservoir elevations.
4. A simple numerical model should be used to complete calibration/parametric studies and if a detailed model is required for say, stress analysis, it should be built separately incorporating results from these studies.

CHAPTER 10

CONCLUSIONS

The following conclusions are *specific to the study of Ruskin Dam*:

1. The strength of ambient signals measured were sufficient to complete meaningful ambient vibration signal analysis.
2. At the ambient amplitude of excitation, the gravity blocks appear to be coupled so that the dam exhibits monolithic behaviour.
3. Ambient vibration testing and analysis, based on a single input-single output system with "relative" transfer functions, successfully predicted the first two natural frequencies and corresponding mode shapes of the dam.
4. Ambient vibration testing and analysis, based on a single input-single output with output noise system, with the bedrock signal as input, successfully predicted the first two natural frequencies of the dam with equal or higher accuracy than relative transfer function analysis.
5. The reliability and accuracy of estimation for each of the natural frequencies and corresponding mode shapes varies. The most reliable estimate is for the first natural

frequency, for both methods utilized.

6. The ambient vibration testing and analysis identified a natural frequency of the bedrock.
7. Dynamic properties identified with ambient vibration testing and analysis have proven useful in calibration/parametric studies of the finite element model of the dam.
8. A numerical model with a lumped mass representation of hydrodynamic effects could only be calibrated to the first natural frequency and corresponding mode shape, probably because calculations suggest water compressibility is significant for Ruskin Dam.
9. Understanding of hydrodynamic effects is facilitated by obtaining dynamic properties at significantly differing reservoir water levels.
10. The size of the base model used in this thesis was too large to permit efficient calibration/parametric studies.

The following conclusions address the *general suitability of ambient vibration and analysis techniques for the study of concrete gravity dams*:

1. Ambient vibration and analysis techniques can be used to provide meaningful estimates of the dynamic properties of concrete gravity dams and useful insights into

their behaviour.

2. There is a need for additional ambient analysis theory which can be used to identify natural frequencies.

CHAPTER 11

RECOMMENDATIONS

The following recommendations are *specific to the study of Ruskin Dam*:

1. To provide further proof of the accuracy of the dynamic properties of Ruskin Dam obtained via the ambient vibration testing and analysis presented herein, the dam should be subjected to forced vibration testing and analysis, at corresponding high/low water levels and at the same time of the year.
2. Future ambient vibration testing and analysis of Ruskin Dam should attempt to construct mode shapes using the gain of single input-single output with output noise transfer functions, with the bedrock signal as input.
3. Future ambient vibration testing of Ruskin Dam should utilize a low pass filter with a cut-off frequency higher than 12.5 Hz in order to assist in determining dynamic properties above this frequency.
4. Water compressibility should be considered in any future numerical modelling of Ruskin Dam.
5. Future numerical modelling of Ruskin Dam should include a review of the

hydrodynamic effect of the reservoir acting on the radial gates.

6. Monolithic behaviour identified at the relatively low ambient amplitude of excitation needs to be critically reviewed for its suitability in extrapolation to larger amplitude excitations, such as large earthquakes.
7. Any future review of the work contained in this thesis would be enhanced considerably by a thorough treatment of the possible errors in the analysis.
8. Parametric studies are best completed at a reservoir elevation at the spillway crest or lower, to eliminate consideration of the hydrodynamic effect of the radial gates on the system.
9. Calibration/parametric studies are best completed on a simple model to facilitate efficiency in this work.

The following recommendations are to for the *general suitability of ambient vibration and analysis techniques for the study of concrete gravity dams*:

1. Ambient vibration and analysis techniques should be considered for use at other gravity dams to determine dynamic properties.
2. A trial test with a limited scope of measurement, is a worthwhile low cost measure which should be considered to quickly ascertain the value of more comprehensive

tests.

3. A trial test should investigate whether there are any measurable excitation sources suitable for use as input signals for single input-single output with output noise system transfer functions.
4. A reservoir drawdown should be employed to obtain two sets of dynamic properties for parametric calibration of the model and for study of the hydrodynamic effects.
5. Further ambient vibration analysis theory needs to be developed which implements non-classical damping considerations.

BIBLIOGRAPHY

ANCO Engineers, Inc., 1982, *Dynamic testing of concrete dams*, National Science Foundation, Washington, D.C., June.

ANSI, 1990, Vibration of buildings-guidelines for the measurement of vibrations and evaluation of their effects on buildings, ANSI S2.47-1990, American National Standard, American Acoustical Society, New York, New York.

ANSYS, 1992, *ANSYS User's Manual for Revision 5.0*, Swanson Analysis Systems, Inc., First Printing, Houston, Pennsylvania.

BCH, 1985, *Ruskin Dam - 1984/85 Investigations*, Report No. H1849, Dam Safety Investigations, November 1988, B.C. Hydro, British Columbia.

BCH, 1988, *Guidelines for selecting and applying seismic criteria for dams*, Report No. H1841, Dam Safety Investigations, Revised March 1988, B.C. Hydro, British Columbia.

BCH, 1995, *Ruskin Dam Deficiency Investigation, 3-D Finite Element Analysis and Assessment of Dam Safety*, Report No. MEP78, Dam Safety Investigations, October 1995, B.C. Hydro, British Columbia.

Battacharjee S.S. and Leger P., 1992, Concrete constitutive models for nonlinear seismic analysis of gravity dams - state-of-the-art, *Can. Journal of Civil Engineering*, No. 19:492-509.

Bazant Z.P. and Gopalaratman V.S., 1992, Fracture mechanics of concrete: an apercu of basic concepts and models, *Fracture Mechanics of Concrete Structures, Proc. First Intl. Conference on Fracture Mechanics of Concrete Structures (FraMCoS1)*, Breckenridge, Colorado, Elsevier Applied Science, New York:145-154.

Bendat J.S. and Piersol A.G., 1993, *Engineering Applications of Correlation and Spectral Analysis*, Second edition, John Wiley and Sons, Inc., Toronto, Ontario.

Bendat J.S. and Piersol A.G., 1986, *Random Data Analysis and Measurement Procedures*,

First edition, John Wiley and Sons, Inc., Toronto, Ontario.

Bougacha S. and Tassoulas J.L., 1991, Seismic analysis of gravity dams. I: Modelling of sediments, *Journal of Engineering Mechanics*, Vol. 117, No.8:1826-1850.

CSA, 1984, *Design of concrete structures for buildings*, CAN3-A23.3-M84 National Standard of Canada, Canadian Standards Association, Rexdale, Ontario

Chiarito V.P. and Mlakar P.F., Modal test of a concrete gravity dam, *Proc. Second Intl. Modal Analysis Conference*:142-148.

Chopra A.K., 1987, Earthquake analysis, design, and safety evaluation of concrete dams, *Proc. Fifth Canadian Conference on Earthquake Engineering*, Ottawa: 39-62.

Chopra A.K. and Zhang L., 1991, Earthquake-induced base sliding of concrete gravity dams, *Journal of Structural Engineering*, Vol. 117, No.12:3698-3719.

Clough R.W. and Penzien J., 1975, *Dynamics of Structures*, First edition, McGraw-Hill, Toronto, Ontario..

Cook R.D., Malkus D.S. and Plesha M.E., 1989, *Concepts and Applications of Finite Element Analysis*, Third edition, John Wiley & Sons, New York, New York.

Cooley J.W. and Tukey J.W., 1965, An algorithm for the machine calculation of complex Fourier series, *Mathematics of Computation*, Vol. 19:297-301.

Danay A. and Adeghe L.N., 1993, Seismic-induced slip of concrete gravity dams, *Journal of Structural Engineering*, Vol. 119, No.1:108-129.

Deinum P.J., Dungar R., Ellis B.R., Jeary A.P., Reed G.A.L. and Severn R.T., 1982, Vibration tests on Emosson arch dam, Switzerland, *Earthquake Engineering and Structural Dynamics*, Vol. 10:447-470.

Deger Y., Cantieni R. and Pietrzko S., 1993, Modal analysis of a concrete gravity dam - fe-modelling versus experiment, *Intl. Workshop on Dam Safety Evaluation*, Vol. 2: 253-262, Grindelwald, Switzerland.

- Dewey R.R., Reich R.W. and Saouma V.E., Uplift modelling for fracture mechanics analysis of concrete dams, *Journal of Structural Engineering*, Vol. 120, No. 10:3025-3044.
- Dungar R., Saouma V.E. and Wittmann F.H., 1991, Conference report: the application of fracture mechanics in dam engineering, *Dam Engineering*, Vol. II, Issue I:3-20.
- Duron Z.H., Ostrom D.K., Aagaard B. and Fischer B., 1994, Evaluating the behaviour of dams during earthquakes, *Hydro Review*, April:54-62.
- Duron Z.H. and Hall J.F., 1991, Experimental investigation of Santa Anita dam, *Proc. Ninth Intl. Modal Analysis Conference*:206-212.
- Duron Z.H. and Hall J.F., 1988, Experimental and finite element studies of the forced vibration response of Morrow Point Dam, *Earthquake Engineering and Structural Dynamics*, Vol. 16:1021-1039.
- Duron Z.H., 1987, Experimental and finite element studies of a large arch dam, *Report No. EERL 87-02*, California Institute Of Technology, Pasadena, California.
- Duron Z.H., Hall J.F., Fink K. and Straser E., 1992, Measuring hydrodynamic pressure during forced vibration testing of concrete dams, *Dam Engineering*, Vol. II, Issue 4:337-355.
- Ewins D.J., 1984, *Modal Testing: Theory and Practise*, First edition, John Wiley and Sons Inc., Toronto, Ontario.
- Fanelli M., Giuseppetti G., Bettinali F., Galimberti C., Castoldi A., Gasirati M., Pizzigalli E., Lozza S., Ruggeri G., 1988, Seismic monitoring of dams a new active surveillance system: basic criteria, operating methods and results obtained, *Proc. Ninth World Conference on Earthquake Engineering*, Vol. VI:409-414.
- Fanelli M., Giuseppetti G., Castoldi A. and Bonaldi P., 1992, Dynamic characterization of Talvacchia dam: experimental activities, numerical modelling, monitoring, *Proc. Tenth World Conference on Earthquake Engineering*, Rotterdam, Holland:2689-2694.
- Felber J.F., 1993, Development of a hybrid bridge evaluation system, *Ph.D. Thesis*, Dept. of

Civil Engineering, University of British Columbia, Vancouver, British Columbia.

Fenves G. and Chopra A.K., 1986, Simplified analysis for earthquake resistant design of concrete gravity dams, *Report No. UCB/EERC-85/10*, Earthquake Engineering Research Centre, University Of California, Berkeley, California.

Fenves G. and Chopra A.K., 1986, EAGD-84 A computer program for earthquake analysis of concrete gravity dams, *Report No. UCB/EERC-84/11*, Earthquake Engineering Research Centre, University Of California, Berkeley, California.

Fenves G. and Chopra A.K. 1985, Reservoir bottom absorption effects in earthquake response of concrete gravity dams, *Journal of Structural Engineering*, Vol. III, No. 3:545-562.

Fenves G., Mojtahedi S. and Reimer R.B., 1989, ADAP-88 - A computer program for nonlinear earthquake analysis of concrete arch dams, *Report No. UCB/EERC-89/12*, Earthquake Engineering Research Centre, University Of California, Berkeley, California.

Fenves G., Mojtahedi S. and Reimer R.B., 1992, Effect of contraction joints on earthquake response of an arch dam, *Journal of Structural Engineering*, Vol. 118, No. 4:1039-1055.

Fok K-L, Hall J.F. and Chopra A.K., 1986, EACD-3D A computer program for three-dimensional earthquake analysis of concrete dams, *Report No. UCB/EERC-86/09*, Earthquake Engineering Research Centre, University Of California, Berkeley, California.

Ghobarah A., El-Nady A. and Tarek A., 1994, Simplified dynamic analysis for gravity dams, *Journal of Structural Engineering*, Vol. 120, No. 9:2697-2715.

Kuo J.S-H, 1982, Fluid-structure interactions: added mass computations for incompressible fluid, *Report No. UCB/EERC-82/09*, Earthquake Engineering Research Centre, University of California, Berkeley, California.

Hall J.F., 1988, The dynamic and earthquake behaviour of concrete dams: review of experimental behaviour and observational evidence, *Soil Mechanics and Earthquake Engineering*, Vol. 7, No. 2, 58-121.

- Hall J.F. and Chopra A.K., 1980, Dynamic response of embankment concrete-gravity and arch dams including hydrodynamic interaction, *Report No. UCB/EERC-80/39*, Earthquake Engineering Research Centre, University of California, Berkeley, California.
- Humar, J.L., 1990, *Dynamics of Structures*, First edition, Prentice-Hall, Toronto, Ontario.
- Luz E., 1991, Experimental modal analysis using ambient vibration, *The Intl. Journal of Analytical and Experimental Modal Analysis*, Vol. 7, No. 1:29-39.
- Mindess, S. and Young J.F., 1981, *Concrete*, First edition, Prentice-Hall, Toronto, Ontario.
- Nuss L.K., 1991, *Current Seismic Structural Analysis For Concrete Dams*, Paper presented at the Second Technical Exchange Between the United States Bureau of Reclamation and the Japan Dam Engineering Centre, 1991, United States Bureau of Reclamation, United States Department of the Interior, Denver, Colorado.
- Pataky T.J., 1994, A need for improvement of existing computational/experimental models used in the assessment of concrete gravity dams, *Proc. Of The Intl. Workshop On Dam Fracture and Damage*, Chambéry, France:195-202.
- Paultre P., Proulx J., Duron Z.H., Phat T.M. and Im O., 1992, Dynamic testing of Outardes 3 gravity dam, *Proc. Tenth World Conference on Earthquake Engineering*, Rotterdam, Holland:3571-3577.
- Pietrzko S., 1993, On the exciter placement for the modal testing of a gravity dam, *Intl. Workshop on Dam Safety Evaluation*, Vol. 2:241-252, Grindelwald, Switzerland.
- Rashad A.A. and Iwan W.D., 1985, Dynamic analysis of short-length gravity dams, *Journal of Engineering Mechanics*, Vol. III, No. 8:1067-1083.
- Rea D., Liaw C-Y and Chopra, A.K., 1975, Mathematical models for the dynamic analysis of concrete gravity dams, *Earthquake Engineering and Structural Dynamics*, Vol. 3: 249-258.
- Rouse, G.C. and Bouwkamp J.G., 1967, Vibration studies of Monticello dam, *Research Report No. 9*, Washington, D.C.: United States Bureau of Reclamation, United States Department of the Interior.

- Saouma V.E., Broz J.J., Bruhwiler E. and Boggs H.L., 1991, Effect of aggregate and specimen size on fracture properties of dam concrete, *Journal of Materials In Civil Engineering*, Vol. 3, No. 3:204-218.
- Schuster N.D., 1994, Dynamic characteristics of a 30 storey building detected during construction from ambient vibration measurements, *M.A.Sc. Thesis*, Dept. of Civil Engineering, University of British Columbia, Vancouver, British Columbia.
- Selvam, V.K., Geethakumari S. and S. Kathirolu, 1993, Natural period of vibration of concrete dams. *Indian Journal Of Power & River Valley Development*, Aug-Sept:170-174.
- SEM, 1993, Combination of test and analysis, *Modal Analysis: Theory and Application Course 28-30 January 1993 Kissimmee Florida*, Society for Experimental Mechanics Inc., Bethel, Connecticut
- Singhal A.C., 1991, Comparison of computer codes for seismic analysis of dams, *Computers & Structures*, Vol. 38, No.1:107-112
- Takahashi, T., 1964, Results of vibration tests and earthquake observations on concrete dams and their considerations, *Proc. Int. Conf. on Large Dams*, Edinburgh, Scotland.
- USBR, 1977, Design criteria for concrete gravity and arch dams, *Monograph No. 19*, United States Bureau of Reclamation, United States Department of the Interior, Revised Printing, Denver, Colorado.
- Westergaard H.M., 1931, Water pressure on dams during earthquakes, *Transactions of the American Society of Civil Engineers*, Vol. 98:418-433.
- Wilson, Bathe and Peterson, 1973, SAPIV, A structural analysis program for static and dynamic response of linear systems, *Report No. EERC-73-11*, Revised April 1973, University of California at Berkeley, Berkeley, California.
- Xuehai L, Wei Z., Wanchun H. and Jinglin D., 1987, Field vibration tests on Ban Xia arch dam by rocket exciters, *Proc. on China-US Workshop on Earthquake Behaviour of Arch Dams*, Dept. of Hydraulic Engineering, Tsinghua University, Beijing, China.

Zangar C.N., 1953, Hydrodynamic pressures on dams due to horizontal earthquakes, *Monograph No. 11*, United States Bureau of Reclamation, United States Department of the Interior, Denver, Colorado.

AMBIENT VIBRATION ASSESSMENT OF RUSKIN DAM DYNAMIC PROPERTIES

APPENDIX A

EQUIPMENT USED, FIELD TESTS AND PHOTOGRAPHS

CONTENTS

<u>Section</u>	<u>Subject</u>	<u>Page</u>
A.1	UBC's Ambient Vibration Testing and Analysis Equipment	171
A.2	Trial Test	172
	A.2.1 Methodology	172
	A.2.2 Preliminary Test Plan	173
	A.2.3 Pre-job Meeting with Ruskin Production	173
	A.2.4 Finalized Test Plan	174
	A.2.3 Trial Test: 23 January 1994	175
A.3	Low/High Reservoir Tests	176
	A.3.1 Methodology	176
	A.3.2 Preliminary Test Plan	177
	A.3.3 Pre-job Meeting with Ruskin Production	177
	A.3.4 Survey/Pre-Installation of Mounting Plate Anchors	178
	A.3.5 Finalized Test Plan	179
	A.3.6 Field Tests	180
	Low Reservoir, 30 April & 1 May 1994	181
	High Reservoir, 7 & 8 May 1994	181
	A.3.7 Post-job Meeting with Ruskin Production	182
A.4	Final Comments on Field Testing	183
	Figures (A1 through A7)	184-190
	Photographs (1 through 11)	191-196

A.1 UBC'S AMBIENT VIBRATION TESTING and ANALYSIS EQUIPMENT

UBC's ambient vibration testing and analysis equipment provides for field measurement, recording and analysis of acceleration. Briefly, the major components of this equipment are:

Sensors

8 sensors (one for each datalogging channel) and their mounting plates. The sensors are Kinemetrics Model FBA-11 accelerometers (Kinemetrics Systems, 222 Vista Avenue, Pasadena, California). They can be configured to measure either horizontal or vertical acceleration of the surface to which they are attached. These accelerometers have an acceleration resolution of 0.2 micro g's. Other specifications of interest are:

- Natural frequency: 50 kHz (damping is 70% of critical)
- Dynamic range: 140 db between 0-10 Hz and 130 db between 0-50 Hz.
- Sensitivity: 5 volts/g.

Cabling

Cabling is necessary to connect the sensors to the stationary signal conditioning, datalogging and monitoring equipment. Cable is available in several runs, in lengths between 50 and 1250 feet. Cabling is shielded to minimize noise.

Data Acquisition and Storage Equipment

Data acquisition and storage equipment consists of the analog/digital convertor, signal conditioners, amplifiers, filters, data storage and control computer

The analog to digital convertor is a Keithley Model 575 Measurement and Control system (Keithley Instrument Inc., 28775 Aurora Road, Cleveland, Ohio, USA, 44139). This unit provides for the sequential sampling of all channels being measured at a rate determined from:

$$\text{Sample rate (in kHz)} = 25/(\text{No. of channels})$$

The Keithley has an AMM2 board which can sample up to 16 channels. However, signal conditioning cards for only 8 channels were available.

The signal conditioner is a Kinemetrics Model VAS-2, containing eight Kinemetrics Model AM-3I signal conditioning cards (one for each datalogging channel). Twelve

different amplification levels are available with this system, from 1 to 2000. The low pass filters can be set to 2.5, 12.5, 25 or 50 Hz. The high pass filters can be set to 0, 0.1 or 5 Hz.

The Keithley analog to digital convertor is controlled by the program AVDA, developed by researchers at UBC (Schuster 1994). This program instructs the Keithley to sample data at a specified rate while also providing for plotting of signals being recorded. AVDA operates on the data storage and control computer. A COMPAQ II portable IBM computer was used for the latter (during an average days testing, about 20 Mb of data were collected).

Spectral Analyzer

The spectral analyzer is a dual channel Zonic model AND 3525. This is used to field review the conditioned signal, so as to provide feedback for field modification of amplification and filtering. The unit can provide for calculation of many frequency domain functions, such as transfer functions, phase, power spectral density and coherence.

Field Analysis Computer and Software

This is used for backup storage and immediate analysis of signals recorded. A generic brande portable PC is used. This computer used programs entitled: P2, ULTRA and VISUAL (see Section 5.3 for a description of these programs). The specifications for this computer were; CPU: Intel 486DX2-66; RAM: 16 Mb; HDD: 546 Mb; Display: high contrast plasma screen.

A.2 TRIAL TEST

A.2.1 Methodology

The following summarizes the major activities in chronological order, undertaken to complete the low/high reservoir tests:

- *Preliminary Test Plan*
- *Pre-job Meetings With Ruskin Production*
- *Finalized Test Plan*
- *Trial Field Test: 23 January 1994*

A.2.1 Preliminary Test Plan

Once approval had been obtained from B.C. Hydro to proceed with a trial test, a preliminary test plan was designed to meet the trial test objectives given in Chapter 7, as well as fitting within the budgetary constraints. The test would need to be completed in one day. As it was uncertain as to whether the HBES could obtain anything of use, the testing was broken up into stages. The first stage would involve measurement of the easily accessible deck across the non-overflow section of the dam. If signals recorded were acceptable, then additional measurements would be taken on the difficult to access ogee.

The preliminary test plan included:

- Measurement Grid
- Manpower/Equipment Requirements
- Time Requirements For Testing

A.2.2 Pre-Job Meeting with Ruskin Production

A Pre-Job meeting with Ruskin Production was held prior to the test, at which the following was discussed:

- *Background*
- *Preliminary Test Plan*
- *Safety (Power System Safety Protection or "PSSP", based on BCHs Workers Compensation Board approved safety procedures)*
- *Work Crew*

Background

Ruskin Production personnel were given some background information for the ambient vibration testing program, including:

- Why ambient vibration testing may be useful to B.C. Hydro
- Funding for the testing
- UBC's experience in the field

Preliminary Test Plan

It was agreed that the proposed measurement grid, including measurements on the ogee, could be completed in a single day. This was important as daylight hours in January were short and there was insufficient funding to conduct tests over two days. The test was scheduled for Saturday 23 January 1994.

Responsibilities for equipment supply were ascertained. UBC would supply all equipment except a safety watch boat and some of the rappelling equipment needed to access the ogee.

Safety

Testing would have to take place on a weekend, to ensure minimal interference with traffic crossing the deck. None of the UBC crew would have BCH's Power System Safety Program (PSSP) training. Ruskin Production would supply appropriately PSSP trained personnel to be present with the UBC crew at all times. Work on the ogee demanded that a clearance be obtained to work downstream of the radial gates. Ruskin Production would supply a person to hold the clearance. In addition during ogee work, a person would need to be located in a boat in the tailwater. The person in the boat would be supplied by Ruskin Production.

Ruskin Production requested proof that members of the UBC crew had accident insurance. This was subsequently provided by UBC. The UBC crew was required to supply themselves with hard hats and steel-toed boots.

Work Crew

The crew makeup was agreed upon. Ruskin Production would supply a three person crew and UBC would supply a six person crew.

A.2.3 Finalized Test Plan

Shown in Figure A1 is a plan of the dam and the measurement grid.

To meet the trial test objectives detailed in Section 7.1, the following was included in the finalized test plan:

- Measurements on the ogee were made on opposite sides of vertical construction joints in the dam.
- Of primary interest was the selection of the reference sensor location. A reference sensor should not be located near an anti-node (inflection

point) or there is a large risk of not identifying the associated natural frequency. To maximize the chance for identification of natural frequencies, two reference sensor locations were chosen to be located where it was suspected that anti-nodes would not be located. Both locations were on the deck, which was easily accessible.

- Points on the east bedrock would be measured to investigate the significance of the bedrock signal (note: no bedrock outcrops were visible on the west abutment).

The resulting model of the measurement grid, used for construction of mode shapes or operating deflected shapes, is shown in Figure A2.

The actual sequencing of measurements is of importance to ensure an efficient use of time during the test. Sensors can be configured to measure either horizontal or vertical acceleration. As well, sensors can be clustered on the mounting plates in arrays, measuring any of the upstream-downstream, vertical or cross-canyon directions. For efficient use of time during the test, it is desirable to minimize the number of changes to sensor measurement orientation and array configuration on a given mounting plate. It is also very desirable to have the sequence of measurements proceed in an orderly fashion across the grid, to minimize cable movements. The final sequence of measurements is shown in Figures A3. Of note:

- It was decided to generally measure only the upstream-downstream and vertical directions. As the upstream-downstream direction was most critical, 2 reference sensors were dedicated to it. A single reference sensor was dedicated to the vertical direction.

Also needed for the Finalized Test Plan is selection of the data acquisition parameters. These are shown in Figure A3 and are discussed in detail in Chapter 7.

A.2.3 Trial Test: 23 January 1994

Ambient conditions during the tests are summarized in Table A1. The reservoir was allowed to fluctuate as power generation requirements during the test dictated.

In addition, there was light road traffic across the deck, consisting of sedans, sport-utility vehicles, light trucks and vans.

Testing began at 8 a.m. A rental van was used to transport equipment to the site. It was parked above the intakes on the east side and was also used to house the HBES equipment.

The initial setup was atop the deck (see Figures A1 and A3). HBES was used to process the signals obtained quickly. Results were found to be acceptable and testing proceeded on the ogee. Two points on the east abutment bedrock were also measured. Sensors were located atop existing concrete stairs which was cast directly against the bedrock.

Climbing onto the ogee was accomplished with the assistance of a chain link ladder and climbing harness attached to a separate rope.

Table A1
Ambient Conditions During Trial Test

RESERVOIR CONDITION	DATE AND TIME	RESERVOIR ELEVATION (ft)	WEATHER	TEMPERATURE, AS RECORDED BY B.C. HYDRO INSTRUMENTATION (degrees Celsius)		RUSKIN POWER GENERATION (MW)
				Alouette Forebay	Stave River above Stave Lake	
Trial	23 January 8 a.m. - 5 p.m.	210.97 - 207.40	Overcast with light showers. No discernible wind.	6.5 - 7.5	not available	70.4 (constant)

A.3 LOW/HIGH RESERVOIR TESTS

A.3.1 Methodology

The following summarizes the major activities in chronological order, undertaken to complete the low/high reservoir tests:

- *Preliminary Test Plan*
- *Pre-job Meeting with Ruskin Production*
- *Finalized Test Plan*
- *Survey/Pre-Installation of Mounting Plate Anchors*
- *Ambient Vibration Field Tests*

- *Post-job Meeting with Ruskin Production*

A.3.2 Preliminary Test Plan

The Preliminary Test Plan was designed to meet the objectives outlined in Chapter 8 and to fit within the budgetary constraints. As such this plan included:

- Measurement Grid
- Manpower/Equipment Requirements
- Scheduling
- Time Requirements for Testing

The Preliminary Test Plan was made prior to meeting with Ruskin Production.

The Preliminary Test Plan called for measurement of considerably more points than the trial test. Planning called for two tests, each at a different reservoir level, of the identical grid of measurement points. In addition, to measurements on the dam deck and ogee, measurements were planned for the dam gallery, to obtain better definition of the mode shapes in the vertical direction and on any bedrock outcrops, to study the bedrock signal.

A.3.3 Pre-Job Meeting with Ruskin Production

A Pre-Job meeting with Ruskin Production was held on 12 April 1994, at which the following was discussed:

- *Preliminary Test Plan*
- *Safety (PSSP based)*
- *Reservoir Control*
- *Work Crew*

Preliminary Test Plan

The measurement grid proposed was acceptable. It was agreed that the proposed measurement grid could be completed in two consecutive days of testing. To finalize the grid, bedrock measurement points had yet to be identified. To save time, concrete/bedrock anchor bolts for securing the sensor

mounting plates would be pre-installed. Bedrock locations required survey to ascertain their positions.

Responsibilities for equipment supply were ascertained. UBC would supply all equipment except a safety watch boat and some of the rappelling equipment needed to access the ogee.

Safety

As with the trial test, the low/high reservoir tests would have to take place during weekend days, to ensure that minimal interference with traffic crossing the deck would occur. Again, none of the UBC crew would be PSSP trained and Ruskin Production would supply appropriately PSSP trained personnel to be present with the UBC crew at all times. However, during ogee work, the person in the boat located in the tailwater would be supplied by UBC.

The UBC crew provided proof of accident insurance. The UBC crew was required to supply themselves with hard hats and steel-toed boots.

Reservoir Control

Ruskin Production indicated that a reservoir drawdown could only be realized during the latter part of April, early part of May, depending on generation requirements. Ruskin Production offered to organize the drawdown. Scheduling hinged on the drawdown test. The second test, at full pool reservoir would have to be as close in time as was reasonable to eliminate any thermal effects on the dynamic characteristics of the dam.

Work Crew

Ruskin Production would supply a three man crew for each day (after the first half day of testing, this was reduced to a two man crew). UBC would supply 4-6.

A.3.4 Survey/Pre-Installation of Mounting Plate Anchors

To finalize the test plan, bedrock measurement locations needed to be identified. While planning for the reservoir control was being made, bedrock measurement locations were determined. An original site plan by Western Power Co. of Canada Ltd., drawing # W5312 (BCH drawing # not available) was reviewed in concert with a field inspection, to best identify bedrock outcrops.

Three full days (19, 26 and 27 April 1994) were required to install anchor bolts for all dam/bedrock measurement locations and to survey the bedrock measurement locations.

A.3.5 Finalized Test Plan

The key item needed to finalize the test plan was the scheduling of the reservoir drawdown. The test was on standby until this was obtained. Final approval for a reservoir drawdown, for the weekend of 30 April/1 May, was eventually obtained by Ruskin Production. To minimize thermal effects, the normal reservoir test would take place the following weekend.

Shown in Figure A4 is a plan of the dam and the final measurement grid for the low/high reservoir tests. Of note is the following:

- The gallery, ogee and deck were measured in a grid across the length of the dam. Ogee measurements were actually made on the nearest pier vertical face.
- Of primary interest was selection of the reference sensor location. A reference sensor should not be located near an anti-node or there is a large risk of not identifying the associated natural frequency.

The trial test had shown the bedrock to exhibit significant signal strength and it was considered briefly for locating the reference sensors. The triaxial reference sensor array was ultimately located on the west side ogee, at node number 13, where the trial test results had suggested no inflection point would be located for the 0-20 Hz frequency range of interest.

- After thorough searching, bedrock was not located on the west side. Therefore, non-dam measurements on the west side were made on the spillway training benches and on a log flume foundation. Bedrock on the east side was extensively measured, where outcrops were accessible.

The resulting model of the measurement grid, used for construction of mode shapes or operating deflected shapes, is shown in Figure A5.

The final sequence of measurements, after taking into account field modifications are shown in Figures A6 and A7. Of note:

- As 8 sensors were available for collecting measurements, it was decided for simplicity to arrange them as two triaxial arrays and one biaxial array. One of the triaxial arrays was dedicated as the reference sensor array, located at node number 13. Triaxial arrays had sensors measuring the upstream-downstream, vertical and cross-canyon

directions, whereas the biaxial array measured the upstream-downstream and vertical directions only.

The data acquisition parameters were kept similar to those chosen for the trial test and are shown in Figures A6 and A7.

A.3.6 Field Tests

Ambient conditions during the tests are summarized in Table A2. The difference in air temperature on the two weekends is not considered to be significant. The relatively low thermal conductivity of concrete would ensure that no stiffness changes would result from the short time span (5 days) between tests.

Table A2
Ambient Conditions During Low/High Reservoir Tests

RESERVOIR CONDITION	DATE AND TIME	RESERVOIR ELEVATION (ft)	WEATHER	TEMPERATURE, AS RECORDED BY B.C. HYDRO INSTRUMENTATION (degrees Celsius)		RUSKIN POWER GENERATION (MW)
				Alouette Forebay	Stave River above Stave Lake	
Low	30 April 10 a.m. - 6 p.m.	188.86 - 189.51	Rain in a.m., clearing by noon, light wind. Sunny in p.m., mild, breezy, sporadic clouds.	not available	9.7 - 10.9	45 - 60
	1 May 9 a.m. - 6 p.m.	188.46 - 188.63	Clear, sunny, mild, no discernible wind	not available	9.4 - 14.8	45
High	7 May 11 a.m. - 7 p.m.	210.34 - 210.41	Sunny, warm, breezy	16.1 - 23.9	14.8 - 28.0	54 -55
	8 May 7 a.m. - 9 p.m.	210.38 - 210.71	Sunny, warm, breezy.	11.5 - 21.7	15.1 - 25.9	42 - 80

In addition, there was light road traffic across the deck, consisting of sedans, sport-utility vehicles, light trucks and vans. The frequency of traffic crossing was markedly less during the early morning or late in the day.

Low Reservoir Test, 30 April & 1 May 1994

Confirmation of a reservoir drawdown was obtained one and a half weeks prior to the actual test. The actual drawdown was 22 ft and required 4 days to complete.

Testing on 30 April did not begin until 10 a.m. A rental van was used to transport equipment to the site. It was parked above the intakes on the east side and was also used to house the HBES equipment for setups on this day, which covered the ogee and east side bedrock. The mounting plates with sensors attached needed to be levelled and aligned with the longitudinal axis of the dam. This proved to be very time consuming on the bedrock (see Photograph 4). Climbing onto the ogee was accomplished with the assistance of a chain link ladder and climbing harness attached to a separate rope. It was noted that water was leaking from the gate seals, even at the lowered water elevation (about 3 1/2 ft above the ogee crest). See Photograph 8. Measurements were completed by about 7:30 p.m. with no significant problems encountered.

On 1 May the equipment was set up in a temporary construction shed located near the east entrance to the deck. On this day the east side, gallery and deck were measured. Photographs 5 and 6 depict activity in the gallery. Work required to level and align mounting plates was minimal and as a result measuring proceeded very quickly, from between 9 a.m. until 6 p.m. It was decided to leave the reference sensors in place through the week.

As a result of the levelling problems encountered on the bedrock, for the high reservoir test, each mounting plate was modified with three threaded holes, in a tripod arrangement, into which were threaded 3 carriage bolts. The mounting plate level could be adjusted by turning the carriage bolts.

High Reservoir Test, 7 & 8 May 1994

Work for the high reservoir test proceeded in the opposite order to the low reservoir test. On 7 May, the east side, gallery and deck were measured. The HBES was set up in the temporary construction shed. Problems were encountered with channels 7 and 8. Occasionally, the data acquisition equipment would not record these channels. The root of this problem was not satisfactorily determined, however, did disappear on the following day. The resulting delays meant that some of the planned measurements for this day were not completed and would have to be included in the following days work.

On 8 May an early start was made. Upon arrival at site, it was noted that water was spilling over the top of the gates. As well, it was noted later that water spilling onto the reference sensors from a leak in the side of the gate which had not been visible during the low reservoir test. It was found later that this leaking water was impinging on the vertical and cross-canyon reference sensors, but not the upstream-downstream sensor. Measurements proceeded smoothly on the east side bedrock. The newly modified mounting plates proved to be easier to level and align. When measurement of the ogee was initiated, a fuse broke in the HBES signal conditioner. A 4 hour delay resulted while a fuse was purchased in the nearby town of Maple Ridge. This delay meant that there was little time to complete the final setups, which consisted of deck measurements left from the previous day. It became necessary to shorten the length of time during which each signal was measured, resulting in only 8 records (data segments) as opposed to the planned 16 (the reduction in the number of data segments will yield higher statistical errors in the frequency domain functions calculated).

A.3.8 Post-Job Meeting with Ruskin Production

The following pertinent comments were agreed regarding the low/high reservoir field testing, at a Post-Job Meeting on 16 May 1994:

- Crew size of 7 was adequate (5 UBC and 2 Ruskin Production).
- Work days were between 12 and 16 hours long, somewhat longer than originally anticipated. Each test would have been better distributed over 3 days, to alleviate crew fatigue and to allow some time for the any problems encountered during testing.
- The reference sensor array should not have been left in place the week between tests. Some data recorded may not be acceptable due to water impinging on the reference sensors from leaks in the radial gate seals. A re-installation of the reference sensor would have revealed the water leak, consequently, it would have been located to avoid water from impinging onto it.
- Pre-installation of concrete/bedrock anchor bolts was a worthwhile time saving measure.
- Levelling and alignment of the mounting plates on the bedrock was improved by the modification of these plates to accept a tripod arrangement of levelling carriage bolts.

A.4 FINAL COMMENTS on FIELD TESTING

The testing is considered to have been well organized and reasonably well executed, however, some problems were encountered.

If BCH undertakes ambient vibration testing in the future, the following should be ensured to maximize the chance for a successful test:

- Effective communication between parties involved.
- Involvement of the local BCH Production office.
- Proper organization including a detailed test plan and clearly identified roles for each member of the crew.
- An experienced crew.
- Familiarity of the dam being tested.
- Good quality equipment.

In addition, it is noted that the trial test was a worthwhile undertaking. In one day, at low cost, the practicality of more comprehensive and expensive testing was able to be investigated. The reservoir drawdown and measurement of bedrock would not have been undertaken if the trial test had not shown the feasibility of ambient testing.

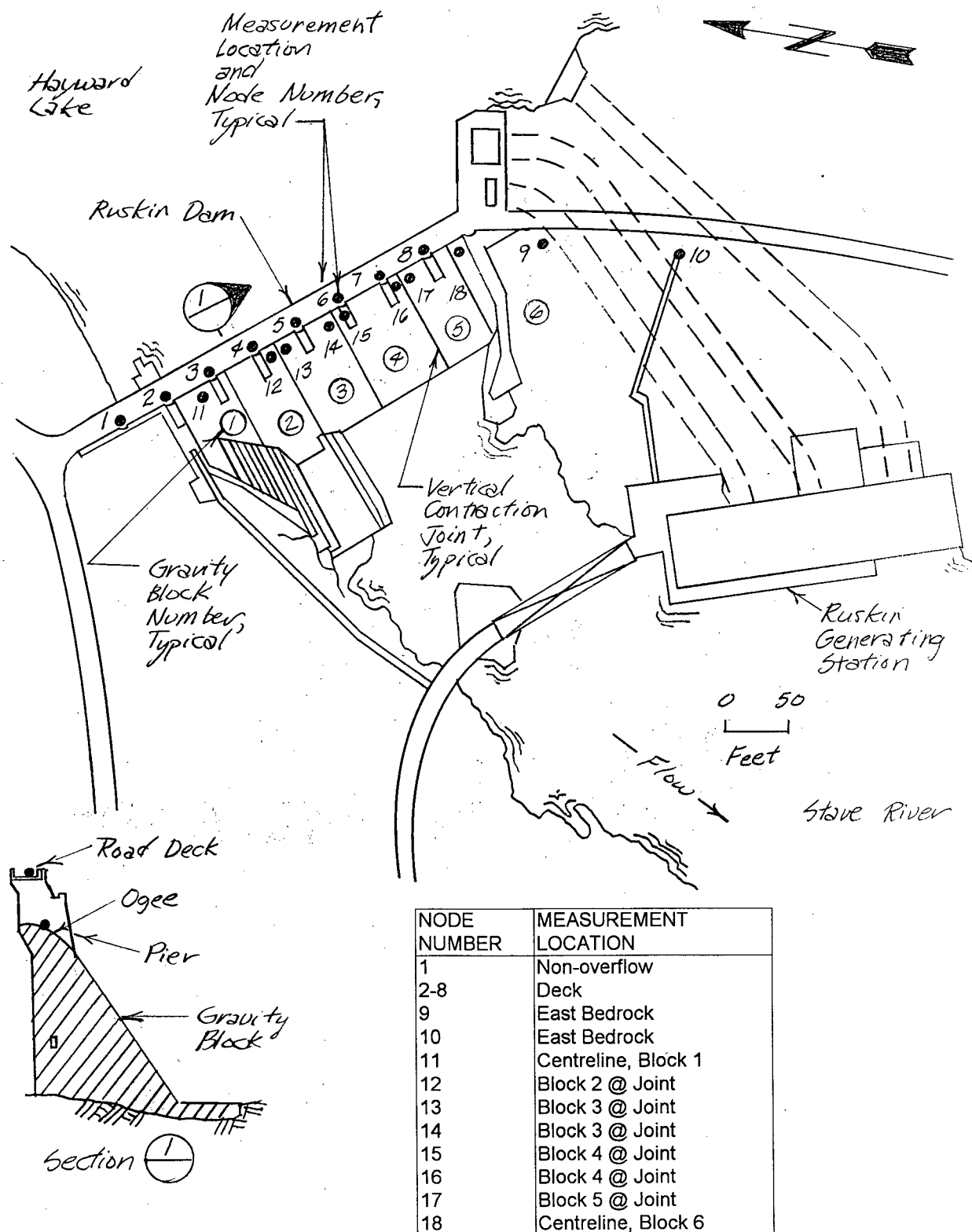
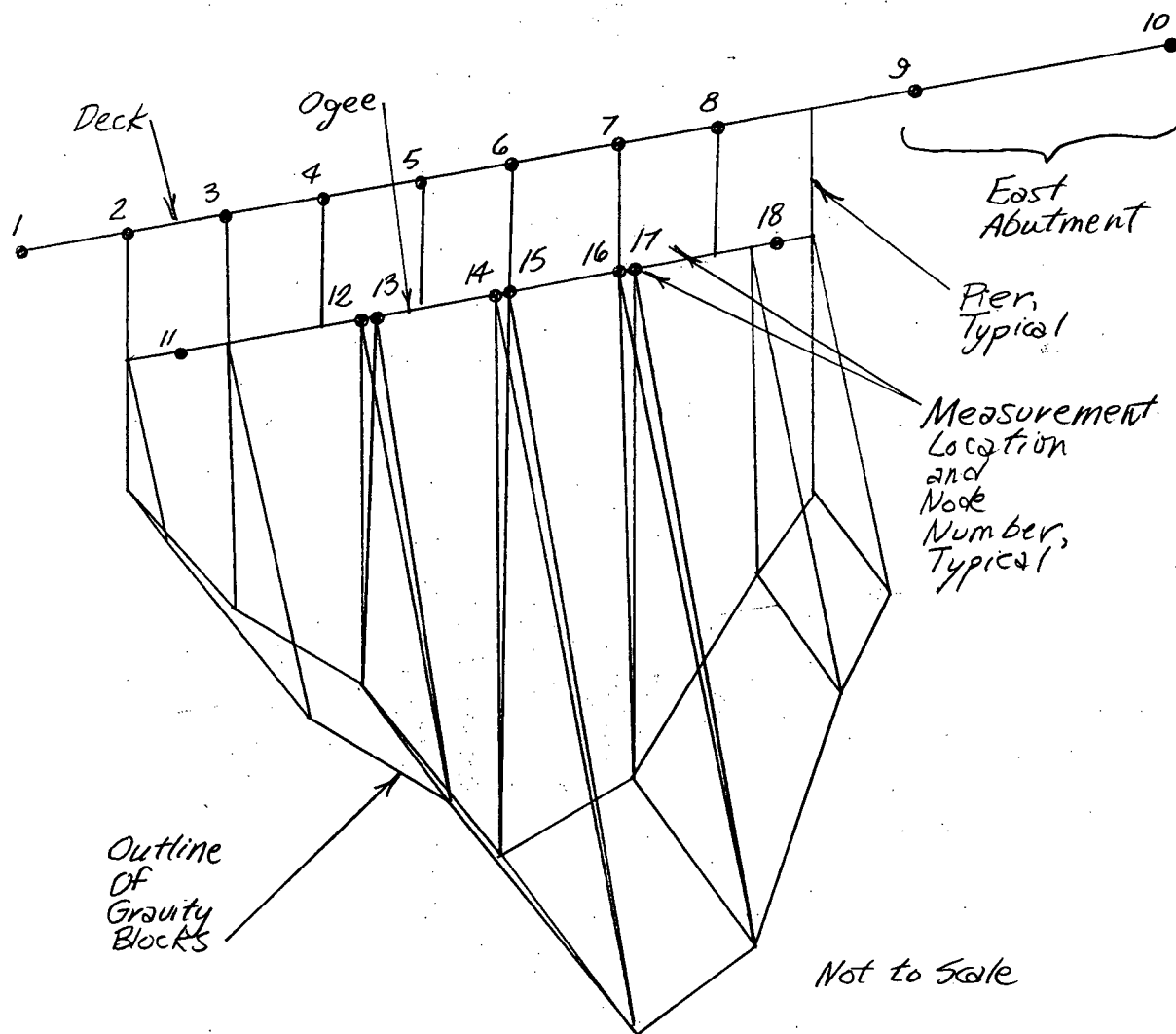


FIGURE A1 PLAN OF RUSKIN DAM AND GENERATION STATION WITH FIELD AMBIENT VIBRATION MEASUREMENT LOCATIONS FOR THE TRIAL TEST

RUSKIN DAM AMBIENT VIBRATION FIELD TRIAL TEST, 23 January 1994



NODE NUMBER	MEASUREMENT LOCATION
1	Non-overflow
2-8	Deck
9	East Bedrock
10	East Bedrock
11	Centreline, Block 1
12	Block 2 @ Joint
13	Block 3 @ Joint
14	Block 3 @ Joint
15	Block 4 @ Joint
16	Block 4 @ Joint
17	Block 5 @ Joint
18	Centreline, Block 6

Notes:

1. See Figure A3 for the sequencing of measurements.

FIGURE A2

MODEL OF RUSKIN DAM (used in "VISUAL") SHOWING
AMBIENT VIBRATION MEASUREMENT LOCATIONS FOR TRIAL TEST

RUSKIN DAM AMBIENT VIBRATION FIELD TESTING, 23 January 1994

DATE	TEST NODE NUMBER AND DIRECTION									COMPUTER FILE (extension: .bbb)
	#	u=upstream-downstream, v=vertical, c=cross-canyon e.g., 5v=node 5 vertical direction								
23 Jan	1	5v	5u	7u	2u	3u	4u	6u	8u	RUSK0101 to RUSK0108
23 Jan	2	5v	5u	7u		12u	12v	13u	13v	RUSK0201 to RUSK0208
23 Jan	3	5v	5u	7u	11u	12u	12v	13u	13v	RUSK0301 to RUSK0308
23 Jan	4	5v	5u	7u	13u	14u	14v	15u	15v	RUSK0401 to RUSK0408
23 Jan	5	5v	5u	7u	13c	14c	14v	15c	15v	RUSK0501 to RUSK0508
23 Jan	6	5v	5u	7u	18u	16u	16v	17u	17v	RUSK0601 to RUSK0608
23 Jan	7	5v	5u	7u	1u	9u	9v	10u	10v	RUSK0701 to RUSK0708
		1	2	3	4	5	6	7	8	
		REFERENCE #								
		CHANNEL #								

DATA ACQUISITION PARAMETER	VALUE
Nyquist Frequency	40 Hz
High Pass Filter	0.1 Hz
Low High Pass Filter	12.5 Hz
No. of Segments	16
Points Per Segment	4096
Global Gain	5 db
Gain	Test #1: Channel # 1: 6 db Others: 18 db Test #'s 2-4: 12 db Test #'s 5-7: 18 db

Notes:

1. For node locations, see Figure A1
2. For computer files, they are of the general form: RUSK0x0y, where x = test # and y = channel #
3. Also recorded were calibration files for every channel of each test, of the general form:
RUSK0xay or RUSK0xby, where x = test #, y = channel #, a = after calibration,
b = before calibration

FIGURE A3	MEASUREMENT SEQUENCE and DATA ACQUISITION PARAMETERS TRIAL TEST
	RUSKIN DAM AMBIENT VIBRATION FIELD TEST, TRIAL, 23 January, 1994

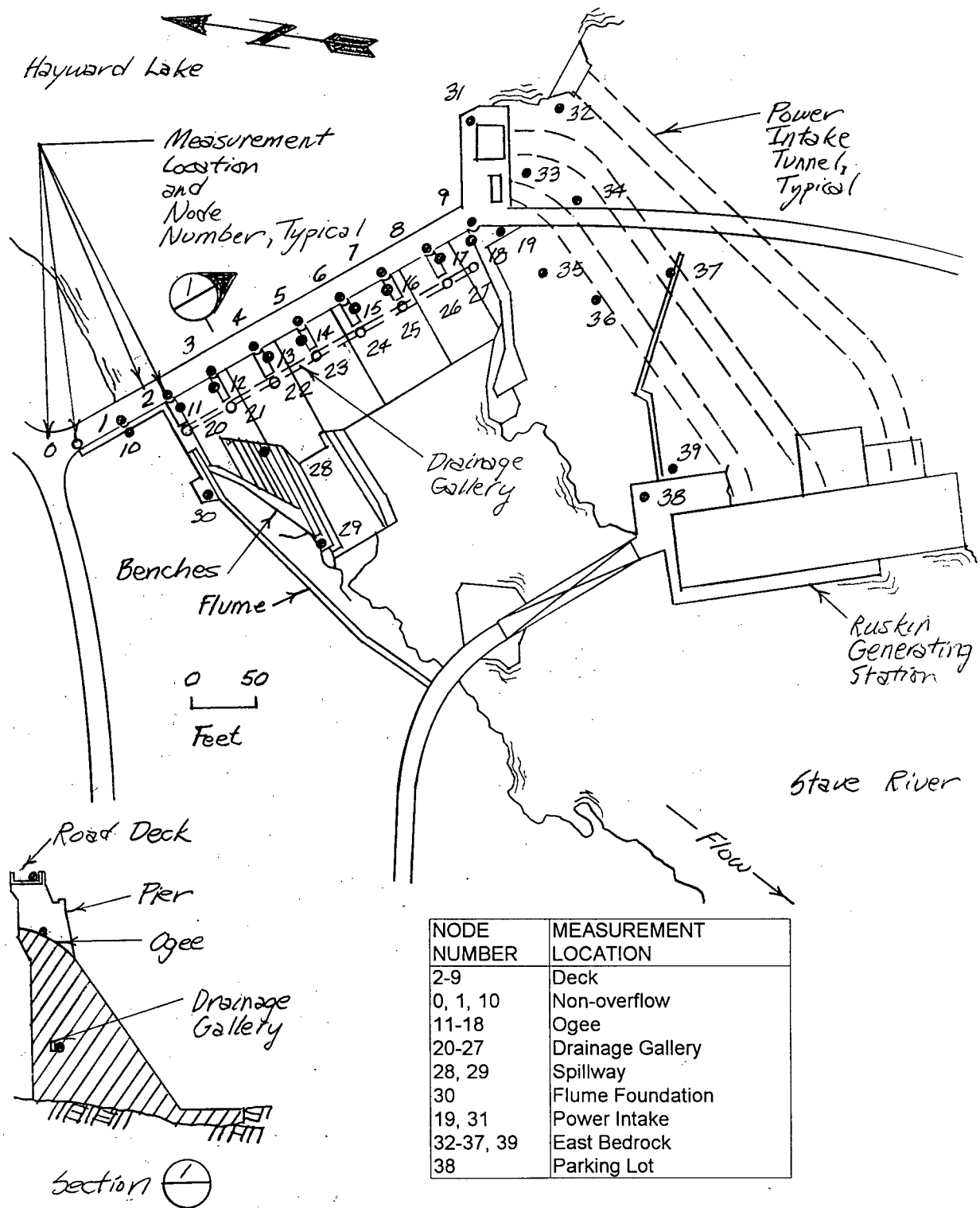
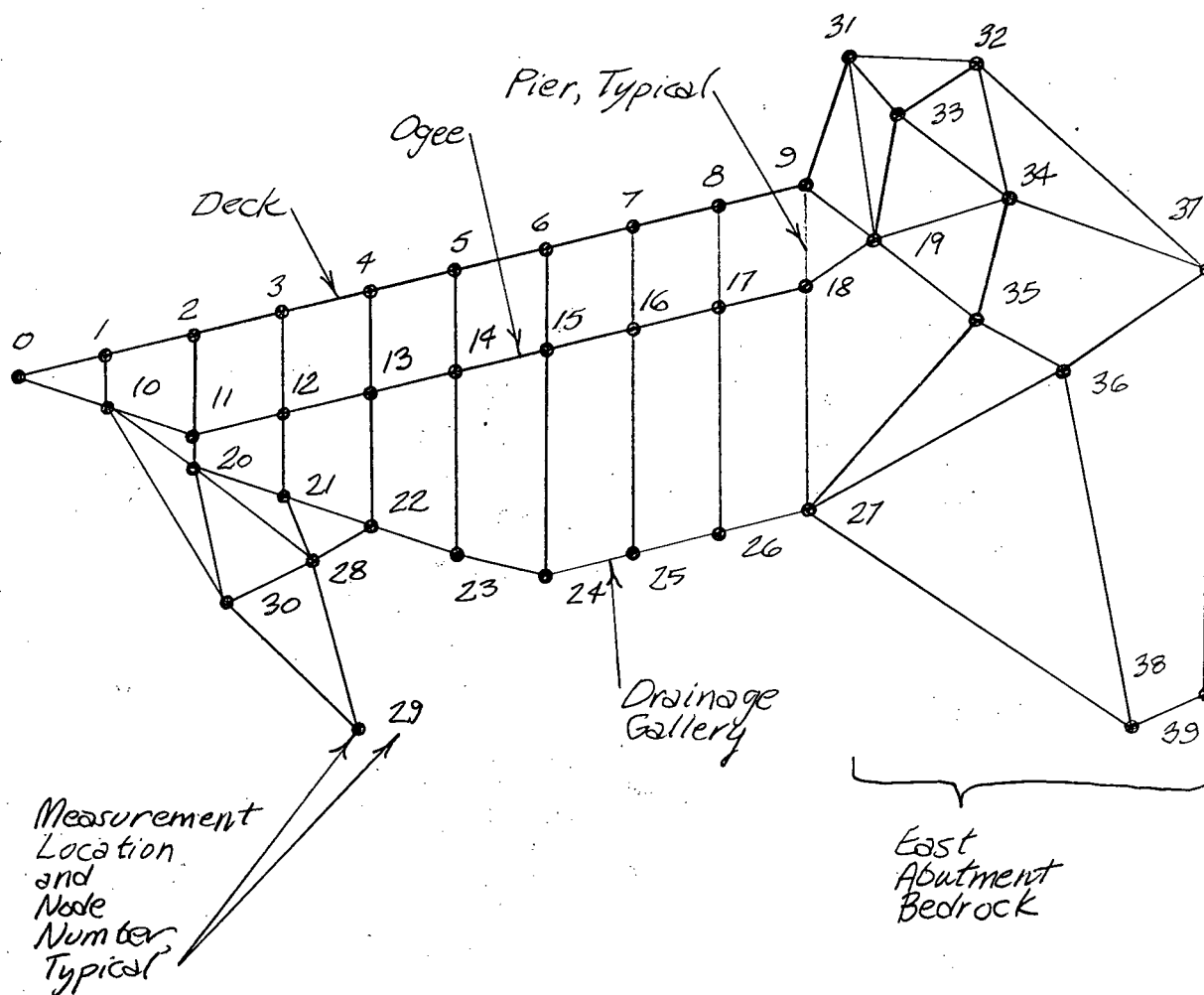


FIGURE A4 PLAN OF RUSKIN DAM AND GENERATING STATION WITH FIELD AMBIENT VIBRATION MEASUREMENT LOCATIONS FOR THE LOW/HIGH RESERVOIR TESTS

RUSKIN DAM AMBIENT-VIBRATION FIELD TESTING, April & May, 1994



NODE NUMBER	MEASUREMENT LOCATION
2-9	Deck
0, 1, 10	Non-overflow
11-18	Ogee
20-27	Drainage Gallery
28, 29	Spillway
30	Flume Foundation
19, 31	Power Intake
32-37, 39	East Bedrock
38	Parking Lot

Notes:

1. See Figures A6 and A7 for the sequencing of measurements.

FIGURE A5	MODEL OF RUSKIN DAM (used in "VISUAL") SHOWING AMBIENT VIBRATION MEASUREMENT LOCATIONS FOR THE LOW/HIGH RESERVOIR TESTS
	RUSKIN DAM AMBIENT VIBRATION FIELD TESTING, April & May, 1994

DATE	TEST NODE NUMBER AND DIRECTION										COMPUTER FILE (extension: .bbb)
	#	u=upstream-downstream, v=vertical, c=cross-canyon e.g., 5v=node 5 vertical direction									
30 April	1	13u	13v	13c	19u	19v	19c	14u	14v	RSKL0101 to RSKL0108	
30 April	2	13u	13v	13c	11u	11v	11c	12u	12v	RSKL0201 to RSKL0208	
30 April	3	13u	13v	13c	15u	15v	15c	16u	16v	RSKL0301 to RSKL0308	
30 April	4	13u	13v	13c	17u	17v	17c	18u	18v	RSKL0401 to RSKL0408	
30 April	5	13u	13v	13c	31u	31v	31c	33u	33v	RSKL0501 to RSKL0508	
30 April	6	13u	13v	13c	32u	32v	32c	34u	34v	RSKL0601 to RSKL0608	
30 April	7	13u	13v	13c	35u	35v	35c	37u	37v	RSKL0701 to RSKL0708	
30 April	8	13u	13v	13c	36u	36v	36c			RSKL0801 to RSKL0806	
30 April	9	13u	13v	13c	38u	38v	38c	39u	39v	RSKL0901 to RSKL0908	
1 May	10	13u	13v	13c	28u	28v	28c	30u	30v	RSKL1001 to RSKL1008	
1 May	11	13u	13v	13c	29u	29v	29c	10u	10v	RSKL1101 to RSKL1108	
1 May	12	13u	13v	13c	26u	26v	26c	27u	27v	RSKL1201 to RSKL1208	
1 May	13	13u	13v	13c	24u	24v	24c	25u	25v	RSKL1301 to RSKL1308	
1 May	14	13u	13u	13v	22u	22v	22c	23u	23v	RSKL1401 to RSKL1408	
1 May	15	13u	13v	13c	20u	20v	20c	21u	21v	RSKL1501 to RSKL1508	
1 May	16	13u	13v	13c	8u	8v	8c	9u	9v	RSKL1601 to RSKL1608	
1 May	17	13u	13v	13c	6u	6v	6c	7u	7v	RSKL1701 to RSKL1708	
1 May	18	13u	13v	13c	4u	4v	4c	5u	5v	RSKL1801 to RSKL1808	
1 May	19	13u	13v	13c	2u	2v	2c	3u	3v	RSKL1901 to RSKL1908	
1 May	20	13u	13v	13c	0u	0v	0c	1u	1v	RSKL2001 to RSKL2008	
		1	2	3	4	5	6	7	8		
		REFERENCE #									
		CHANNEL #									

DATA ACQUISITION PARAMETER	VALUE
Nyquist Frequency	40 Hz
High Pass Filter	0.1 Hz
Low High Pass Filter	12.5 Hz
No. of Segments	16
Points Per Segment	4096
Global Gain	5 db
Gain	Test #'s 1-9, 1-20: 6 db Test # 10, seg.1-12: 6 db Test # 10, seg.13-16: 0 db

Notes:	
1. For node locations, see Figure A4	
2. For computer files, they are of the general form: RSKLxx0y, where xx = test # and y = channel #	
3. Also recorded were calibration files for every channel of each test, of the general form: RSKLxxay or RSKLxxby, where xx = test #, y = channel #, a = after calibration, b = before calibration	
FIGURE A6	MEASUREMENT SEQUENCE and DATA ACQUISITION PARAMETERS
	LOW RESERVOIR
	RUSKIN DAM AMBIENT VIBRATION FIELD TEST, LOW RESERVOIR, 30 April & 1 May, 1994

DATE	TEST NODE NUMBER AND DIRECTION									COMPUTER FILE (extension: .bbb)
	#	u=upstream-downstream, v=vertical, c=cross-canyon e.g., 5v=node 5 vertical direction								
7 May	1	13u	13v	13c	28u	28v	28c	30u	30v	RSKH0101 to RSKH0108
7 May	2	13u	13v	13c	29u	29v	29c	10u	10v	RSKH0201 to RSKH0208
7 May	3	13u	13v	13c	26u	26v	26c	27u	27v	RSKH0301 to RSKH0308
7 May	4	13u	13v	13c	24u	24v	24c	25u	25v	RSKH0401 to RSKH0408
7 May	5	13u	13v	13c	22u	22v	22c	23u	23v	RSKH0501 to RSKH0508
7 May	6	13u	13v	13c	20u	20v	20c	21u	21v	RSKH0601 to RSKH0608
7 May	7	13u	13v	13c	25u	25v	25c	27u	27v	RSKH0701 to RSKH0708
7 May	8	13u	13v	13c	8u	8v	8c	9u	9v	RSKH0801 to RSKH0808
7 May	9	13u	13v	13c	6u	6v	6c	7u	7v	RSKH0901 to RSKH0908
8 May	10	13u	13v	13c	38u	38v	38c	39u	39v	RSKH1001 to RSKH1008
8 May	11	13u	13v	13c	36u	36v	36c	37u	37v	RSKH1101 to RSKH1108
8 May	12	13u	13v	13c	35u	35v	35c	37u	37v	RSKH1201 to RSKH1208
8 May	13	13u	13v	13c	32u	32v	32c	34u	34v	RSKH1301 to RSKH1308
8 May	14	13u	13v	13c	31u	31v	31c	33u	33v	RSKH1401 to RSKH1408
8 May	15	13u	13v	13c	17u	17v	17c	18u	18v	RSKH1501 to RSKH1508
8 May	16	13u	13v	13c	15u	15v	15c	16u	16v	RSKH1601 to RSKH1608
8 May	17	13u	13v	13c	19u	19v	19c	14u	14v	RSKH1701 to RSKH1708
8 May	18	13u	13v	13c	11u	11v	11c	12u	12v	RSKH1801 to RSKH1808
8 May	19	13u	13v	13c	0u	0v	0c	0u	0v	RSKH1901 to RSKH1908
8 May	20	13u	13v	13c	2u	2v	2c	3u	3v	RSKH2001 to RSKH2008
8 May	21	13u	13v	13c	4u	4v	4c	5u	5v	RSKH2101 to RSKH2108
8 May	22	13u	13v	13c	8u	8v	8c	9u	9v	RSKH2201 to RSKH2208
		1	2	3	4	5	6	7	8	
		REFERENCE #								
		CHANNEL #								

DATA ACQUISITION PARAMETER	VALUE
Nyquist Frequency	40 Hz
High Pass Filter	0.1 Hz
Low High Pass Filter	12.5 Hz
No. of Segments	Test #'s 2, 16, 18 and 22: 8 All other Tests #'s: 16
Points Per Segment	4096
Global Gain	5 db
Gain	Test #'s 1-9, 19: 6 db Test #'s 10-15: 0 db Test #'s 20 & 21: 0 db Test # 16: 6 & 12 db Test #'s 17, 18 & 22: 12 db

Notes:

1. For node locations, see Figure A4
2. For computer files, they are of the general form: RSKHxx0y, where xx = test # and y = channel #
3. Also recorded were calibration files for every channel of each test, of the general form:
RSKHxxay or RSKHxxby, where xx = test #, y = channel #, a = after calibration,
b = before calibration

FIGURE A7	MEASUREMENT SEQUENCE and DATA ACQUISITION PARAMETERS HIGH RESERVOIR
	RUSKIN DAM AMBIENT VIBRATION FIELD TEST, HIGH RESERVOIR, 7 & 8 May, 1994



PHOTOGRAPH 1

View from east abutment, towards west abutment, showing the spillway training benches, the disused flume and also detail of the gate/deck/pier arrangement.
RUSKIN DAM AMBIENT VIBRATION FIELD TEST, LOW RESERVOIR, 30 APRIL 94



PHOTOGRAPH 2

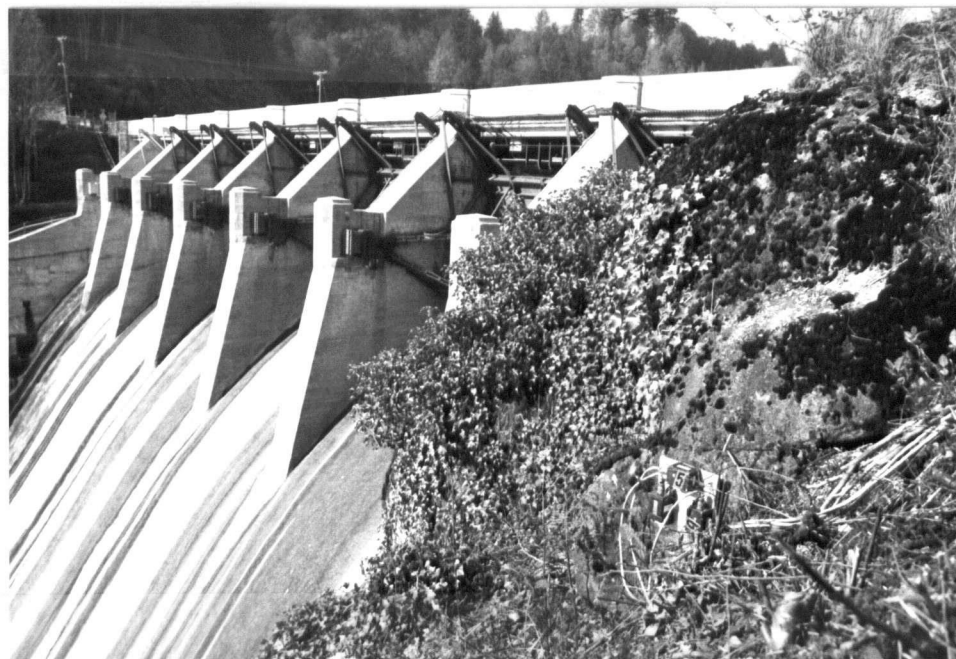
View from east abutment, looking along the deck.
RUSKIN DAM AMBIENT VIBRATION FIELD TEST, LOW RESERVOIR, 30 APRIL 94



PHOTOGRAPH 3

View looking westward along deck. Cabling connecting sensors to HBES equipment is visible.

RUSKIN DAM AMBIENT VIBRATION FIELD TEST, LOW RESERVOIR, 30 APRIL 94



PHOTOGRAPH 4

Detail of sensors at node 35, mounted on an approximately vertical face of bedrock.

RUSKIN DAM AMBIENT VIBRATION FIELD TEST, LOW RESERVOIR, 30 APRIL 94



PHOTOGRAPH 5 (TOP)

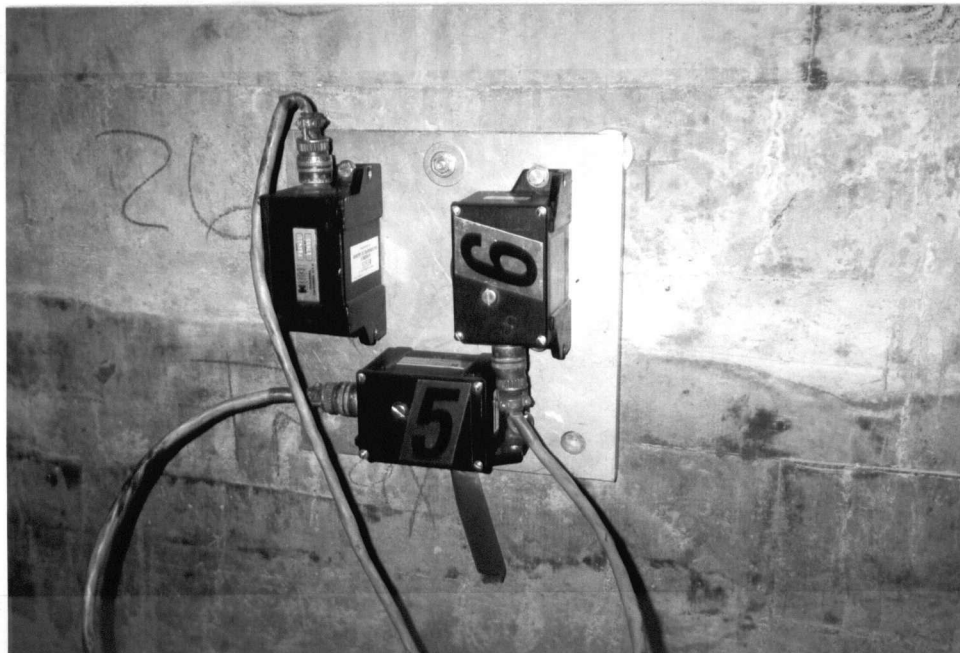
Sensors mounted at nodes 26 and 27, at east end of gallery.

RUSKIN DAM AMBIENT VIBRATION
FIELD TEST, LOW RESERVOIR,
1 MAY 94

PHOTOGRAPH 6 (BOTTOM)

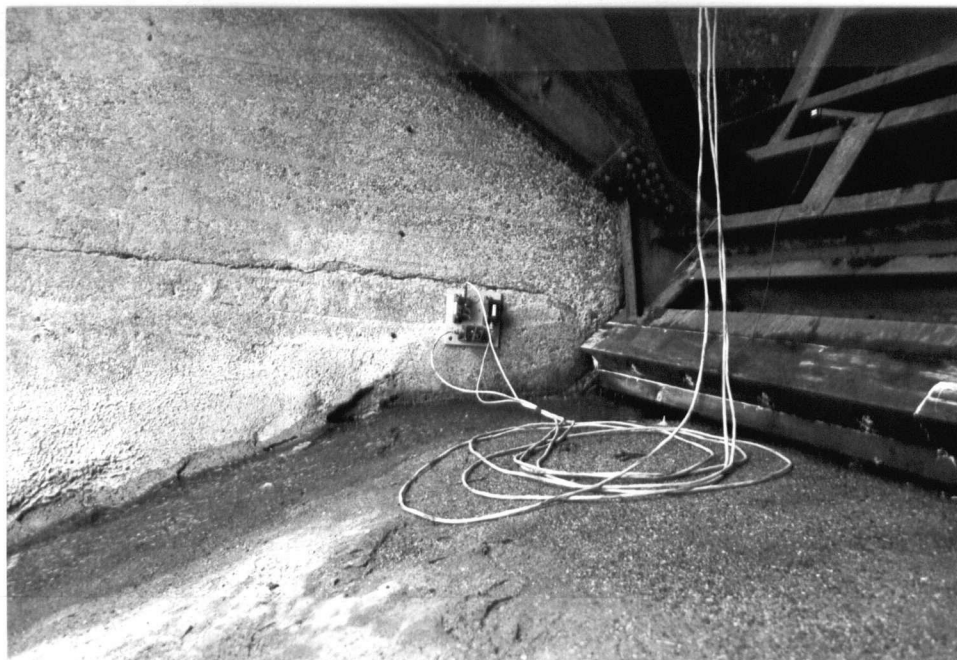
Detail of sensors shown in
Photograph 5.

RUSKIN DAM AMBIENT VIBRATION
FIELD TEST, LOW RESERVOIR,
1 MAY 94





PHOTOGRAPH 7	Sensors located on west side of pier at node 16.
	RUSKIN DAM AMBIENT VIBRATION FIELD TEST, LOW RESERVOIR, 30 APRIL 94



PHOTOGRAPH 8	Detail of sensors located on east side of pier at node 15.
	RUSKIN DAM AMBIENT VIBRATION FIELD TEST, LOW RESERVOIR, 30 APRIL 94

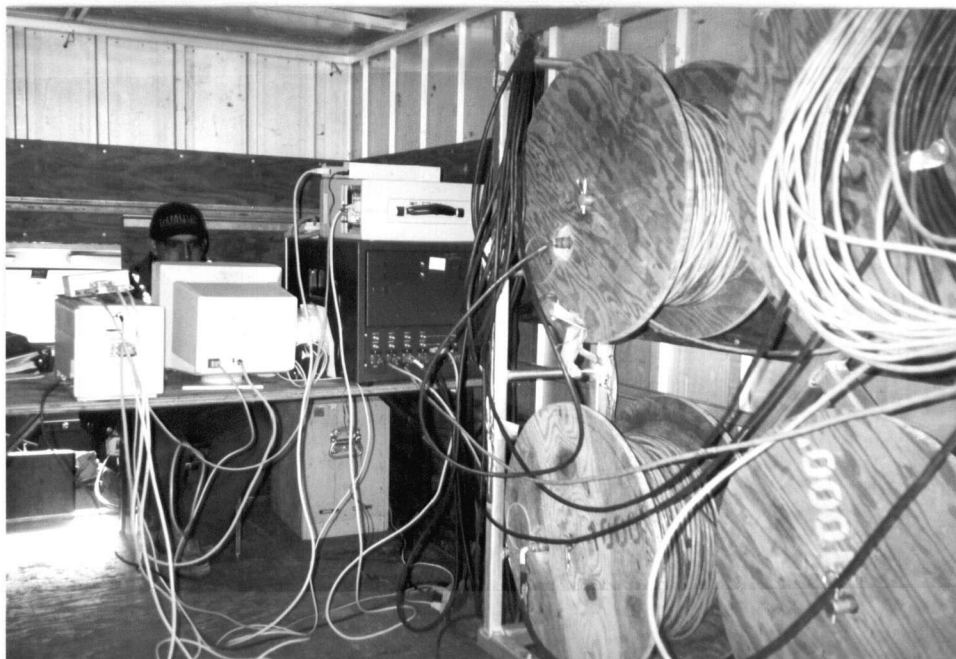


PHOTOGRAPH 9	Looking down stairway on east abutment. Sensors at Node 37 are visible in the foreground. The powerhouse is visible in the left background. RUSKIN DAM AMBIENT VIBRATION FIELD TEST, LOW RESERVOIR, 30 APRIL 94
--------------	--



PHOTOGRAPH 10

HBES equipment: signal conditioner with amplifiers/filters (background), analog to digital convertor (not shown, within signal conditioner), data collection control computer (atop signal conditioner), data analysis computer (foreground).
 RUSKIN DAM AMBIENT VIBRATION FIELD TEST, HIGH RESERVOIR, 8 MAY 94



PHOTOGRAPH 11

HBES equipment, as setup in the back of a rental van. Note the cabling connected to the back of the signal processor. Spectrum analyzer is located in box on floor.
 RUSKIN DAM AMBIENT VIBRATION FIELD TEST, HIGH RESERVOIR, 8 MAY 94

**AMBIENT VIBRATION ASSESSMENT OF RUSKIN DAM
DYNAMIC PROPERTIES**

APPENDIX B

ANALYSIS OF TRIAL TEST, 23 JANUARY 1994

CONTENTS

<u>Section</u>	<u>Subject</u>	<u>Page</u>
B.1	Hybrid Bridge Evaluation System (HBES) Analysis	198
	B.1.1 General	198
	B.1.2 Average Normalized Power Spectral Densities (ANPSDs)	199
	B.1.3 ULTRA and VISUAL	200
	B.1.4 Hybrid Bridge Evaluation System (HBES) Analysis Summary . . .	201
B.2	Complementary Analysis	202
	B.2.1 Coincident Time Histories	202
B.3	Trial Test Conclusions	203
	Figures (B1 through B10)	205-214

B.1 HYBRID BRIDGE EVALUATION SYSTEM (HBES) ANALYSIS

B.1.1 General

Initial field review of signals using HBES from the first setup of sensors on the deck only, indicated that the signal amplitude was adequate. Therefore the decision was made to proceed with measurements on the ogee and abutments.

In the office, locations measured were sorted by descending order of signal amplitude. This was done by calculating an average positive peak acceleration for a representative sampling of the segments. The following is the resulting order. In brackets is shown the calculated average acceleration value in units of micro-g's, along with the fraction of the total segments which were used in calculating the average:

1. Deck atop ogee, upstream-downstream (860, 112/304)
2. Deck, non overflow section, upstream-downstream (710, 16/16)
3. Ogee, upstream-downstream (360, 96/176)
4. Deck atop ogee, vertical (210, 63/112)
5. East Bedrock, upstream-downstream (170, 32/32)
6. East Bedrock, vertical (140, 32/32)
7. Ogee, vertical (120, 80/160)
8. Ogee, cross-canyon (70, 24/48)

The values shown above compare with the accelerometer resolution of 0.2 micro-g's. It is found that maximum amplitudes are between 4300 and 350 times greater than the sensor resolution.

UBC has conducted ambient vibration testing on several other structures. The stiffest of these was a piled wharf at Squamish, B.C. This structure exhibited a maximum acceleration amplitude in the order of 50 micro-g's. Data obtained was judged to be adequate to complete meaningful analysis of the main dynamic characteristics of the wharf.

It is concluded that the ambient vibrations obtained during the Ruskin trial test were of sufficient amplitude to permit meaningful analysis of the main dynamic characteristics of the dam.

B.1.2 Average Normalized Power Spectral Densities (ANPSDs)

Plotted in Figure B1 are ANPSDs for the ogee and east abutment, plotted in low resolution as an average of 16 segments, with between 2-8 measurement locations (nodes) used. The nodes used are listed in Table B1 and shown in Figure A1 in Appendix A.

Table B1
Nodes Used in ANPSD Calculation

LOCATION	NODES
Ogee	11-18
East Bedrock	9 and 10

The frequency ranges which show the greatest strength are shown in Table B2.

Table B2
ANPSD Frequency Ranges/Peaks Of Significant Strength
Trial Test (Low Resolution, 0.0781 Hz)

LOCATION	DIRECTION	RANGE (Hz)	PEAK (Hz)
Ogee	Upstream-Downstream and Vertical	7.0-8.0 8.5-9.2 11.9-12.2 12.8-13.7 13.9-14.1 15.8-16.2 17.9-18.1	7.7 9.0 12.1 13.6 14.0 16.1 18.0
East Bedrock	Upstream-Downstream	8.5-9.0 11.9-12.8 15.9-16.7 17.9-18.1	8.8 12.1, 12.4 16.1, 16.5 18.0

Of note:

1. The ogee exhibits ANPSD maximas and the east bedrock ANPSDs do not over the ranges:
 - 7.0-8.0 Hz
 - 12.8-14.2 Hz

This suggests independent amplified action of the dam and therefore these ranges are considered to include potential natural frequencies of the dam.

2. The east bedrock and ogee have common ANPSD maximas at:

- 8.5-9.2 Hz
- 11.9-12.8 Hz
- 15.8-16.7 H.
- 17.9-18.1 Hz

These ranges therefore include potential natural frequencies which may encompass both the dam and east bedrock or could be representative of frequency components of the excitation within the east bedrock which is causing large amplitude motion in the dam.

It is important to note that only two points on the east bedrock were measured, one of these was very close to the east abutment of the dam. To better understand the significance of the east bedrock signal, additional measurements are necessary to study it, for instance, to see if there is any spatial relationship to what is measured.

The use of a low pass filter equal to 12.5 Hz has probably hampered determination of dynamic properties above this frequency.

B.1.3 ULTRA and VISUAL

Shown in Figs. B2 through B4 are the operating deflected shapes corresponding to each of the significant frequencies (as identified below) in each potential natural frequency range indicated from the ANPSD analysis. Each plot was made without coherence or phase windows.

The following details each operating deflected shape identified, as defined along the ogee/deck in the upstream-downstream direction. Insufficient data was recorded for the vertical direction. The operating deflected shapes constructed with reference sensor 5, as it yielded the most sensible data.

Coherence: 0.9 Phase: 10 degrees

7.0-8.0 Hz: Single curvature of the ogee and the deck. Very good resilience of the operating deflected shape to the phase/coherence windows is indicated, with the best

judged to be at 7.2-7.4 Hz. Its fundamental single curvature shape indicates that it probably is the first natural frequency and corresponding mode shape of the dam.

8.5-9.2 Hz: Single curvature over the central portion of the ogee, with two inflection points near its ends. Almost all nodes do not participate for the phase/coherence windows indicated, suggesting that the frequency range does not contain a probable natural frequency.

11.9-12.8 Hz: Single curvature over most of the ogee. An inflection point near the east side of the ogee and in the non-overflow section. The east side bedrock may be participating in the response, which exhibits good resilience with application of the phase/coherence window indicated. The best resilience is judged to be at 11.9-12.3 Hz.

12.8-14.2 Hz: Almost double curvature of the ogee. One inflection point on Block 4 and a second in the non-overflow section. The 13.2-13.6 Hz frequency range is judged the most resistant to the application of the phase/coherence window.

15.8-16.7 Hz: Double curvature plus of the ogee, with possibly additional curvatures extending into the abutment bedrock and the non-overflow section. One inflection point on Block 3, the other block locations are not determined. This frequency range does not exhibit strong resilience to the phase/coherence window. At 16.9 Hz the best resilience is found.

For analysis of the low/high reservoir tests analysis with VISUAL will concentrate on using the phase factor alone, as it appears to be the more fundamental indicator of a probable natural frequency.

B.1.4 Hybrid Bridge Evaluation System (HBES) Analysis Summary

Probable natural frequencies and the corresponding mode shapes are found at:

1. 7.3 +/- 0.1 Hz for which the corresponding mode shape is a single curvature of the ogee in the upstream-downstream direction.
2. 12.1 +/- 0.2 Hz for which the corresponding mode shape contains a single inflection point near the east side of the ogee.

3. 13.4 +/- 0.2 Hz for which the corresponding mode shape contains one inflection point on the ogee.

Probable natural frequencies at 7.5-9.2, \pm 9.0 Hz and 15.8-16.7 Hz suggested by ANPSD analysis are not supported with phase/coherence criteria as found in the ULTRA and VISUAL analysis.

Additional measurements are felt to be needed to better detail response shapes. The non-overflow section and the overflow section gallery should be instrumented. As well, more extensive measurements in the vertical and cross-canyon directions are needed.

Additional measurements on the east bedrock are also required to study its significance

It is recognized that the use of a low pass filter equal to 12.5 Hz has probably hampered identification of natural frequencies above this value.

B.2 COMPLEMENTARY ANALYSIS

B.2.1 Coincident Time Histories

Acceleration time histories were obtained near vertical contraction joints on adjacent gravity blocks. Each of these, as well as all others recorded at Ruskin Dam is 16 segments long, with each segment containing 4096 points. It is not practical to reproduce all of this data for this report. Manually scanning of these records shows that the gravity block motions are highly coupled in the three directions measured (upstream-downstream, cross-canyon and vertical). Shown in Figures B5 through B7 are short intervals of these records. These figures illustrate the highly coupled motion found in the data.

When response shapes were determined, the modal ratios for nodes located on opposite sides of a vertical contraction joint are very close in magnitude, but not identical. This effect is shown in Figures B2 through B4, where the symbols which indicate node points along the ogee are not coincident in amplitude for a given response frequency. In some instances this may simply be a function of the curvature of the mode shape and the distance between the measurement points. However, the difference does appear incorrect in some cases, e.g.: Figure B3, 12.1 Hz, vertical motion (downstream elevation), modes 12 and 13 exhibit a significant dislocation. The gain of the relative transfer function is used to plot these operating deflected shapes. Error in the gain calculation is suspected of causing the misalignment.

Visual inspection of the shotcrete on the ogee showed cracking above the design location of the vertical contraction joints. This suggests differential

movement of at least the outer downstream skin of the gravity blocks has occurred. The movement is most likely caused by thermal loading. Thermal expansion and contraction would be most severe in the outermost thickness of the dam gravity blocks, where the average concrete (and shotcrete) temperature change due to ambient temperature fluctuations, would be greatest.

On the day of the test, 23 January 1994, the average temperature of the outer thickness of the dam concrete (and shotcrete) is expected to have been close to its annual minimum temperature and thermal contraction effects would be near their most influential. If differential movement between blocks were to be detected, it would be most probable when conditions were as on the day of the test. However, the data clearly shows that no significant independent motion was detectable.

Shown in Figures B8 through B10 are plots of cross-spectral density, coherence and phase for each pair of accelerometers. These clearly show that above 5 Hz, the coherence is very nearly equal to 1 and the phase is equal to zero (the exception is the cross-canyon measurement for nodes 14 and 15 where the phase is equal to nearly 180 degrees, probably because the accelerometers were placed incorrectly in the field). The high coherence and consistent phase suggests the blocks are moving together.

It is concluded that the gravity blocks did not exhibit any independent motion, in any of the three directions measured.

It must be kept in mind, that the low level of ambient vibration during the day of the test may have been insufficient to cause independent action. Large excitations, such as earthquakes, may cause non-linear independent action. Further analysis of the dam, considering the shear/tensile strengths of the vertical contraction joints, is required to determine whether this is possible.

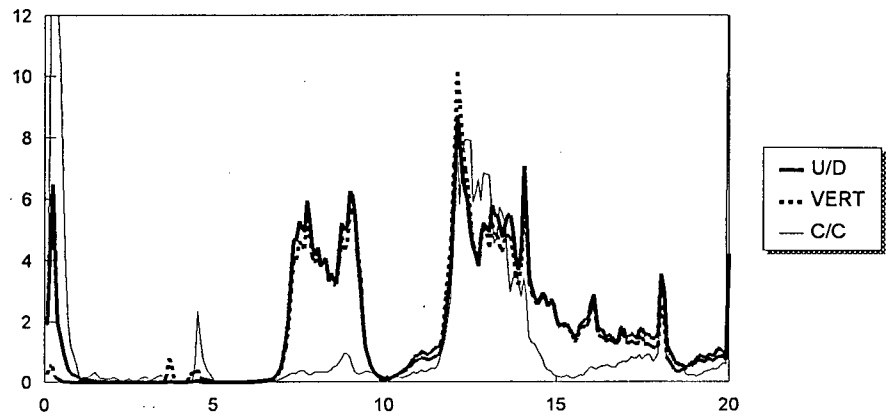
B.3 TRIAL TEST CONCLUSIONS

The following conclusions are drawn with respect to the objectives set for the trial test, as discussed in Section 7.1 of the main text:

1. *Objective 1, Determine Suitability Of Ambient Vibration Signal Strength:* The signal strength was concluded sufficiently strong to allow for ambient vibration signal analysis.
2. *Objective 2, Cursory Determination Of Dynamic Properties Of Dam:* The signal strength was concluded sufficient to allow for determination of dynamic properties. The natural frequencies and mode shapes (as defined along the ogee) determined were:
 - 7.4 +/- 0.1 Hz, single curvature

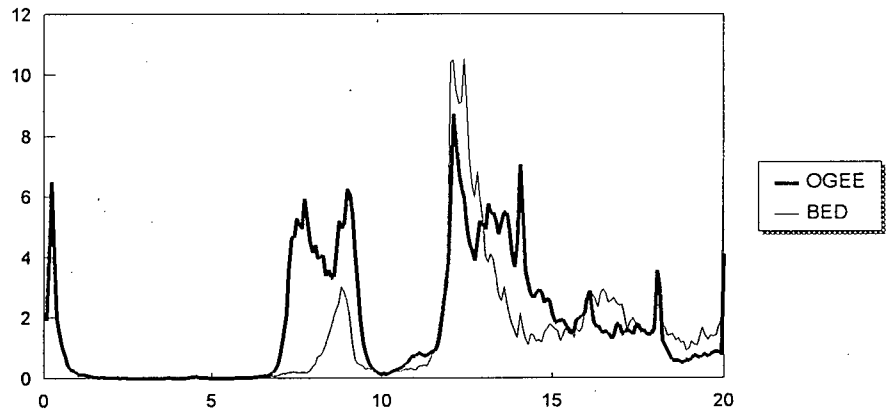
- 12.1 +/- 0.2 Hz, near single curvature (one inflection point)
 - 13.4 +/- 0.2 Hz, near one and one half curvatures (one inflection point)
3. *Objective 3, Determine Whether Gravity Blocks Exhibit Monolithic Or Independent Dynamic Behaviour:* It was concluded that at the ambient level of excitation, the gravity blocks indicated monolithic behaviour.
 4. *Objective 4, Cursory Analysis Of Bedrock Signals:* It was concluded that insufficient measurements of the east bedrock had been made to complete understanding of their significance.

OGEE



OGEE & EAST BEDROCK

Upstream-
Downstream
Direction



NOTES:

1. Resolution: Low (0.0781 Hz), Window: Hanning
2. Number of segments: 16, number of sensors to produce averages:
Ogee: upstream-downstream: 8, cross-canyon: 6, vertical: 6
East Bedrock: upstream-downstream: 2
4. In legends shown, U/D=upstream-downstream direction, V = vertical direction, C/C = cross-canyon direction, BED = east bedrock
5. Abscissa: frequency (Hz), ordinate: ANPSD magnitude

FIGURE B1

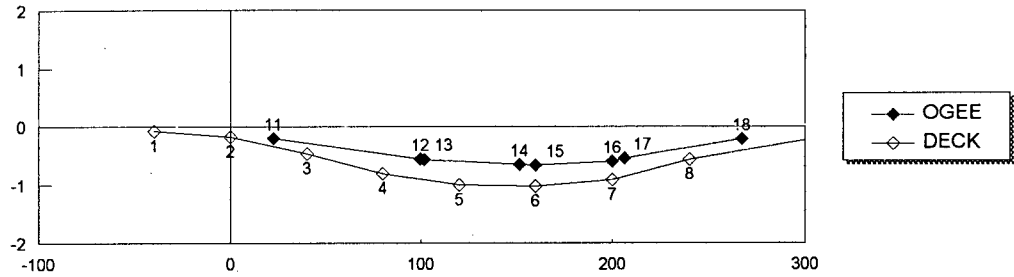
ANPSD Functions

Ogee and East Bedrock

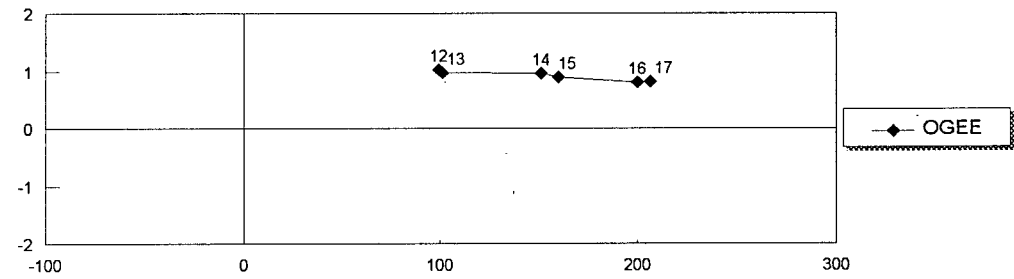
RUSKIN DAM AMBIENT VIBRATION TRIAL FIELD TEST, 23 January 94

7.3 Hz

UPSTREAM
DOWNSTREAM

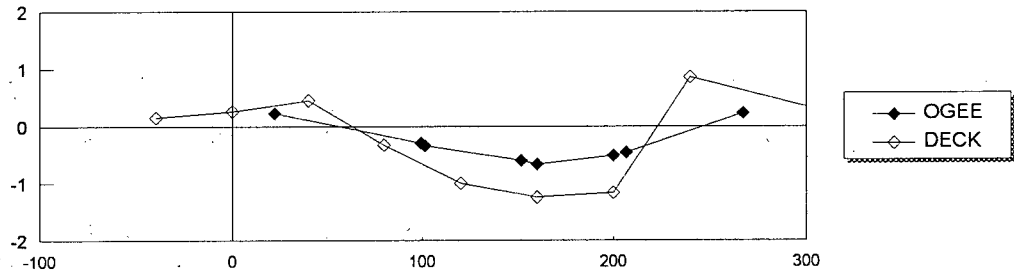


VERTICAL

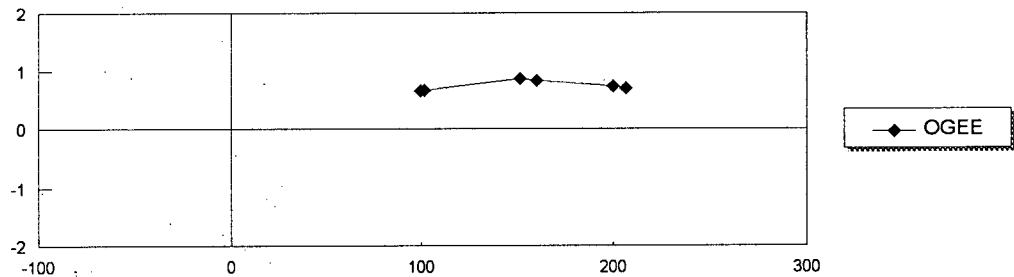


9.0 Hz

UPSTREAM
DOWNSTREAM



VERTICAL



NOTES:

1. Abscissa: normalized amplitudes.
2. Ordinate: measured in feet from centreline of pier on west side of overflow section, overflow length is 280 feet
3. Reference sensor: Node 5
4. PHASE WINDOW: 0-180 degrees, COHERENCE WINDOW: 0-1, Resolution: Low (0.0781 Hz), Window: Hanning
5. Node numbers shown for response at 7.3 Hz only, see Figure A1 for location
6. Positive sense: upstream in upstream-downstream plots, up in vertical plots

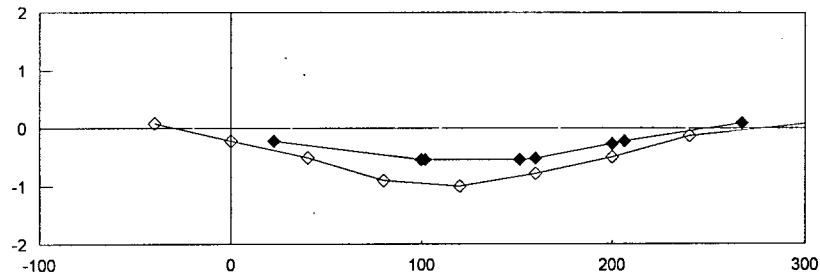
FIGURE B2

OPERATING DEFLECTED SHAPE (defined at ogee and deck)
7.3 Hz and 9.0 Hz

RUSKIN DAM AMBIENT VIBRATION TRIAL FIELD TEST, 23 January 94

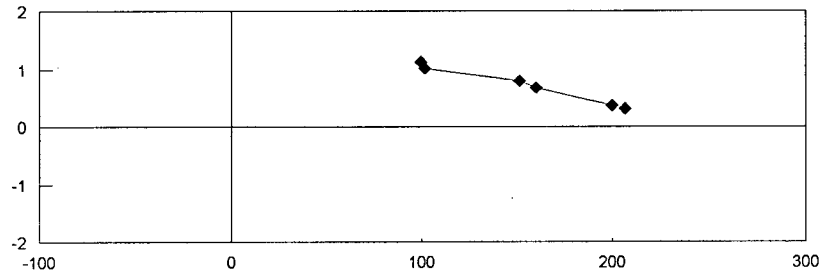
12.1 Hz

UPSTREAM
DOWNSTREAM



—◆— OGEE
- - -◆- - DECK

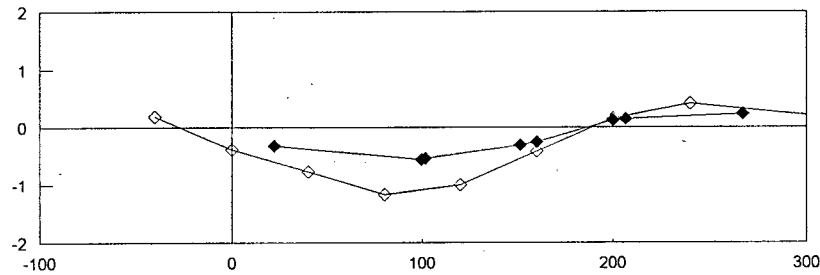
VERTICAL



—◆— OGEE

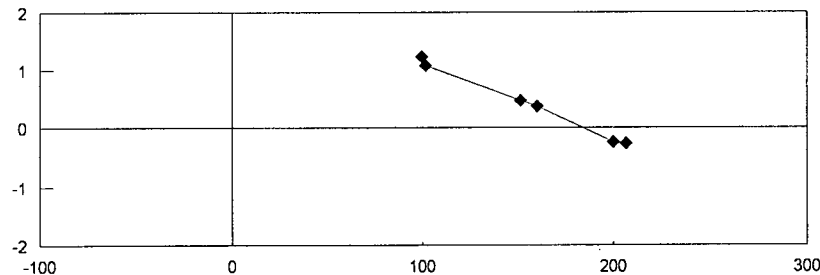
13.4 Hz

UPSTREAM
DOWNSTREAM



—◆— OGEE
- - -◆- - DECK

VERTICAL



—◆— OGEE

NOTES:

1. Abscissa: normalized amplitudes.
2. Ordinate: measured in feet from centreline of pier on west side of overflow section, overflow length is 280 feet
3. Reference sensor: Node 5
4. PHASE WINDOW: 0-180 degrees, COHERENCE WINDOW: 0-1, Resolution: Low (0.0781 Hz), Window: Hanning
5. Node numbers shown for response at 7.3 Hz only, see Figure A1 for location
6. Positive sense: upstream in upstream-downstream plots, up in vertical plots

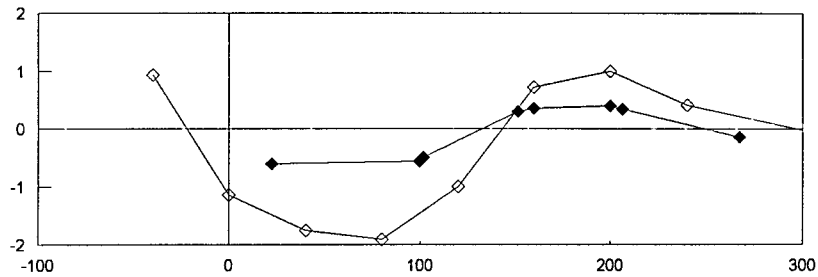
FIGURE B3

OPERATING DEFLECTED SHAPE (defined at ogee and deck)
12.1 Hz and 13.4 Hz

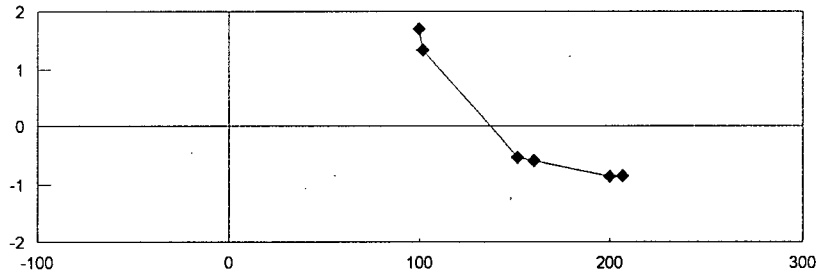
RUSKIN DAM AMBIENT VIBRATION TRIAL FIELD TEST, 23 January 94

16.9 Hz

UPSTREAM
DOWNSTREAM



VERTICAL



NOTES:

1. Abscissa: normalized amplitudes.
2. Ordinate: measured in feet from centreline of pier on west side of overflow section, overflow length is 280 feet
3. Reference sensor: Node 5
4. PHASE WINDOW: 0-180 degrees, COHERENCE WINDOW: 0-1, Resolution: Low (0.0781 Hz), Window: Hanning
5. Node numbers shown for response at 7.3 Hz only, see Figure A1 for location
6. Positive sense: upstream in upstream-downstream plots, up in vertical plots

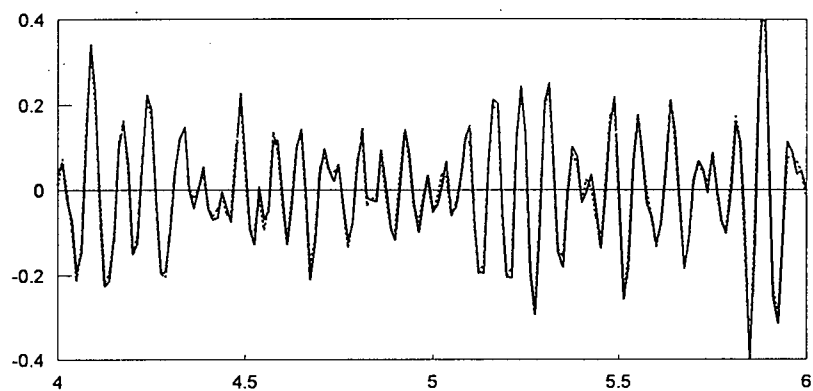
FIGURE B4

OPERATING DEFLECTED SHAPE (defined at ogee and deck)

16.9 Hz

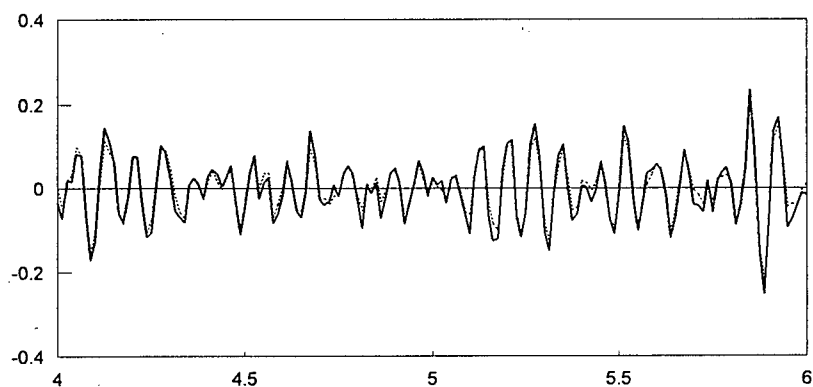
RUSKIN DAM AMBIENT VIBRATION TRIAL FIELD TEST, 23 January 94

UPSTREAM-
DOWNSTREAM



— BLOCK 2
..... BLOCK 3

VERTICAL



— BLOCK 2
..... BLOCK 3

NOTES:

1. Abscissa: acceleration in mg's, ordinate: time in seconds

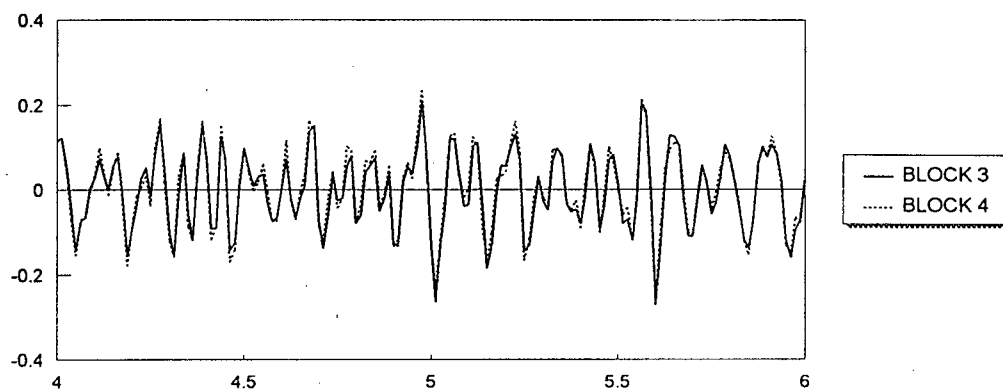
FIGURE B5

ACCELERATION TIME HISTORIES

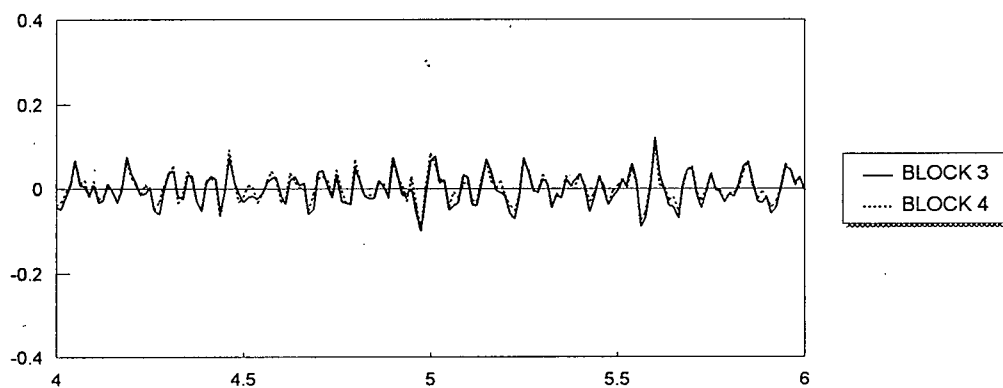
BLOCKS 2 and 3 (Structural Model Nodes 12 and 13)

RUSKIN DAM AMBIENT VIBRATION TRIAL FIELD TEST, 23 January 94

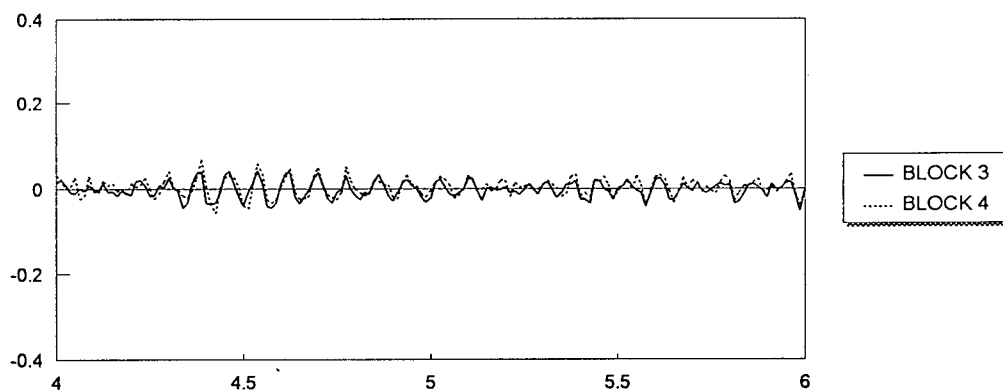
UPSTREAM-
DOWNSTREAM



VERTICAL



CROSS-
CANYON



NOTES:

1. Abscissa: acceleration in mg's, ordinate: time in seconds

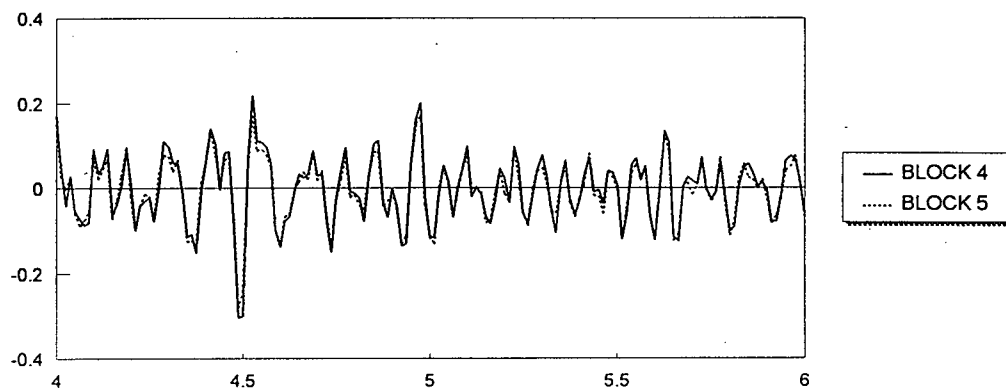
FIGURE B6

ACCELERATION TIME HISTORIES

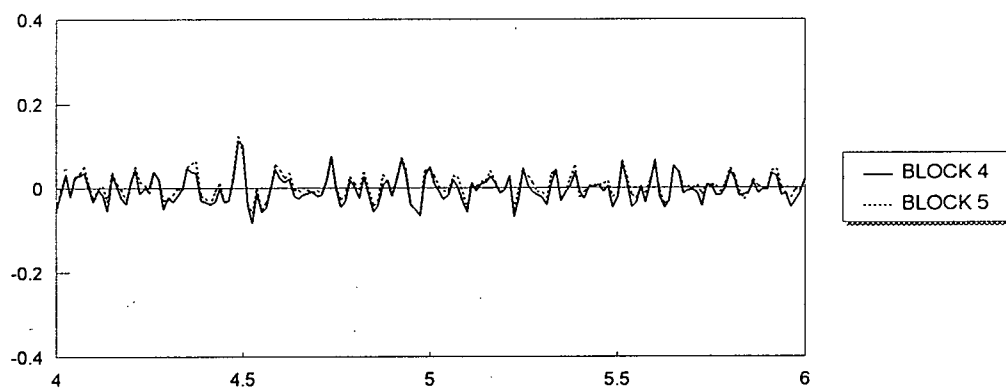
BLOCKS 3 and 4 (Structural Model Nodes 14 and 15)

RUSKIN DAM AMBIENT VIBRATION TRIAL FIELD TEST, 23 January 94

UPSTREAM-
DOWNSTREAM



VERTICAL



NOTES:

1. Abscissa: acceleration in mg's, ordinate: time in seconds

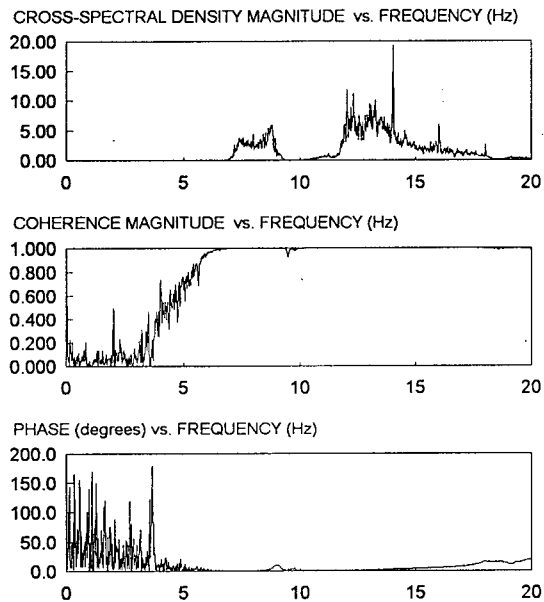
FIGURE B7

ACCELERATION TIME HISTORIES

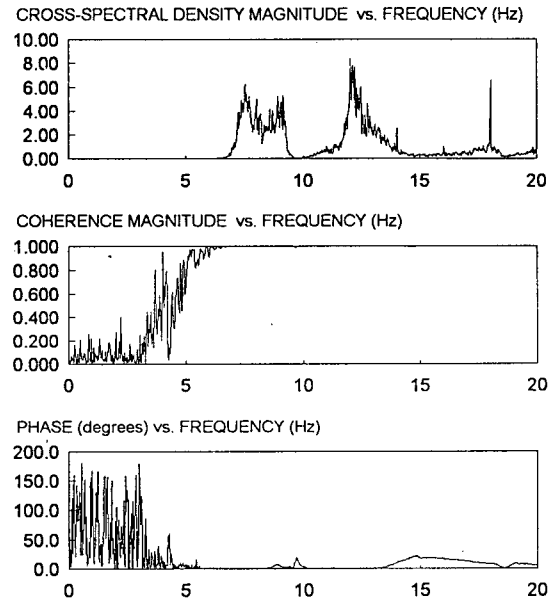
BLOCKS 4 and 5 (Structural Model Nodes 16 and 17)

RUSKIN DAM AMBIENT VIBRATION TRIAL FIELD TEST, 23 January 94

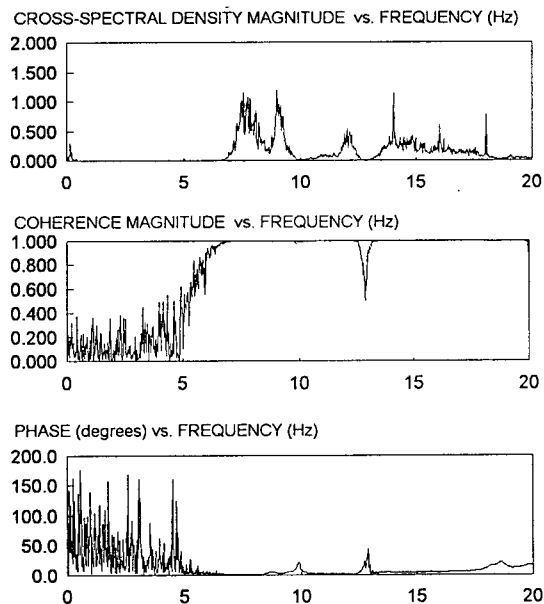
BLOCKS 2 AND 3 (NODES 12 AND 13):



BLOCKS 3 AND 4 (NODES 14 AND 15):



BLOCKS 4 AND 5 (NODES 16 AND 17):



NOTES:

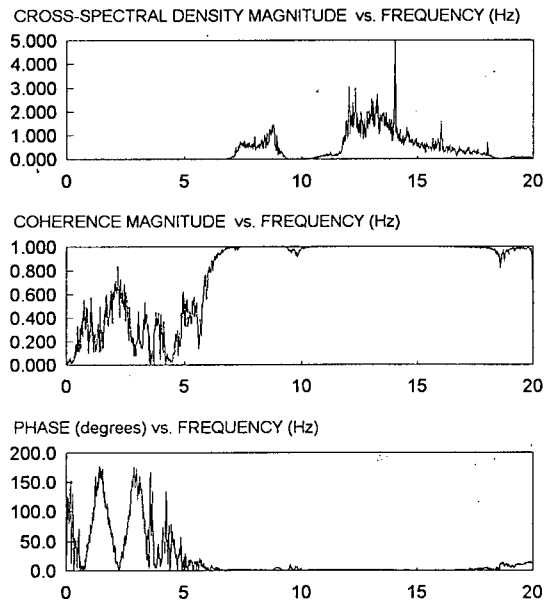
1. All plots completed with high resolution frequency (0.0195Hz) and with 16 segments

FIGURE B8

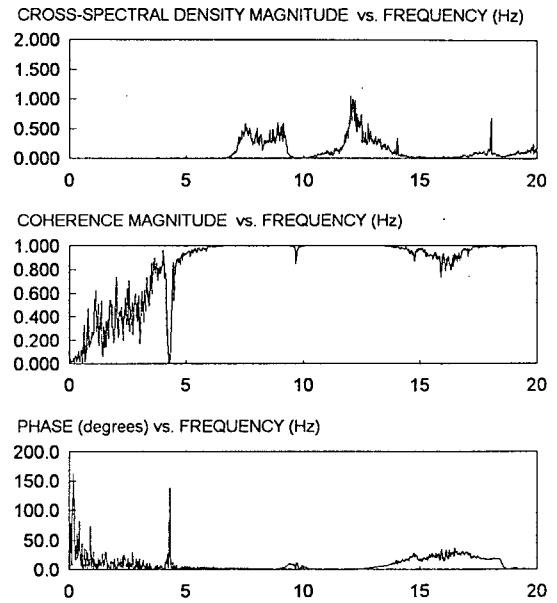
CROSS-SPECTRAL DENSITY, COHERENCE and PHASE FACTOR FUNCTIONS
Blocks 2&3, 3&4, 4&5, Upstream-Downstream Direction

RUSKIN DAM AMBIENT VIBRATION TRIAL FIELD TEST, 23 January 1994

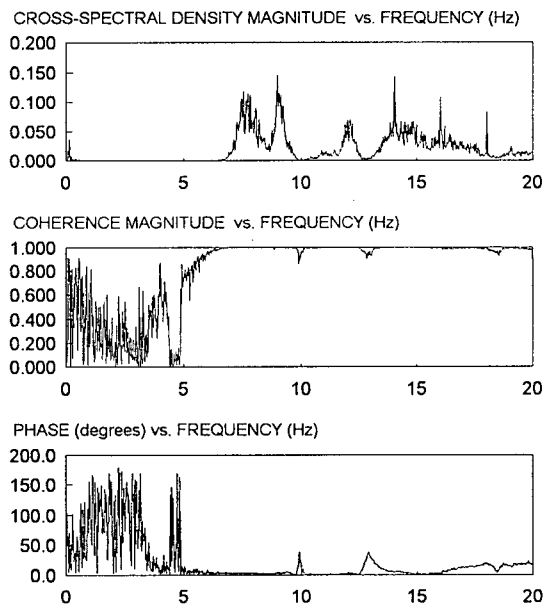
BLOCKS 2 AND 3 (NODES 12 AND 13):



BLOCKS 3 AND 4 (NODES 14 AND 15):



BLOCKS 4 AND 5 (NODES 16 AND 17):



NOTES:

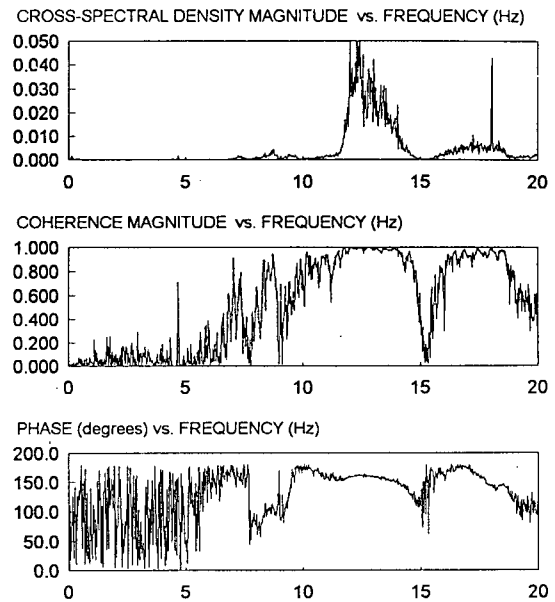
1. All plots completed with high resolution frequency (0.0195Hz) and with 16 segments

FIGURE B9

CROSS-SPECTRAL DENSITY, COHERENCE and PHASE FACTOR FUNCTIONS
Blocks 2&3, 3&4, 4&5, Vertical Direction

RUSKIN DAM AMBIENT VIBRATION TRIAL FIELD TEST, 23 January 1994

BLOCKS 3 AND 4 (NODES 14 AND 15):



NOTES:

1. All plots completed with high resolution frequency (0.0195Hz) and with 16 segments

FIGURE B10

CROSS-SPECTRAL DENSITY, COHERENCE and PHASE FACTOR FUNCTIONS
Blocks 2&3, 3&4, 4&5, Cross-Canyon Direction

RUSKIN DAM AMBIENT VIBRATION TRIAL FIELD TEST, 23 January 1994

**AMBIENT VIBRATION ASSESSMENT OF RUSKIN DAM
DYNAMIC PROPERTIES**

APPENDIX C

ANALYSIS OF LOW RESERVOIR TEST, 30 APRIL & 1 MAY 1994

CONTENTS

<u>Section</u>	<u>Subject</u>	<u>Page</u>
C.1	Hybrid Bridge Evaluation System (HBES) Analysis	216
	C.1.1 Average Normalized Power Spectral Densities (ANPSDs)	216
	C.1.2 ULTRA and VISUAL	218
	C.1.3 Hybrid Bridge Evaluation System (HBES) Analysis Summary . . .	221
C.2	Complementary Analyses	222
	C.2.1 Detailed Phase Change	222
	C.2.2 Power Spectral Densities (PSDs), Cross-spectral Densities (XSDs), Phase and Coherence	223
	Ogee	223
	East Bedrock and Reference Sensor	224
	East Bedrock and East Bedrock	225
	C.2.3 Transfer Function	226
	All Nodes	226
	Node 33	227
	Phase Shift	228
C.3	Low Reservoir Conclusions	229
	Figures (C1 through C36)	231-266

C.1 HYBRID BRIDGE EVALUATION SYSTEM (HBES)

C.1.1 Average Normalized Power Spectral Densities (ANPSDs)

Plotted in Figures C1 and C2 are the ANPSDs for the deck, ogee and east abutment nodes, plotted in high resolution for the average of 16 segments and low resolution for the average of 64 segments. Signals were modified with the "Hanning" window to reduce leakage.

Table C1 gives the breakdown of nodes used in plotting the ANPSDs.

Table C1
Nodes Used in ANPSD Calculation

LOCATION	NODES
Ogee	11-18
Deck	0-9
East Bedrock	19, 31-39

Shown in Table C2 is a list of the most significant frequencies and frequency ranges noted in the ANPSDs. The following is also noted:

1. The east bedrock exhibits significant ANPSD maximas and the ogee/deck do not, over the ranges:
 - 4.0-5.0 Hz
 - 12.0-13.0 Hz

These ranges are considered to contain potential natural frequencies of the east bedrock or frequency components of the excitation originating from within the east bedrock.

2. The deck/ogee ANPSDs exhibit significant ANPSD maximas and the east bedrock does not, over the ranges:
 - 8.0-10.0 Hz
 - 13.0-15.0 Hz

This suggests independent amplified action of the dam and therefore

Table C2
ANPSD Frequency Ranges/Peaks of Significant Strength
Low Reservoir (Low Resolution, 0.0781 Hz, 64 segments)

LOCATION	DIRECTION	RANGE (Hz)	PEAK (Hz)
Deck	Upstream-Downstream	8.0-10.0 11.5-12.5 12.5-14.5 17.0-19.0	8.7, 8.9 12.0 13.6 16.1 18.1
	Vertical	4.0-5.0 8.0-10.0 12.5-14.5 17.0-19.0	4.6 8.7, 8.9 12.1 13.6 16.1, 18.1
	Cross-Canyon	12.5-14.5 15.0-17.0 17.0-19.0	12.1 13.6 16.1 18.1
Ogee	Upstream-Downstream	4.0-5.0 8.0-10.0 11.5-12.5 12.5-16.0 17.0-19.0	8.8, 9.1 12.1 13.4 18.0
	Vertical	4.0-5.0 8.0-10.0 12.5-14.5 14.5-15.5 17.0-19.0	4.7 9.1 12.1 13.6 14.8, 15.2 18.0
	Cross-Canyon	12.5-14.5 17.0-19.0	13.5 18.1 (many small peaks)
East Bedrock	Upstream-Downstream	4.0-5.0 10.0-15.0 17.0-19.0	4.5 11.6, 12.1, 13.4 16.1, 18.0
	Vertical	4.0-5.0 7.5-9.5 10.5-14.5 17.0-19.0	4.6 9.1 12.1, 13.6 16.1 18.0
	Cross-Canyon	4.0-5.0 6.0-7.5 8.0-9.5 10.5-14.5 17.0-19.0	4.6 7.0 9.1 12.1, 13.6 16.0 18.0

these ranges are considered to contain potential natural frequencies of the dam.

3. The east bedrock and deck/ogee jointly exhibit significant ANPSD maximas over the ranges:

- 16.0-16.1 Hz
- 17.0-19.0 Hz

These ranges are considered to contain potential natural frequencies encompassing the dam alone or both the dam and bedrock or they could be representative of frequency components of the excitation originating from within the east bedrock which are causing a large motion of the dam.

C.1.2 ULTRA and VISUAL

In Figures C3 to C8 are operating deflected shapes at the most significant frequencies, as defined by the vectors of the relative transfer function gains and phases from ULTRA. These are plotted for two different phase windows: 90 degrees (i.e., wide open, all nodes are allowed to participate) and 20 degrees (i.e., only nodes where the phase is within 0-20 degrees and 160-180 degrees are allowed to participate). The 20 degree phase window results are shown as this phase was considered to be the highest allowable for reasonable determination of a probable natural frequency with VISUAL.

In general, note in Figures C3 to C8 that the vertical component is significantly less than the upstream-downstream component. In addition, the sense of the coupled vertical/horizontal motion is: vertical up coupled with downstream in the horizontal direction.

All VISUAL work is completed with the signals having been treated with the "Hanning" window.

The following are notes made regarding the VISUAL analysis using successively tighter phase factor and coherence window. Reference to "animate" indicates the effect of VISUAL allowing a node to move if it meets the coherence and phase window values (see Section 4.3).

Coherence: 0 Phase: 90 degrees:

Using wide open coherence and phase factors allows a unique and insightful opportunity for a visual representation of the changing operating deflected shape of the dam with increasing frequency. It was expected that due to modal

interference and noise in the signals, changes in phase would not be smooth. This was indeed found. See the Detailed Phase Change study, discussed later in C.2.1.

Between 0 and 4.0 Hz there is no consistency in the operating deflected shape. Nodes seem to randomly animate in and out of phase with one another with slight frequency shifts.

At about 4.0 Hz the first signs of stabilization appear. Here the dam and surrounding bedrock is shown to move together. As one approaches 4.5 Hz the movement takes on a distinctively rigid body type of motion, with the east side amplitude much greater than the west side. The most consistent frequency range is about 4.6 \pm 0.3 Hz although intermittently the odd node animates out-of-phase. The operating deflected shape at the ogee is shown in Figure C3.

Increasing frequency shows the dam taking a more independent shape, however still moving in-phase with the surrounding bedrock. The dam begins to take on a distinctively independent single curvature shape in both vertical and upstream-downstream directions, at about 8.0 Hz. An inflection point in both the vertical and upstream-downstream directions appears in the non-overflow section. In the vertical, it appears at about 8.0 Hz, whereas in the upstream-downstream, it appears at about 8.5 Hz. This inflection point remains in the non-overflow section, more often than not, until 20 Hz.

The east bedrock now begins to animate out of phase with the dam. This occurs first in the vertical direction between 8.3 and 8.9 Hz and later in the upstream-downstream between 9.1 and 9.5 Hz. Operating deflected shapes at the ogee for 8.7 and 9.1 Hz, are shown in Figures C4 and C5.

At 9.0 Hz an inflection point begins to creep in from the east side vertical direction, showing up in the ogee and deck. There is a frequency lag before it appears in the upstream-downstream direction, however it does show up at about 9.7 Hz. At about 9.8 Hz an inflection point also appears in the gallery east end in plan but not in elevation. This shape holds in general until about 11.8 Hz, however, the animation pattern is unstable through this range, with inflection points moving to and fro. The shape and amplitude of the single curvature in the dam body constantly shifts with increasing frequency. It does not exhibit any stability throughout the 10.0 to 11.8 Hz range..

At 11.8 Hz, the inflection points are shown to jump westward one node, on each of the ogee, deck and gallery. At 12.0 Hz a very large vertical amplitude motion appears briefly in the east bedrock. The ogee operating deflected shape at 12.1 Hz is shown in Figure C6. Above 12.0 Hz, dam animation pattern exhibits little stability with increasing frequency. The inflection point is found to move quickly westward until about 13.0 Hz.

Between 13.0-13.8 Hz great stability is found in the operating deflected shape

in both the vertical and upstream-downstream directions. The ogee operating deflected shape in this range is shown in Figure C7.

Between 14.0 and 14.8 Hz the inflection point in the ogee jumps westward one node.

Between 14.9 and 16.4 Hz another inflection point forms on the west side. Stability is not reached until about 17.7 Hz. Thereafter the shape, which consists of a double curvature with 3 inflection points, exists until about 18.0 Hz. See Figure C8 for the ogee operating deflected shape at 17.9 Hz.

After 18.0 Hz very little frequency stability is found in the operating deflected shape of the dam.

Coherence: 0 Phase: 40 degrees

4.0-5.0 Hz: Nodes in the east bedrock and extreme west side of dam begin to de-activate.

8.0-10.0 Hz: Nodes in the perimeter of the dam and the east bedrock begin to de-activate. This effect is most prominent with increasing frequency after 8.5 Hz.

11.5-15.0 Hz: Nodes at the perimeter of the dam and in the east bedrock begin to de-activate.

17.0-19.0 Hz: A large number of nodes are found de-activated. This includes much of the ogee, deck and gallery. It is very difficult to determine an optimum frequency range for a probable natural frequency. The generous phase factor suggests that a probable natural frequency does not exist.

Coherence: 0 Phase: 20 degrees

4.0-5.0 Hz: Many west side nodes are de-activated. As well, sporadically nodes in the east bedrock, ogee or deck de-activate. In Figure C3, the breakdown in the vertical direction (elevation) direction of the operating deflected shape is most apparent.

8.0-10.0 Hz: The best range appears to be 8.3 +/- 0.3 Hz. After 8.5 Hz nodes on the east side of the dam tend to de-activate in the vertical direction. After 8.5 Hz, the majority of the east bedrock is de-activated. After 9.5 Hz additional dam nodes de-activate. Operating deflected shapes at 8.7 and

9.1 Hz are shown in Figures C4 and C5. Referring to these figures, both frequencies exhibit phase resilience.

11.5-15.0 Hz: At 12.1 +/- 0.1 Hz the majority of dam nodes are still active, however much of the east bedrock is de-activated. At 12.0-13.0 Hz, sporadic de-activation of nodes occurs. At 13.0-14.0 Hz there are signs of breakdown of the shape. Several nodes in the ogee, gallery and deck de-activate on the east end of the dam. The best range seems to be 13.6 +/- 0.3 Hz. See Figure C7.

17.0-19.0 Hz: Most nodes are inactive. This is exhibited in Figure C8, where only 2-3 nodes are indicated active, in both of the deck and ogee.

C.1.3 Hybrid Bridge Evaluation (HBES) Summary

1. There is strong evidence of a probable natural frequency of the bedrock at 4.6 +/- 0.3 Hz. The mode shape appears to be a rigid body resonance. Cross-spectral density, phase and coherence functions between bedrock nodes measured coincident need to be reviewed to confirm this (see Section C.2).
2. There is strong evidence of a probable natural frequency of the dam at 8.3 +/- 0.3 Hz. The large range is due to the conflicting results between the ANPSD and VISUAL studies. Further complementary analyses detailed in section C.2 may help narrow this range. The mode shape is a single curvature shape in both principle directions.
3. There is reasonable evidence of a probable natural frequency of the dam at 13.6 +/- 0.3 Hz. The mode shape has one inflection point along the ogee in both the upstream-downstream and vertical directions.
4. There is slight evidence of a potential natural frequencies at 18.0 +/- 1.0 Hz and 12.1 +/- 0.1 Hz.

C.2 COMPLEMENTARY ANALYSES

All plots presented were completed without a window to reduce leakage. Comparative plots with and without a window did not indicate any substantial difference.

C.2.1 Detailed Phase Change

Data was studied at the frequency resolution of the recording, i.e., 0.0195 Hz.

No hard copy of the phase change data is included herein due to the large amount of space it would require. The following describes what was observed:

4.3-7.7 Hz: In both of the vertical and upstream-downstream directions there were several lengthy but discontinuous frequency ranges in which all nodes moved in phase. The range of this behaviour extended from 4.3 to 7.7 Hz (the hard copy phase change data contains no information regarding amplitude, therefore, it is not possible to determine when the first indication of the independent single curvature shape of the dam manifests itself, which VISUAL shows to be about 8.0 Hz, as reported in Section C.1.2).

7.8-9.8 Hz: Through this frequency range two significant mode shapes were found to have stability. The first, from about 7.8-9.0 Hz, has the overflow section of the dam moving in phase, with some out of phase motion in the non-overflow west end. The second, between 9.0-9.8 Hz is similar but contains a single inflection point, in the vertical direction, in the extreme east end of the overflow section, deck and ogee.

Between the nodes on the deck/ogee and the reference sensor, good to excellent coherence is exhibited in both vertical and upstream-downstream directions. Above 0.8 is common in this regard. Therefore the phase factor has a standard deviation of no more than 3 degrees (see Table 5.2 in Section 5.2) and the inflection point location has been accurately identified.

11.5-15.0 Hz: Between 11.5-12.5 Hz there is very little indication of phase stability, in both upstream-downstream and vertical directions coincident. It is common to see coherences below 0.2 for nodes at the east end of the deck/ogee and in the east bedrock, indicating phase errors greater than 10 degrees (see Table 5.2 in Section 5.2).

Stability occurs about 13.0 Hz and continues to about 14.3 Hz. There is intermittent evidence of phase change for one node in the gallery throughout this range. As only one node was exhibiting this instability, VISUAL was used to confirm what was occurring. It was found that an inflection point is very close to this node, thus explaining the changing phase.

17.0-19.0 Hz: The most significant range of stability occurs between 17.6 and 17.9 Hz.

Detailed Phase Change Conclusions

1. Detail phase change study is limited in its ability to interpret the data. It should be considered as a means to augment the VISUAL analysis. To assist interpretation of the importance of phase instabilities, coherence data also needs to be available to allow for consideration of the standard deviation of the phase estimate (see Section 5.2).
2. Of the important frequency ranges identified with HBES the one with significant phase instability for the dam nodes is 12.1 +/- 0.1 Hz.
3. Of the important frequency ranges identified with the HBES system, those with significant phase stability for the dam nodes were found to be 4.6 +/- 0.3, 8.3 +/- 0.3, 13.6 +/- 0.3, and 17.8 +/- 0.2 Hz (the latter a tighter range than the HBES range of 18.0 +/- 1.0 Hz).

C.2.2 Power Spectral Densities (PSDs), Cross-spectral Densities (XSDs), Phase and Coherence

Ogee

PSDs

See Figures C9 and C10.

Considering each individual node, the PSDs for the upstream-downstream and vertical directions are usually similar, the only significant differences are found at the ends, or at Nodes 11, 12 and 19 where the frequency content varies. The great strength in Node 12 at 15.0 Hz in the vertical seems incorrect (it is the origin of the corresponding strength in the vertical ogee ANPSD).

No significant relative strength is noted in the HBES predicted bedrock probable natural frequency range of 4.6 +/- 0.3 Hz.

Significant peaking exists between 8.0-10.0 Hz. These peaks appear to be concentrated at two frequencies: 8.7 and 9.1 Hz, therein corresponding to the two very similar near single curvature response shapes noted with VISUAL. Although the plots are non-normalized, the relative magnitude of these peaks rise up for nodes at the centre of the dam. This is indicative of a single curvature mode shape, as magnitudes of PSDs can be used to construct mode

shapes (Bendat and Piersol 1993, 201).

Significant peaks exist between 11.5 and 15.0 Hz. These are more dominant in the nodes for the east and west ends of the dam corresponding to the HBES predicted probable natural frequency range of 13.6 ± 0.3 Hz. If the PSD magnitudes were used to construct a mode shape, it would be a double curvature shape.

XSDs, Phase and Coherence

See Figures C11 to C14

As with PSDs, the shapes of XSDs at a given node, in both the vertical and upstream-downstream directions, are similar.

Phase plots exhibit their best values in the 7.5-8.5 Hz range. The minimum appears to be approximately 7.5 Hz for most. This is in direct contrast to the peaks in the XSDs, PSDs (and ANPSDs) which exist closer to 9.0 Hz. The coherence function is above 0.8 for most dam nodes over this latter range, indicating from Table 5.2 in Section 5.2 that the phase factor is accurate to within 3 degrees \pm .

Node 16 exhibits a large drop in coherence between 12.5-13.0 Hz, which is coincident with a valley in the XSD, and is just before a series of peaks in the XSD between 12.5 and 14.0 Hz. This is coincident with the HBES predicted probable natural frequency range of 13.6 ± 0.3 Hz, with the corresponding mode shape having an inflection point near Node 16.

The phase function for most nodes near 18.0 Hz is very poor. There is a peak in the XSD. Some nodes exhibit a drop in coherence just before this peak, witness node 17. Similar to the 8.0-9.5 Hz range, the coherence is high at this frequency, again indicating the phase factor is accurate. It should be concluded that no natural frequency exists.

East Bedrock and Reference Sensor

PSDs

See Figures C15 and C16.

White noise conditions are not found. Vertical PSDs vary with location. Upstream-downstream plots are much more consistent.

Nodes 31 to 34, located near the intake at the lead end of the tunnels, exhibit

high strength in the 12.0 +/- Hz range. The strength is manifested as a very narrow band peak in the vertical direction. This suggests a frequency component of the excitation from the bedrock.

Vertical plots exhibit considerably more independent narrow band peaks than the upstream-downstream plots.

Spikes at 2.0 Hz and multiples thereof are evident. See Node 32 vertical PSD for the most evidence of this spiking. These 2.0 Hz spikes are also noted in many PSD and XSD plots for the ogee and are probably representative of the 2.0 Hz turbine spinning frequency at the Ruskin Generating Station. Therefore, these 2.0 Hz spikes are probably frequency components of the excitation emanating from the bedrock.

XSDs, Phase and Coherence

See Figures C17 to C22.

Shapes of the XSD are very similar in the upstream-downstream and vertical directions. There is strength at 8.0-10.0, 12.5-14.5, 17.5-18.5 Hz ranges usually.

Plots in general are not as good as those obtained for the ogee. Coherences are sometimes very low. Peaks in the coherence and phase plots are not as broadband.

Of interest are the phase plots. Some very distinctive smooth crossings from 0 to 180 degrees are noted. The most intriguing pass through 90 degrees near potential natural frequencies at 8.5-9.5 Hz and 13.5-14.5 Hz (see nodes 31-35 in the vertical and nodes 31-37 in the upstream-downstream). Of note, only the vertical plots show the crossing through the 13.5-14.5 Hz range. In the upstream-downstream plot the crossing occurs at a higher frequency and is noticeably inconsistent between nodes. These results suggest a transfer function can be constructed, treating the bedrock as input. This will be studied in the section C.2.3.

East Bedrock and East Bedrock

XSDs, Phase and Coherence

See Figures C23 and C24 for XSD, phase and coherence functions between nodes in the east bedrock which were measured simultaneously.

All of the measured pairs are in phase throughout most of the frequency range

5.0-20.0 Hz.

Significant peaks are found, particularly in the vertical XSD, between 4.5-5.0 Hz for all coupled nodes and particularly between nodes 35 and 37. The corresponding coherence and phase data is very strong suggesting a natural frequency and mode shape encompassing the east bedrock.

PSDs, XSDs, Phase and Coherence Conclusions:

1. For the ogee, the following is concluded:
 - Poor phase in the 17.0-19.0 Hz range, coupled with high coherence suggests that no natural frequencies exist for the dam.
 - Between 7.5-9.0 Hz, the best phase factor does not correspond to the peaks in the PSDs and XSDs. Coherence indicates accurate phase factors. The best range for the natural frequency remains that predicted with HBES as 8.3 +/- 0.3 Hz.
2. For the east bedrock, the following is concluded:
 - White noise conditions are not exhibited in the bedrock signals.
 - Vertical PSDs have a significant zone of strength at 4.0-5.0 Hz. This is also found in the XSD for the vertical direction between east bedrock nodes, with excellent coherence and phase exhibited. This suggests a natural frequency and mode shape encompassing the east bedrock. XSD with the reference sensor do not exhibit this strength, thereby supporting the idea of an independent bedrock natural frequency.
 - Phase for the XSD with the reference sensor exhibits crossings through 90 degrees near peaks in the XSD. This intriguing result indicates that transfer functions may be successfully constructed using the bedrock signals as the input.

C.2.3 Transfer Function

All Nodes

Transfer Functions

Transfer functions and selected phases were calculated and plotted, as shown in

Figures C25 to C31. These plots are made at the highest resolution of the data possible.

There is no evidence of signal strength between 4.5 and 5.0 Hz.

Between 8-10 Hz is generally found a rounded peak, with the maximum value occurring between 8.5 and 9.0 Hz. The next significant peak, again rounded, occurs between 13.3 and 13.9 Hz. There is sometimes another rounded peak at 17.5-18.5 Hz.

Phase Factors

Referring to Figures C29 to C31, in the vertical direction the plotted nodes show a surprisingly close agreement at the first point where they cross through 90 degrees. This occurs at 8.7 ± 0.1 Hz. In the upstream-downstream direction, the crossing point is also evident, however the variation of the frequency at the crossing is greater. The average crossing point of the upstream-downstream direction is 9.1 ± 0.2 Hz, for a difference of about 0.4 Hz between the two directions.

A second 90 degree crossing is not as consistently indicated. In the vertical direction a crossing through 90 degrees is found at 14.0 ± 1.0 Hz. The upstream-downstream direction show additional 90 degree crossing activity, at $11.0 \pm$ Hz and $18.0 \pm$ Hz. Referring to figures C17 to C19, coherences at $11.0 \pm$ Hz are very low, indicating high error in the estimate of the phase which therefore weakens the evidence for a natural frequency. At $18.0 \pm$ Hz, the coherence is better, however, closer examination of the phase plots in Figures C17 to C19 indicates very few decisively cross at 90 degrees within a reasonable frequency range, thereby weakening the evidence for a natural frequency.

Node 33

Node 33 yields the best results for consideration as the optimum transfer function. This node is located near the upstream end of the power intake tunnels, approximately between intakes 1 and 2. Node 33s transfer function, phase and coherence was then re-calculated at a low resolution, to improve on the accuracy of the gain. The resulting plots are shown in Figures C32 and C33.

Transfer function signal strength between 8.0 and 10.0 Hz contains a rounded peak. Coincident with these, are crossings of the phase through 90 degrees. In the upstream-downstream direction this occurs at 9.5 Hz. In the vertical direction, this occurs at 8.7 Hz. Coherence values are reasonable only in the vertical direction. At the upstream-downstream phase crossing, the standard

deviation in the phase, using Table 5.2 in Section 5.2, is 12 degrees +/-, indicating high noise in the transfer function. Using the low noise vertical transfer function matches the HBES results the best.

Signal strength exists between 13.0 and 14.0 Hz, with a rounded peak. The phase exhibits a crossing through 90 degrees at about 13.6 degrees for the vertical direction with reasonable coherence, however in the upstream-downstream direction, no such crossing is found. Once again, using the vertical transfer function matches the HBES results.

A final zone of transfer function strength is found at 17.0 to 19.0 Hz in the upstream-downstream direction only, with another rounded peak. As it turns out, comparison with other upstream-downstream transfer functions shows that Node 33s is the only one to show a 90 degree crossing near this peak. The evidence for a natural frequency is therefore not conclusive.

Phase Shift

The discrepancy in the prediction of the first natural frequency between the vertical and upstream-downstream signals was further investigated.

A study was made to see whether the vertical or upstream-downstream signal would yield the same 90 degree crossing point with an orthogonal output signal, as mode shapes typically have components in the three principle directions. Shown in Figure C34 are plots made with the bedrock signal at node 33 and the reference signal (remember, that the only signals recorded coincident with any of the bedrock signals, is the triaxial array of reference signals). These plots indicate that consistency is found. Either the vertical or upstream-downstream input bedrock signal will yield the same 90 crossing point irrespective of whether a vertical or upstream-downstream reference signal is chosen for output. This strengthens the evidence for construction of a transfer function using a bedrock signal for input, as consistency intuitively should be exhibited.

It was wondered if a time lag between the recorded vertical and upstream-downstream signals could explain the difference in the 90 degree crossings found at the first natural frequency. Plots were made of coincident time domain signals, which were then viewed for evidence of time lagging. Shown in Figure C35 are plots of typical segments of coincident bedrock and reference sensor signals in the vertical and upstream-downstream directions. The reference sensor signals are shown to be near perfectly in phase. Whereas, the bedrock signals do suggest time lag. Shown in Figure C36 is the identical segment of the bedrock signals, with a plot indicating the affect of a time shift equal to one time discretization. This figure shows what appears to be the signals becoming more in phase.

The reason for a potential error in recording of the bedrock signals was then

investigated. Instrumentation error seemed unlikely given that no evidence of time lag in the coincidentally recorded reference sensor signals was found. It is hypothesized that the upstream-downstream component of the signal measured at a given point may be delayed relative to the vertical signal due to varying density in the bedrock, or because it is contaminated with other information such as resonances from dam natural frequencies. The vertical signal does not appear to have been affected by such phenomena.

Transfer Function Conclusions

1. It has been demonstrated that the vertical signal recorded from the bedrock can be successfully used as input for transfer functions with the dam signals, based on reasonable correlation to the HBES results. The upstream-downstream signals, when used as input in a similar transfer function, were not found to be as reliable.
2. Using the vertical signal based transfer function, the following was found:
 - The first natural frequency is predicted to be at 8.7 ± 0.1 Hz, yielding good correlation to the range of 8.3 ± 0.3 Hz found with the HBES system.
 - The second natural frequency is predicted to be at 14.0 ± 1.0 Hz and is therein poorly correlated to the HBES prediction of 13.6 ± 0.3 Hz.
 - Potential natural frequencies at 12.1 ± 0.1 Hz, 16.1 ± 0.1 Hz and 18.0 ± 1.0 Hz are not indicated.
3. Node 33s vertical transfer function yielded the best correlation with the HBES results.

C.3 LOW RESERVOIR CONCLUSIONS

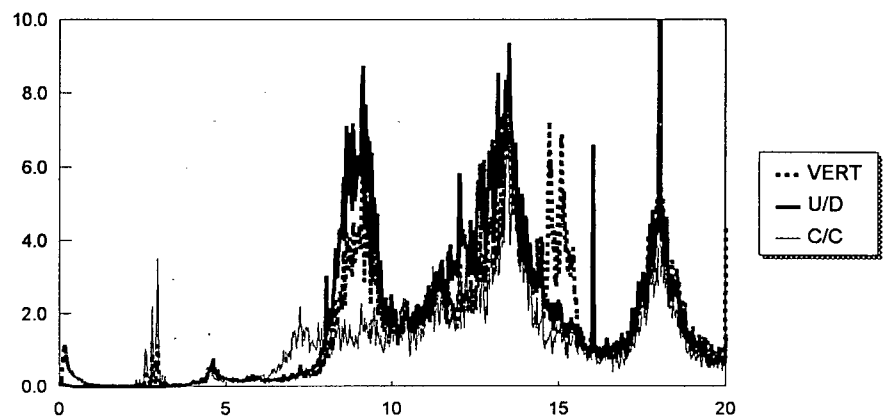
1. HBES shows evidence of a probable natural frequency of the bedrock at 4.6 ± 0.3 Hz, with the corresponding mode shape a rigid body motion, with a much greater amplitude on the east side.. The east bedrock PSDs, XSDs, phase and coherence studies indicate a natural frequency and resonance within the east bedrock in this frequency range. Transfer function studies finds that this very strong signal is not exciting the dam.
2. HBES finds strong evidence of a probable natural frequency of the dam at 8.3 ± 0.3 Hz, with the large range due to contradictory evidence between the ANPSD strength and the phase data. Transfer function analysis using the

vertical signal would indicate 8.7 ± 0.1 Hz. As a result, a compromise frequency range of 8.6 ± 0.4 Hz is suggested. The mode shape is a near symmetric single curvature in both the vertical and upstream-downstream directions. As such it probably represents the first or fundamental frequency of the dam.

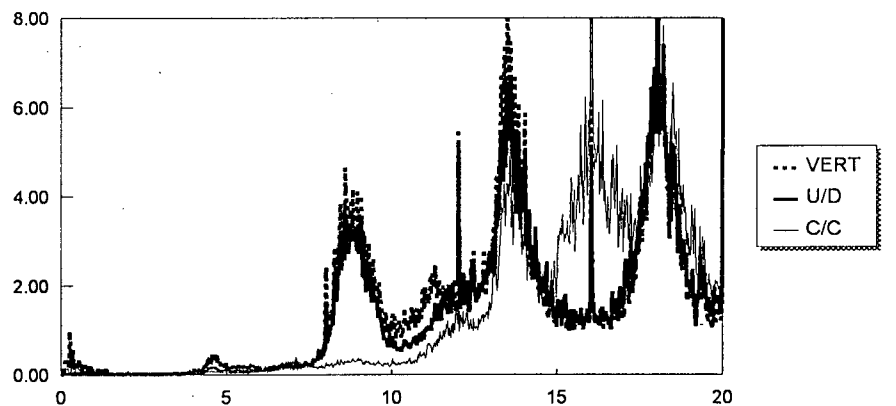
3. HBES finds reasonable evidence of a probable natural frequency of the dam at 13.6 ± 0.3 Hz. This also finds rough correlation in the transfer function analysis for the vertical direction signal only. The mode shape has one inflection point just east of centre along the ogee, in both vertical and upstream-downstream directions.
4. HBES finds evidence of a probable natural frequency at 12.1 ± 0.1 Hz. No other substantial support for this range was found. Based on the high bedrock PSD and XSD strength coupled with reasonable phase and coherence at this frequency, it is considered to represent a frequency component of the excitation originating within the bedrock.
5. HBES finds slight evidence for a probable natural frequency at 18.0 ± 1.0 Hz, in the form of ANPSD strength. Poor phase coupled with good coherence indicates that it most likely is not a natural frequency.

As noted with the trial test, the low pass filter was set at 12.5 Hz. It is considered that use of this filter has hampered identification of dynamic properties above 12.5 Hz.

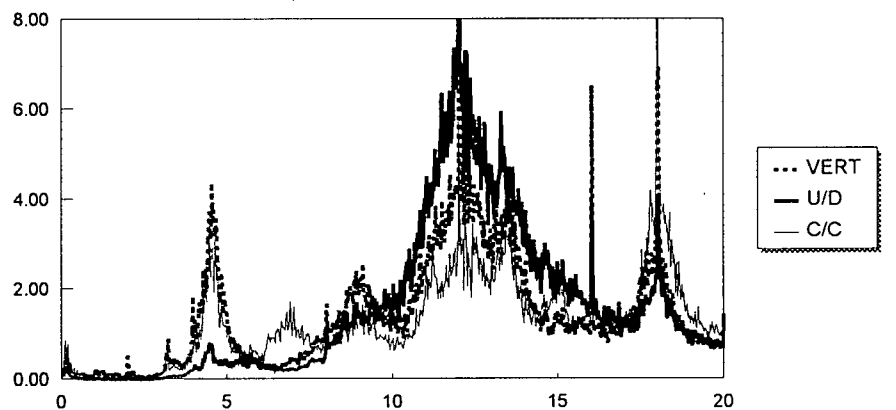
OGEE



DECK



EAST BEDROCK



NOTES:

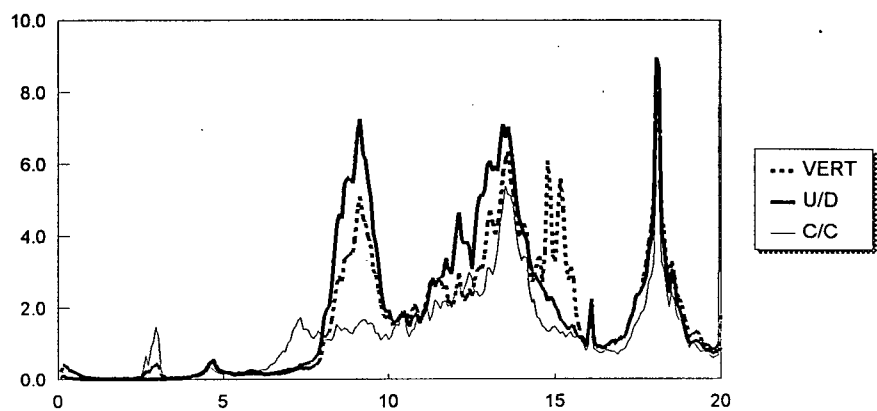
1. All plots made with high resolution (0.0195 Hz) and with 16 segments.
2. In legends shown, U/D = upstream-downstream direction, V = vertical direction, C/C = cross-canyon direction
3. All plots, abscissa: frequency (Hz), ordinate: ANPSD magnitude

FIGURE C1

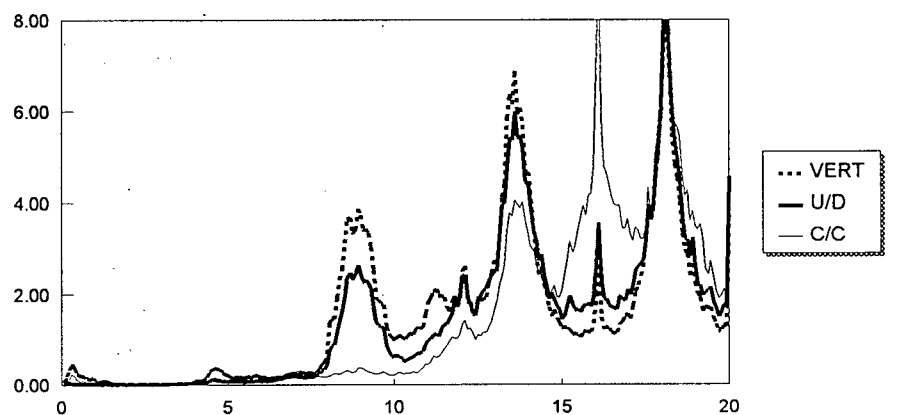
ANPSD Functions
Ogee, Deck and East Bedrock

RUSKIN DAM AMBIENT VIBRATION FIELD TEST, LOW RESERVOIR, 30 April & 1 May 1994

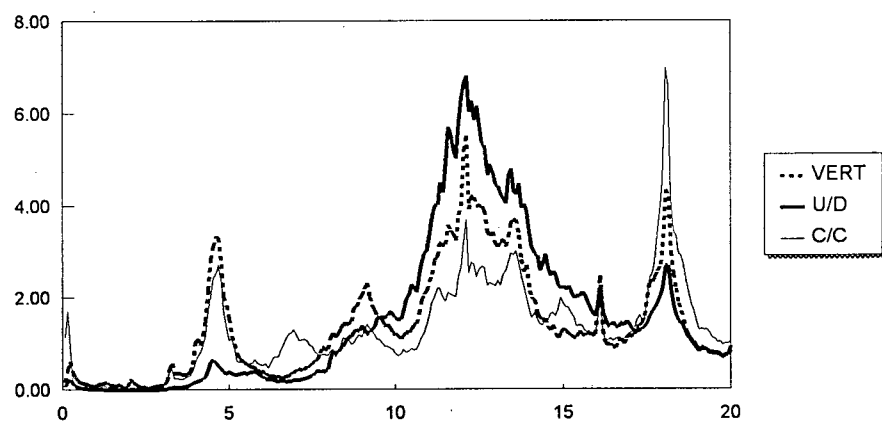
OGEE



DECK



EAST BEDROCK



NOTES:

1. All plots made with low resolution (0.0781 Hz) and with 64 segments.
2. In legends shown, U/D = upstream-downstream direction, V = vertical direction, C/C = cross-canyon direction
3. All plots, abscissa: frequency (Hz), ordinate: ANPSD magnitude

FIGURE C2

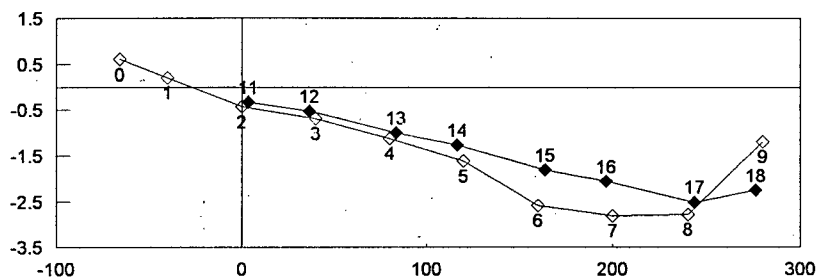
ANPSD Functions

Ogee, Deck and East Bedrock

RUSKIN DAM AMBIENT VIBRATION FIELD TEST, LOW RESERVOIR, 30 April & 1 May 1994

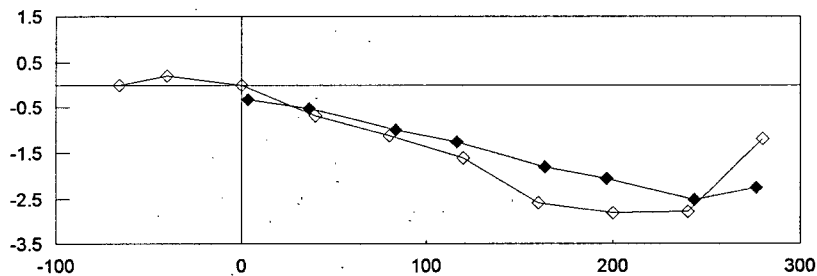
UPSTREAM-DOWNSTREAM

PHASE WINDOW:
0-180 degrees



OGEE
DECK

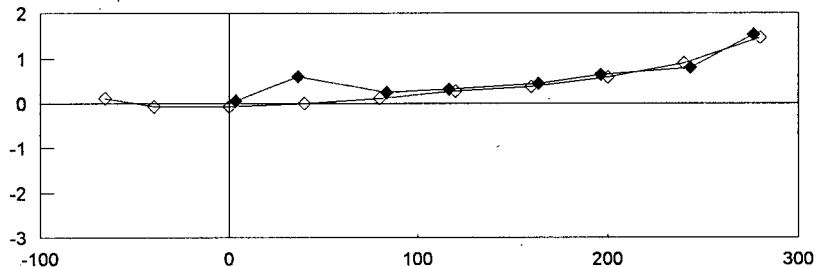
PHASE WINDOW:
0-20 & 160-180 degrees



OGEE
DECK

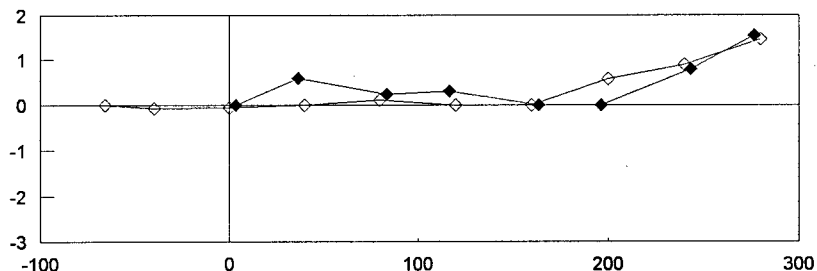
VERTICAL

PHASE WINDOW:
0-180 degrees



OGEE
DECK

PHASE WINDOW:
0-20 & 160-180 degrees



OGEE
DECK

NOTES:

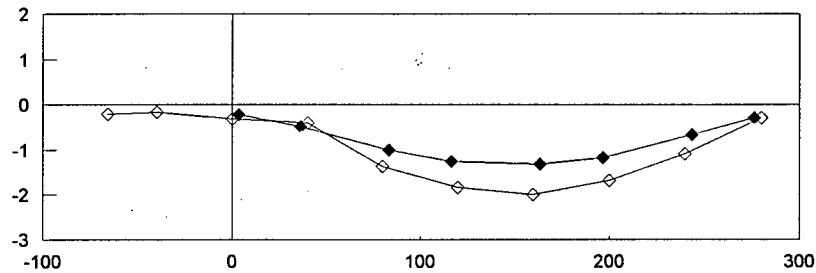
1. All plots completed with high resolution frequency (0.0195Hz) and 16 segments
2. Abscissa: normalized amplitudes
3. Ordinate: measured in feet from centreline of pier on west side of overflow section, overflow length is 280 feet
4. Coherence window: 0-1, phase window: as noted
5. Node numbers shown, for locations see Figure A4.
6. Reference sensor: node 13 upstream-downstream direction
7. Positive sense: upstream in upstream-downstream plots, up in vertical plots

FIGURE C3 OPERATING DEFLECTED SHAPE (defined at ogee and deck)
4.6 Hz

RUSKIN DAM AMBIENT VIBRATION FIELD TEST, LOW RESERVOIR, 30 April & 1 May 1994

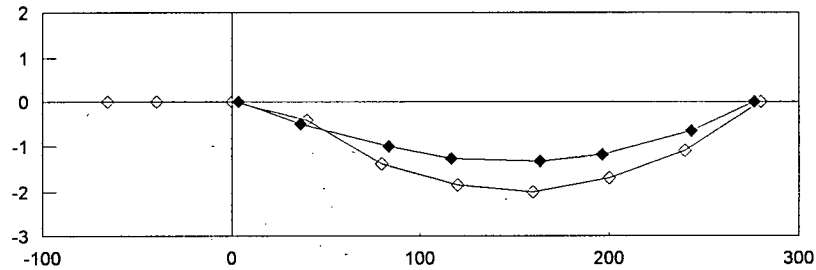
UPSTREAM-
DOWNSTREAM

PHASE
WINDOW:
0-180 degrees



—◆— OGEE
- -◆- - DECK

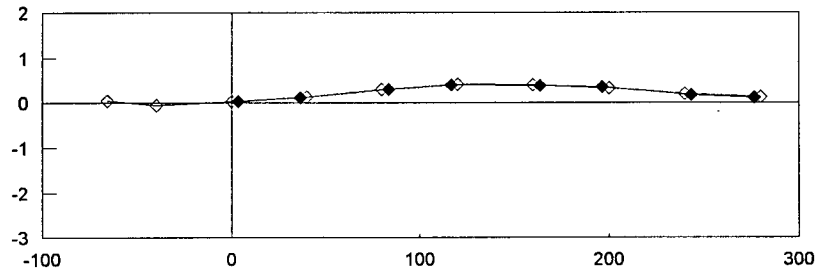
PHASE
WINDOW:
0-20 & 160-180
degrees



—◆— OGEE
- -◆- - DECK

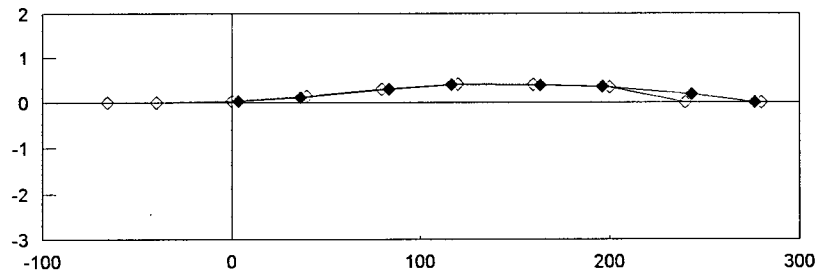
VERTICAL

PHASE
WINDOW:
0-180 degrees



—◆— OGEE
- -◆- - DECK

PHASE
WINDOW:
0-20 & 160-180
degrees



—◆— OGEE
- -◆- - DECK

NOTES:

1. All plots completed with high resolution frequency (0.0195Hz) and 16 segments
2. Abscissa: normalized amplitudes
3. Ordinate: measured in feet from centreline of pier on west side of overflow section, overflow length is 280 feet
4. Coherence window: 0-1, phase window: as noted
5. Node numbers shown on Figure C3, for locations see Figure A4.
6. Reference sensor: node 13 upstream-downstream direction
7. Positive sense: upstream in upstream-downstream plots, up in vertical plots

FIGURE C4

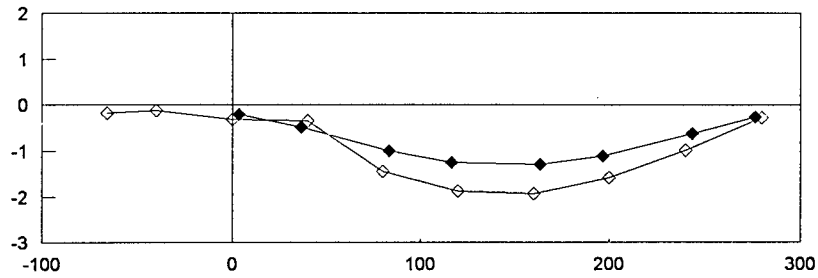
OPERATING DEFLECTED SHAPE (defined at ogee and deck)

8.7 Hz

RUSKIN DAM AMBIENT VIBRATION FIELD TEST, LOW RESERVOIR, 30 April & 1 May 1994

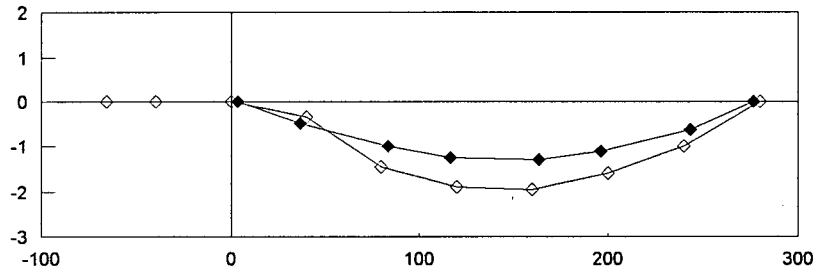
UPSTREAM-
DOWNSTREAM

PHASE
WINDOW:
0-180 degrees



—◆— OGEE
- - -◆- - DECK

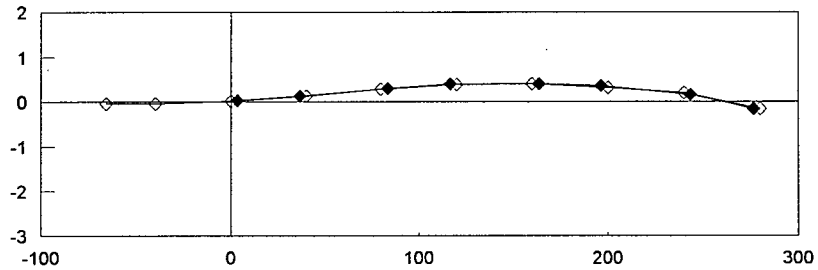
PHASE
WINDOW:
0-20 & 160-180
degrees



—◆— OGEE
- - -◆- - DECK

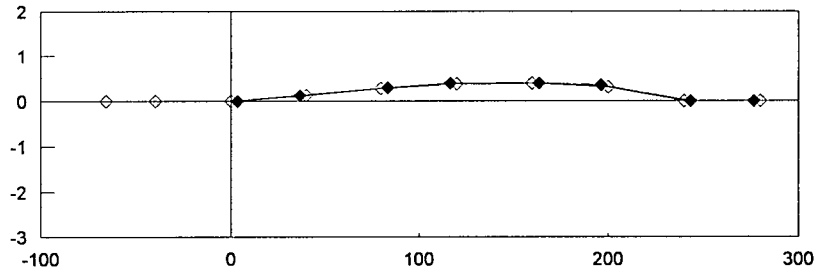
VERTICAL

PHASE
WINDOW:
0-180 degrees



—◆— OGEE
- - -◆- - DECK

PHASE
WINDOW:
0-20 & 160-180
degrees



—◆— OGEE
- - -◆- - DECK

NOTES:

1. All plots completed with high resolution frequency (0.0195Hz) and 16 segments
2. Abscissa: normalized amplitudes
3. Ordinate: measured in feet from centreline of pier on west side of overflow section, overflow length is 280 feet
4. Coherence window: 0-1, phase window: as noted
5. Node numbers shown on Figure C3, for locations see Figure A4.
6. Reference sensor: node 13 upstream-downstream direction
7. Positive sense: upstream in upstream-downstream plots, up in vertical plots

FIGURE C5

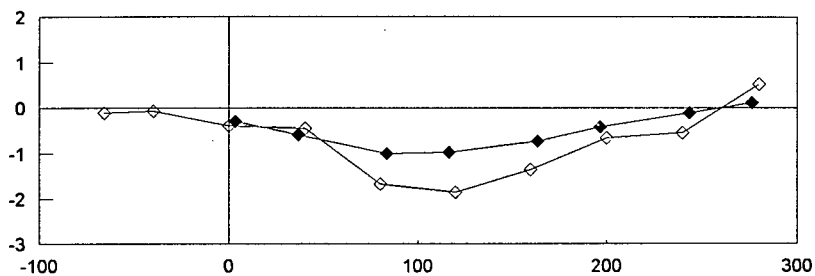
OPERATING DEFLECTED SHAPE (defined at ogee and deck)

9.1 Hz

RUSKIN DAM AMBIENT VIBRATION FIELD TEST, LOW RESERVOIR, 30 April & 1 May 1994

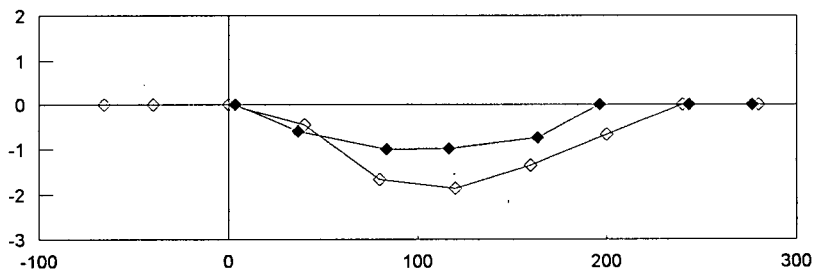
UPSTREAM-DOWNSTREAM

PHASE
WINDOW:
0-180 degrees



OGEE
DECK

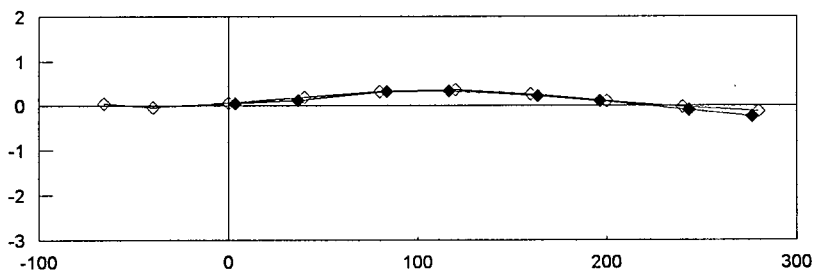
PHASE
WINDOW:
0-20 & 160-180
degrees



OGEE
DECK

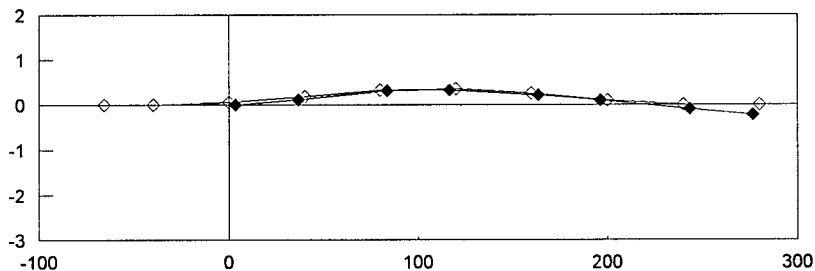
VERTICAL

PHASE
WINDOW:
0-180 degrees



OGEE
DECK

PHASE
WINDOW:
0-20 & 160-180
degrees



OGEE
DECK

NOTES:

1. All plots completed with high resolution frequency (0.0195Hz) and 16 segments
2. Abscissa: normalized amplitudes
3. Ordinate: measured in feet from centreline of pier on west side of overflow section, overflow length is 280 feet
4. Coherence window: 0-1, phase window: as noted
5. Node numbers shown on Figure C3, for locations see Figure A4.
6. Reference sensor: node 13 upstream-downstream direction
7. Positive sense: upstream in upstream-downstream plots, up in vertical plots

FIGURE C6

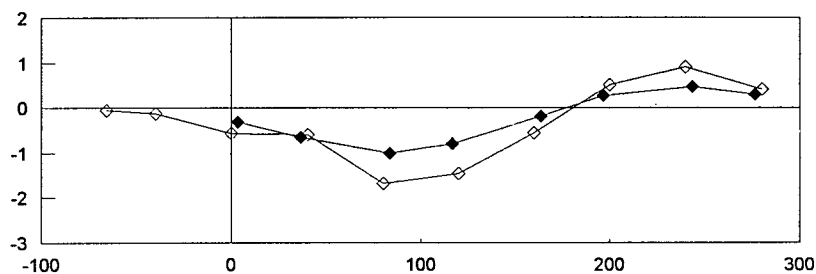
OPERATING DEFLECTED SHAPE (defined at ogee and deck)

12.1 Hz

RUSKIN DAM AMBIENT VIBRATION FIELD TEST, LOW RESERVOIR, 30 April & 1 May 1994

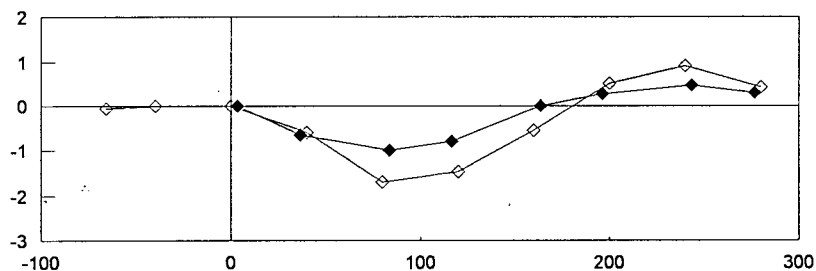
UPSTREAM-DOWNSTREAM

PHASE
WINDOW:
0-180 degrees



OGEE
DECK

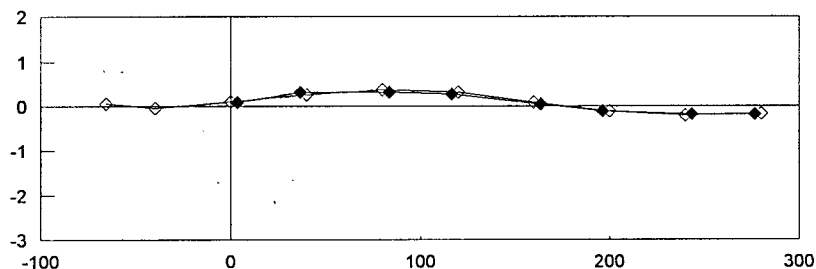
PHASE
WINDOW:
0-20 & 160-180
degrees



OGEE
DECK

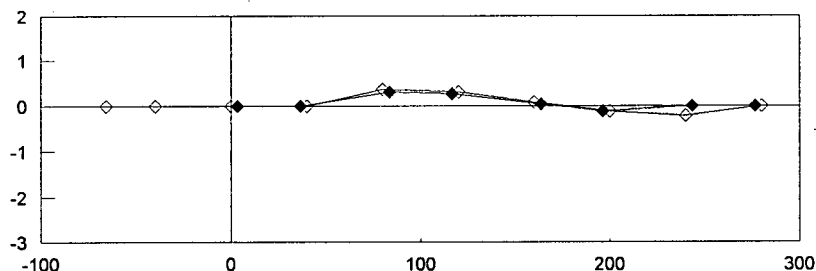
VERTICAL

PHASE
WINDOW:
0-180 degrees



OGEE
DECK

PHASE
WINDOW:
0-20 & 160-180
degrees



OGEE
DECK

NOTES:

1. All plots completed with high resolution frequency (0.0195Hz) and 16 segments
2. Abscissa: normalized amplitudes
3. Ordinate: measured in feet from centreline of pier on west side of overflow section, overflow length is 280 feet
4. Coherence window: 0-1, phase window: as noted
5. Node numbers shown on Figure C3, for locations see Figure A4.
6. Reference sensor: node 13 upstream-downstream direction
7. Positive sense: upstream in upstream-downstream plots, up in vertical plots

FIGURE C7

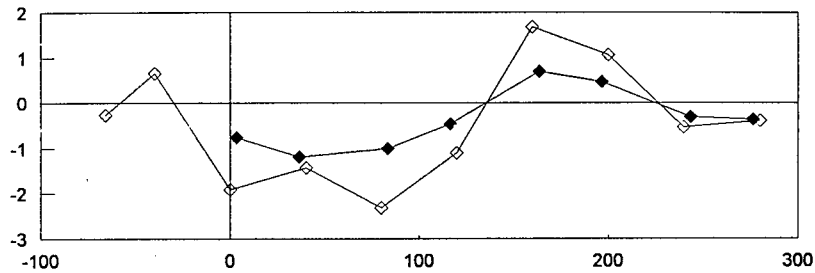
OPERATING DEFLECTED SHAPE (defined at ogee and deck)

13.6 Hz

RUSKIN DAM AMBIENT VIBRATION FIELD TEST, LOW RESERVOIR, 30 April & 1 May 1994

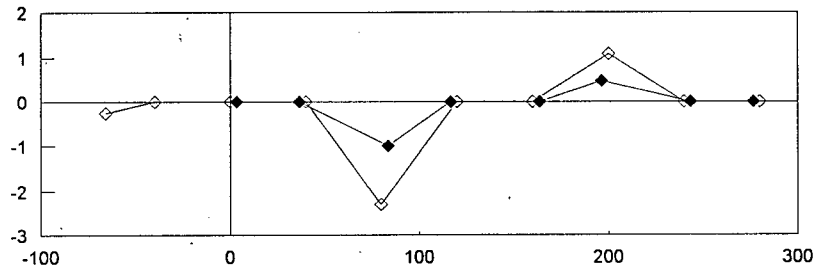
UPSTREAM-DOWNSTREAM

PHASE
WINDOW:
0-180 degrees



OGEE
DECK

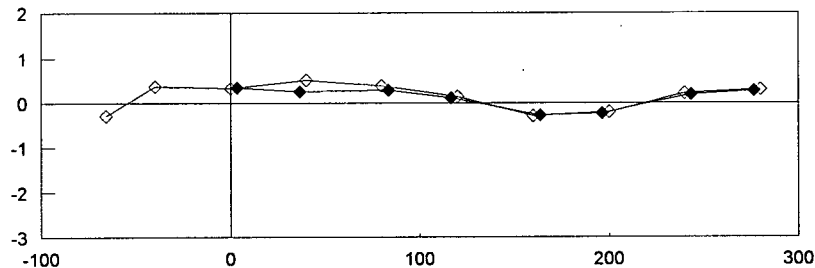
PHASE
WINDOW:
0-20 & 160-180
degrees



OGEE
DECK

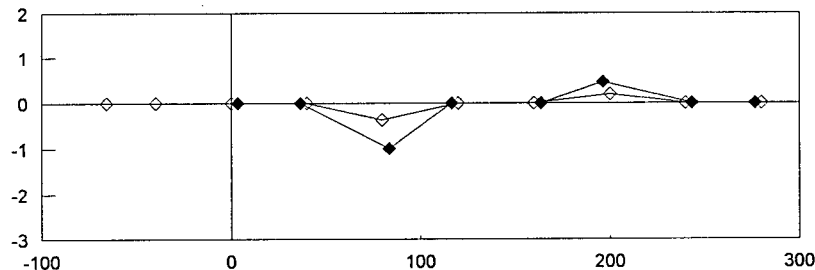
VERTICAL

PHASE
WINDOW:
0-180 degrees



OGEE
DECK

PHASE
WINDOW:
0-20 & 160-180
degrees



OGEE
DECK

NOTES:

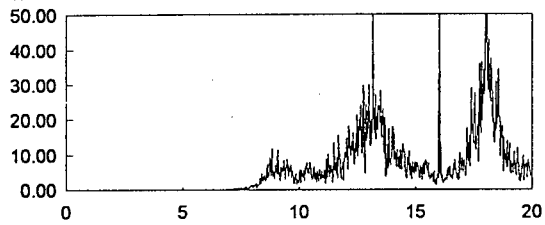
1. All plots completed with high resolution frequency (0.0195Hz) and 16 segments
2. Abscissa: normalized amplitudes
3. Ordinate: measured in feet from centreline of pier on west side of overflow section, overflow length is 280 feet
4. Coherence window: 0-1, phase window: as noted
5. Node numbers shown on Figure C3, for locations see Figure A4.
6. Reference sensor: node 13 upstream-downstream direction
7. Positive sense: upstream in upstream-downstream plots, up in vertical plots

FIGURE C8

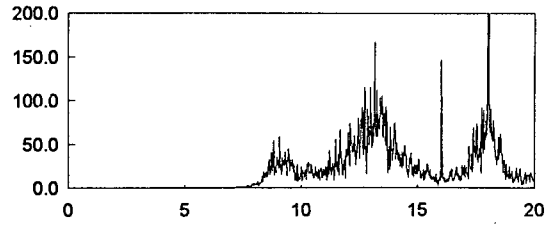
OPERATING DEFLECTED SHAPE (defined at ogee and deck)
17.9 Hz

RUSKIN DAM AMBIENT VIBRATION FIELD TEST, LOW RESERVOIR, 30 April & 1 May 1994

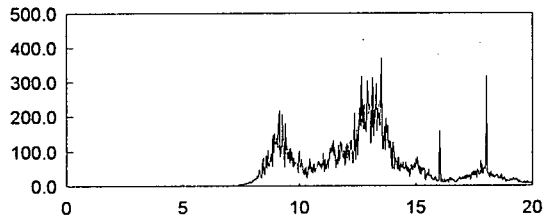
NODE 11



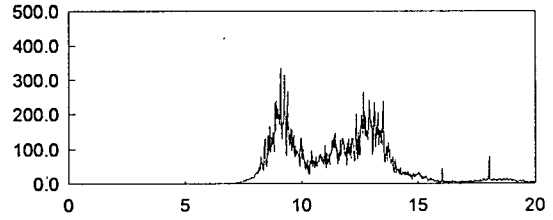
NODE 12



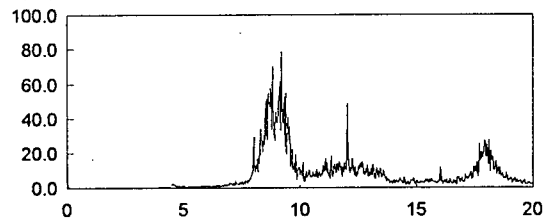
NODE 13



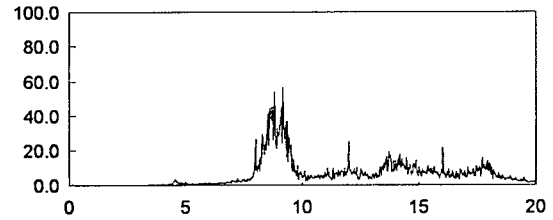
NODE 14



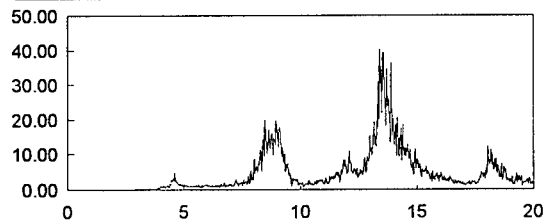
NODE 15



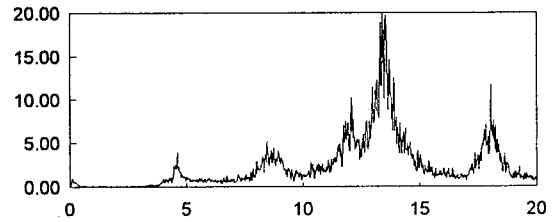
NODE 16



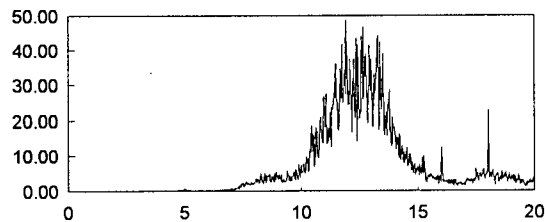
NODE 17



NODE 18



NODE 19



NOTES:

1. All plots high resolution frequency (0.0195Hz), 16 segments, abscissa: frequency (Hz), ordinate: PSD magnitude

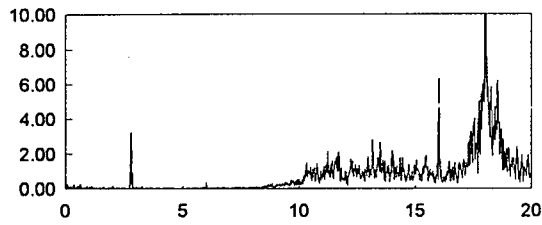
FIGURE C9

POWER SPECTRAL DENSITY FUNCTIONS

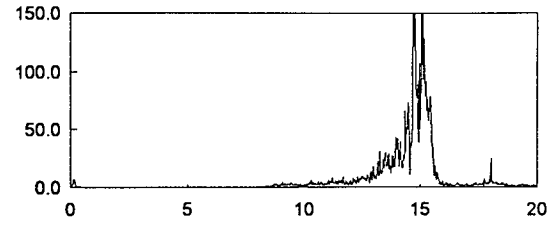
Ogee, Upstream-Downstream Direction

RUSKIN DAM AMBIENT VIBRATION FIELD TEST, LOW RESERVOIR, 30 April & 1 May 1994

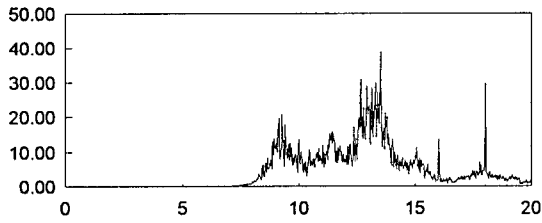
NODE 11



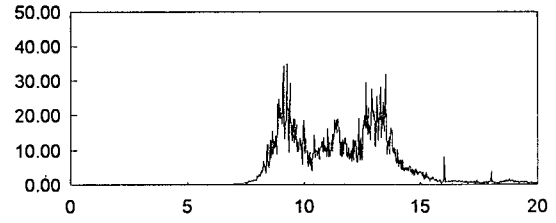
NODE 12



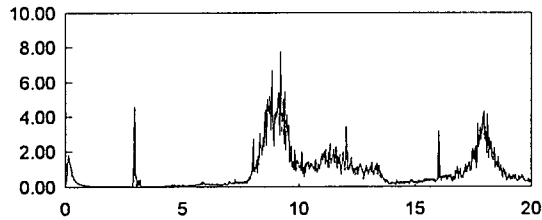
NODE 13



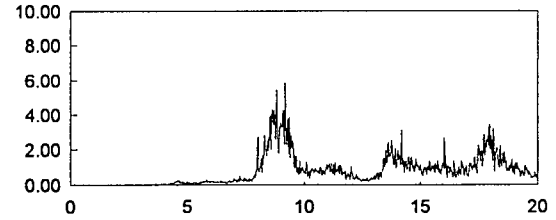
NODE 14



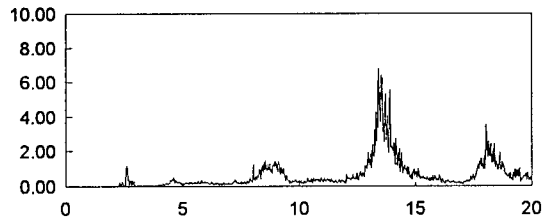
NODE 15



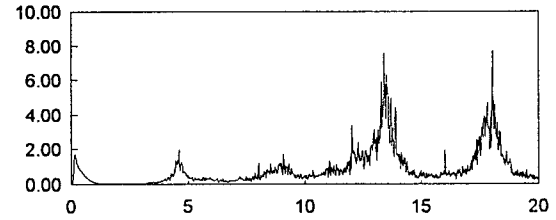
NODE 16



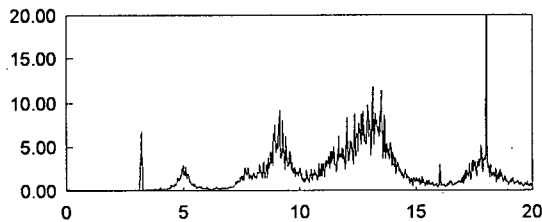
NODE 17



NODE 18



NODE 19



NOTES:

1. All plots high resolution frequency (0.0195Hz), 16 segments, abscissa: frequency (Hz), ordinate: PSD magnitude

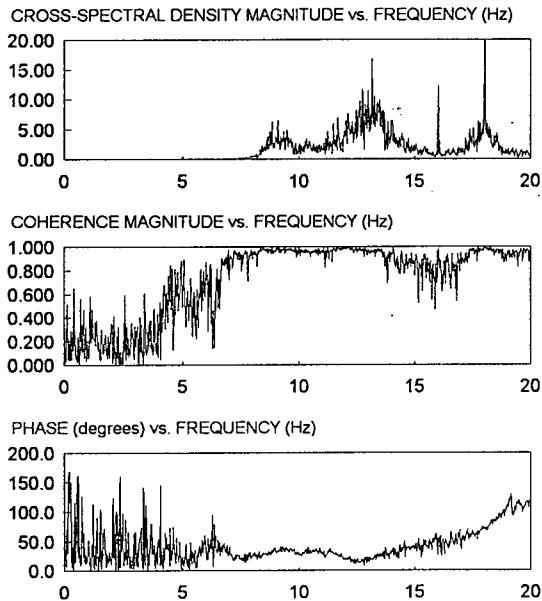
FIGURE C10

POWER SPECTRAL DENSITY FUNCTIONS

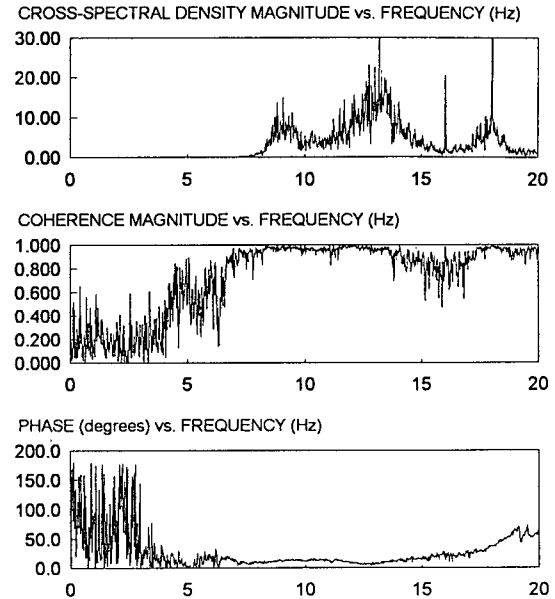
Ogee, Vertical Direction

RUSKIN DAM AMBIENT VIBRATION FIELD TEST, LOW RESERVOIR, 30 April & 1 May 1994

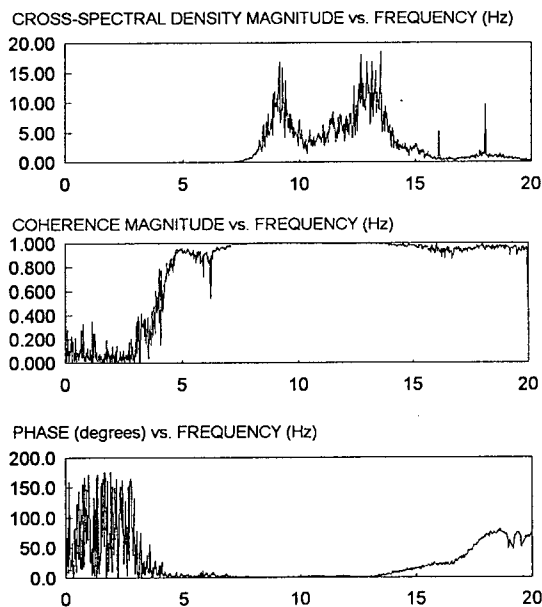
NODES 13 AND 11:



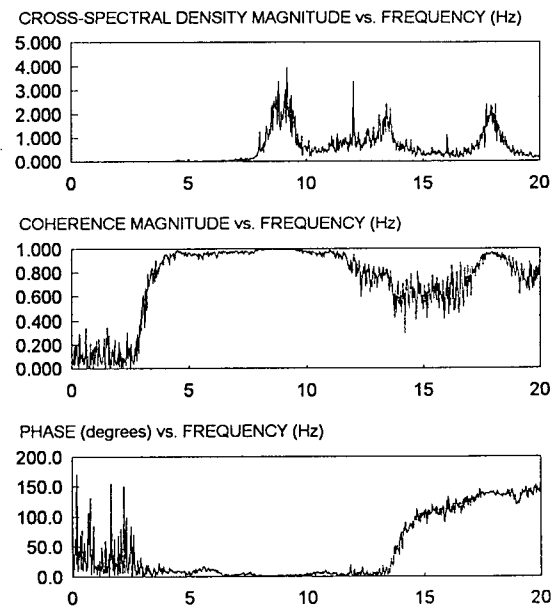
NODES 13 AND 12:



NODES 13 AND 14:



NODES 13 AND 15:



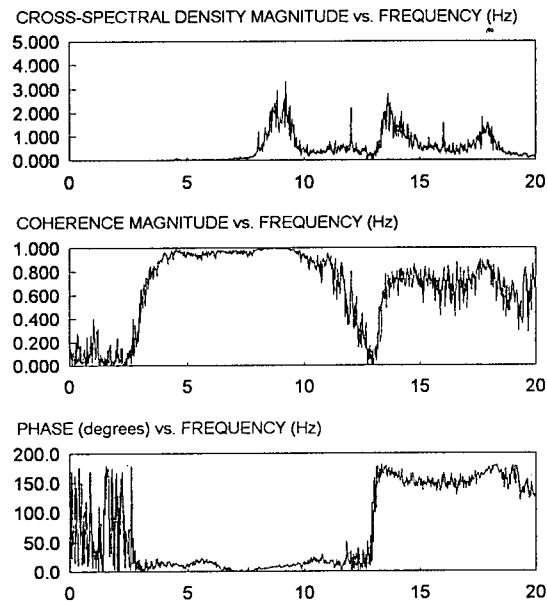
NOTES:

1. All plots completed with high resolution frequency (0.0195Hz) and with 16 segments

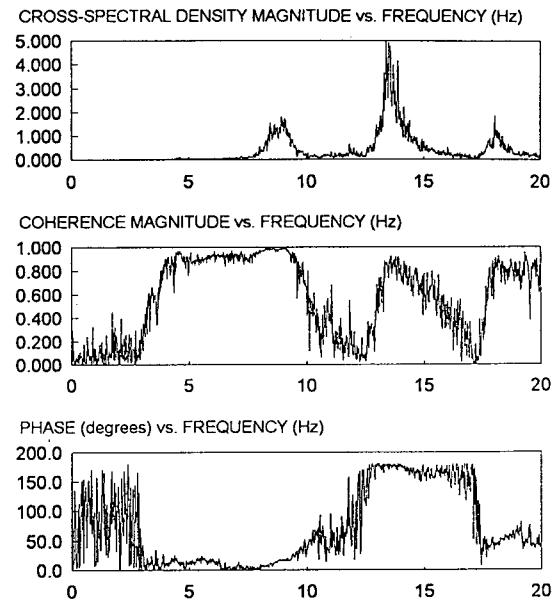
FIGURE C11

CROSS-SPECTRAL DENSITY, COHERENCE and PHASE FACTOR FUNCTIONS
Ogee and Reference Sensor, Upstream-Downstream Direction
RUSKIN DAM AMBIENT VIBRATION FIELD TEST, LOW RESERVOIR, 30 April & 1 May 1994

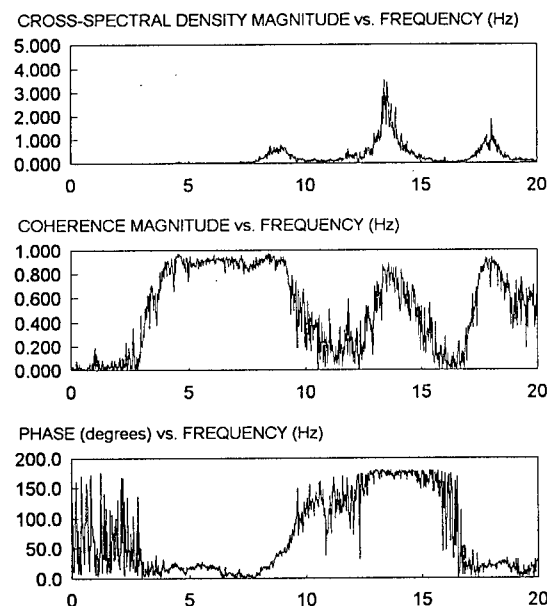
NODES 13 AND 16:



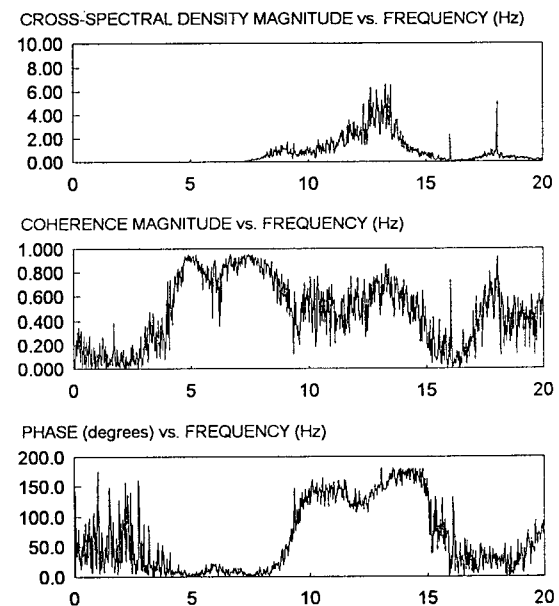
NODES 13 AND 17:



NODES 13 AND 18:



NODES 13 AND 19:



NOTES:

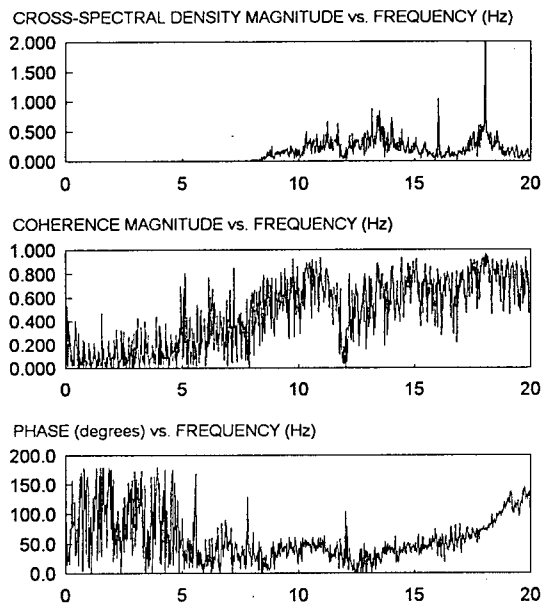
1. All plots completed with high resolution frequency (0.0195Hz) and with 16 segments

FIGURE C12

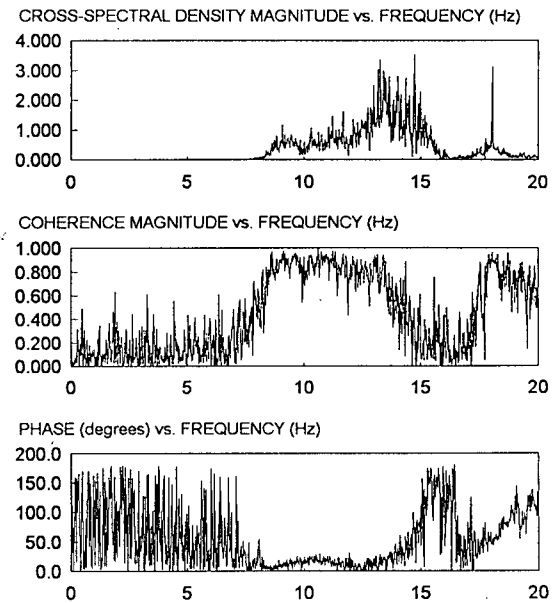
CROSS-SPECTRAL DENSITY, COHERENCE and PHASE FACTOR FUNCTIONS
Ogee and Reference Sensor, Upstream-Downstream Direction

RUSKIN DAM AMBIENT VIBRATION FIELD TEST, LOW RESERVOIR, 30 April & 1 May 1994

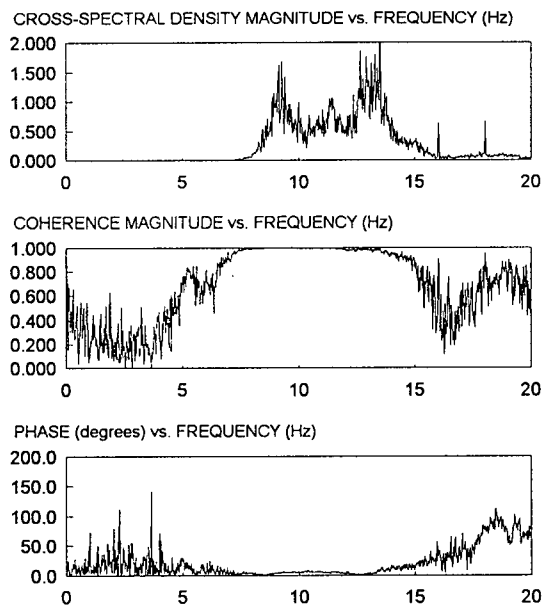
NODES 13 AND 11:



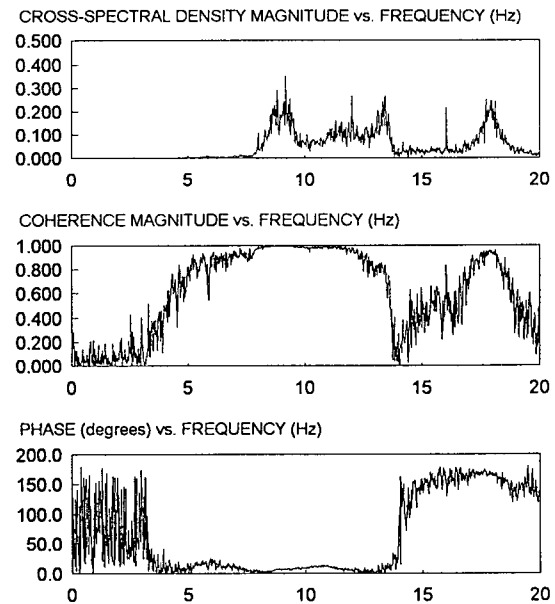
NODES 13 AND 12:



NODES 13 AND 14:



NODES 13 AND 15:



NOTES:

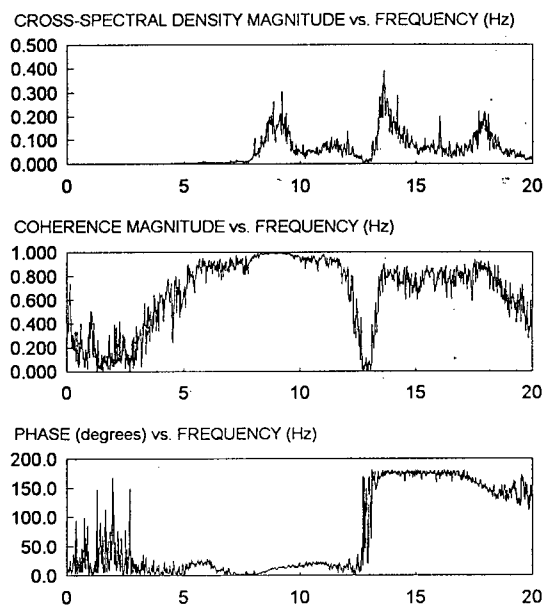
1. All plots completed with high resolution frequency (0.0195Hz) and with 16 segments

FIGURE C13

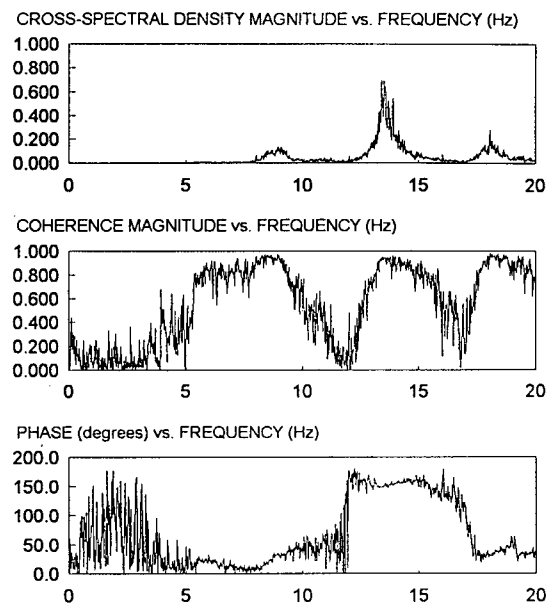
CROSS-SPECTRAL DENSITY, COHERENCE and PHASE FACTOR FUNCTIONS
Ogee and Reference Sensor, Vertical Direction

RUSKIN DAM AMBIENT VIBRATION FIELD TEST, LOW RESERVOIR, 30 April & 1 May 1994

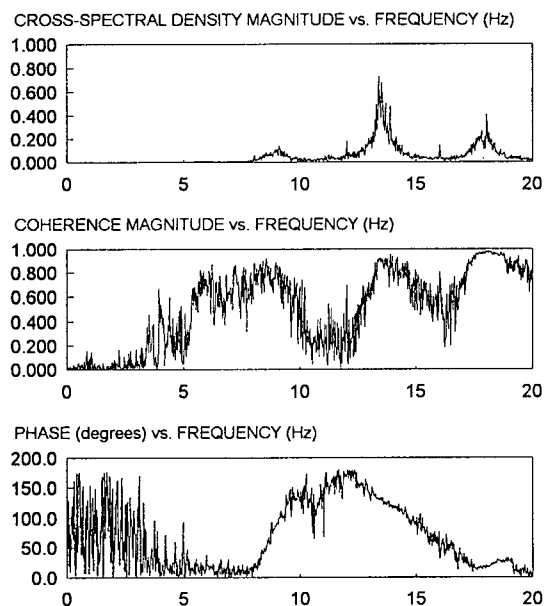
NODES 13 AND 16:



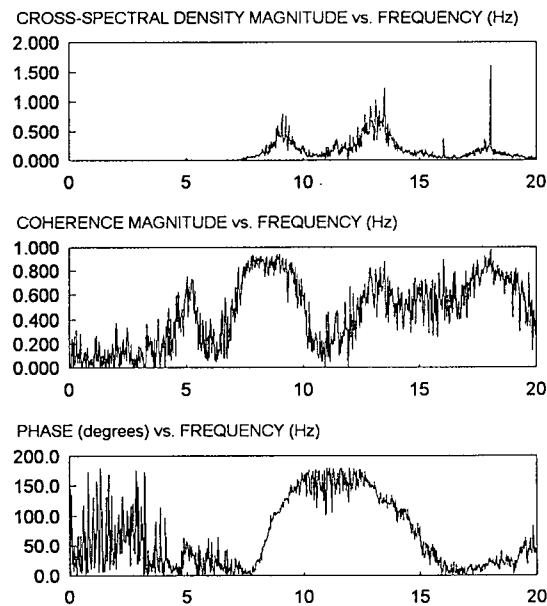
NODES 13 AND 17:



NODES 13 AND 18:



NODES 13 AND 19:



NOTES:

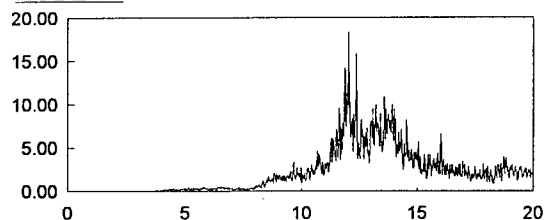
1. All plots completed with high resolution frequency (0.0195Hz) and with 16 segments

FIGURE C14

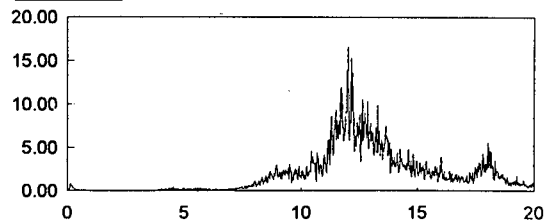
CROSS-SPECTRAL DENSITY, COHERENCE and PHASE FACTOR FUNCTIONS
Ogee and Reference Sensor, Vertical Direction

RUSKIN DAM AMBIENT VIBRATION FIELD TEST, LOW RESERVOIR, 30 April & 1 May 1994

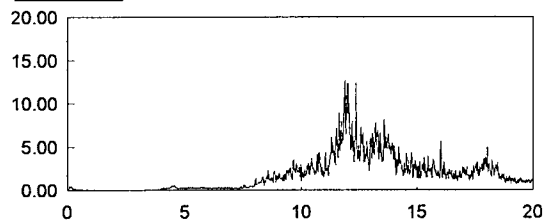
NODE 31



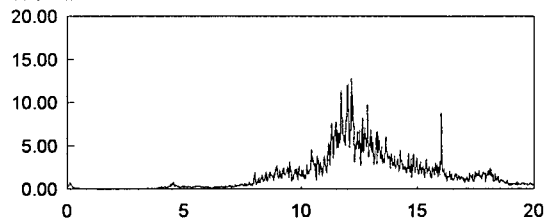
NODE 32



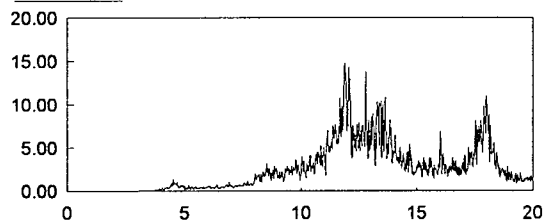
NODE 33



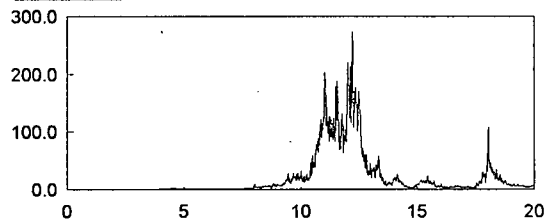
NODE 34



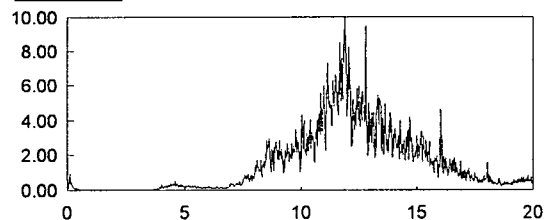
NODE 35



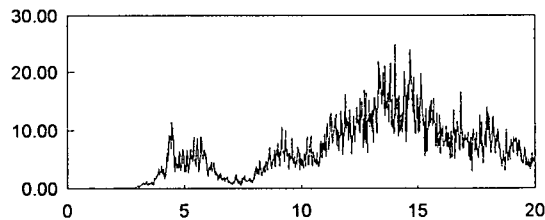
NODE 36



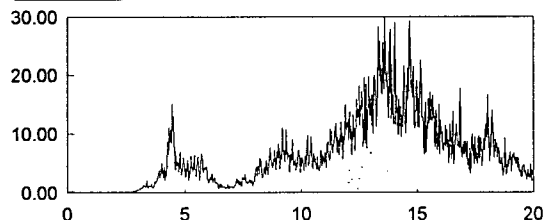
NODE 37



NODE 38



NODE 39



NOTES:

1. All plots high resolution frequency (0.0195Hz), 16 segments, abscissa: frequency (Hz), ordinate: PSD magnitude

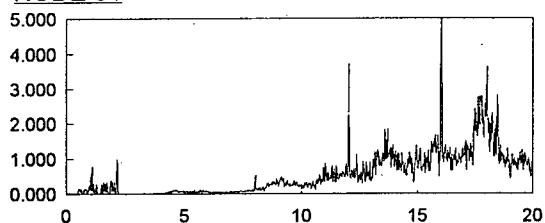
FIGURE C15

POWER SPECTRAL DENSITY FUNCTIONS

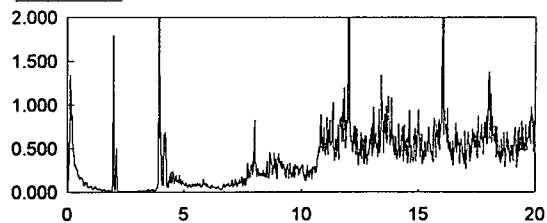
East Bedrock, Upstream-Downstream Direction

RUSKIN DAM AMBIENT VIBRATION FIELD TEST, LOW RESERVOIR, 30 April & 1 May 1994

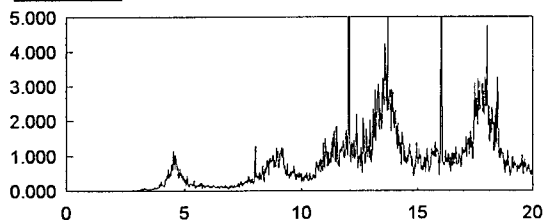
NODE 31



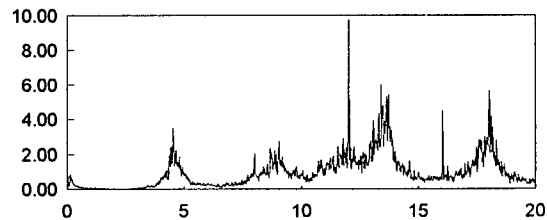
NODE 32



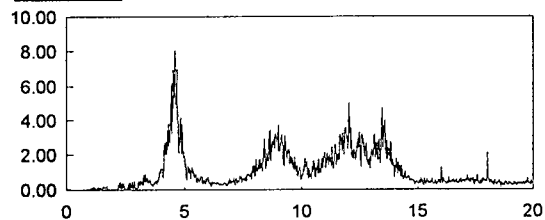
NODE 33



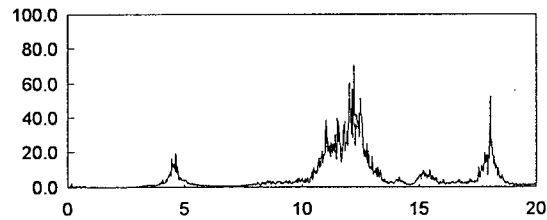
NODE 34



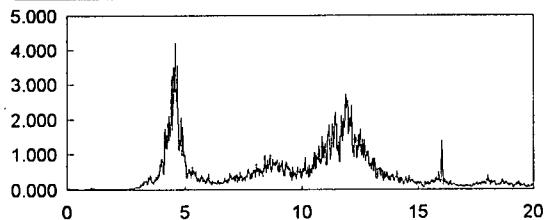
NODE 35



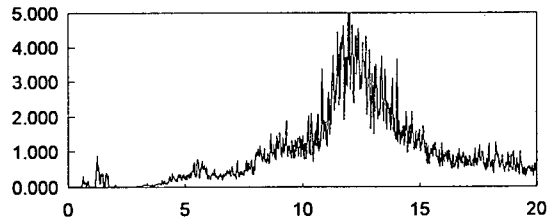
NODE 36



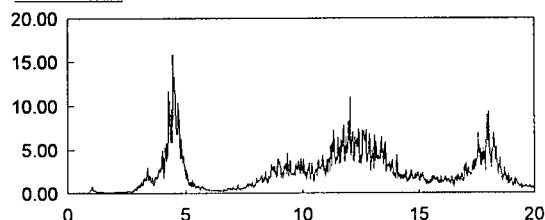
NODE 37



NODE 38



NODE 39



NOTES:

1. All plots high resolution frequency (0.0195Hz), 16 segments, abscissa: frequency (Hz), ordinate: PSD magnitude

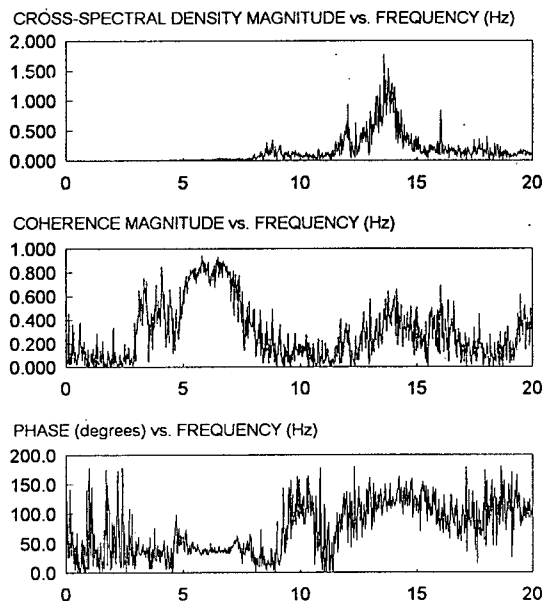
FIGURE C16

POWER SPECTRAL DENSITY FUNCTIONS

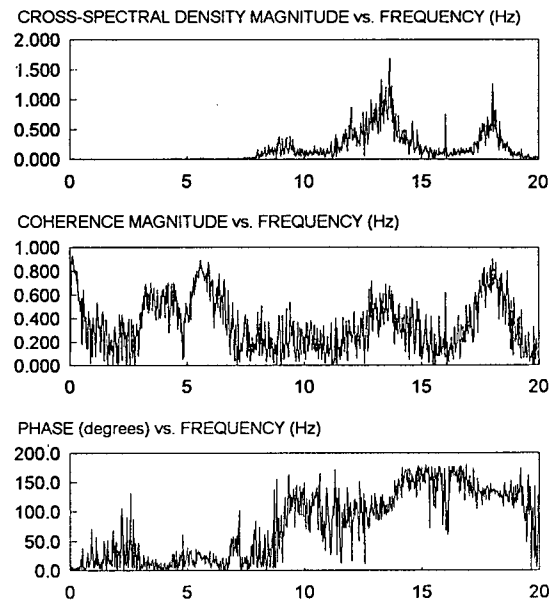
East Bedrock, Vertical Direction

RUSKIN DAM AMBIENT VIBRATION FIELD TEST, LOW RESERVOIR, 30 April & 1 May 1994

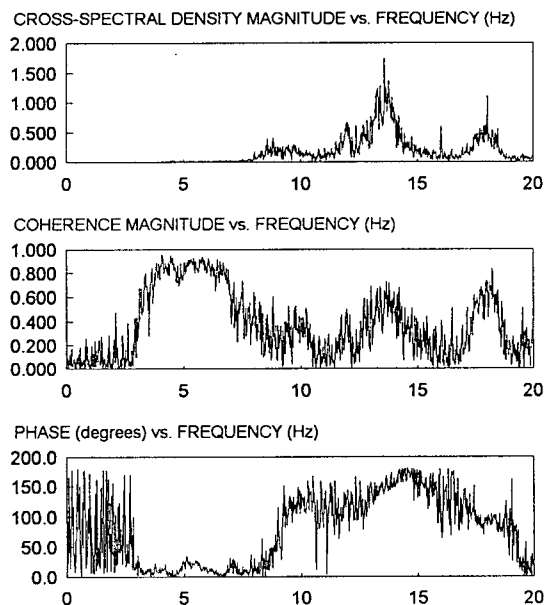
NODES 13 AND 31:



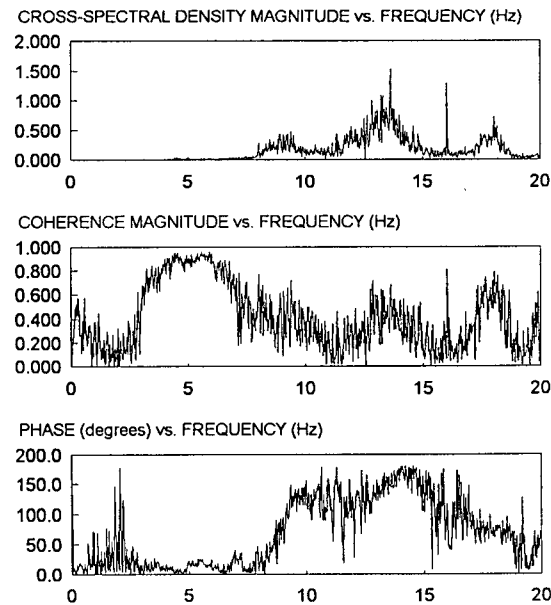
NODES 13 AND 32:



NODES 13 AND 33:



NODES 13 AND 34:



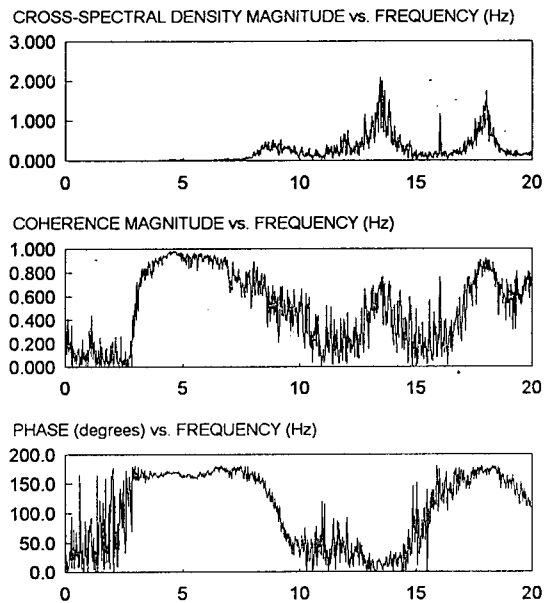
NOTES:

1. All plots completed with high resolution frequency (0.0195Hz) and with 16 segments

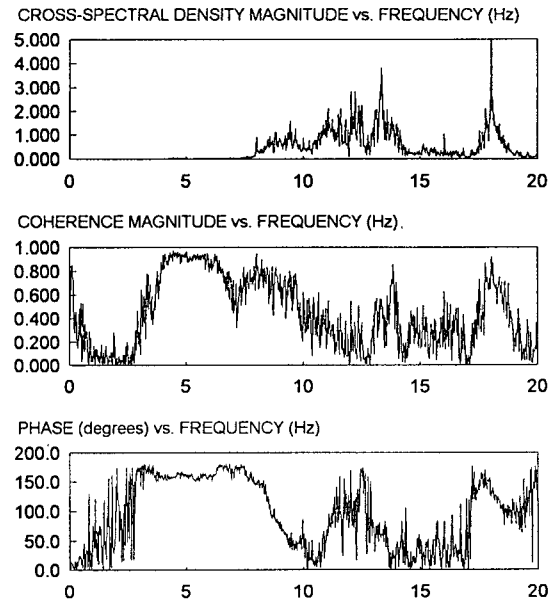
FIGURE C17

CROSS-SPECTRAL DENSITY, COHERENCE and PHASE FACTOR FUNCTIONS
East Bedrock and Reference Sensor, Upstream-Downstream Direction
RUSKIN DAM AMBIENT VIBRATION FIELD TEST, LOW RESERVOIR, 30 April & 1 May 1994

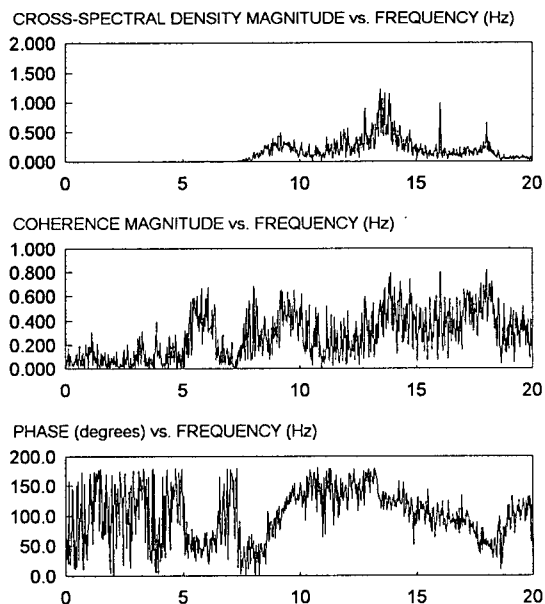
NODES 13 AND 35:



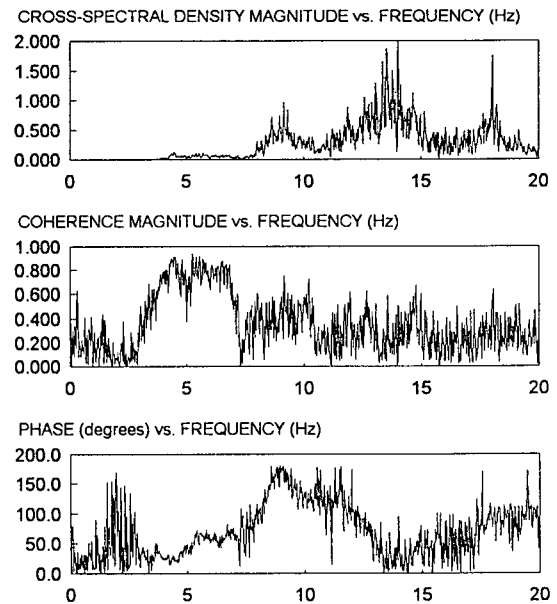
NODES 13 AND 36:



NODES 13 AND 37:



NODES 13 AND 38:



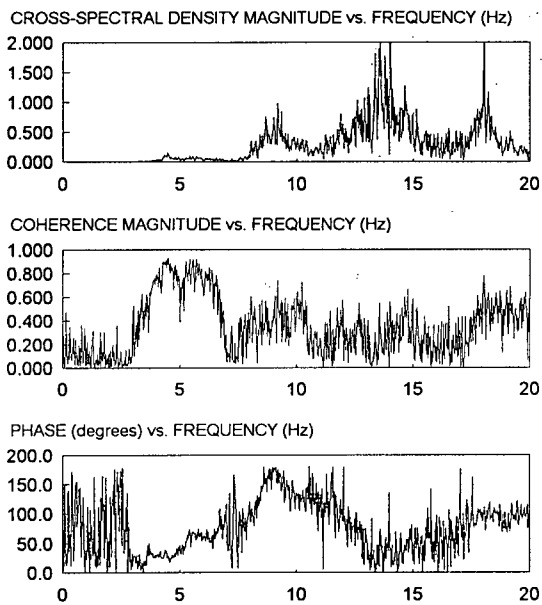
NOTES:

1. All plots completed with high resolution frequency (0.0195Hz) and with 16 segments

FIGURE C18

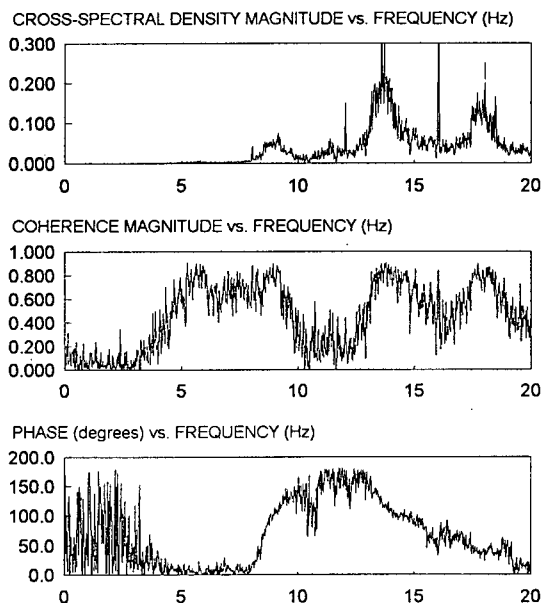
CROSS-SPECTRAL DENSITY, COHERENCE and PHASE FACTOR FUNCTIONS
East Bedrock and Reference Sensor, Upstream-Downstream Direction
RUSKIN DAM AMBIENT VIBRATION FIELD TEST, LOW RESERVOIR, 30 April & 1 May 1994

NODES 13 AND 39:

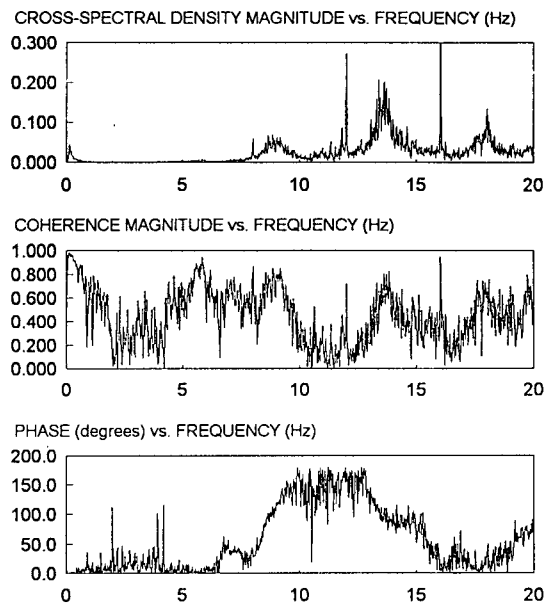


NOTES:	
1. All plots completed with high resolution frequency (0.0195Hz) and with 16 segments	
FIGURE C19	CROSS-SPECTRAL DENSITY, COHERENCE and PHASE FACTOR FUNCTIONS
	East Bedrock and Reference Sensor, Upstream-Downstream Direction
	RUSKIN DAM AMBIENT VIBRATION FIELD TEST, LOW RESERVOIR, 30 April & 1 May 1994

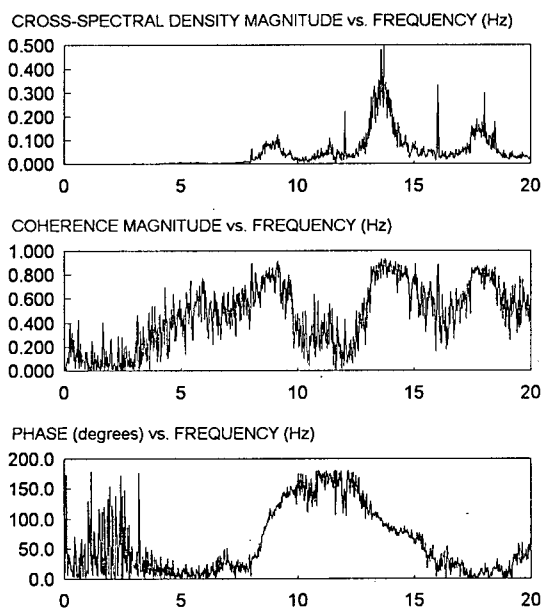
NODES 13 AND 31:



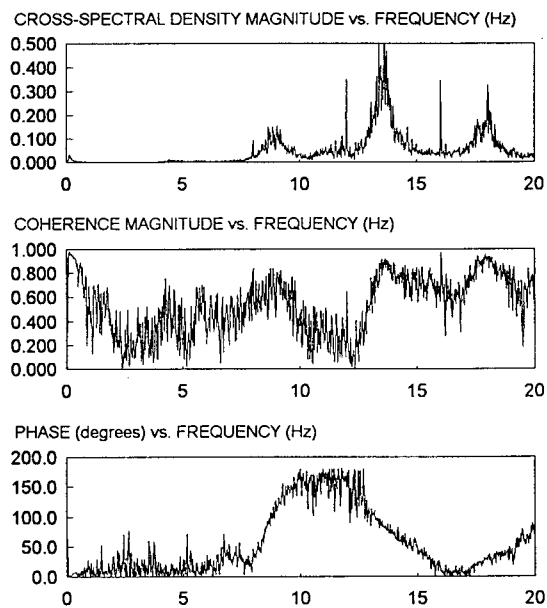
NODES 13 AND 32:



NODES 13 AND 33:



NODES 13 AND 34:



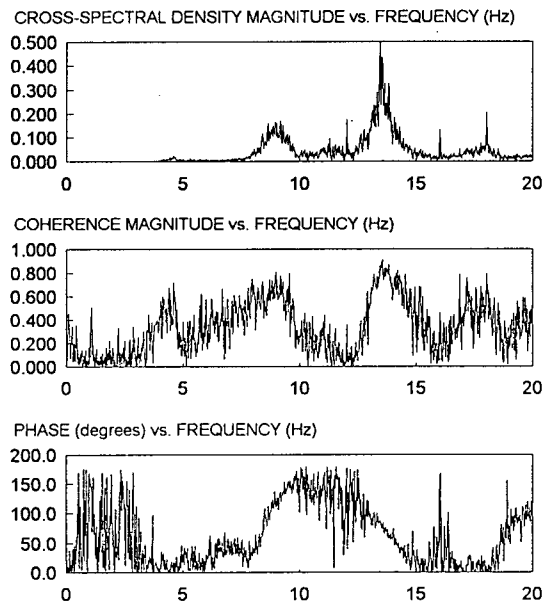
NOTES:

1. All plots completed with high resolution frequency (0.0195Hz) and with 16 segments

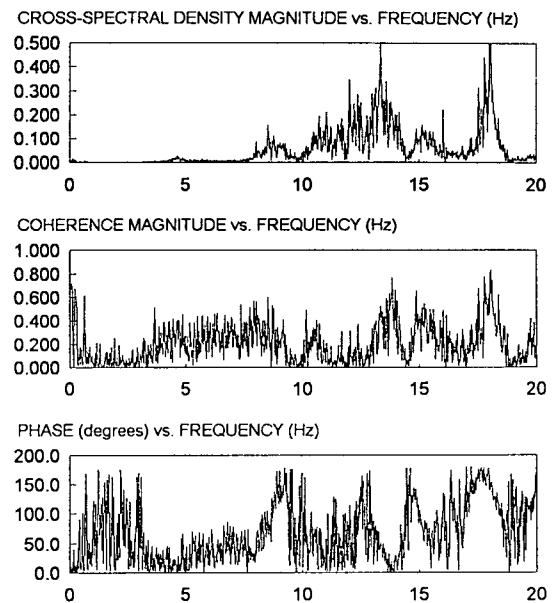
FIGURE C20

CROSS-SPECTRAL DENSITY, COHERENCE and PHASE FACTOR FUNCTIONS
East Bedrock and Reference Sensor, Vertical Direction
RUSKIN DAM AMBIENT VIBRATION FIELD TEST, LOW RESERVOIR, 30 April & 1 May 1994

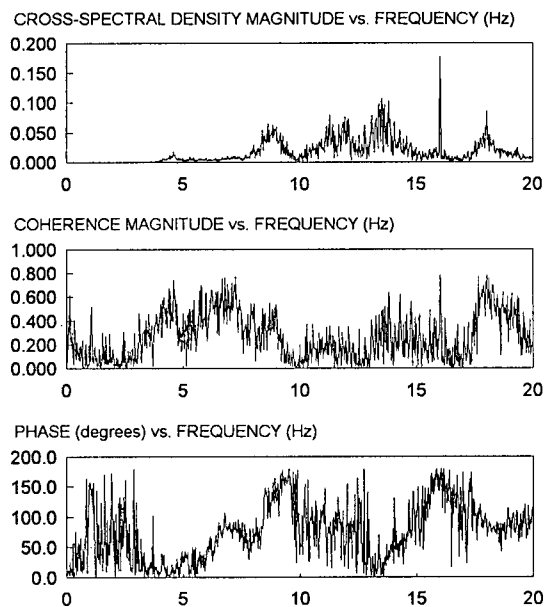
NODES 13 AND 35:



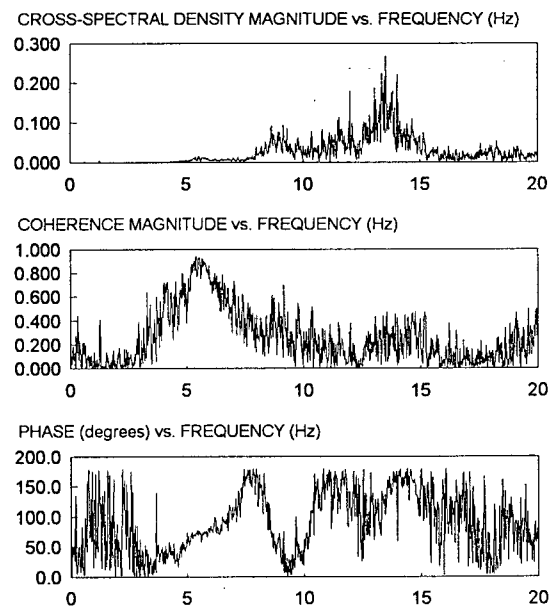
NODES 13 AND 36:



NODES 13 AND 37:



NODES 13 AND 38:



NOTES:

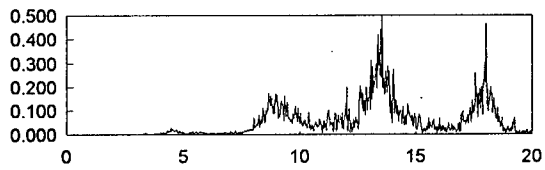
1. All plots completed with high resolution frequency (0.0195Hz) and with 16 segments

FIGURE C21

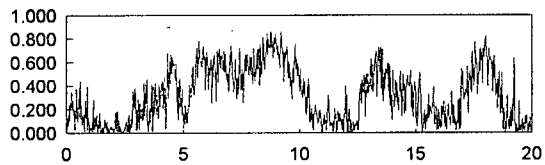
CROSS-SPECTRAL DENSITY, COHERENCE and PHASE FACTOR FUNCTIONS
East Bedrock and Reference Sensor, Vertical Direction
RUSKIN DAM AMBIENT VIBRATION FIELD TEST, LOW RESERVOIR, 30 April & 1 May 1994

NODES 13 AND 39:

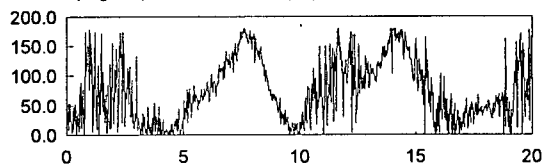
CROSS-SPECTRAL DENSITY MAGNITUDE vs. FREQUENCY (Hz)



COHERENCE MAGNITUDE vs. FREQUENCY (Hz)



PHASE (degrees) vs. FREQUENCY (Hz)



NOTES:

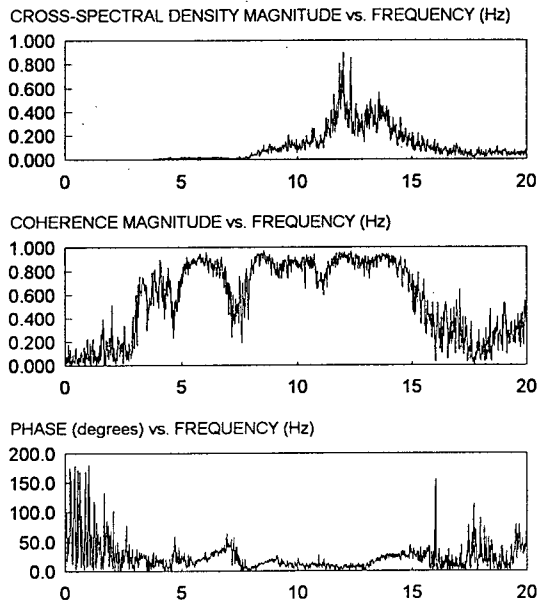
1. All plots completed with high resolution frequency (0.0195Hz) and with 16 segments

FIGURE C22

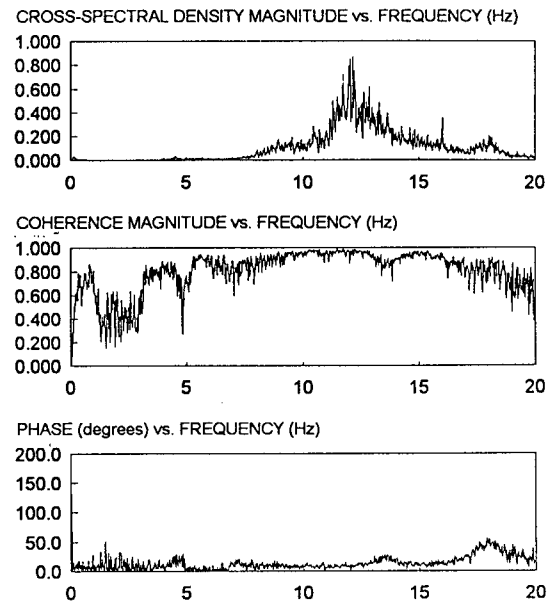
CROSS-SPECTRAL DENSITY, COHERENCE and PHASE FACTOR FUNCTIONS
East Bedrock and Reference Sensor, Vertical Direction

RUSKIN DAM AMBIENT VIBRATION FIELD TEST, LOW RESERVOIR, 30 April & 1 May 1994

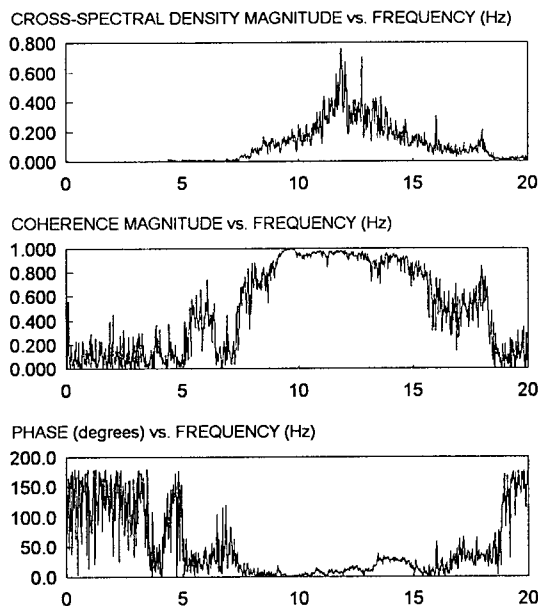
NODES 31 and 33



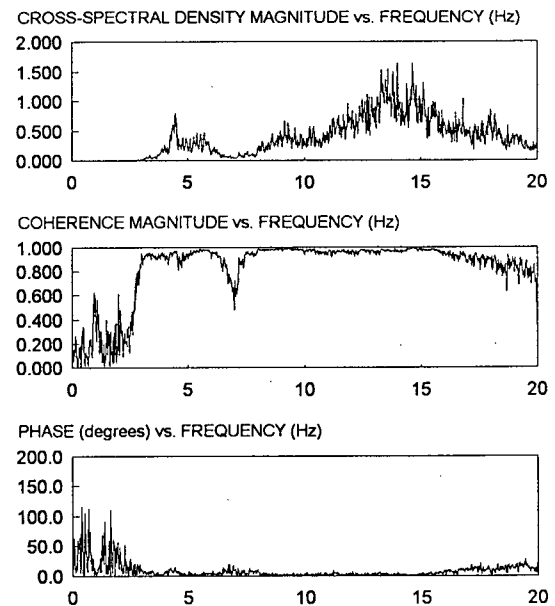
NODES 32 and 34



NODES 35 and 37



NODES 38 and 39



NOTES:

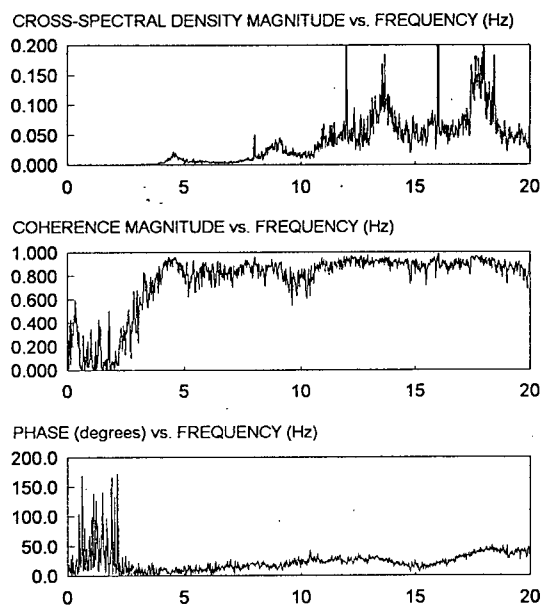
1. All plots completed with high resolution frequency (0.0195 Hz) and 16 segments

FIGURE C23

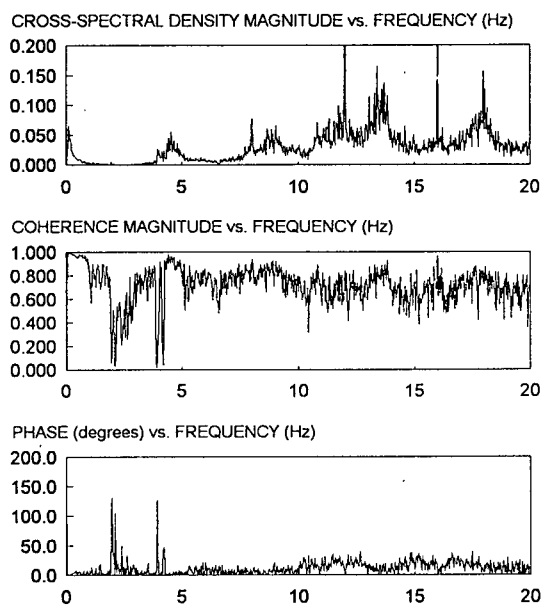
CROSS-SPECTRAL DENSITY, COHERENCE and PHASE FACTOR FUNCTIONS
East Bedrock, Upstream-Downstream Direction

RUSKIN DAM AMBIENT VIBRATION FIELD TEST, LOW RESERVOIR, 30 April & 1 May 1994

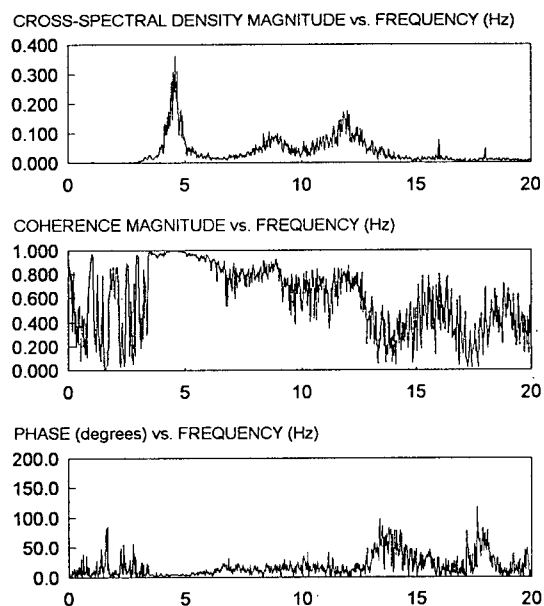
NODES 31 and 33



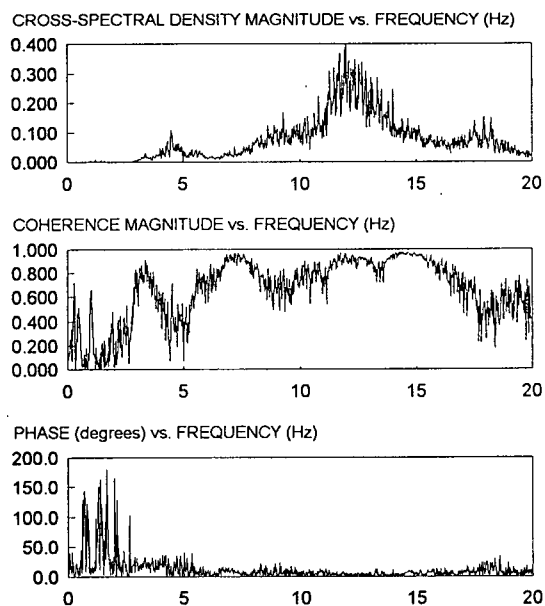
NODES 32 and 34



NODES 35 and 37



NODES 38 and 39



NOTES:

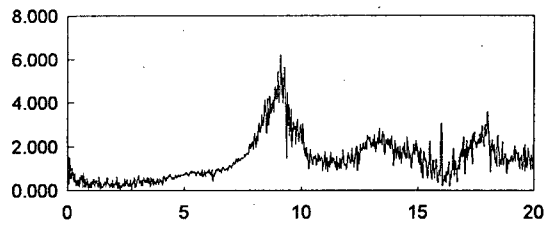
1. All plots completed with high resolution frequency (0.0195 Hz) and 16 segments

FIGURE C24

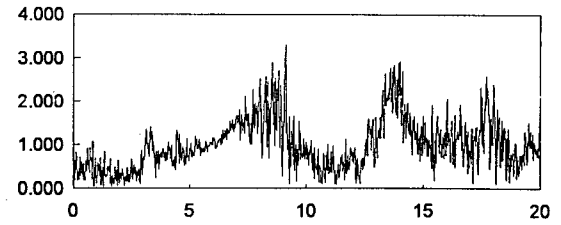
CROSS-SPECTRAL DENSITY, COHERENCE and PHASE FACTOR FUNCTIONS
East Bedrock, Vertical Direction

RUSKIN DAM AMBIENT VIBRATION FIELD TEST, LOW RESERVOIR, 30 April & 1 May 1994

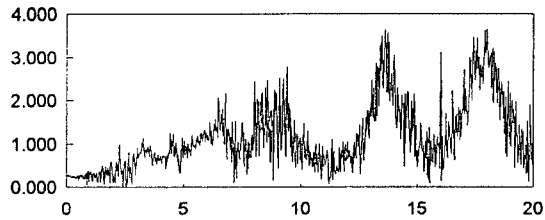
NODE 19



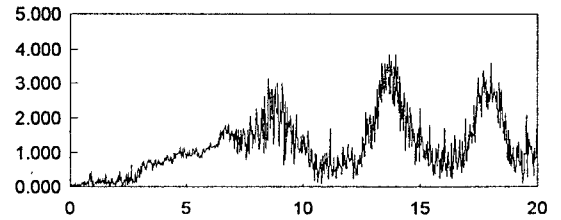
NODE 31



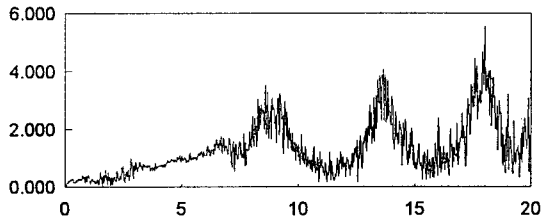
NODE 32



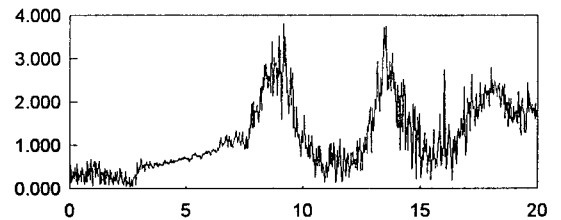
NODE 33



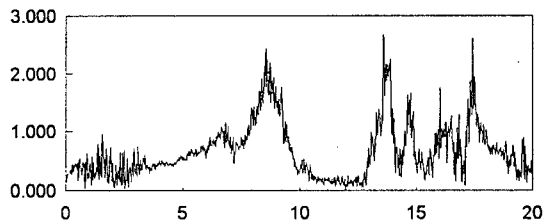
NODE 34



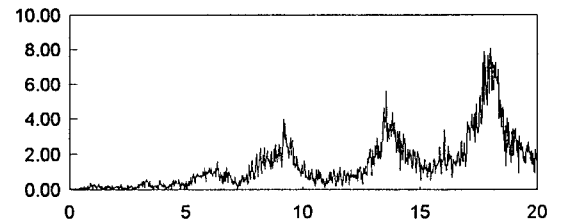
NODE 35



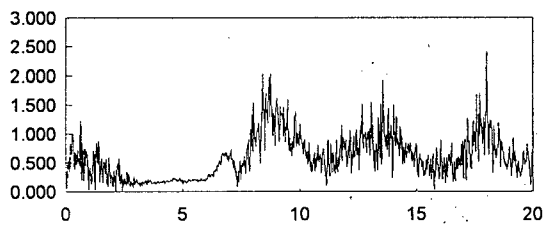
NODE 36



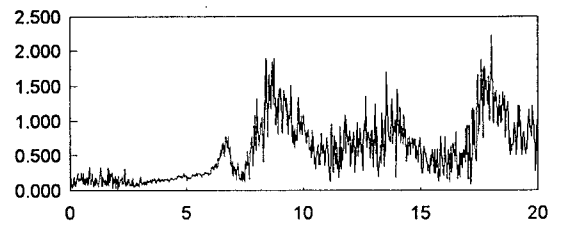
NODE 37



NODE 38



NODE 39



NOTES:

1. All plots completed with high resolution (0.0195 Hz) and 16 segments
2. Abscissa: frequency (Hz), ordinate: transfer function gain magnitude

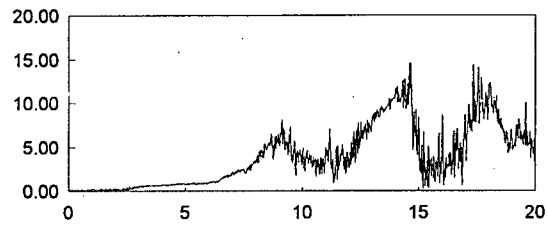
FIGURE C25

TRANSFER FUNCTION GAIN

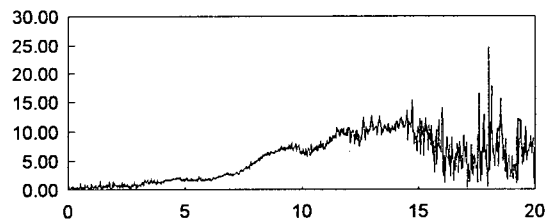
East Bedrock and Reference Sensor, Upstream-Downstream Direction

RUSKIN DAM AMBIENT VIBRATION FIELD TEST, LOW RESERVOIR, 30 April & 1 May 1994

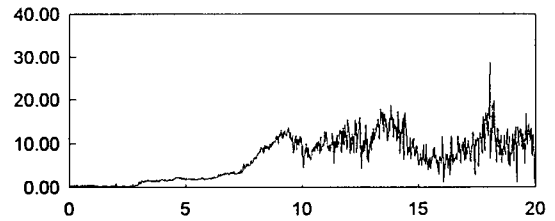
NODE 27



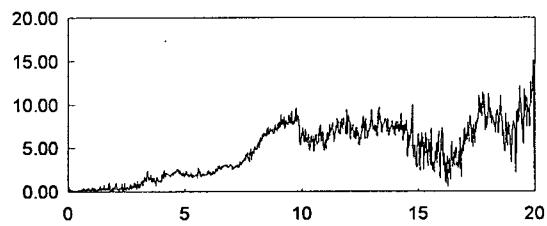
NODE 28



NODE 29

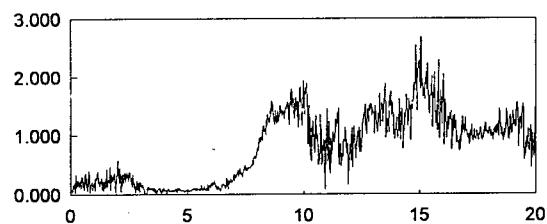


NODE 30

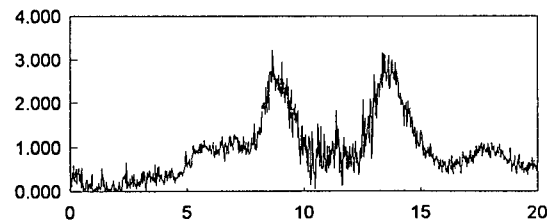


<u>NOTES:</u> 1. All plots completed with high resolution (0.0195 Hz) and 16 segments 2. Abscissa: frequency (Hz), ordinate: transfer function gain magnitude	
<u>FIGURE C26</u>	<u>TRANSFER FUNCTION GAIN</u>
	<u>East Bedrock and Reference Sensor, Upstream-Downstream Direction</u>
	RUSKIN DAM AMBIENT VIBRATION FIELD TEST, LOW RESERVOIR, 30 April & 1 May 1994

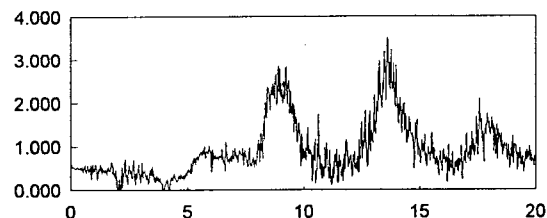
NODE 19



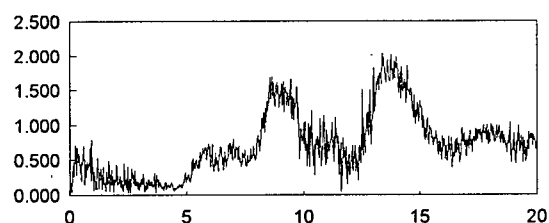
NODE 31



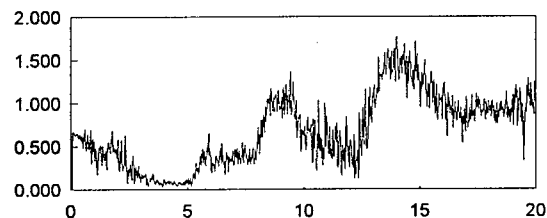
NODE 32



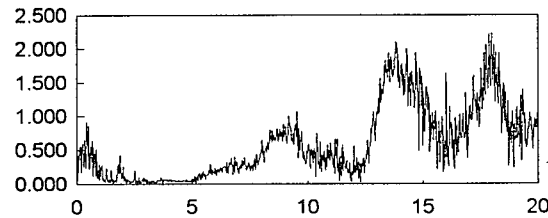
NODE 33



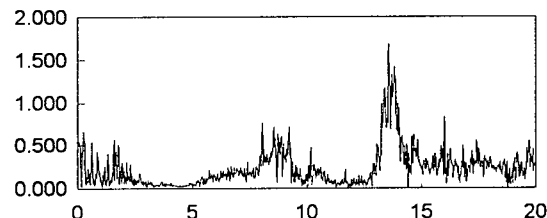
NODE 34



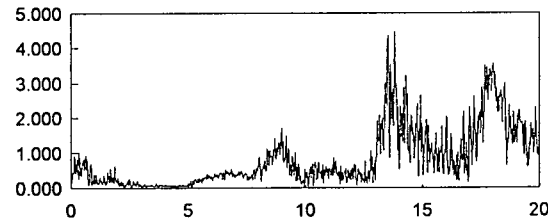
NODE 35



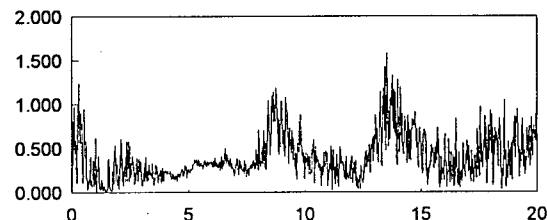
NODE 36



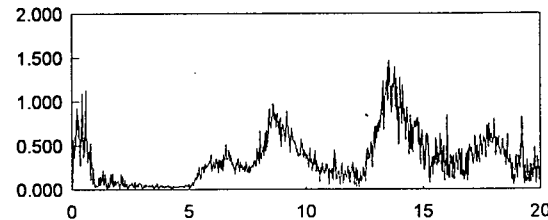
NODE 37



NODE 38



NODE 39



NOTES:

1. All plots completed with high resolution (0.0195 Hz) and 16 segments
2. Abscissa: frequency (Hz), ordinate: transfer function gain magnitude

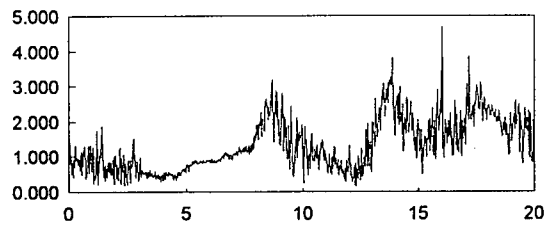
FIGURE C27

TRANSFER FUNCTION GAIN

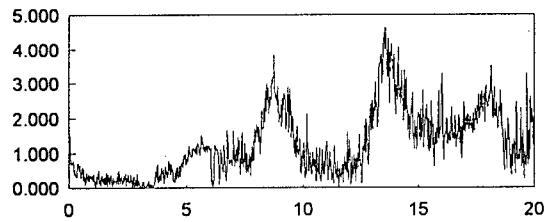
East Bedrock and Reference Sensor, Vertical Direction

RUSKIN DAM AMBIENT VIBRATION FIELD TEST, LOW RESERVOIR, 30 April & 1 May 1994

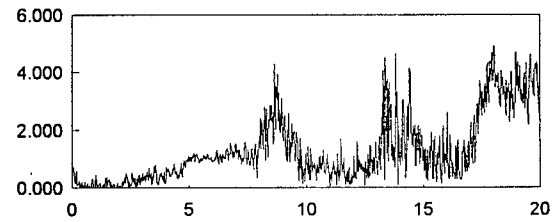
NODE 27



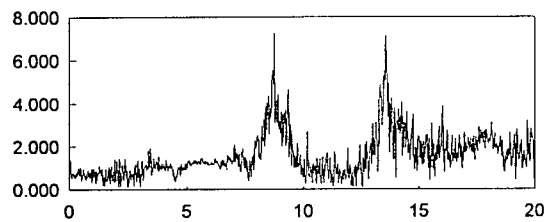
NODE 28



NODE 29



NODE 30



NOTES:

1. All plots completed with high resolution (0.0195 Hz) and 16 segments
2. Abscissa: frequency (Hz), ordinate: transfer function gain magnitude

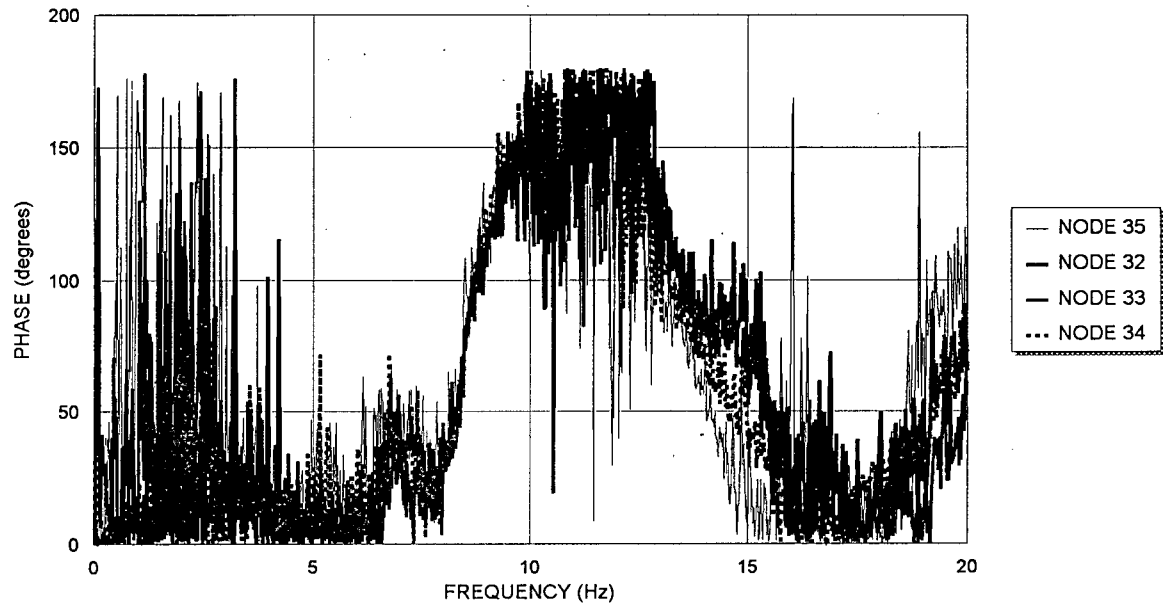
FIGURE C28

TRANSFER FUNCTION GAIN

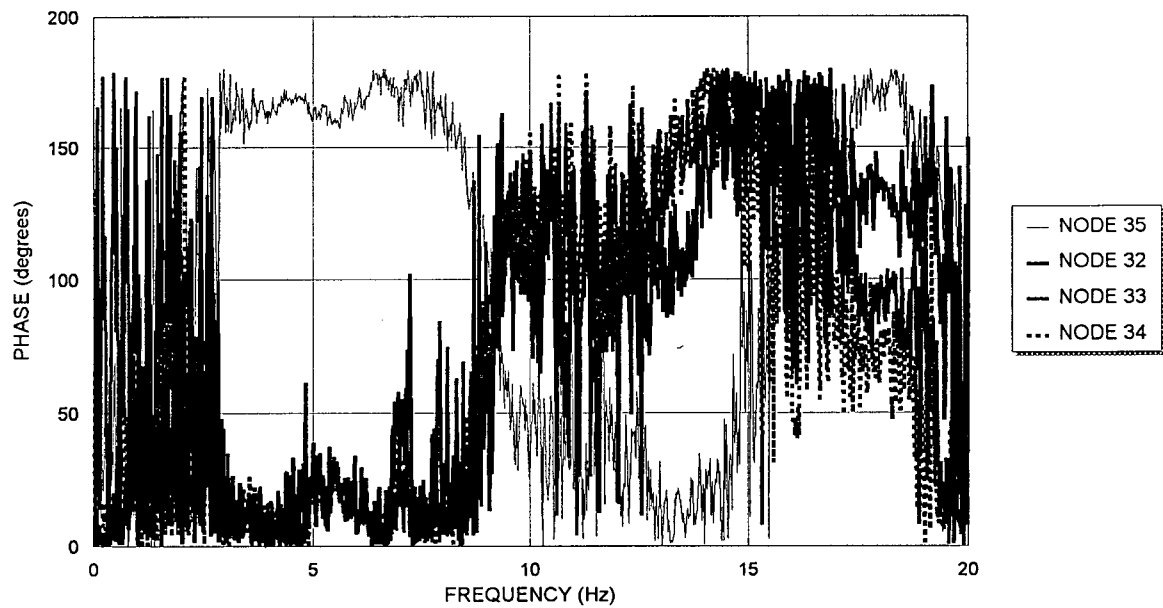
East Bedrock and Reference Sensor, Vertical Direction

RUSKIN DAM AMBIENT VIBRATION FIELD TEST, LOW RESERVOIR, 30 April & 1 May 1994

VERTICAL

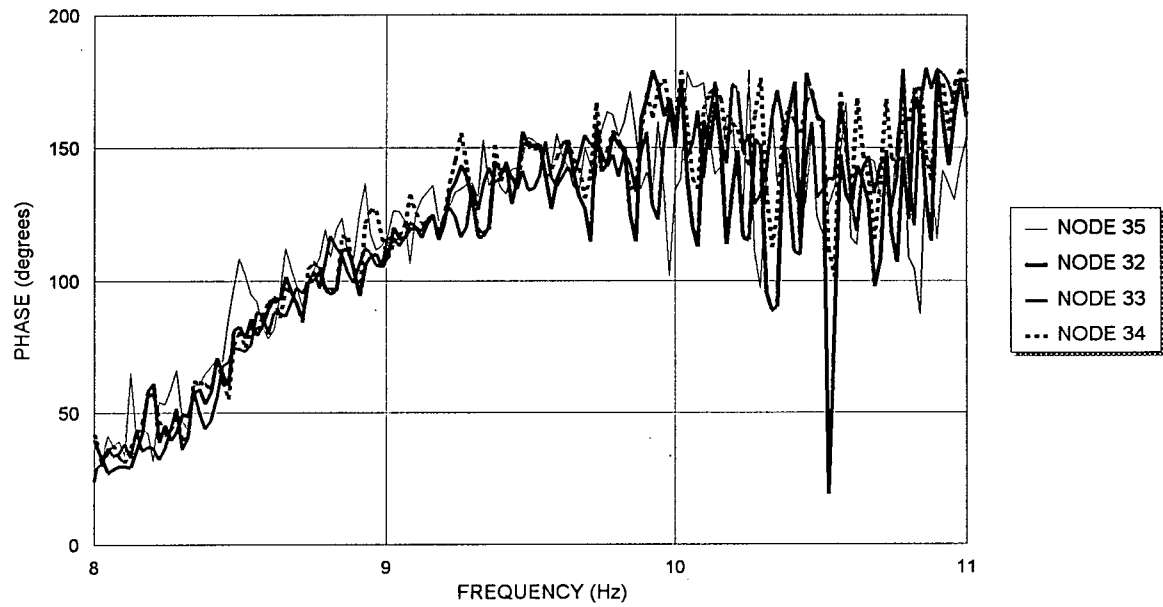


UPSTREAM-DOWNSTREAM

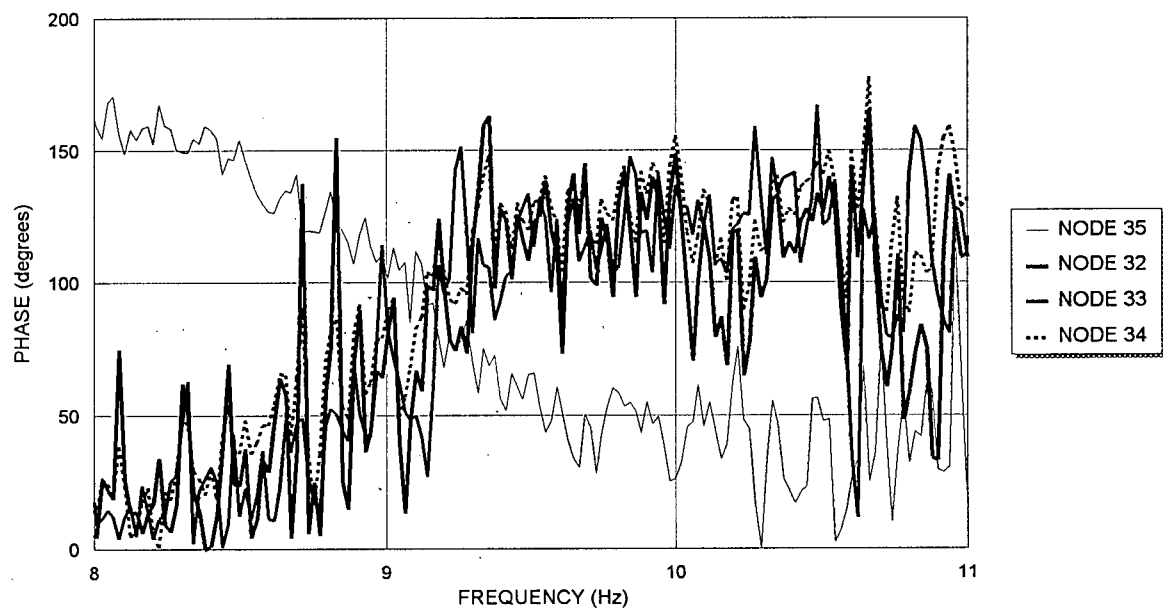


NOTES:	
1. All plots completed with high resolution frequency (0.0195Hz) and 16 segments	
FIGURE C29	PHASE FACTOR FUNCTION 0-20 Hz
	U/S & Vert., Input: Nodes 32-35 (East Bedrock), Output: Node 13 (Ogee)
	RUSKIN DAM AMBIENT VIBRATION FIELD TEST, LOW RESERVOIR, 30 April & 1 May 1994

VERTICAL



UPSTREAM-DOWNSTREAM



NOTES:

1. All plots completed with high resolution frequency (0.0195Hz) and 16 segments

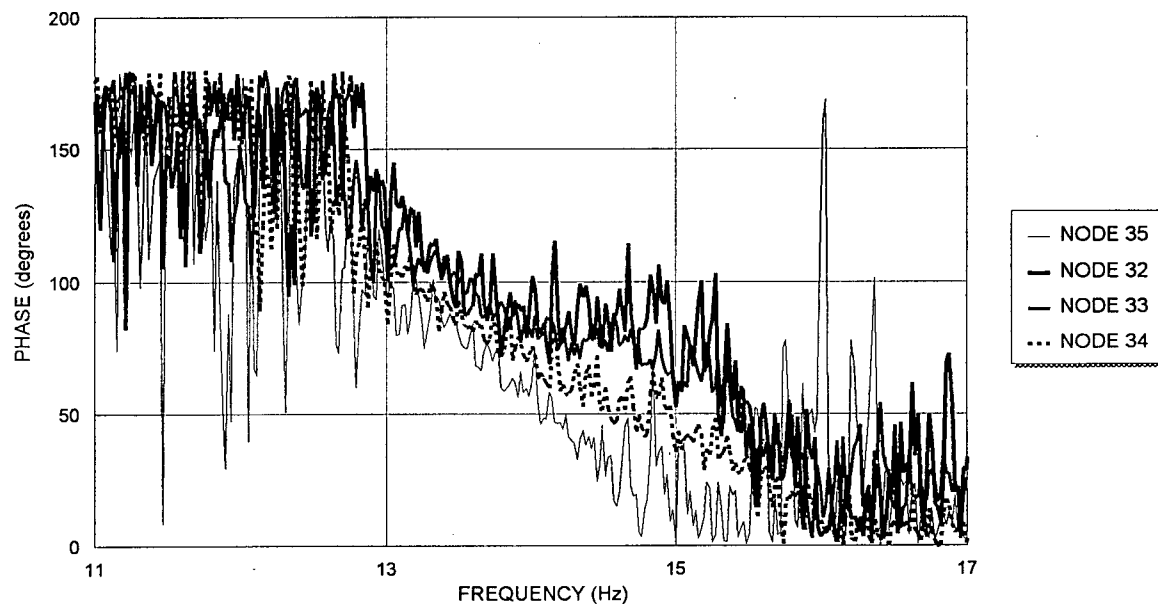
FIGURE C30

PHASE FACTOR FUNCTION 8-11 Hz

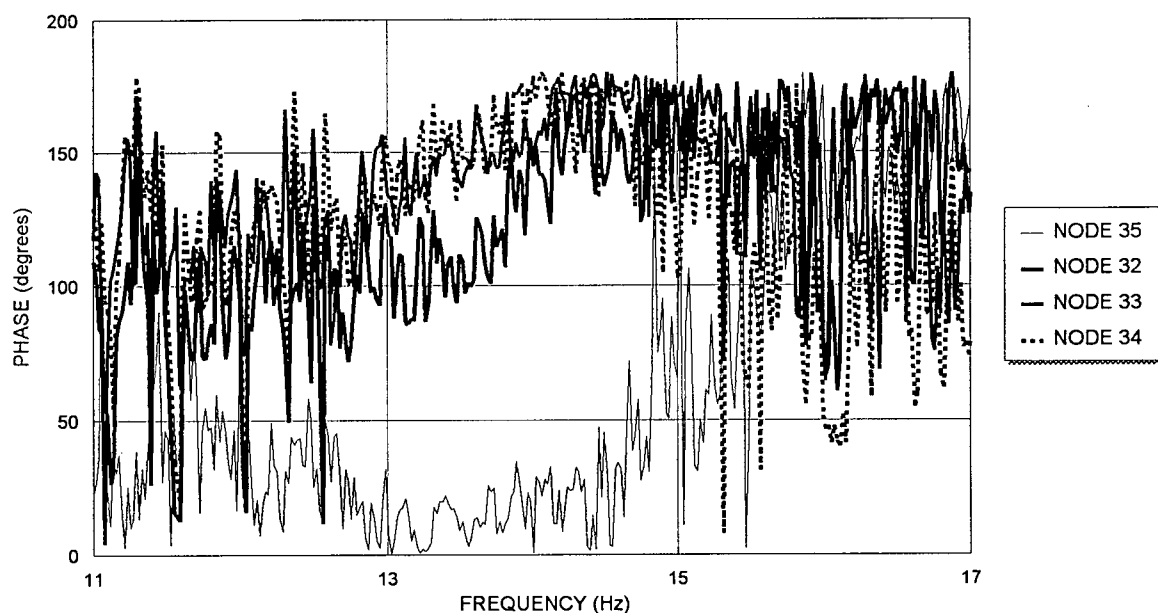
U/S & Vert., Input: Nodes 32-35 (East Bedrock), Output: Node 13 (Ogee)

RUSKIN DAM AMBIENT VIBRATION FIELD TEST, LOW RESERVOIR, 30 April & 1 May 1994

VERTICAL



UPSTREAM-DOWNSTREAM



NOTES:

1. All plots completed with high resolution frequency (0.0195Hz) and 16 segments

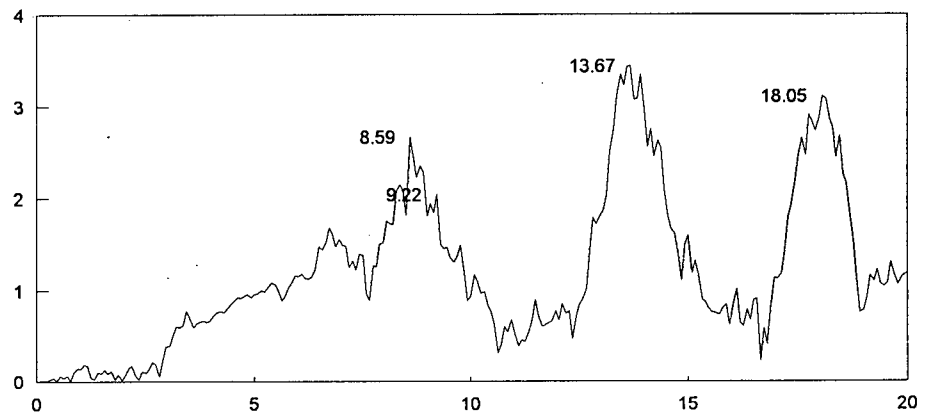
FIGURE C31

PHASE FACTOR FUNCTION 11-17 Hz

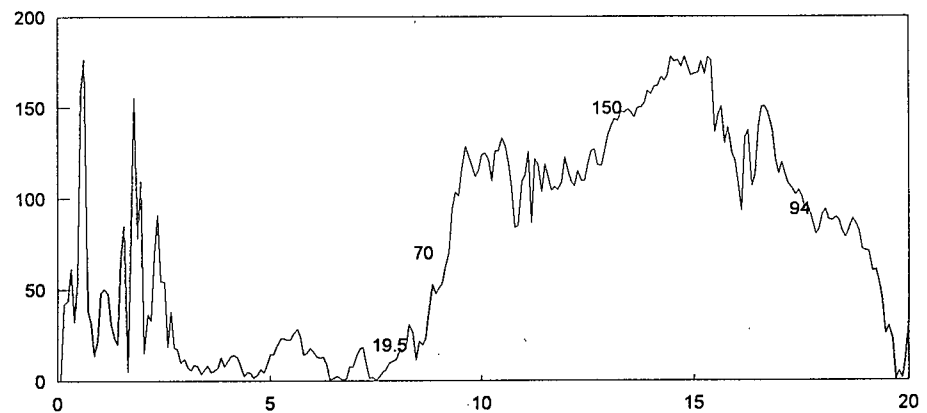
U/S & Vert., Input: Nodes 32-35 (East Bedrock), Output: Node 13 (Ogee)

RUSKIN DAM AMBIENT VIBRATION FIELD TEST, LOW RESERVOIR, 30 April & 1 May 1994

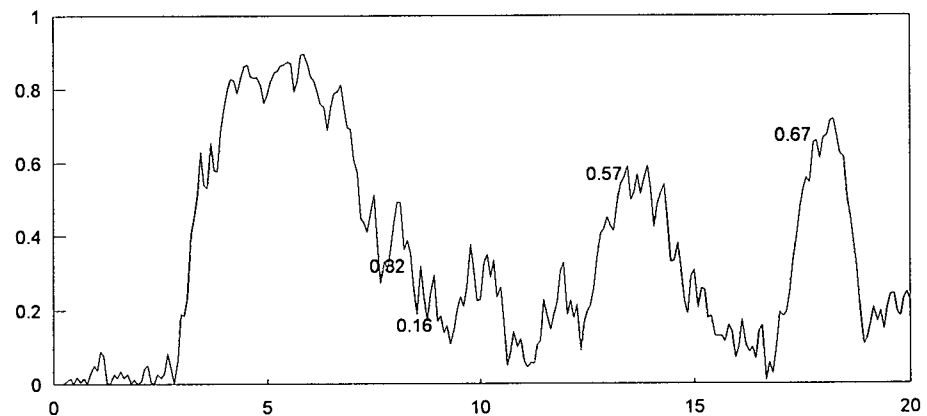
TRANSFER
FUNCTION GAIN
MAGNITUDE
vs.
FREQUENCY (Hz)



PHASE
(degrees)
vs
FREQUENCY (Hz)



COHERENCE
MAGNITUDE
vs
FREQUENCY (Hz)



NOTES:

1. All plots at low resolution (0.0781 Hz) and with 64 segments
2. Transfer function gain local maxima frequencies are indicated, as are the corresponding phase factor and coherence values

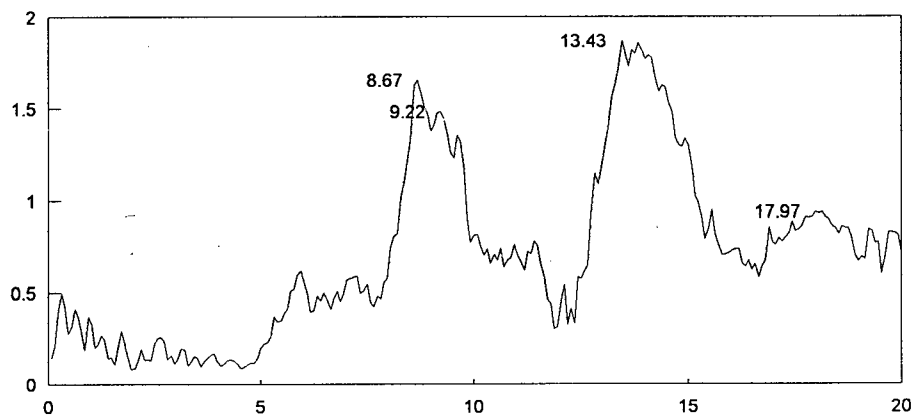
FIGURE C32

TRANSFER FUNCTION GAIN, PHASE FACTOR AND COHERENCE

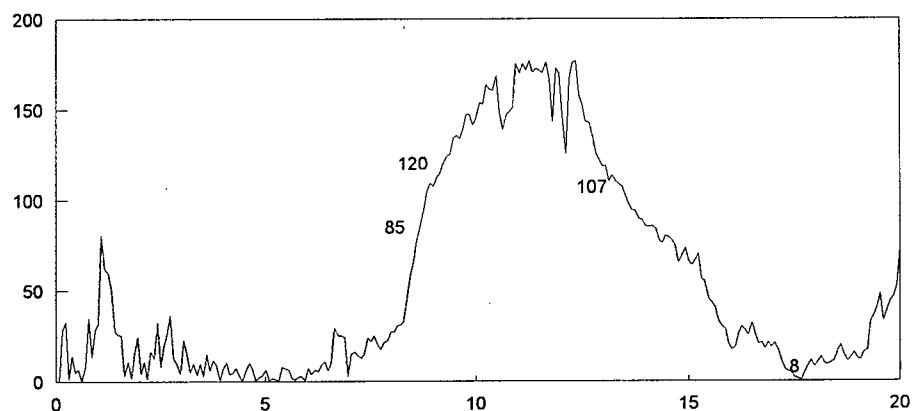
Upstream-Downstream Direction, Input: Node 33 (Bedrock), Output: Node 13 (Ogee)

RUSKIN DAM AMBIENT VIBRATION FIELD TEST, LOW RESERVOIR, 30 April & 1 May 1994

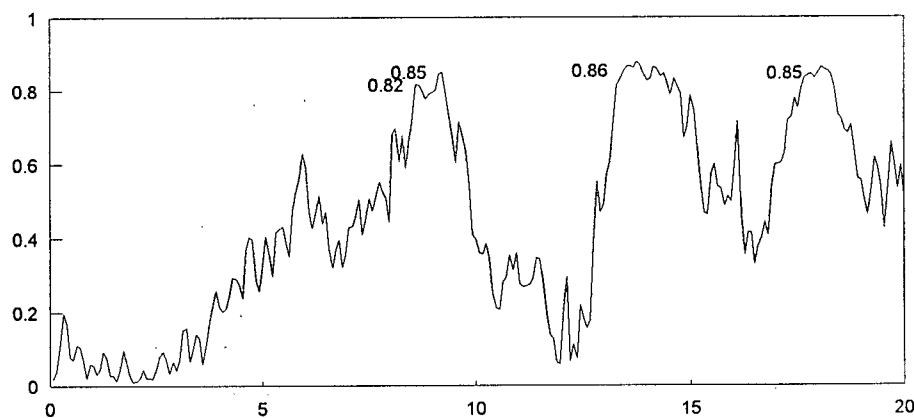
TRANSFER
FUNCTION GAIN
MAGNITUDE
vs.
FREQUENCY (Hz)



PHASE
(degrees)
vs
FREQUENCY (Hz)



COHERENCE
MAGNITUDE
vs
FREQUENCY (Hz)



NOTES:

1. All plots at low resolution (0.0781 Hz) and with 64 segments
2. Transfer function gain local maxima frequencies are indicated, as are the corresponding phase factor and coherence values

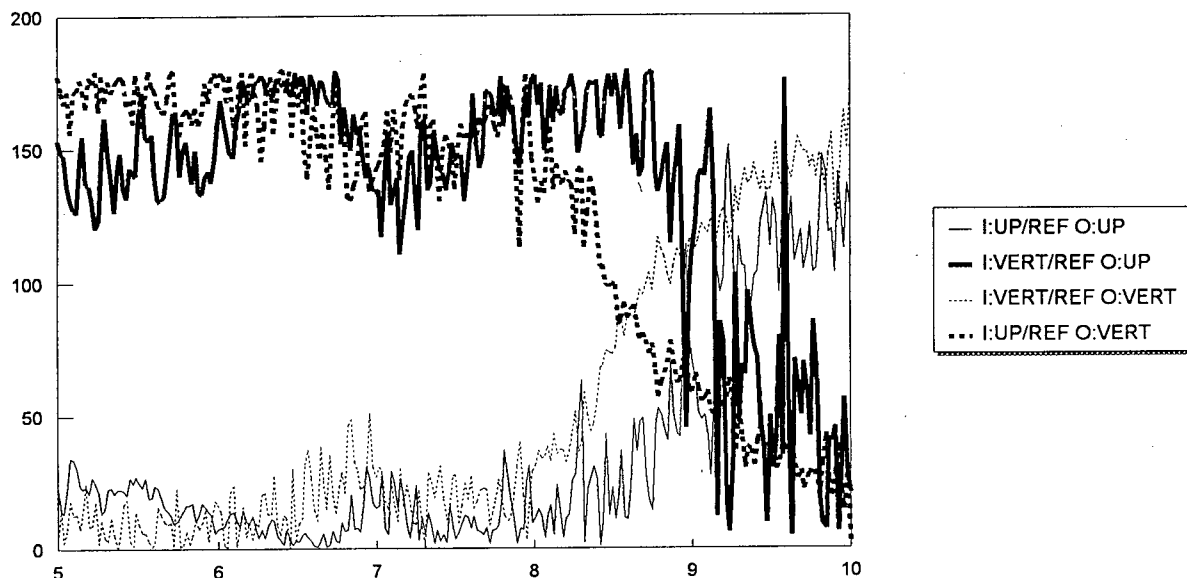
FIGURE C33

TRANSFER FUNCTION GAIN, PHASE FACTOR AND COHERENCE

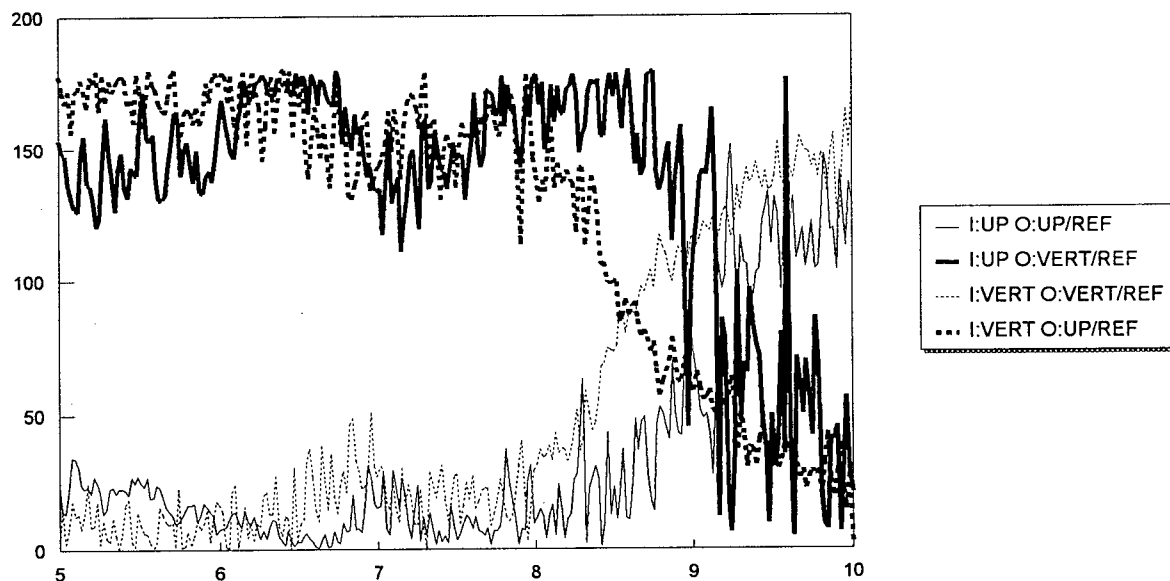
Vertical Direction, Input: Node 33 (Bedrock), Output: Node 13 (Ogee)

RUSKIN DAM AMBIENT VIBRATION FIELD TEST, LOW RESERVOIR, 30 April & 1 May 1994

INPUT: REFERENCE SENSORS



INPUT: BEDROCK



NOTES:

1. All plots completed with high resolution frequency (0.0195 Hz), 16 segments and a Hanning window
2. In legend, I: input, O: output, UP: upstream-downstream bedrock signal, VERT: vertical bedrock signal
UP/REF: upstream-downstream reference signal, VERT/REF: vertical reference signal.
3. All plots abscissa: frequency (Hz), ordinate: phase (degrees).

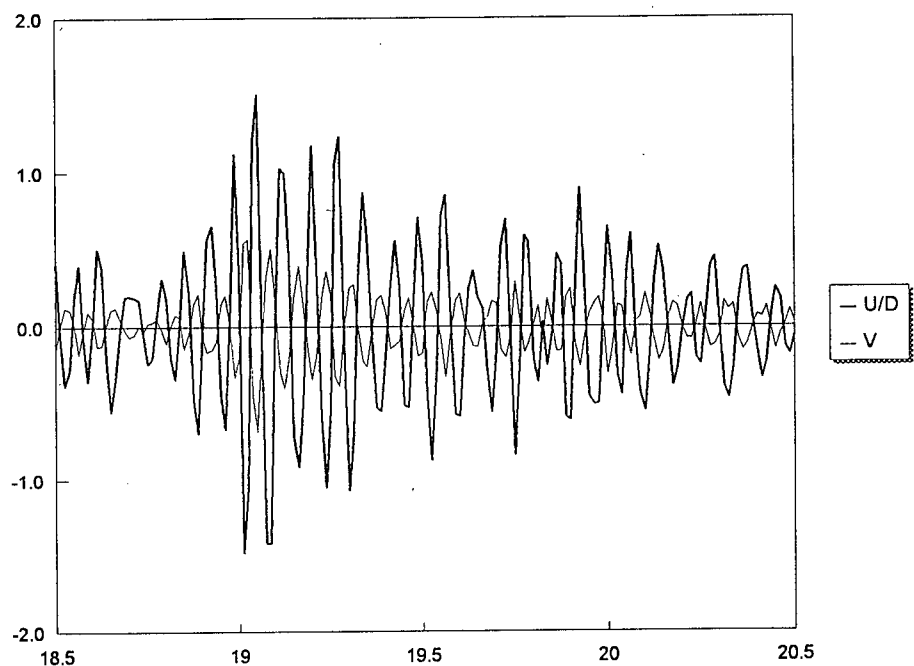
FIGURE C34

PHASE FACTOR FUNCTION COMPARISON

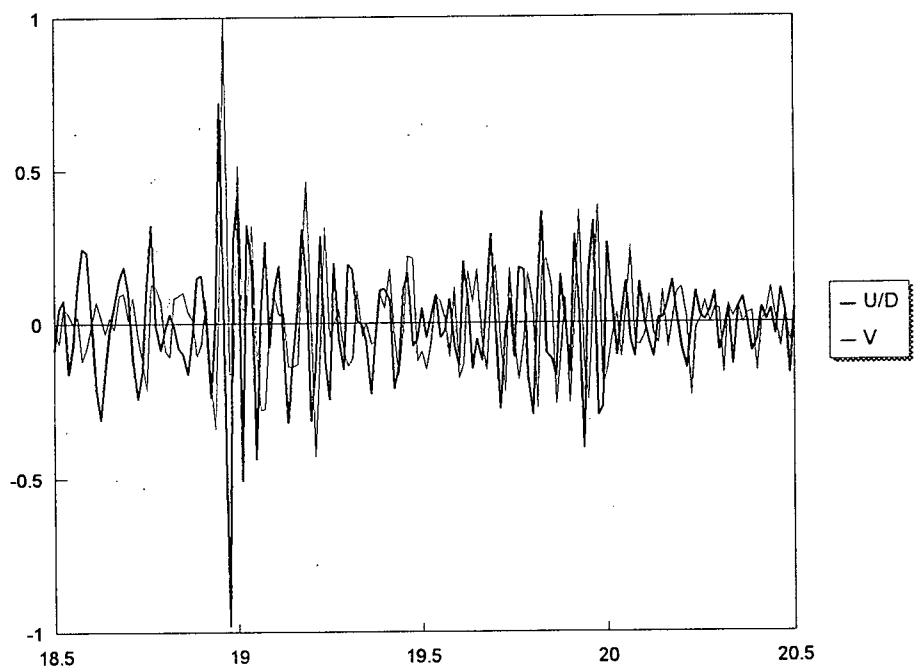
Variable Input and Output Signals, Node 13 (Reference) and Node 33 (East Bedrock)

RUSKIN DAM AMBIENT VIBRATION FIELD TEST, LOW RESERVOIR, 30 April & 1 May 1994

Node 13
(Reference
Sensor)



Node 33
(Bedrock)



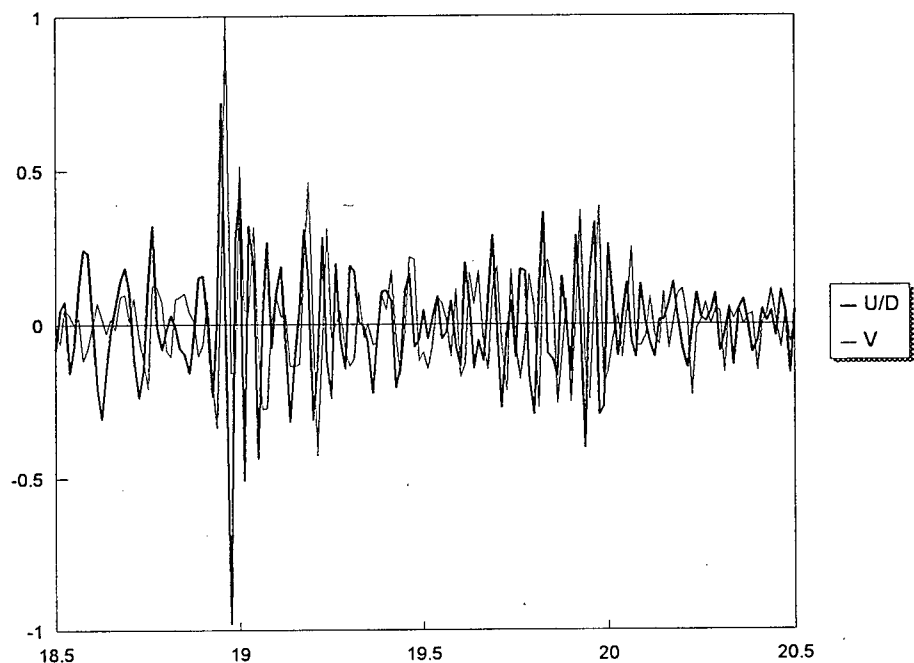
Notes:

1. In legends shown, U/D = upstream-downstream direction, V = vertical direction
2. All plots, abscissa: time (seconds), ordinate: signal magnitude (volts)

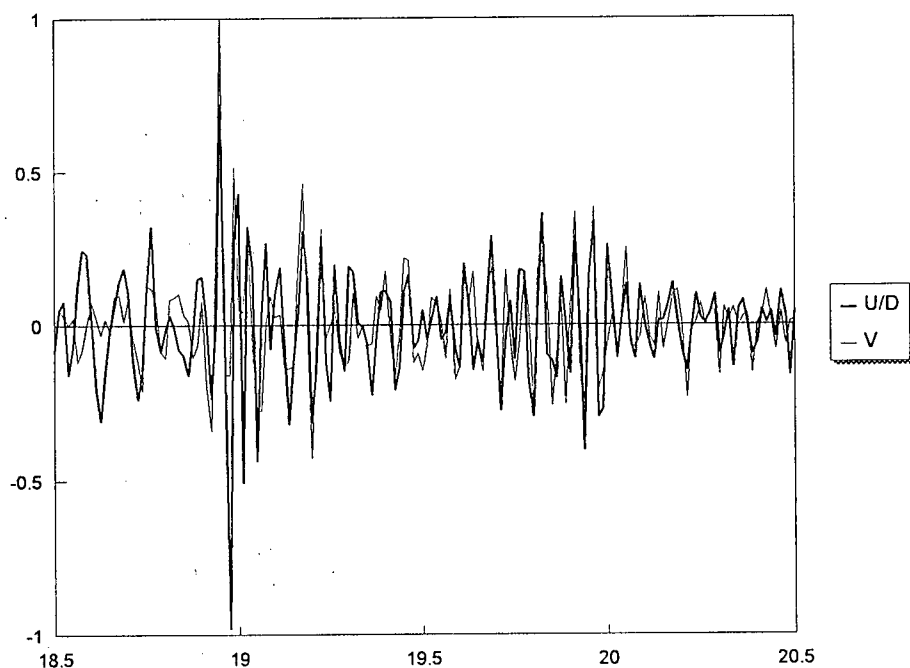
FIGURE C35

TIME DOMAIN COMPARISON OF COINCIDENT BEDROCK AND OGEE SIGNALS
Upstream-Downstream and Vertical, Node 13 (Reference) and Node 33 (East Bedrock)
RUSKIN DAM AMBIENT VIBRATION FIELD TEST, LOW RESERVOIR, 30 April and 1 May 1994

UNSHIFTED



TIME SHIFTED



Notes:

1. In legends shown, U/D = upstream-downstream direction, V = vertical direction
2. All plots, abscissa: time (seconds), ordinate: signal magnitude (volts)

FIGURE C36 EFFECT OF TIME DELAY EQUIVALENT TO ONE TIME DOMAIN DISCRETIZATION
Upstream-Downstream and Vertical, Node 33 (East Bedrock)
RUSKIN DAM AMBIENT VIBRATION FIELD TEST, LOW RESERVOIR, 30 April and 1 May 1994

**AMBIENT VIBRATION ASSESSMENT OF RUSKIN DAM
DYNAMIC PROPERTIES**

APPENDIX D

ANALYSIS OF HIGH RESERVOIR TEST, 7 & 8 MAY 1994

CONTENTS

<u>Section</u>	<u>Subject</u>	<u>Page</u>
D.1	Hybrid Bridge Evaluation System (HBES) Analysis	268
	D.1.1 Average Normalized Power Spectral Densities (ANPSDs)	268
	D.1.2 ULTRA and VISUAL	269
	D.1.3 Hybrid Bridge Evaluation System (HBES) Analysis Summary . . .	273
D.2	Complementary Analysis	273
	D.2.1 Detailed Phase Change	273
	D.2.2 Power Spectral Densities (PSDs), Cross-spectral Densities (XSDs), Phase and Coherence	275
	Ogee	275
	East Bedrock and Reference Sensor	276
	East Bedrock and East Bedrock	277
	D.2.3 Transfer Function	278
	All Nodes	278
	Node 33	279
D.3	High Reservoir Conclusions	280
	Figures (D1 through D33)	281-313

D.1 HYBRID BRIDGE EVALUATION SYSTEM (HBES) ANALYSIS

D.1.1 Average Normalized Power Spectral Densities (ANPSDs)

Plotted in Figures D1 and D2 are the ANPSDs for the deck, ogee and east abutment nodes, plotted in high resolution for the average of 8-16 segments and low resolution for the average of 32 segments, respectively. The number of averages is lower for a few deck nodes due to a shorter time record. See Appendix A for a description of the test and the reasoning for this. Signals were modified with the "Hanning" window to reduce leakage.

The nodes used in plotting the ANPSDs were identical for those used for the low reservoir test, shown in Table C1 in Appendix C.

Shown in Table D1, for the low resolution plot are the frequency ranges/peaks which exhibit the most significant strength.

The following is noted:

1. The deck/ogee ANPSDs exhibit significant ANPSD maximas and the bedrock ANPSDs do not at:

- 6.8-8.0 Hz

This suggests amplified action of the dam and therefore this range is considered to contain a potential natural frequency of the dam.

2. The east bedrock and deck/ogee jointly exhibit significant ANPSD maximas and the east bedrock does not at:

- 4.0-5.0 Hz
- 8.0-9.0 Hz
- 11.8-13.5 Hz
- 13.5-15.0 Hz
- 15.0-17.9 Hz

These ranges are considered to contain potential natural frequencies encompassing the dam alone or both the dam and bedrock or they could be representative of frequency components of the excitation originating from within the east bedrock which are causing a large motion of the dam.

D.1.2 ULTRA and VISUAL

In Figures D3 to D8 are operating deflected shapes at the most significant frequencies. These are plotted for two different phase windows: 90 degrees (i.e., wide open, all nodes are allowed to participate) and 20 degrees (i.e., only nodes where the phase is within 0-20 degrees and 160-180 degrees are allowed to participate). The 20 degree phase window results are shown as this phase was considered to be the highest allowable for reasonable determination of a probable natural frequency with VISUAL.

In general, note in Figures D3 to D8 that the vertical component is significantly less than the upstream-downstream component. In addition, the sense of the coupled vertical/horizontal motion is: vertical up coupled with horizontal in the downstream direction.

All VISUAL work is completed with the signals having been treated with the "Hanning" window.

Coherence: 0 Phase: 90 degrees

Between 0 and 3.0 Hz, there is very little stability in the animated shape. About 3.0 Hz the ogee begins to show signs of stability.

There is evidence of rigid body motion between 4.0 and 5.0 Hz. The gallery does not participate, rather it exhibits very unstable animation patterns. The best shape is about 4.5 Hz and is shown in Figure D3.

At about 6.0 Hz the dam begins to take on a single curvature shape. The stability and smoothness of this curvature improves steadily with increasing frequency. The best appearance is between 7.0 and 7.3 Hz. The shape at 7.1 Hz is shown in Figure D4. Here, an inflection point is evident in the vertical direction of the non-overflow section on the west side.

The east bedrock begins to animate out of phase with the dam after 6.7 Hz. This process is completed in the vertical direction first, by about 7.1 Hz, followed by the upstream-downstream direction, by about 7.3 Hz.

An inflection point appears on the east side of the overflow section, firstly in the vertical direction at 7.3 Hz and then in the upstream-downstream direction at 7.6 Hz.

Between 8.0 and 9.0 Hz the animated shape undergoes a rapid transition through several different shapes with successively greater numbers of inflection points evident. Each shape is very brief in appearance. Towards 9.0 Hz the animated shape begins to break down and exhibit considerable instability.

Table D1
ANPSD Frequency Ranges/Peaks Of Significant Strength
High Reservoir (Low Resolution, 0.0781 Hz, 32-64 segments)

LOCATION	DIRECTION	RANGE (Hz)	PEAK (Hz)
Deck	Upstream-Downstream and Vertical	4.0-5.5 6.5-8.0 8.0-9.0 12.0-13.2 13.2-15.0 16.0-17.7 17.7-18.4	5.0 7.2 8.4 12.5 13.8, 14.1 16.1, 16.6 18.0
	Cross-Canyon	8.0-9.0 12.0-15.0 15.0-20.0	8.4 12.5, 13.9, 14.1, 14.5 16.1, 16.6, 17.0, 17.5, 18.1, 19.2
Ogee	Upstream-Downstream	4.4-4.8 6.0-6.7 6.7-8.0 8.0-9.5 11.9-13.4 13.4-14.8 15.3-18.0	4.6 6.4 7.2 8.5 12.1, 12.5 13.9, 14.1 16.1, 16.6, 16.7
	Vertical	6.7-9.2 10.3-12.0 12.0-13.4 15.3-18.0	7.3 8.4 12.1, 12.5 13.9, 14.1 16.1, 16.5, 16.7
	Cross-Canyon	4.3-4.8 8.0-9.2 10.3-12.0 12.0-13.4 15.3-18.0	4.8 8.3 11.0 12.5 16.1, 16.5, 16.8
East Bedrock	Upstream-Downstream	4.5-5.0 7.7-11.8 11.8-13.6 13.6-15.0 15.0-17.7	4.8 10.1, 11.1 12.1, 12.5 14.1 16.1, 16.7 18.0
	Vertical	4.0-5.0 7.5-10.0 10.0-11.8 11.8-13.7 13.7-15.0 15.0-17.9	4.6 8.4 11.0 12.1, 12.5 14.1 16.1, 16.6 18.0
	Cross-Canyon	8.2-8.8 10.3-12.0 12.0-13.5 13.5-14.5 15.0-17.9	8.5 10.9 12.1, 12.5, 13.0 14.1 16.1, 16.5, 16.8 18.0

Thereafter it reverts to a single curvature shape in the upstream-downstream direction and a rigid body shape in the vertical direction.

The animated shape appearance improves with increasing frequency, eventually becoming single curvature in both vertical and upstream-downstream directions. By 11.8 Hz the inflection point has reappeared on the east side of the overflow section.

Between 12.0 and 13.3 Hz the inflection point creeps westward as the frequency is increased. By 13.3 Hz it is located at about the eastern third point of the dam length. The shape at 12.5 Hz is shown in Figure D5.

Between 13.3 Hz and 16.0 Hz the inflection point slowly creeps westward. At 16.0 Hz it is located at the mid point of the dam and it remains there until 20.0 Hz.

There are several periods of stability between 13.3 and 17.3 Hz, each with a differing combination of inflection point locations in the deck/ogee/gallery. The transition between them is very orderly. The shape at 13.4 Hz is shown in Figure D6.

First appearing in the vertical between 15.0 and 17.3 Hz, and later in the upstream-downstream between 15.3 and 17.3 Hz, a second inflection point moves in from the east side of the overflow section. The operating deflected shapes at 14.1 and 16.6 Hz are shown in Figures D7 and D8.

Between 17.3 and 17.7 Hz, the shape containing two inflection points in the overflow section is relatively stable.

After 18.0 Hz, less stability is exhibited, particularly in the vertical direction.

Coherence: 0 Phase: 40 degrees

<i>4.0-6.0 Hz:</i>	Gallery de-activated most of the range.
<i>6.0-8.0 Hz:</i>	All east bedrock nodes de-activated 6.8-7.3 Hz. The east abutment nodes of the dam begin to de-activate after 7.0 Hz.
<i>8.0-12.0 Hz:</i>	Through the 8.5 +/- 0.5 Hz range most nodes are de-activated. Re-activation occurs after about 10.0 Hz. By 11.8 Hz, most nodes are re-activated.
<i>12.0-13.0 Hz:</i>	Most nodes are active. Some perimeter nodes on the dam randomly de-activate.

- 13.0-14.0 Hz:* Nodes of the east bedrock and west dam tends to de-activate in the vertical direction. In the upstream-downstream direction most nodes are active, until about 13.9 Hz, where the east bedrock nodes de-activate.
- 14.0-16.5 Hz:* Some central dam nodes randomly de-activate. In the upstream-downstream direction, most east bedrock and west dam nodes are de-activated, until 16.0 Hz where the east bedrock re-activates in both directions. Gallery tends to de-active near 16.3 Hz.
- 16.5+ Hz:* Nodes active until about 17.0 Hz. when the central dam nodes tend to de-activate.

Coherence: 0 Phase: 20 degrees

- 4.0-6.0 Hz:* Most of the gallery and east bedrock are de-activated. The most activity occurs at about 4.5 Hz. See Figure D3 for the resilience of the operating deflected shape at a phase window of 20 degrees.
- 6.0-8.0 Hz:* Perimeter nodes in the dam and the east bedrock are de-activated to 6.8 Hz. Thereafter, many dam nodes re-activate. The best range appears to be 7.1-7.2 Hz. By 8.0 Hz many nodes on the east side of the dam are de-activated. Figure D4 shows the shape at 7.1 Hz.
- 8.0-12.0 Hz:* Most nodes de-activated through the 8.5 +/- 0.5 Hz range. Thereafter, the activation pattern is very unstable until about 11.9 Hz.
- 12.0-13.0 Hz:* Sporadic de-activation of nodes through range. Only the perimeter dam nodes de-activate regularly. The ogee is very good throughout most of the range. The range 12.8-12.9 Hz has the most active ogee nodes. The operating deflected shape at 12.5 Hz is shown in Figure D5.
- 13.0-14.0 Hz:* Most ogee nodes activated throughout range. Best up to about 13.4 Hz. See Figure D6 for the shape at 13.4 Hz.
- 14.0-16.5 Hz:* The animated shape breaks down significantly after 15.4 Hz. See Figure D7 for the operating deflected shape at 14.1 Hz.
- 16.5+ Hz:* Very unstable animation patterns, with few nodes moving. As shown, in Figure D8 at 16.6 Hz, very few

nodes are left animated with a phase window of 20 degrees.

D.1.3 Hybrid Bridge Evaluation System (HBES) Analysis Summary

1. There is evidence of a probable natural frequency of the bedrock at 4.5 +/- 0.1 Hz. The mode shape is a rigid body motion. Cross-spectral density, phase and coherence functions should be calculated between bedrock nodes measured coincident to help confirm this and to attempt to determine the mode shape of the bedrock in this frequency range (see Section D.2).
2. There is strong evidence of a probable natural frequency of the dam at 7.1 +/- 0.1 Hz. The mode shape is a single curvature in both the upstream-downstream and vertical directions.
3. There is slight evidence of other natural frequencies at 12.1 +/- 0.1, 12.5 +/- 0.1, 14.0 +/- 0.2, 16.8 +/- 0.7 Hz, based on ANPSD strength. It was not possible to discern their authenticity any more conclusively with VISUAL.
4. Using VISUAL, the 13.2 +/- 0.2 Hz range also provides slight evidence of a probable natural frequency. This range does not have corresponding significant ANPSD strength.
5. ANPSD strength noted between 8.5 +/- 0.5 Hz does not correspond to a probable natural frequency due to inadequate phase for the majority of dam nodes. Interestingly, the animated shape seemingly progresses through an orderly progression of higher modes, with successively greater number of inflection points. This animation behaviour and the relative ANPSD strength are not completely understood. It is noted that the east bedrock has significant ANPSD strength in the vertical direction through the same frequency range.

D.2 COMPLEMENTARY ANALYSIS

All plots presented were completed without a window to reduce side-lob leakage. Comparative plots with and without a window did not indicate any substantial difference.

D.2.1 Detailed Phase Change

Data was studied at the frequency resolution of its recording, i.e., 0.0195 Hz. No hard copy of the phase change data is included herein due to the large

amount of space it would require. The following describes what was observed:

- 4.0-6.0 Hz:* Between 4.0 and 5.0 Hz there is no substantial frequency range where even just the deck and ogee nodes are in phase. The best is at about 4.5 Hz.
- 6.0-8.0 Hz:* After about 6.5 Hz, most nodes on the dam, including the gallery, move in phase. This continues to about 7.5 Hz, with the most stable range being 6.8-7.2 Hz. There is an inflection point in the non-overflow section in the vertical direction. Towards 8.0 Hz, an inflection point appears on the east side of the overflow section.
- 8.0-9.0 Hz:* As indicated with VISUAL in section D.1.2, there is a rapidly changing sequence of mode shapes through the range, ending in complete instability in the animation pattern. The best stability occurs between 8.1 and 8.3 Hz. Coherence is very high for most nodes through this range indicating a low error in the phase estimate.
- 9.0-12.0 Hz:* Interestingly, after the instability of the previous range, the phase eventually returns to a pattern similar to that before 7.5 Hz, i.e., all nodes on the dam, except those in the non-overflow section, moving in phase. By 11.8 Hz, the inflection point on the east side re-appears.
- 12.0-13.0 Hz:* Through this range, the eastern inflection point tracks westward. The best stability is noted between 12.5-12.7, 12.7-13.0 Hz. The former corresponds to a peak in the ANPSDs. Near 12.0 Hz, the stability is very poor, yet an ANPSD peak resides there.
- 13.0-14.0 Hz:* Again through this range, the eastern inflection point continues to track westward with increasing frequency. The best ranges of stability are 13.4-13.5, 13.8-13.9 Hz. All of the nodes on the overflow section begin a very long segment of stability at 13.8 Hz.
- 14.0-16.5 Hz:* In this range a second eastern inflection point appears, beginning about 15.0 Hz in the vertical deck and ending at 17.3 Hz with the upstream-downstream gallery. The best ranges for stability are 14.7-15.0, 16.1-16.4, 16.6-16.9 Hz. The latter two contain two inflection points in the overflow section of the deck and ogee, whereas the former has but a single inflection point. A significantly long period of stability exists for the overflow dam nodes in the vertical between 16.2 and 17.0 Hz.

16.5+ Hz: A significant stability exists between 17.5-17.6 Hz, with two inflection points in the overflow section of the deck, ogee and gallery. After 17.8 Hz, the vertical direction is very unstable.

Detailed Phase Change Conclusions

1. Of the important frequency ranges identified with HBES, those with significant phase stability for the dam nodes were found to be 7.1 +/- 0.1, 12.5 +/- 0.1, 13.2 +/- 0.2, 14.0 +/- 0.2, 16.8 +/- 0.7 Hz.
2. Of the important frequency ranges identified with HBES, those with significant phase instability for the dam nodes were found to be 8.5 +/- 0.5 and 12.1 +/- 0.1 Hz.

D.2.2 Power Spectral Densities (PSDs), Cross-spectral Densities (XSDs), Phase and Coherence

Ogee

PSDs

See Figures D9 and D10.

At a given node, the vertical and upstream-downstream plots are very similar. The only major difference is that only upstream-downstream plots show relatively high strength in the 4.5 Hz+/- zone.

Other significant zones of strength are 7.0-7.2, 8.0-9.0, 12.0-13.0, 13.0-15.0, 15.5-17.0 Hz.

Similar to the low reservoir case, the mode shape in the 7.0-7.2 Hz range can be identified with careful study of the PSD amplitudes.

XSDs, Phase and Coherence

See Figures D11 to D14.

Immediately evident is the poor phase existing through the 8.0-9.0 Hz range, which was exhibited with VISUAL. Coherence is generally reasonable through this range thereby indicating a low error (standard deviation) in the phase estimate. Interestingly, the coherence does exhibit a sharp drop generally just

after this range.

In general, the best phase is found at 6.5-7.5 Hz and 12.0-13.0 Hz.

The best coherence is found at 6.5-7.5 Hz in both directions. As well, coherence is very good in the upstream-downstream direction in the 4.5 Hz +/- range.

Node 16 plots exhibits a sharp drop in coherence between 13.0-13.5 Hz, which is coincident with a valley in the XSD, and is just before a series of peaks in the XSD between 13.5 and 14.5 Hz. Again, similar to the low reservoir test, this is coincident with the HBES predicted probable natural frequency range of 13.2 +/- 0.2 Hz.

East Bedrock and Reference Sensor

PSDs

See Figures D15 and D16.

White noise conditions are not found. Low coherence indicates poor data was collected for nodes 38 and 39 (see Figures D18, D19, D21 and D22).

Strength is exhibited in the 4.0-5.0, 8.0-10.0, 12.0-13.0, 15.5-17.5 Hz ranges for the vertical plots.

Node 36 exhibits exceptionally high strength in the upstream-downstream at 12.0-13.0 Hz.

Comparing with the low reservoir PSD indicates few similarities. Some strength is evident for both reservoir levels in the 4-5 Hz range.

XSDs, Phase and Coherence

See Figures D17 to D22.

Further evidence of the poor quality of the data obtained is apparent with the vertical phase and coherence plots for nodes 35 through 39, and the upstream-downstream plots for nodes 38 and 39. Here coherences are very low and phase is unstable.

Noticeable peaks occur at 8.0-9.0, 12.5-13.5, 15.5-17.5 Hz for the vertical and upstream-downstream directions for nodes 19, 31-34, nearest the dam.

As with the low reservoir condition, of interest are the phase plots. They exhibit crossings through 90 degrees near 7.0, 8.5, 12.0 and 13.5 Hz. There is the potential for transfer function construction for signals which are reasonable. Unfortunately, many signals, including the vertical signals, appear to have been contaminated and will not be useful.

East Bedrock and East Bedrock

XSDs, Phase and Coherence

See Figures D23 and D24.

Unlike the low reservoir test, not all measured pairs are in phase throughout the entire 5.0-20.0 Hz range, probably reflective of the poor quality data recorded.

Strength in the XSDs, coupled with good coherence and phase is evident in the 4.0-5.0 Hz range, of the uncontaminated signals. This is similar to what was found with the low reservoir data in Appendix C. It is suggestive of a natural frequency in the bedrock at this frequency.

PSDs, XSDs, Phase and Coherence Conclusions

1. For the ogee, the following is concluded:
 - Poor phase in the range 8.5 +/- 0.5 Hz coupled with reasonable coherence suggests that no natural frequency resides there.
2. For the east bedrock, the following is concluded:
 - Data appears to have been contaminated in some bedrock signals. This is true of most of the signals nearest the powerhouse. White noise conditions are not noted.
 - Significant PSD strength is found in the 4.0-5.0 Hz range. As well, significant XSD strength, coupled with good coherence and phase is found amongst the east bedrock pairings over this range. This suggests a natural frequency in the east bedrock in this frequency range, which is similar to what was found for the low reservoir condition, as reported in Appendix C.
 - Review of the phase plots indicates that the potential for transfer function construction is possible.

D.2.3 Transfer Function

All Nodes

Transfer Functions

Transfer functions, and some selected phases were calculated and are shown in Figures D25 through D31. These plots are made at the highest resolution of the data possible.

Vertical plots have provided very poor transfer functions. Reasonable results appear for only nodes 27-31 and 33. This is probably due to contaminated data. Problems were encountered with the UBC measurement equipment the day prior to recording these signals.

Peaks are noted at 7.0-7.2, 8.1-8.4 12.0-12.4 and 16.0-16.2 Hz. The sharpest peaks are in the first two ranges.

Phase Factors

Referring to Figures D29 to D31, the first 90 degree crossing corresponds roughly with a transfer function peak, noted in Figures D25 to D28. In the vertical direction, the crossing occurs about 6.9 Hz, whereas in the upstream-downstream direction it occurs about 7.2 Hz. A frequency shift between the vertical and upstream-downstream predictions was also noted in the low reservoir case as well.

An irregular crossing at 90 degrees occurs through the 8.4-9.0 Hz range. This does correspond with a transfer function peak, and the coherence is only reasonable, being between 0.5 and 0.6 indicating some error in its magnitude (see Figures D17 to D22 for the coherence). This is suggestive of a natural frequency, however, other results (HBES and complementary analyses) indicated poor phase between points on the dam (see Figures D11 to D14), indicative of a non-natural frequency.

Another 90 degree crossing occurs in the vertical at 9.5-10.5 Hz, seemingly corresponding to a 90 degree crossing in the upstream-downstream at 11.0-12.5 Hz. The vertical evidence is more compelling. There are corresponding nearby transfer function and coherence function peaks (see Figures D20 to D28). However, these are small peaks, and the HBES results provide no support for a natural frequency in these ranges. The evidence is very weak for a natural frequency.

A 90 degree crossing also is shown in the vertical at 13.0-14.0 Hz, seemingly

corresponding to a 90 degree crossing in the upstream-downstream at 13.5-16.0 Hz. The vertical crossing is very regular and there are nearby transfer function and coherence function peaks in the vertical direction (see Figures D20 to D28). However, these peaks are not indicated in the upstream-downstream direction plots. Evidence is slight for a natural frequency.

Node 33

In order to compare to the low reservoir case, node 33 was chosen for consideration as the optimum transfer function. As well, its vertical transfer function and PSD appeared reasonably uncontaminated. Shown in Figures D32 and D33 are the low resolution plots of the transfer function, phase and coherence.

The natural frequency in the 7.0 +/- 0.1 Hz range is readily identified, with vertical showing a peak at 7.0 Hz (not the highest in the vicinity however), a phase of 90 degrees and a coherence of 0.31. In the horizontal, the peak is at 7.2 Hz, the phase is 80 degrees and the coherence is 0.49. The coherences are low and not coincident with local peaks, suggesting that the error in the phase is significant. A glance at Table 5.2 in Section 5.2 shows the error to be 7.7 and 5.0 degrees respectively. This is not sufficient to suggest that the identified frequency is substantially incorrect and probably reflects the poor quality of the vertical signal recorded.

In the vertical direction, a 90 crossing at 13.4 Hz is representative of one of many peaks, none of which stand out above the others, in the 12.0-17.5 Hz range. The corresponding coherence of 0.53 is not a peak. Another crossing exists at 10.2 Hz, which roughly corresponds to a low peaking region.

Transfer function peaks exist near 8.4 Hz, however corresponding phases of 154 and 161 degrees for the vertical and upstream-downstream directions respectively indicate no natural frequency.

Transfer Function Conclusions

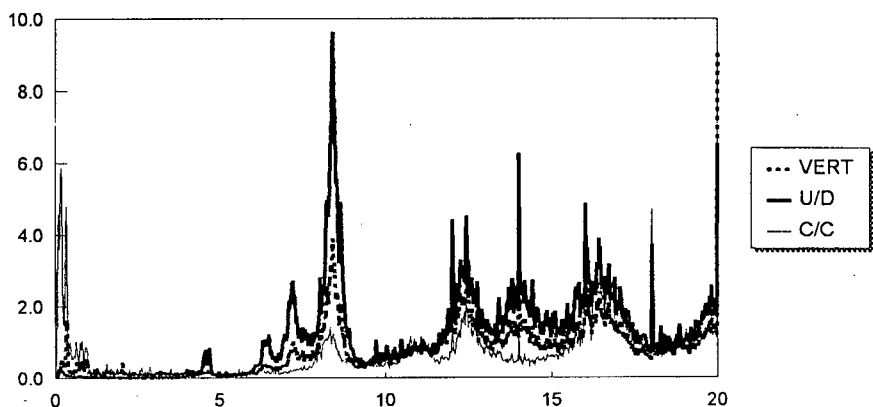
1. Even with the poor quality data (low coherence) recorded for the bedrock signals for the high reservoir test, it has been demonstrated that the vertical signal recorded from the bedrock can be successfully used as input for transfer functions with the dam signals, yielding good correlation to the HBES results. The upstream-downstream signals, when used as input in a similar transfer function, were not found to be as reliable.
2. Using the vertical signal based transfer function, the following was found:

- The first natural frequency is predicted to be at 7.0 ± 0.1 Hz, yielding very good correlation to the range of 7.1 ± 0.1 Hz found with the HBES system.
- The second natural frequency is predicted to be at 13.3 ± 0.3 Hz yielding reasonable correlation to the HBES prediction of 13.2 ± 0.2 Hz.

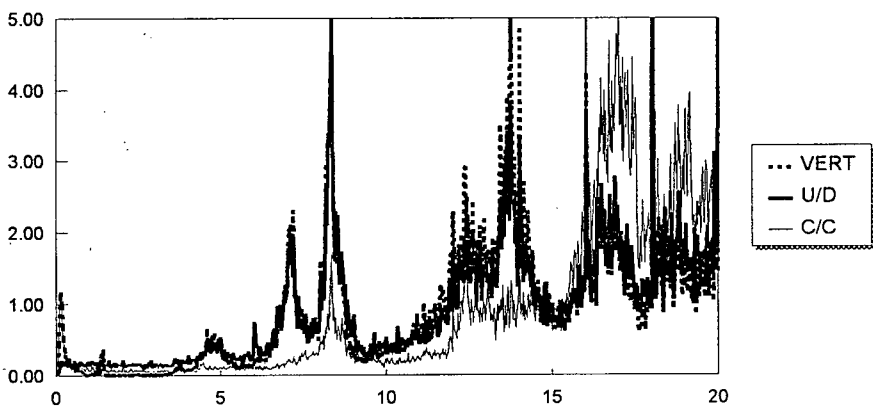
D.3 HIGH RESERVOIR CONCLUSIONS

1. HBES shows evidence of a probable natural frequency of the bedrock at 4.5 ± 0.1 Hz, with the corresponding mode shape a rigid body motion, with a much greater amplitude on the east side. The east bedrock PSDs, XSD, phase and coherence studies indicate a natural frequency and resonance within the east bedrock in this frequency range. Transfer function studies finds that this very strong signal is not exciting the dam.
2. HBES finds strong evidence of a probable natural frequency of the dam at 7.1 ± 0.1 Hz. Transfer function analysis using the vertical signal would indicate 7.0 ± 0.1 Hz. As a result, a compromise frequency range of 7.1 ± 0.2 Hz is suggested. The mode shape is probably a near symmetric single curvature in both the vertical and upstream-downstream directions. As such it probably represents the first or fundamental frequency of the dam.
3. HBES finds slight evidence of a probable natural frequency of the dam at 13.2 ± 0.2 Hz. This also finds reasonable correlation in the transfer function analysis for the vertical direction signal only, which predicts a natural frequency at 13.3 ± 0.3 Hz. The compromise range will be the latter. The mode shape contains one inflection point on the ogee in both the vertical and upstream-downstream.
4. HBES finds slight evidence for probable natural frequencies at 12.1 ± 0.1 ; 12.5 ± 0.1 , 14.0 ± 0.2 and 16.8 ± 0.7 Hz. None of these found support in the transfer function analysis. They are concluded not to be natural frequencies.

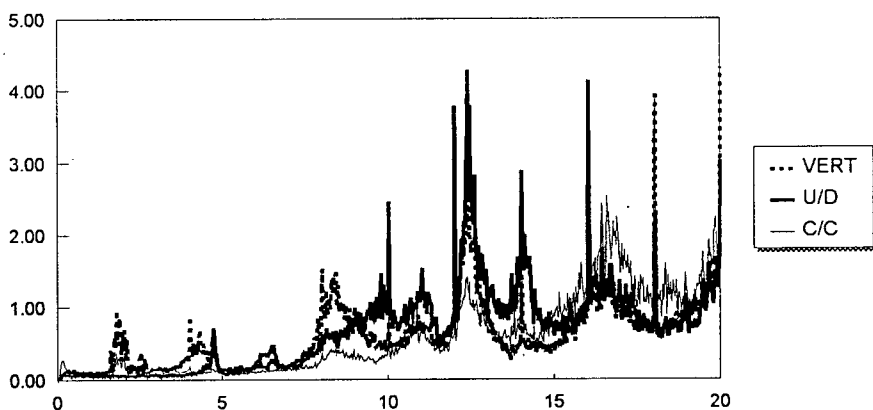
OGEE



DECK



EAST BEDROCK



NOTES:

1. All plots made with high resolution (0.0195 Hz) and with 8-16 segments.
2. In legends shown, U/D = upstream-downstream direction, V = vertical direction, C/C = cross-canyon direction
3. All plots, abscissa: frequency (Hz), ordinate: ANPSD magnitude

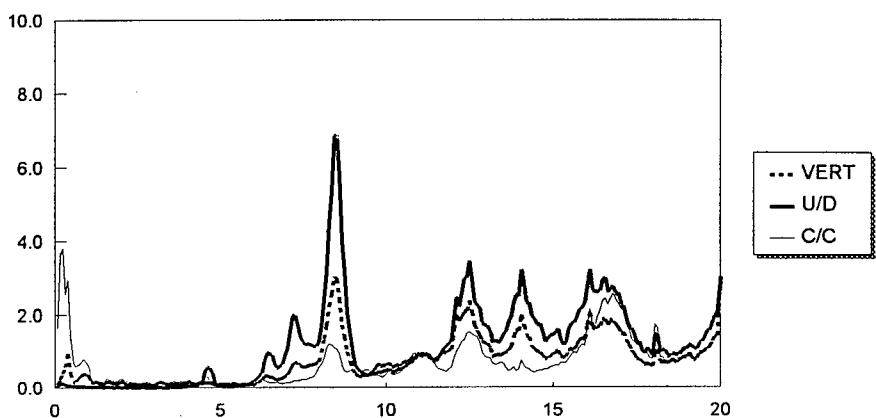
FIGURE D1

ANPSD Functions

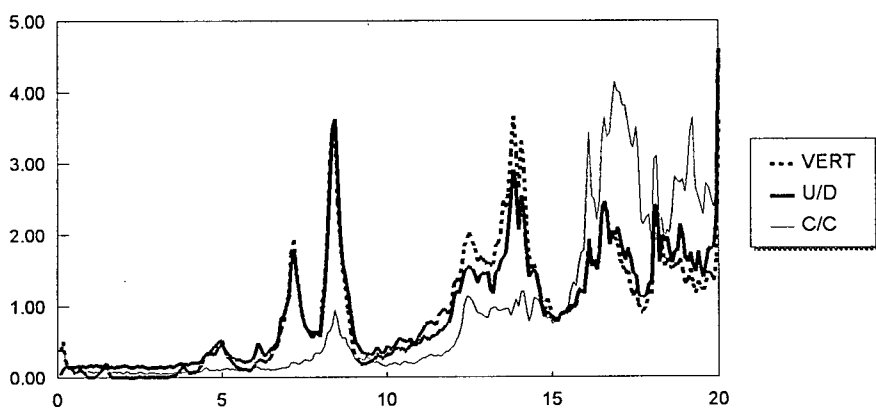
Ogee, Deck and East Bedrock

RUSKIN DAM AMBIENT VIBRATION FIELD TEST, HIGH RESERVOIR, 7 & 8 May 1994

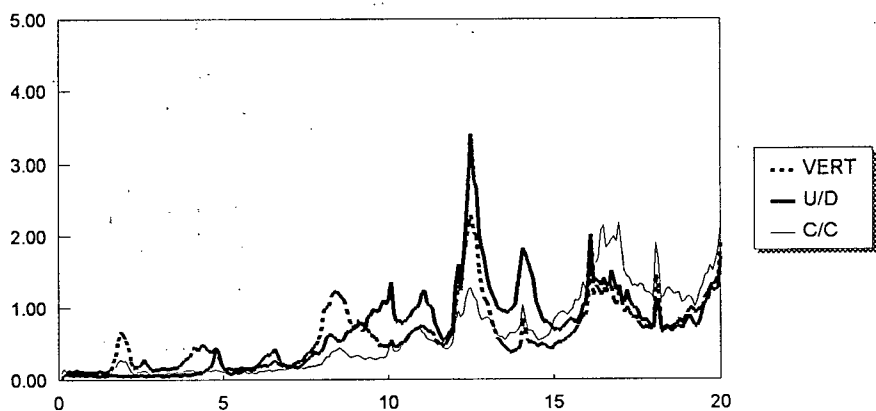
OGEE



DECK



EAST BEDROCK



NOTES:

1. All plots made with low resolution (0.0781 Hz) and with 32-64 segments.
2. In legends shown; U/D = upstream-downstream direction, V = vertical direction, C/C = cross-canyon direction
3. All plots, abscissa: frequency (Hz), ordinate: ANPSD magnitude

FIGURE D2

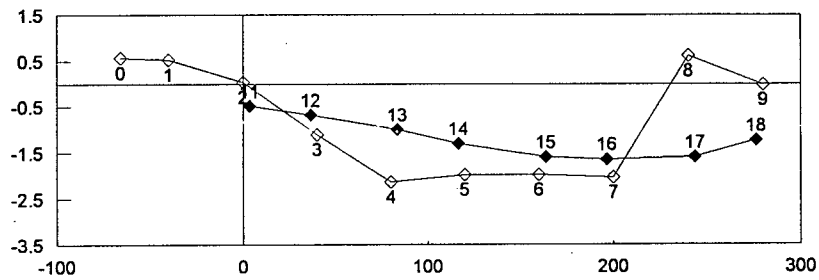
ANPSD Functions

Ogee, Deck and East Bedrock

RUSKIN DAM AMBIENT VIBRATION FIELD TEST, HIGH RESERVOIR, 7 & 8 May 1994

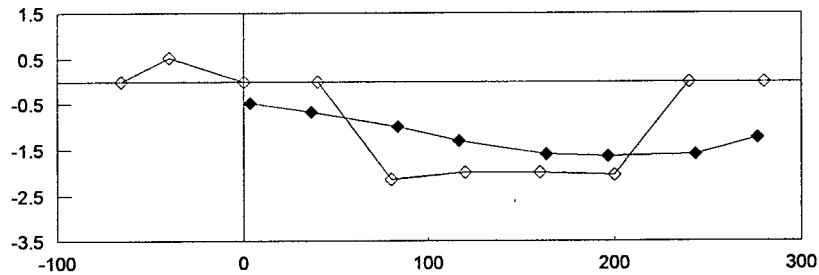
UPSTREAM-
DOWNSTREAM

PHASE
WINDOW:
0-180 degrees



—◆— OGEE
- -◆- - DECK

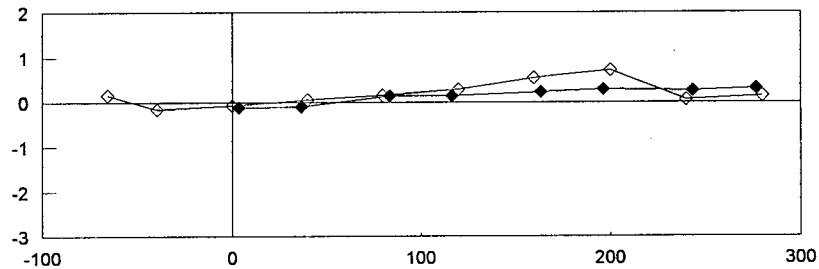
PHASE
WINDOW:
0-20 & 160-180
degrees



—◆— OGEE
- -◆- - DECK

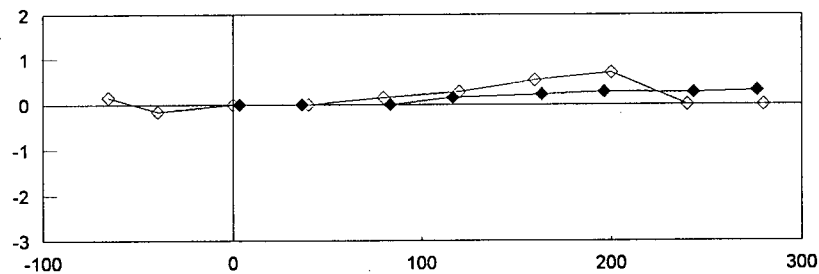
VERTICAL

PHASE
WINDOW:
0-180 degrees



—◆— OGEE
- -◆- - DECK

PHASE
WINDOW:
0-20 & 160-180
degrees



—◆— OGEE
- -◆- - DECK

NOTES:

1. All plots completed with high resolution frequency (0.0195 Hz) and 16 time segments
2. Abscissa: normalized amplitudes
3. Ordinate: measured in feet from centreline of pier on west side of overflow section, overflow length is 280 feet
4. Coherence window: 0-1, phase window: as noted
5. Node numbers shown, for locations see Figure A4.
6. Reference sensor: node 13 upstream-downstream direction
7. Positive sense: upstream in upstream-downstream plots, up in vertical plots

FIGURE D3

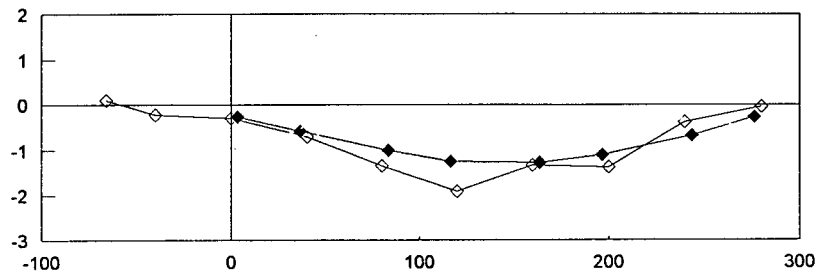
OPERATING DEFLECTED SHAPE (defined at ogee and deck)

4.5 Hz

RUSKIN DAM AMBIENT VIBRATION FIELD TEST, HIGH RESERVOIR, 7 & 8 May 1994

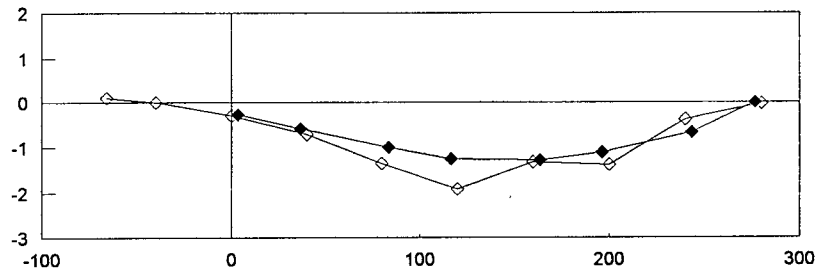
UPSTREAM-
DOWNSTREAM

PHASE
WINDOW:
0-180 degrees



—◆— OGEE
—◇— DECK

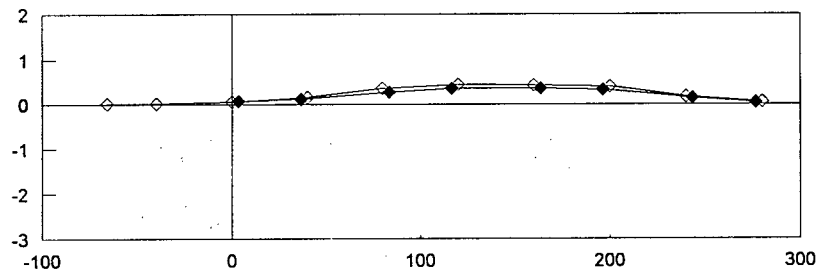
PHASE
WINDOW:
0-20 & 160-180
degrees



—◆— OGEE
—◇— DECK

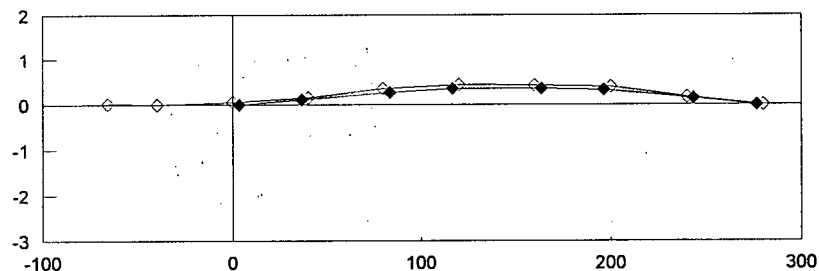
VERTICAL

PHASE
WINDOW:
0-180 degrees



—◆— OGEE
—◇— DECK

PHASE
WINDOW:
0-20 & 160-180
degrees



—◆— OGEE
—◇— DECK

NOTES:

1. All plots completed with high resolution frequency (0.0195 Hz) and 16 time segments
2. Abscissa: normalized amplitudes
3. Ordinate: measured in feet from centreline of pier on west side of overflow section, overflow length is 280 feet
4. Coherence window: 0-1, phase window: as noted
5. Node numbers shown on Figure D3, for locations see Figure A4.
6. Reference sensor: node 13 upstream-downstream direction
7. Positive sense: upstream in upstream-downstream plots, up in vertical plots

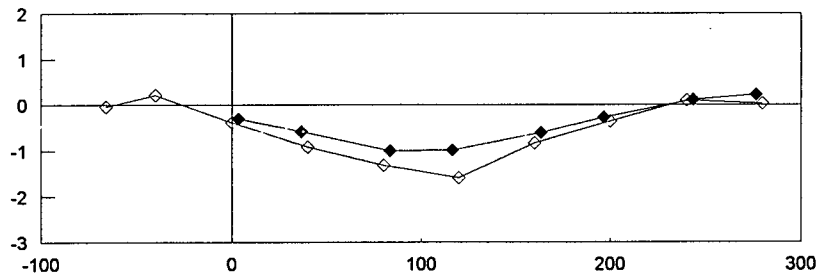
FIGURE D4

OPERATING DEFLECTED SHAPE (defined at ogee and deck)
7.1 Hz

RUSKIN DAM AMBIENT VIBRATION FIELD TEST, HIGH RESERVOIR, 7 & 8 May 1994

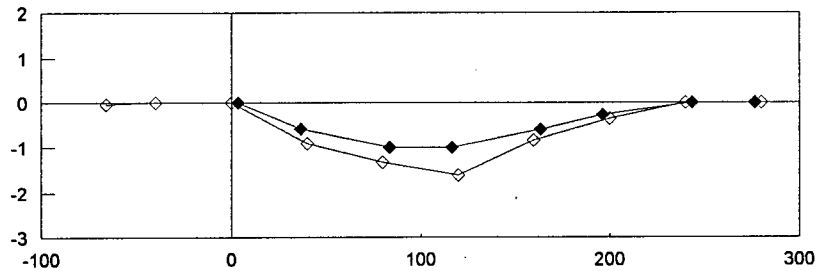
UPSTREAM-
DOWNSTREAM

PHASE
WINDOW:
0-180 degrees



—◆— OGEE
- - -◆- - DECK

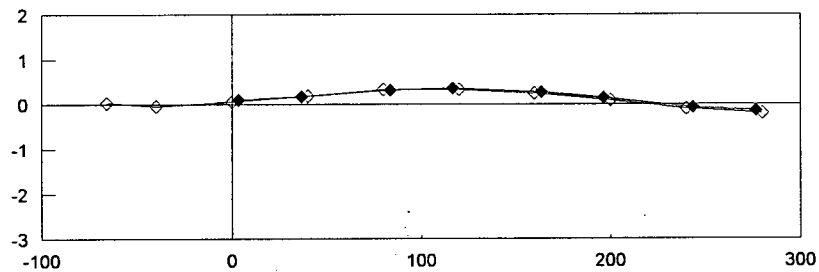
PHASE
WINDOW:
0-20 & 160-180
degrees



—◆— OGEE
- - -◆- - DECK

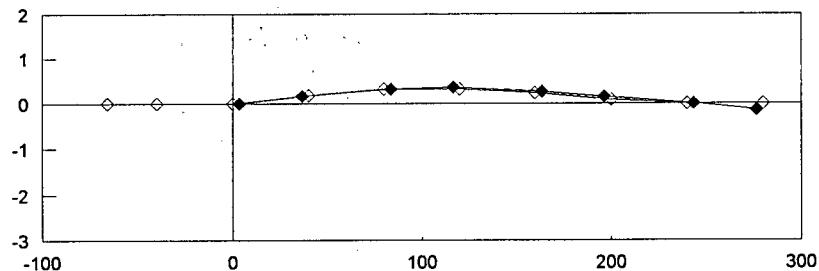
VERTICAL

PHASE
WINDOW:
0-180 degrees



—◆— OGEE
- - -◆- - DECK

PHASE
WINDOW:
0-20 & 160-180
degrees



—◆— OGEE
- - -◆- - DECK

NOTES:

1. All plots completed with high resolution frequency (0.0195 Hz) and 16 time segments
2. Abscissa: normalized amplitudes
3. Ordinate: measured in feet from centreline of pier on west side of overflow section, overflow length is 280 feet
4. Coherence window: 0-1, phase window: as noted
5. Node numbers shown on Figure D3, for locations see Figure A4.
6. Reference sensor: node 13 upstream-downstream direction
7. Positive sense: upstream in upstream-downstream plots, up in vertical plots

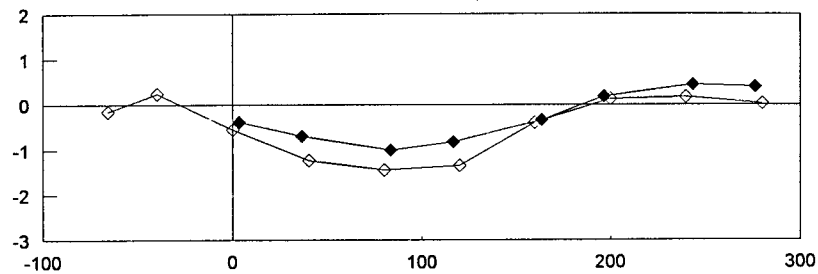
FIGURE D5

OPERATING DEFLECTED SHAPE (defined at ogee and deck)
12.5 Hz

RUSKIN DAM AMBIENT VIBRATION FIELD TEST, HIGH RESERVOIR, 7 & 8 May 1994

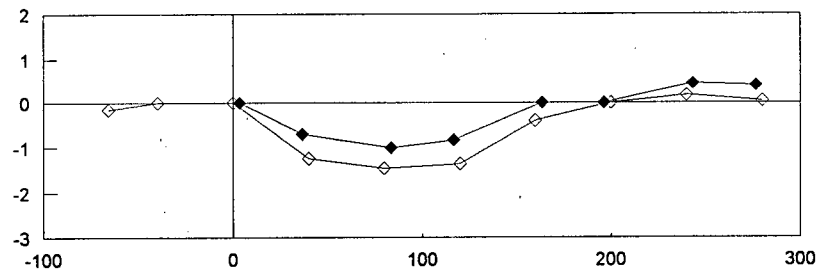
UPSTREAM-
DOWNSTREAM

PHASE
WINDOW:
0-180 degrees



—◆— OGEE
- -◆- - DECK

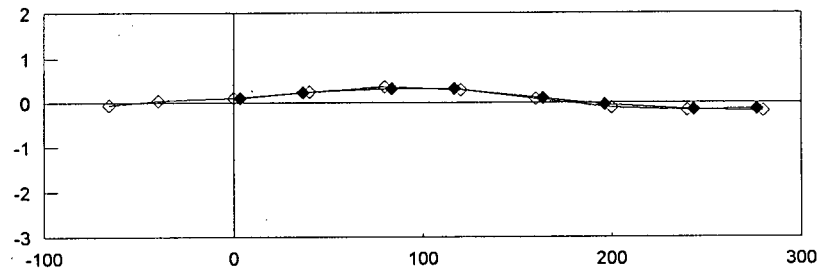
PHASE
WINDOW:
0-20 & 160-180
degrees



—◆— OGEE
- -◆- - DECK

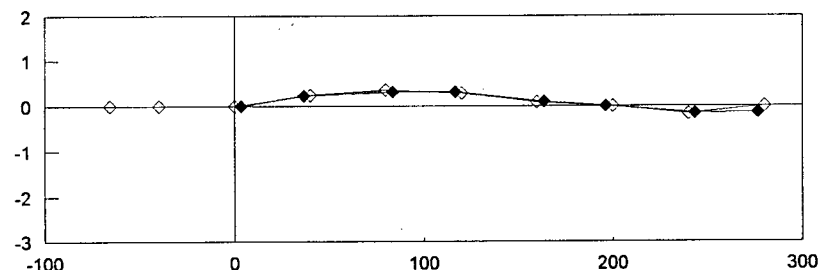
VERTICAL

PHASE
WINDOW:
0-180 degrees



—◆— OGEE
- -◆- - DECK

PHASE
WINDOW:
0-20 & 160-180
degrees



—◆— OGEE
- -◆- - DECK

NOTES:

1. All plots completed with high resolution frequency (0.0195 Hz) and 16 time segments
2. Abscissa: normalized amplitudes
3. Ordinate: measured in feet from centreline of pier on west side of overflow section, overflow length is 280 feet
4. Coherence window: 0-1, phase window: as noted
5. Node numbers shown on Figure D3, for locations see Figure A4.
6. Reference sensor: node 13 upstream-downstream direction
7. Positive sense: upstream in upstream-downstream plots, up in vertical plots

FIGURE D6

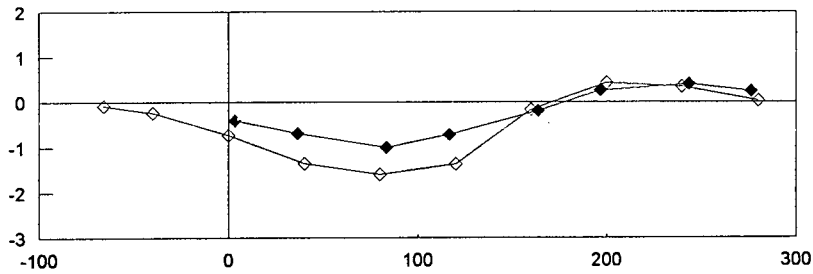
OPERATING DEFLECTED SHAPE (defined at ogee and deck)

13.4 Hz

RUSKIN DAM AMBIENT VIBRATION FIELD TEST, HIGH RESERVOIR, 7 & 8 May 1994

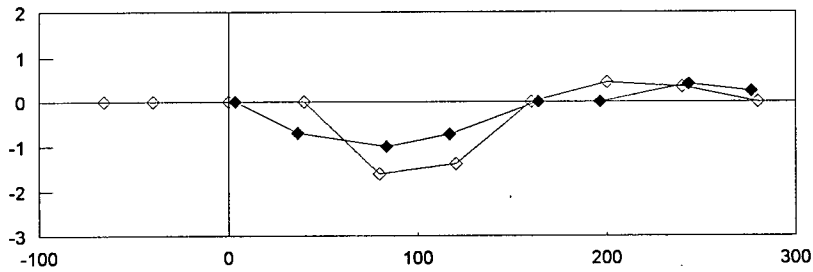
UPSTREAM- DOWNSTREAM

PHASE
WINDOW:
0-180 degrees



—◆— OGEE
—◇— DECK

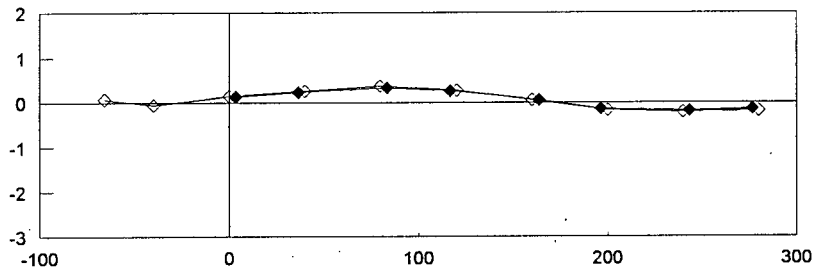
PHASE
WINDOW:
0-20 & 160-180
degrees



—◆— OGEE
—◇— DECK

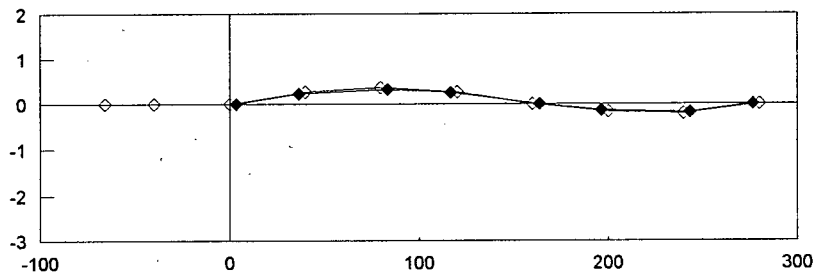
VERTICAL

PHASE
WINDOW:
0-180 degrees



—◆— OGEE
—◇— DECK

PHASE
WINDOW:
0-20 & 160-180
degrees



—◆— OGEE
—◇— DECK

NOTES:

1. All plots completed with high resolution frequency (0.0195 Hz) and 16 time segments
2. Abscissa: normalized amplitudes
3. Ordinate: measured in feet from centreline of pier on west side of overflow section, overflow length is 280 feet
4. Coherence window: 0-1, phase window: as noted
5. Node numbers shown on Figure D3, for locations see Figure A4.
6. Reference sensor: node 13 upstream-downstream direction
7. Positive sense: upstream in upstream-downstream plots, up in vertical plots

FIGURE D7

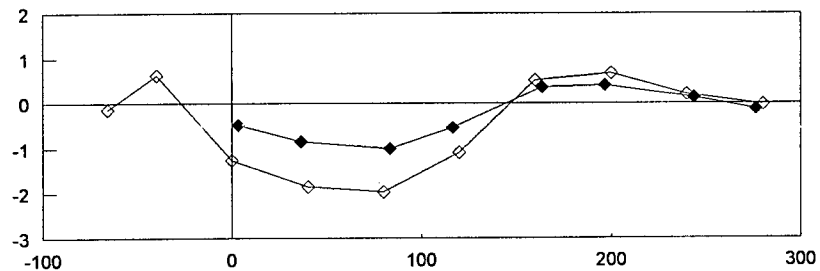
OPERATING DEFLECTED SHAPE (defined at ogee and deck)

14.1 Hz

RUSKIN DAM AMBIENT VIBRATION FIELD TEST, HIGH RESERVOIR, 7 & 8 May 1994

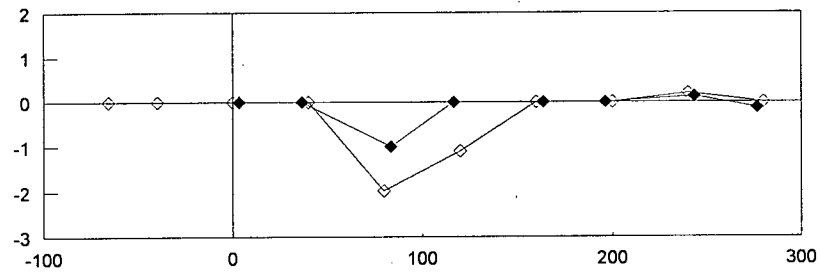
UPSTREAM-
DOWNSTREAM

PHASE
WINDOW:
0-180 degrees



—◆— OGEE
—◇— DECK

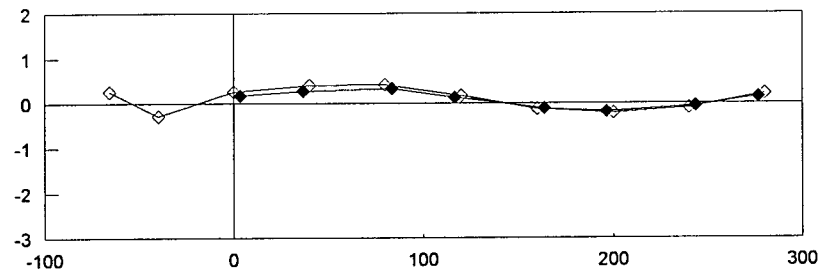
PHASE
WINDOW:
0-20 & 160-180
degrees



—◆— OGEE
—◇— DECK

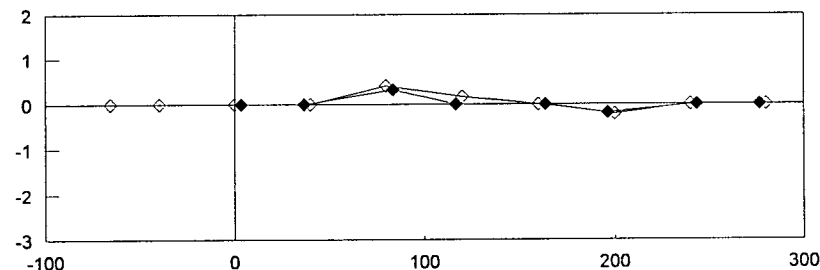
VERTICAL

PHASE
WINDOW:
0-180 degrees



—◆— OGEE
—◇— DECK

PHASE
WINDOW:
0-20 & 160-180
degrees



—◆— OGEE
—◇— DECK

NOTES:

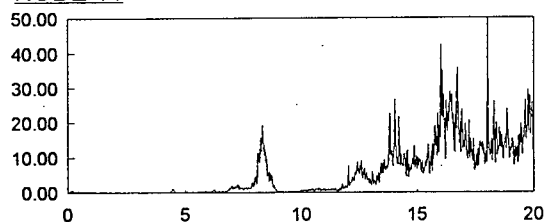
1. All plots completed with high resolution frequency (0.0195 Hz) and 16 time segments
2. Abscissa: normalized amplitudes
3. Ordinate: measured in feet from centreline of pier on west side of overflow section, overflow length is 280 feet
4. Coherence window: 0-1, phase window: as noted
5. Node numbers shown on Figure D3, for locations see Figure A4.
6. Reference sensor: node 13 upstream-downstream direction
7. Positive sense: upstream in upstream-downstream plots, up in vertical plots

FIGURE D8

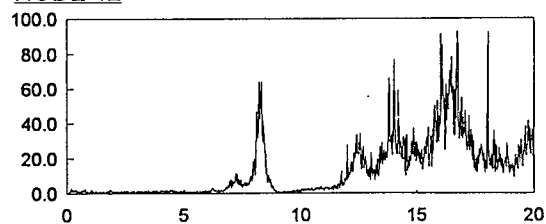
OPERATING DEFLECTED SHAPE (defined at ogee and deck)
16.6 Hz

RUSKIN DAM AMBIENT VIBRATION FIELD TEST, HIGH RESERVOIR, 7 & 8 May 1994

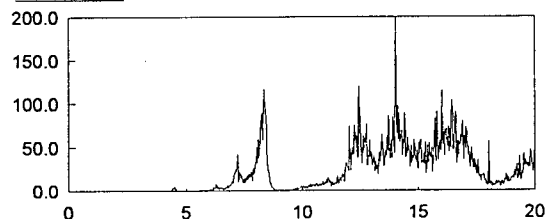
NODE 11



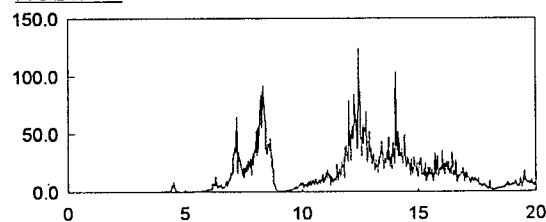
NODE 12



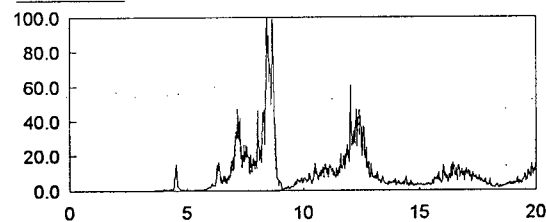
NODE 13



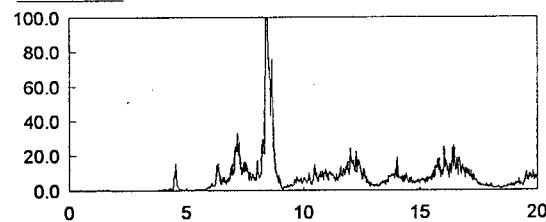
NODE 14



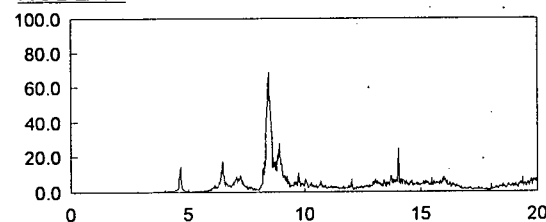
NODE 15



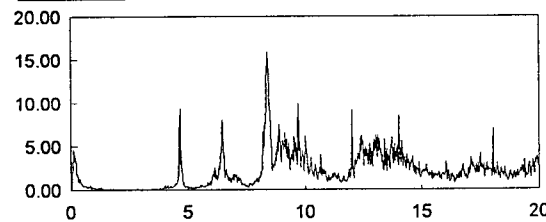
NODE 16



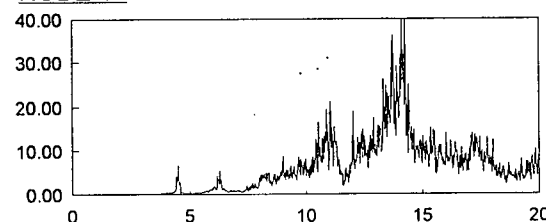
NODE 17



NODE 18



NODE 19



NOTES:

1. All plots high resolution frequency (0.0195Hz), 16 segments, abscissa: frequency (Hz), ordinate: PSD magnitude

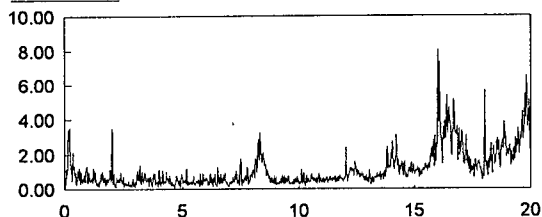
FIGURE D9

POWER SPECTRAL DENSITY FUNCTIONS

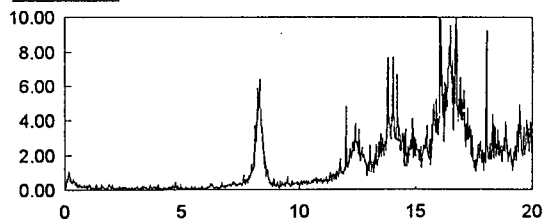
Ogee, Upstream-Downstream Direction

RUSKIN DAM AMBIENT VIBRATION FIELD TEST, HIGH RESERVOIR, 7 & 8 May 1994

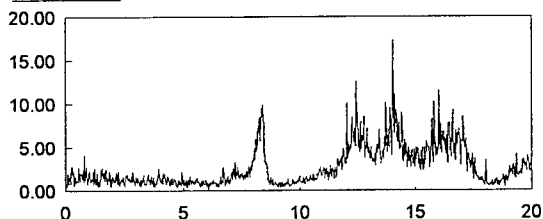
NODE 11



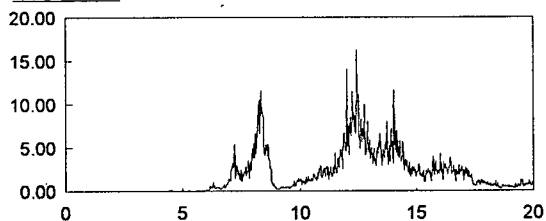
NODE 12



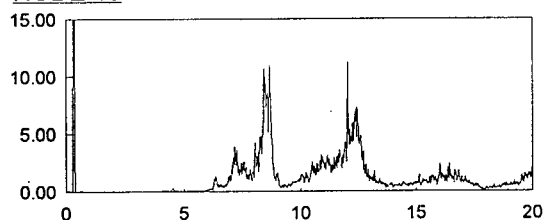
NODE 13



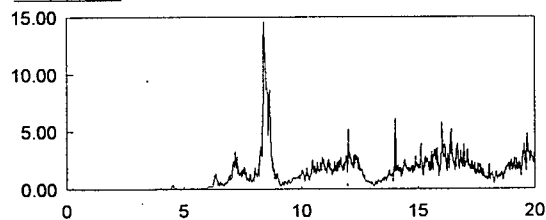
NODE 14



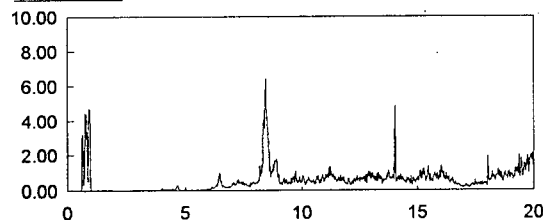
NODE 15



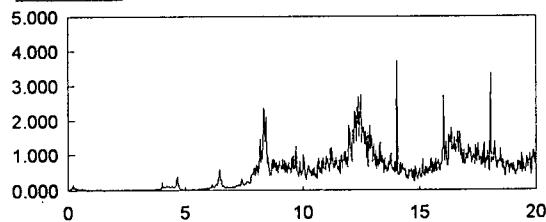
NODE 16



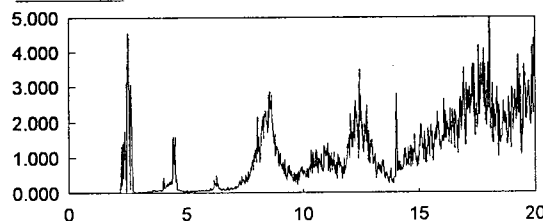
NODE 17



NODE 18



NODE 19



NOTES:

1. All plots high resolution frequency (0.0195Hz), 16 segments, abscissa: frequency (Hz), ordinate: PSD magnitude

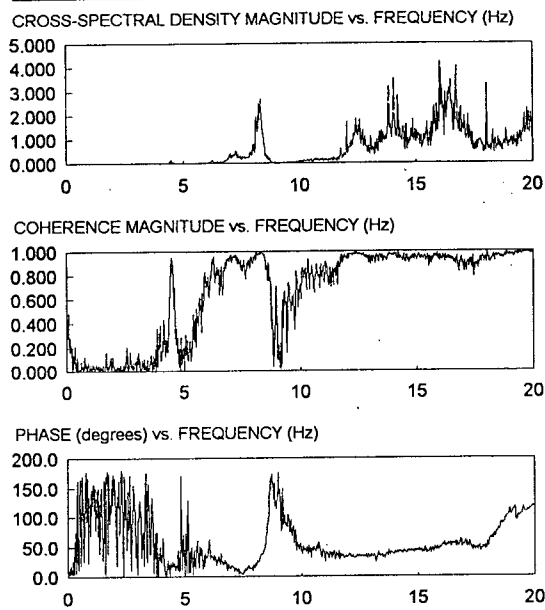
FIGURE D10

POWER SPECTRAL DENSITY FUNCTIONS

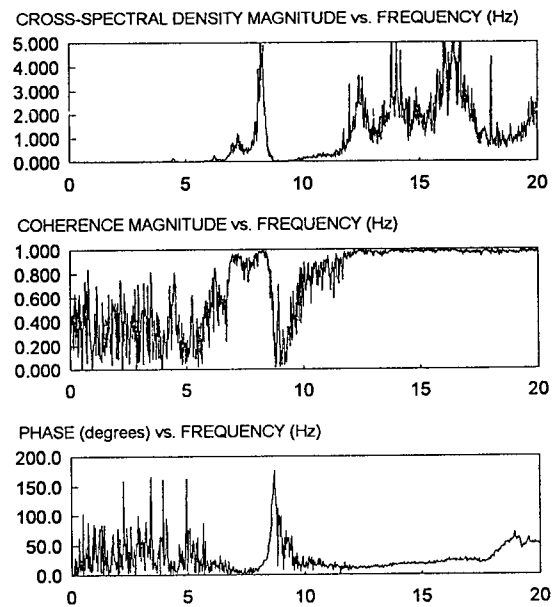
Ogee, Vertical Direction

RUSKIN DAM AMBIENT VIBRATION FIELD TEST, HIGH RESERVOIR, 7 & 8 May 1994

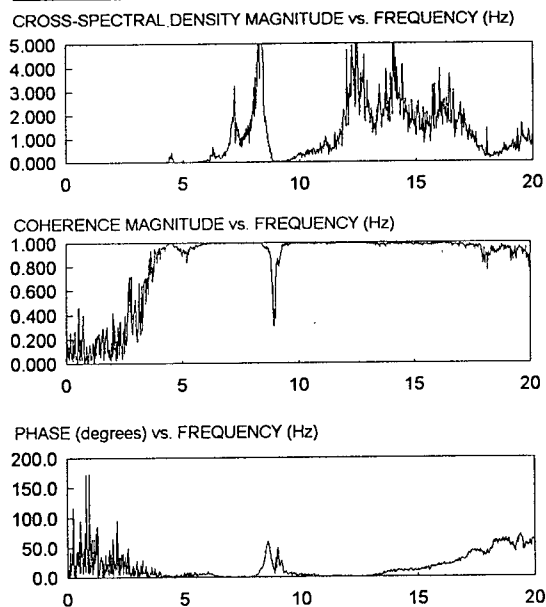
NODES 13 AND 11:



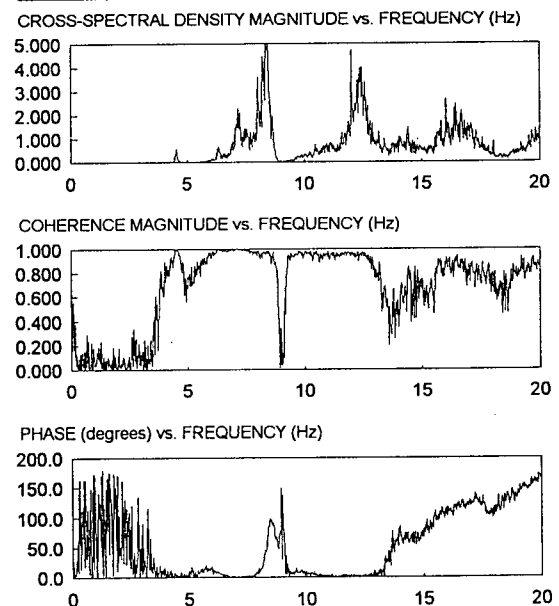
NODES 13 AND 12:



NODES 13 AND 14:



NODES 13 AND 15:



NOTES:

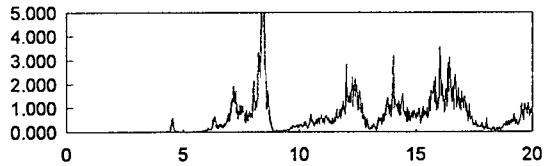
1. All plots completed with high resolution frequency (0.0195 Hz) and with 16 segments

FIGURE D11

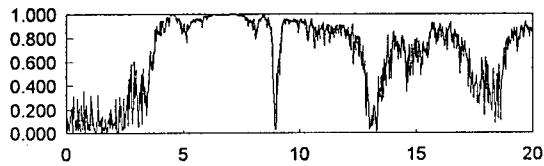
CROSS-SPECTRAL DENSITY, COHERENCE and PHASE FACTOR FUNCTIONS
Ogee and Reference Sensor, Upstream-Downstream Direction
RUSKIN DAM AMBIENT VIBRATION FIELD TEST, HIGH RESERVOIR, 7 & 8 May 1994

NODES 13 AND 16:

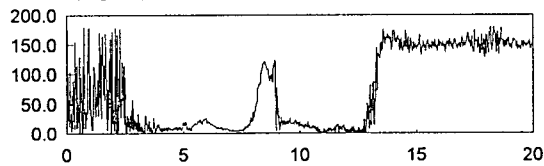
CROSS-SPECTRAL DENSITY MAGNITUDE vs. FREQUENCY (Hz)



COHERENCE MAGNITUDE vs. FREQUENCY (Hz)

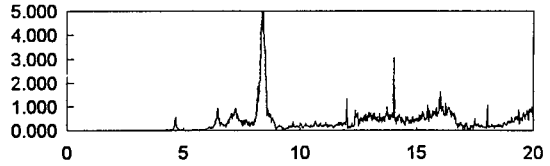


PHASE (degrees) vs. FREQUENCY (Hz)

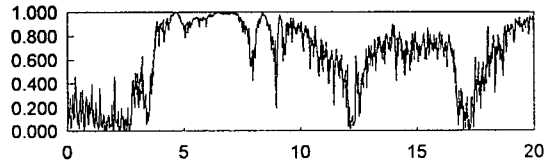


NODES 13 AND 17:

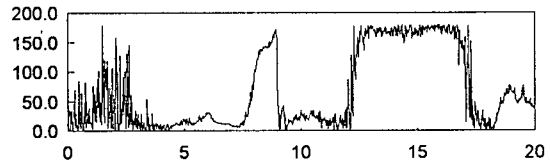
CROSS-SPECTRAL DENSITY MAGNITUDE vs. FREQUENCY (Hz)



COHERENCE MAGNITUDE vs. FREQUENCY (Hz)

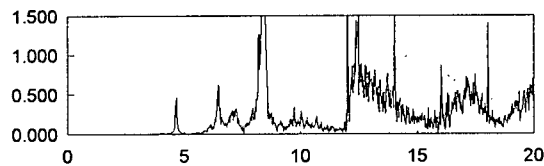


PHASE (degrees) vs. FREQUENCY (Hz)

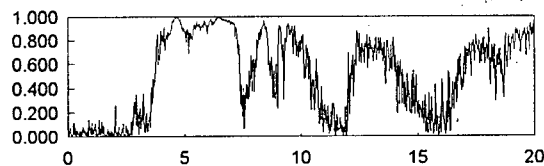


NODES 13 AND 18:

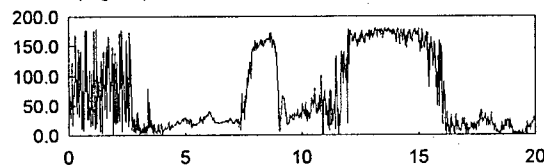
CROSS-SPECTRAL DENSITY MAGNITUDE vs. FREQUENCY (Hz)



COHERENCE MAGNITUDE vs. FREQUENCY (Hz)

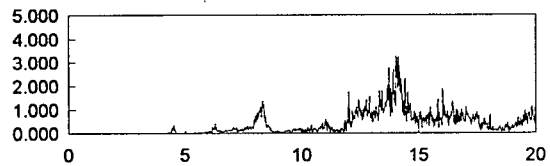


PHASE (degrees) vs. FREQUENCY (Hz)

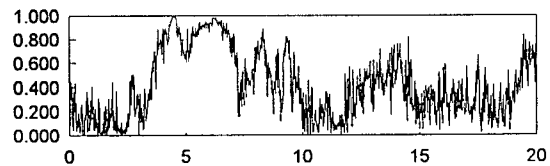


NODES 13 AND 19:

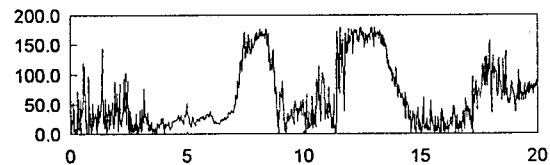
CROSS-SPECTRAL DENSITY MAGNITUDE vs. FREQUENCY (Hz)



COHERENCE MAGNITUDE vs. FREQUENCY (Hz)



PHASE (degrees) vs. FREQUENCY (Hz)



NOTES:

1. All plots completed with high resolution frequency (0.0195 Hz) and with 16 segments

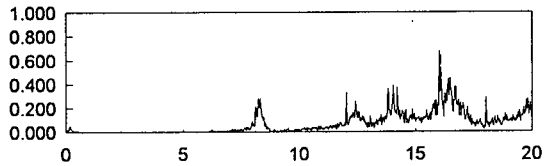
FIGURE D12

CROSS-SPECTRAL DENSITY, COHERENCE and PHASE FACTOR FUNCTIONS
Ogee and Reference Sensor, Upstream-Downstream Direction

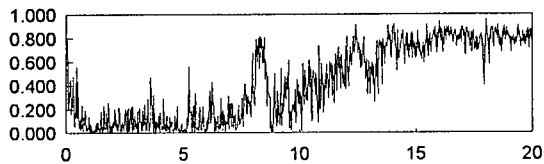
RUSKIN DAM AMBIENT VIBRATION FIELD TEST, HIGH RESERVOIR, 7 & 8 May 1994

NODES 13 AND 11:

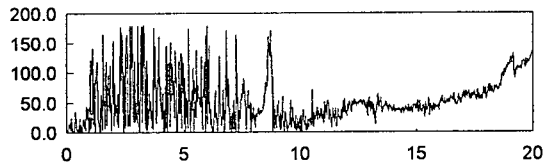
CROSS-SPECTRAL DENSITY MAGNITUDE vs. FREQUENCY (Hz)



COHERENCE MAGNITUDE vs. FREQUENCY (Hz)



PHASE (degrees) vs. FREQUENCY (Hz)

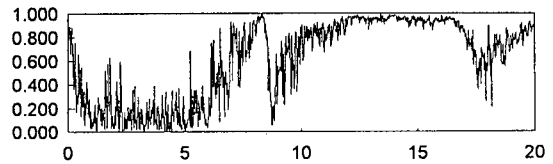


NODES 13 AND 12:

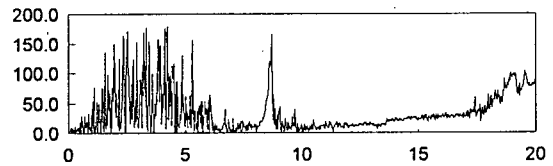
CROSS-SPECTRAL DENSITY MAGNITUDE vs. FREQUENCY (Hz)



COHERENCE MAGNITUDE vs. FREQUENCY (Hz)

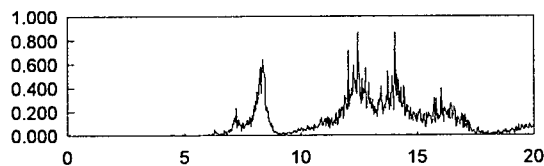


PHASE (degrees) vs. FREQUENCY (Hz)

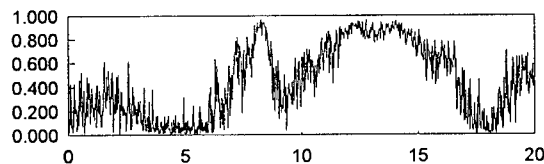


NODES 13 AND 14:

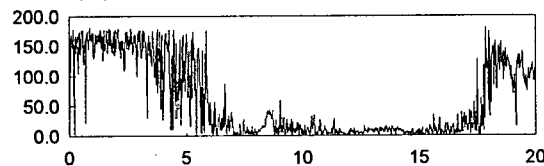
CROSS-SPECTRAL DENSITY MAGNITUDE vs. FREQUENCY (Hz)



COHERENCE MAGNITUDE vs. FREQUENCY (Hz)

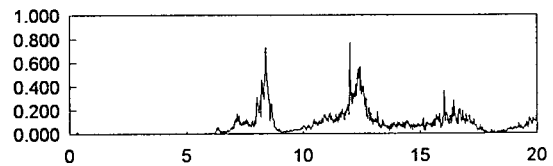


PHASE (degrees) vs. FREQUENCY (Hz)

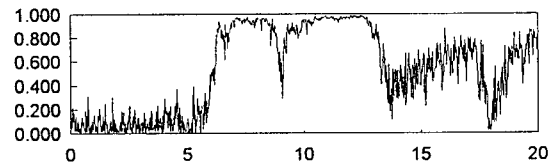


NODES 13 AND 15:

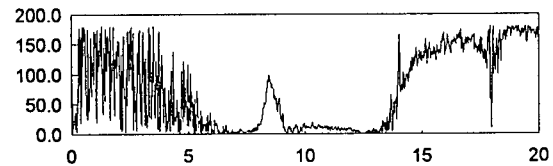
CROSS-SPECTRAL DENSITY MAGNITUDE vs. FREQUENCY (Hz)



COHERENCE MAGNITUDE vs. FREQUENCY (Hz)



PHASE (degrees) vs. FREQUENCY (Hz)



NOTES:

1. All plots completed with high resolution frequency (0.0195 Hz) and with 16 segments

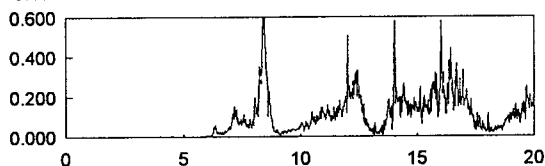
FIGURE D13

CROSS-SPECTRAL DENSITY, COHERENCE and PHASE FACTOR FUNCTIONS
Ogee and Reference Sensor, Vertical Direction

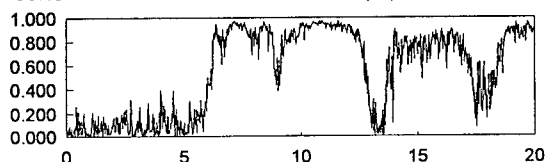
RUSKIN DAM AMBIENT VIBRATION FIELD TEST, HIGH RESERVOIR, 7 & 8 May 1994

NODES 13 AND 16:

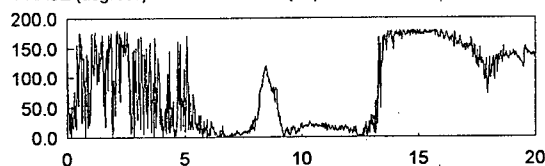
CROSS-SPECTRAL DENSITY MAGNITUDE vs. FREQUENCY (Hz)



COHERENCE MAGNITUDE vs. FREQUENCY (Hz)

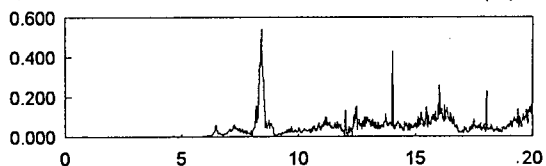


PHASE (degrees) vs. FREQUENCY (Hz)

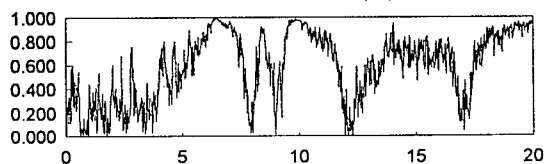


NODES 13 AND 17:

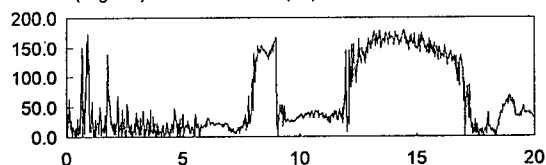
CROSS-SPECTRAL DENSITY MAGNITUDE vs. FREQUENCY (Hz)



COHERENCE MAGNITUDE vs. FREQUENCY (Hz)

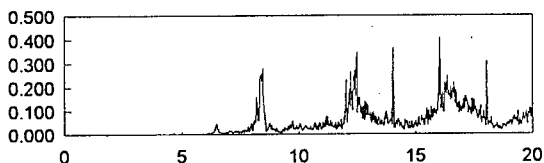


PHASE (degrees) vs. FREQUENCY (Hz)

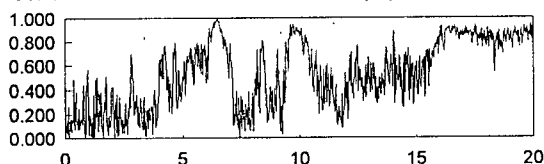


NODES 13 AND 18:

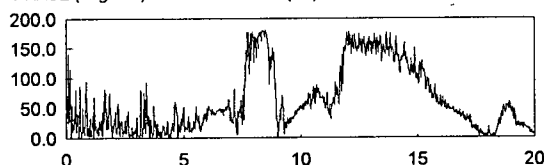
CROSS-SPECTRAL DENSITY MAGNITUDE vs. FREQUENCY (Hz)



COHERENCE MAGNITUDE vs. FREQUENCY (Hz)

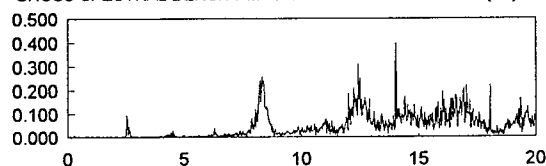


PHASE (degrees) vs. FREQUENCY (Hz)

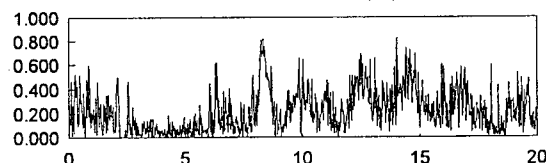


NODES 13 AND 19:

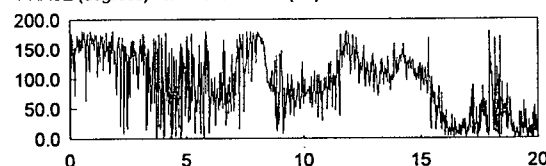
CROSS-SPECTRAL DENSITY MAGNITUDE vs. FREQUENCY (Hz)



COHERENCE MAGNITUDE vs. FREQUENCY (Hz)



PHASE (degrees) vs. FREQUENCY (Hz)



NOTES:

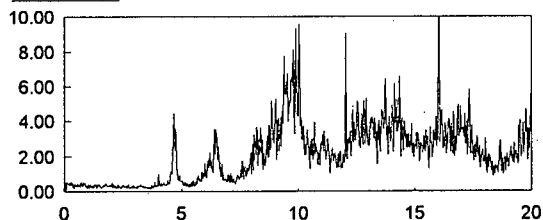
1. All plots completed with high resolution frequency (0.0195 Hz) and with 16 segments

FIGURE D14

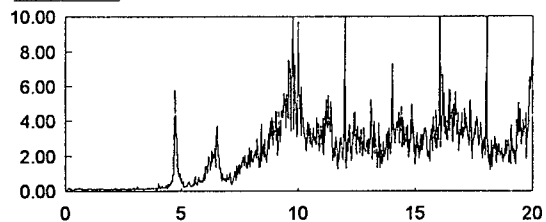
CROSS-SPECTRAL DENSITY, COHERENCE and PHASE FACTOR FUNCTIONS
Ogee and Reference Sensor, Vertical Direction

RUSKIN DAM AMBIENT VIBRATION FIELD TEST, HIGH RESERVOIR, 7 & 8 May 1994

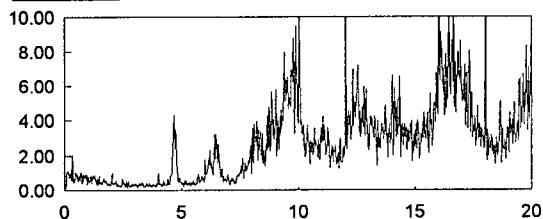
NODE 31



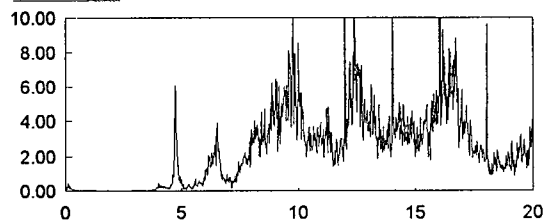
NODE 32



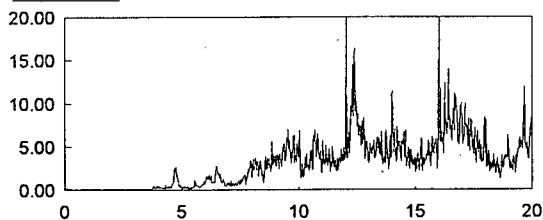
NODE 33



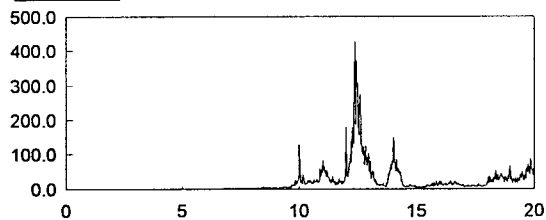
NODE 34



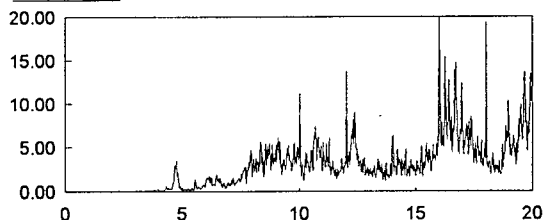
NODE 35



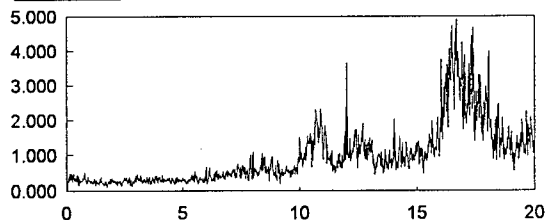
NODE 36



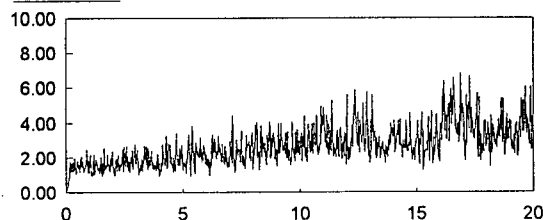
NODE 37



NODE 38



NODE 39



NOTES:

1. All plots high resolution frequency (0.0195Hz), 16 segments, abscissa: frequency (Hz), ordinate: PSD magnitude

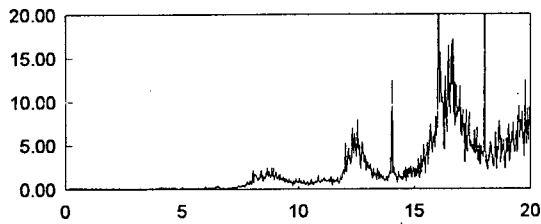
FIGURE D15

POWER SPECTRAL DENSITY FUNCTIONS

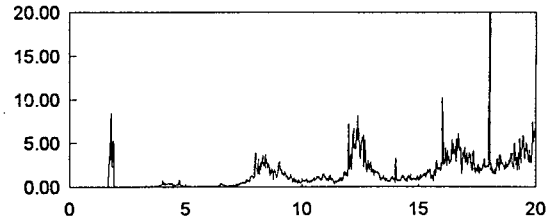
East Bedrock, Upstream-Downstream Direction

RUSKIN DAM AMBIENT VIBRATION FIELD TEST, HIGH RESERVOIR, 7 & 8 May 1994

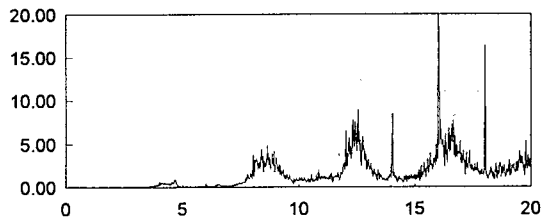
NODE 31



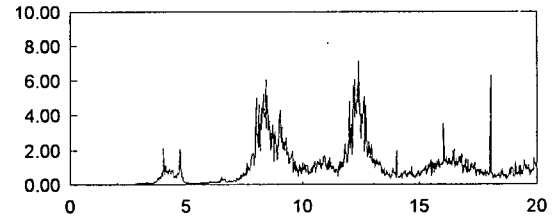
NODE 32



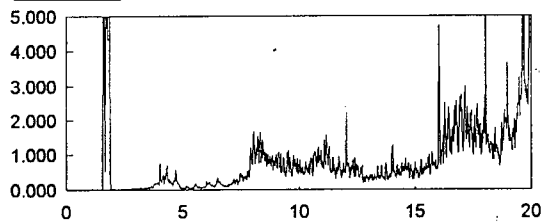
NODE 33



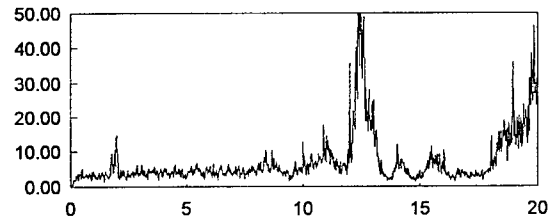
NODE 34



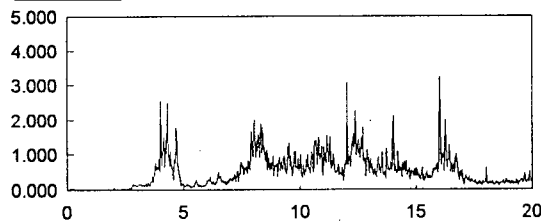
NODE 35



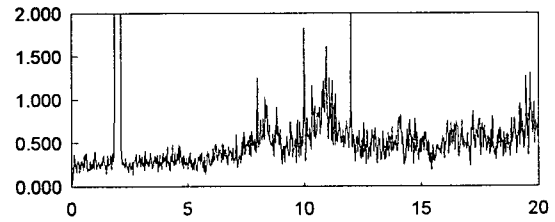
NODE 36



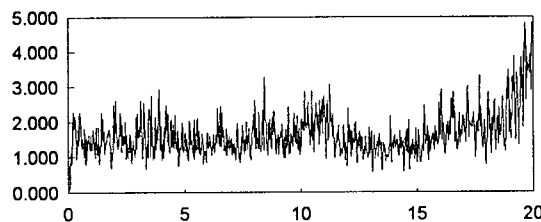
NODE 37



NODE 38



NODE 39



NOTES:

1. All plots high resolution frequency (0.0195Hz), 16 segments, abscissa: frequency (Hz), ordinate: PSD magnitude

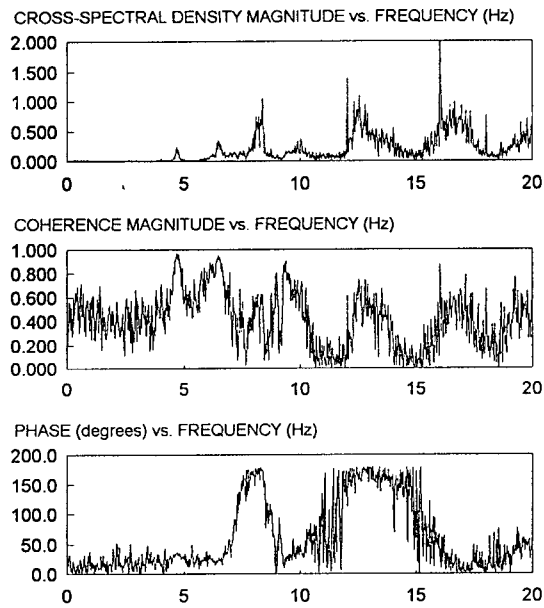
FIGURE D16

POWER SPECTRAL DENSITY FUNCTIONS

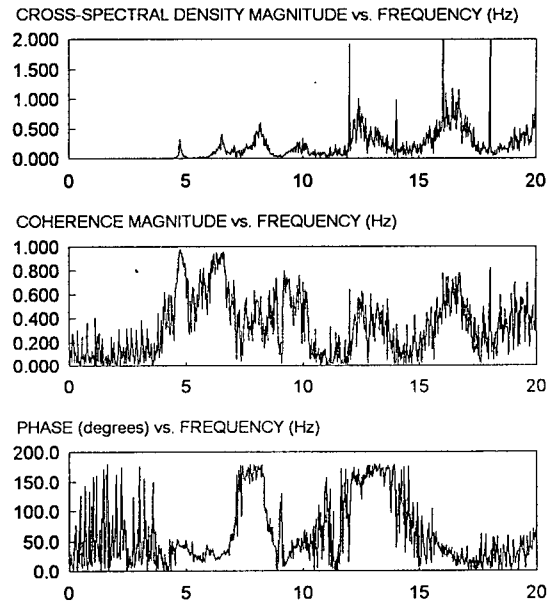
East Bedrock, Vertical Direction

RUSKIN DAM AMBIENT VIBRATION FIELD TEST, HIGH RESERVOIR, 7 & 8 May 1994

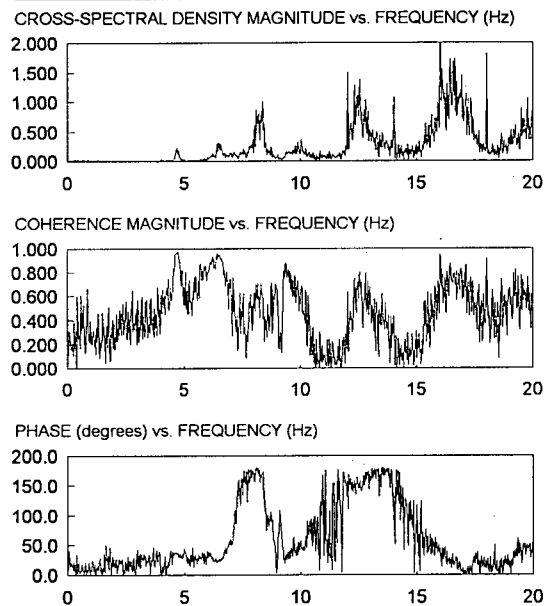
NODES 13 AND 31:



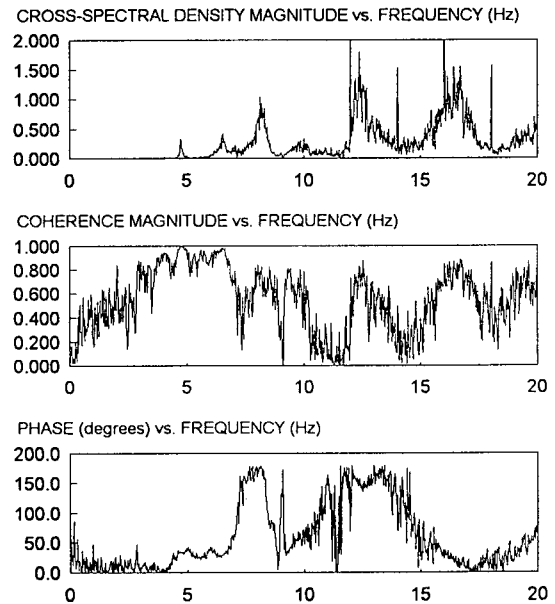
NODES 13 AND 32:



NODES 13 AND 33:



NODES 13 AND 34:



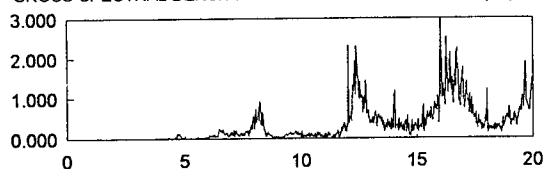
NOTES:

1. All plots completed with high resolution frequency (0.0195 Hz) and with 16 segments

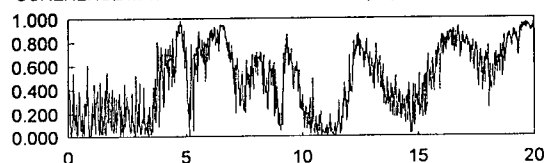
FIGURE D17 CROSS-SPECTRAL DENSITY, COHERENCE and PHASE FACTOR FUNCTIONS
East Bedrock and Reference Sensor, Upstream-Downstream Direction
RUSKIN DAM AMBIENT VIBRATION FIELD TEST, HIGH RESERVOIR, 7 & 8 May 1994

NODES 13 AND 35:

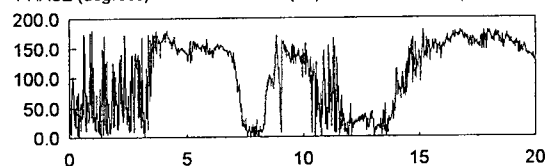
CROSS-SPECTRAL DENSITY MAGNITUDE vs. FREQUENCY (Hz)



COHERENCE MAGNITUDE vs. FREQUENCY (Hz)

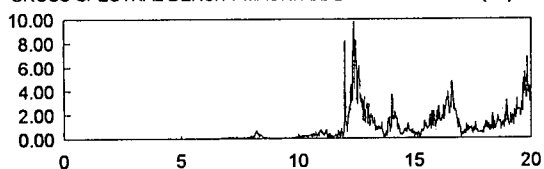


PHASE (degrees) vs. FREQUENCY (Hz)

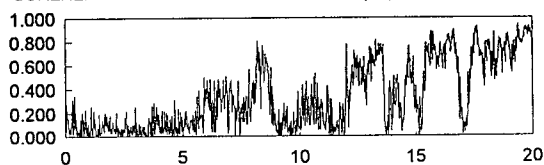


NODES 13 AND 36:

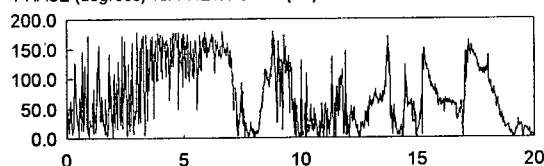
CROSS-SPECTRAL DENSITY MAGNITUDE vs. FREQUENCY (Hz)



COHERENCE MAGNITUDE vs. FREQUENCY (Hz)

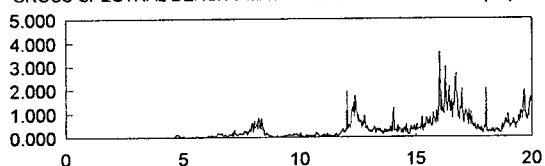


PHASE (degrees) vs. FREQUENCY (Hz)

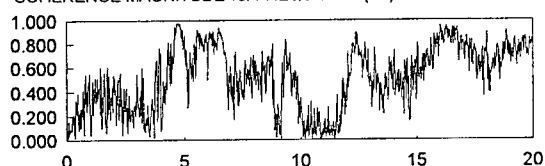


NODES 13 AND 37:

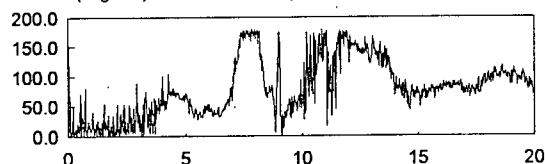
CROSS-SPECTRAL DENSITY MAGNITUDE vs. FREQUENCY (Hz)



COHERENCE MAGNITUDE vs. FREQUENCY (Hz)

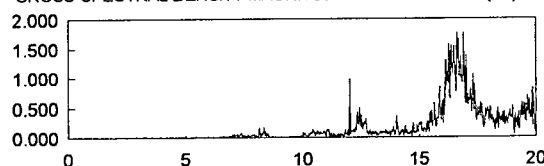


PHASE (degrees) vs. FREQUENCY (Hz)

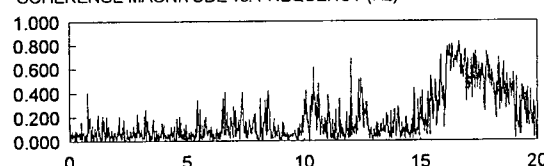


NODES 13 AND 38:

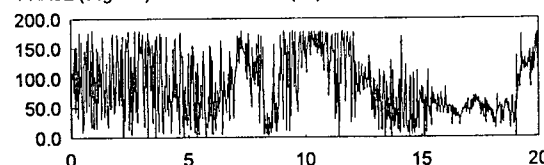
CROSS-SPECTRAL DENSITY MAGNITUDE vs. FREQUENCY (Hz)



COHERENCE MAGNITUDE vs. FREQUENCY (Hz)



PHASE (degrees) vs. FREQUENCY (Hz)



NOTES:

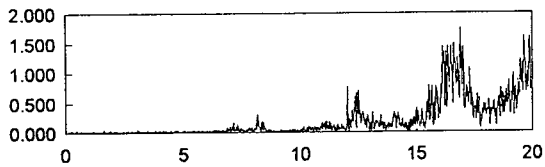
1. All plots completed with high resolution frequency (0.0195 Hz) and with 16 segments

FIGURE D18

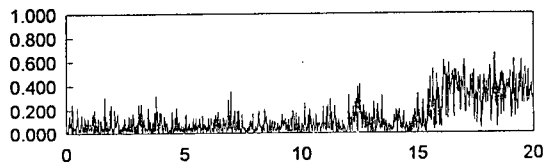
CROSS-SPECTRAL DENSITY, COHERENCE and PHASE FACTOR FUNCTIONS
East Bedrock and Reference Sensor, Upstream-Downstream Direction
RUSKIN DAM AMBIENT VIBRATION FIELD TEST, HIGH RESERVOIR, 7 & 8 May 1994

NODES 13 AND 39:

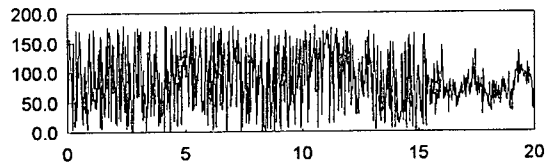
CROSS-SPECTRAL DENSITY MAGNITUDE vs. FREQUENCY (Hz)



COHERENCE MAGNITUDE vs. FREQUENCY (Hz)



PHASE (degrees) vs. FREQUENCY (Hz)



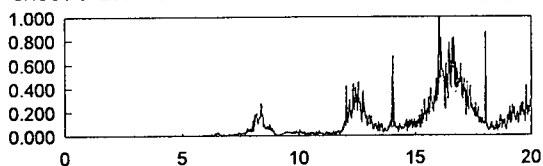
NOTES:

1. All plots completed with high resolution frequency (0.0195 Hz) and with 16 segments

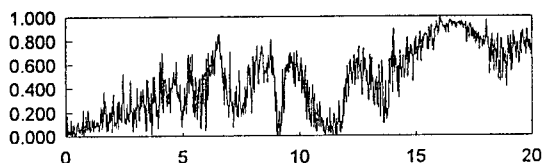
FIGURE D19	CROSS-SPECTRAL DENSITY, COHERENCE and PHASE FACTOR FUNCTIONS
	East Bedrock and Reference Sensor, Upstream-Downstream Direction
	RUSKIN DAM AMBIENT VIBRATION FIELD TEST, HIGH RESERVOIR, 7 & 8 May 1994

NODES 13 AND 31:

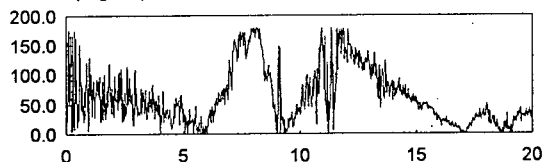
CROSS-SPECTRAL DENSITY MAGNITUDE vs. FREQUENCY (Hz)



COHERENCE MAGNITUDE vs. FREQUENCY (Hz)

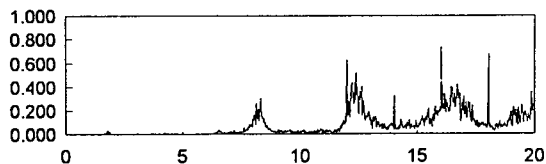


PHASE (degrees) vs. FREQUENCY (Hz)

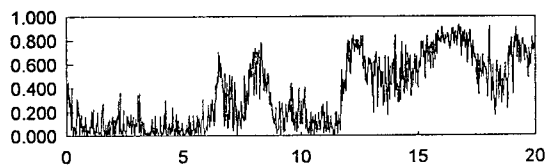


NODES 13 AND 32:

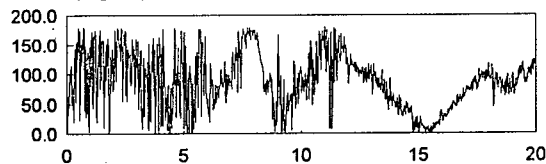
CROSS-SPECTRAL DENSITY MAGNITUDE vs. FREQUENCY (Hz)



COHERENCE MAGNITUDE vs. FREQUENCY (Hz)

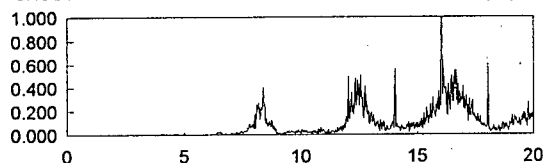


PHASE (degrees) vs. FREQUENCY (Hz)

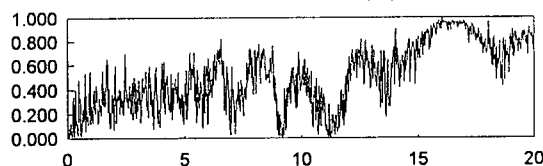


NODES 13 AND 33:

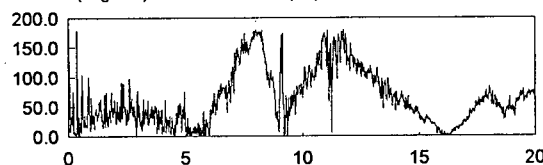
CROSS-SPECTRAL DENSITY MAGNITUDE vs. FREQUENCY (Hz)



COHERENCE MAGNITUDE vs. FREQUENCY (Hz)

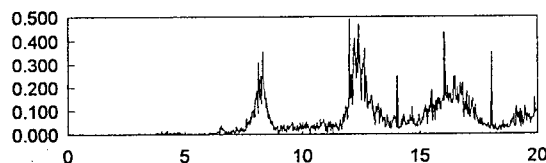


PHASE (degrees) vs. FREQUENCY (Hz)

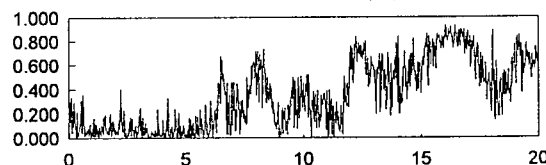


NODES 13 AND 34:

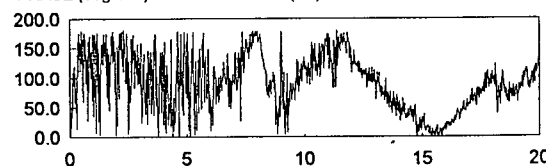
CROSS-SPECTRAL DENSITY MAGNITUDE vs. FREQUENCY (Hz)



COHERENCE MAGNITUDE vs. FREQUENCY (Hz)



PHASE (degrees) vs. FREQUENCY (Hz)



NOTES:

1. All plots completed with high resolution frequency (0.0195 Hz) and with 16 segments

FIGURE D20

CROSS-SPECTRAL DENSITY, COHERENCE and PHASE FACTOR FUNCTIONS
East Bedrock and Reference Sensor, Vertical Direction

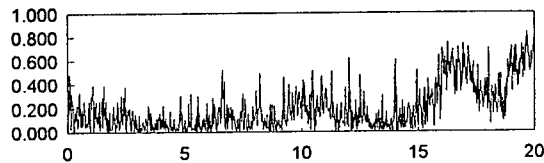
RUSKIN DAM AMBIENT VIBRATION FIELD TEST, HIGH RESERVOIR, 7 & 8 May 1994

NODES 13 AND 35:

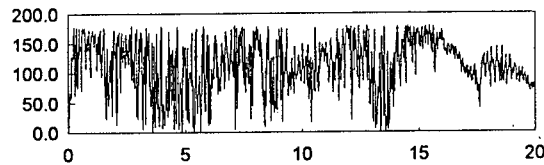
CROSS-SPECTRAL DENSITY MAGNITUDE vs. FREQUENCY (Hz)



COHERENCE MAGNITUDE vs. FREQUENCY (Hz)

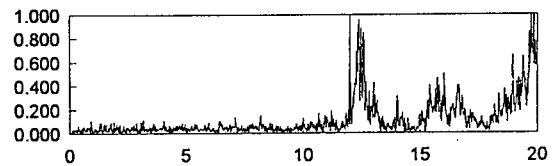


PHASE (degrees) vs. FREQUENCY (Hz)

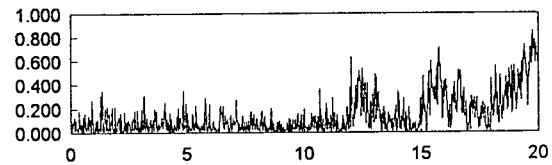


NODES 13 AND 36:

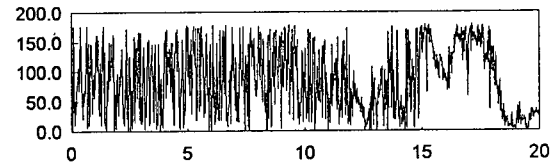
CROSS-SPECTRAL DENSITY MAGNITUDE vs. FREQUENCY (Hz)



COHERENCE MAGNITUDE vs. FREQUENCY (Hz)

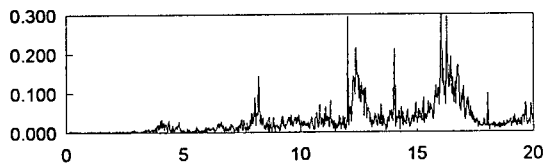


PHASE (degrees) vs. FREQUENCY (Hz)

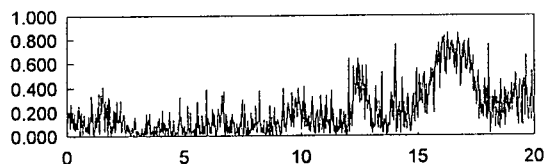


NODES 13 AND 37:

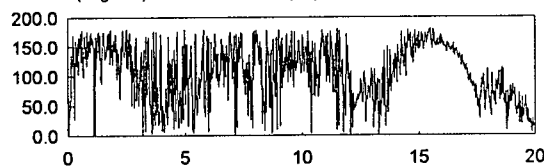
CROSS-SPECTRAL DENSITY MAGNITUDE vs. FREQUENCY (Hz)



COHERENCE MAGNITUDE vs. FREQUENCY (Hz)

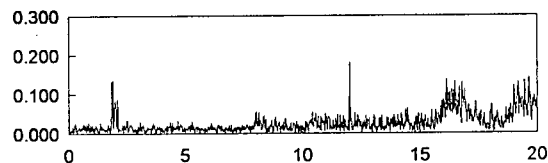


PHASE (degrees) vs. FREQUENCY (Hz)

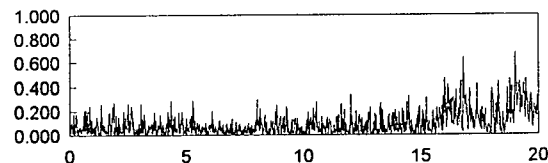


NODES 13 AND 38:

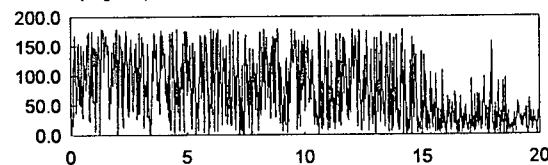
CROSS-SPECTRAL DENSITY MAGNITUDE vs. FREQUENCY (Hz)



COHERENCE MAGNITUDE vs. FREQUENCY (Hz)



PHASE (degrees) vs. FREQUENCY (Hz)



NOTES:

1. All plots completed with high resolution frequency (0.0195 Hz) and with 16 segments

FIGURE D21

CROSS-SPECTRAL DENSITY, COHERENCE and PHASE FACTOR FUNCTIONS
East Bedrock and Reference Sensor, Vertical Direction

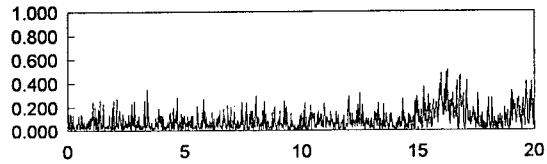
RUSKIN DAM AMBIENT VIBRATION FIELD TEST, HIGH RESERVOIR, 7 & 8 May 1994

NODES 13 AND 39:

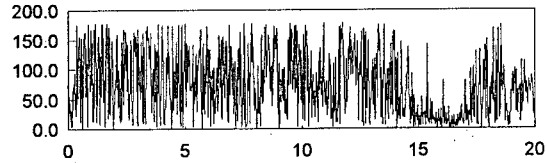
CROSS-SPECTRAL DENSITY MAGNITUDE vs. FREQUENCY (Hz)



COHERENCE MAGNITUDE vs. FREQUENCY (Hz)



PHASE (degrees) vs. FREQUENCY (Hz)



NOTES:

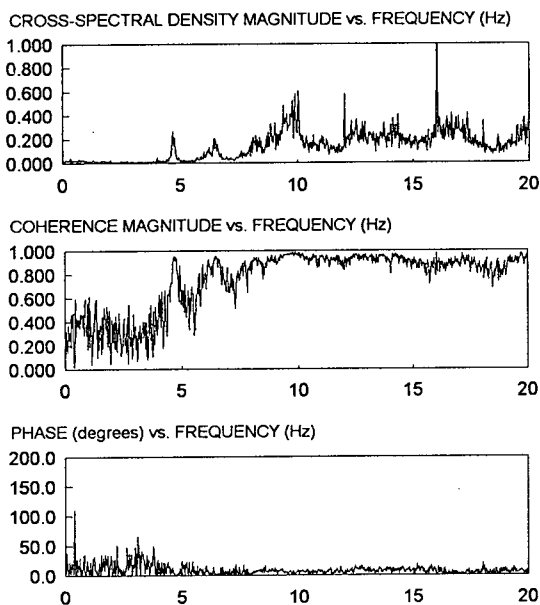
1. All plots completed with high resolution frequency (0.0195 Hz) and with 16 segments

FIGURE D22

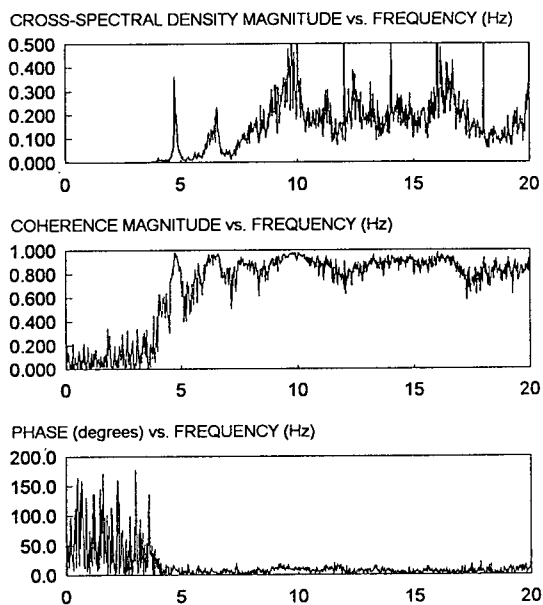
CROSS-SPECTRAL DENSITY, COHERENCE and PHASE FACTOR FUNCTIONS
East Bedrock and Reference Sensor, Vertical Direction

RUSKIN DAM AMBIENT VIBRATION FIELD TEST, HIGH RESERVOIR, 7 & 8 May 1994

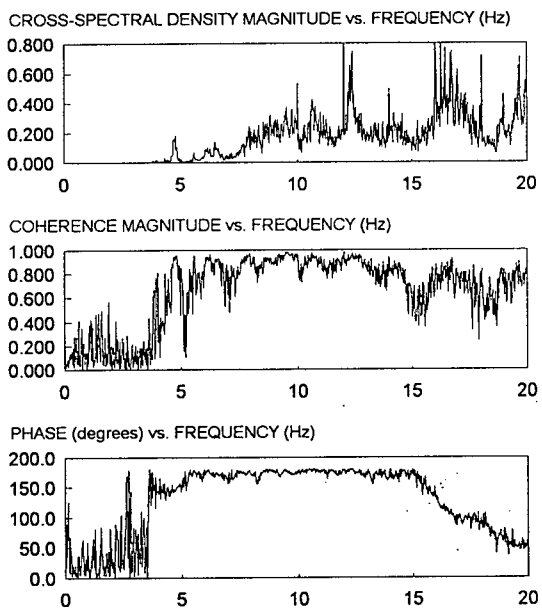
NODES 31 and 33



NODES 32 and 34



NODES 35 and 37



NOTES:

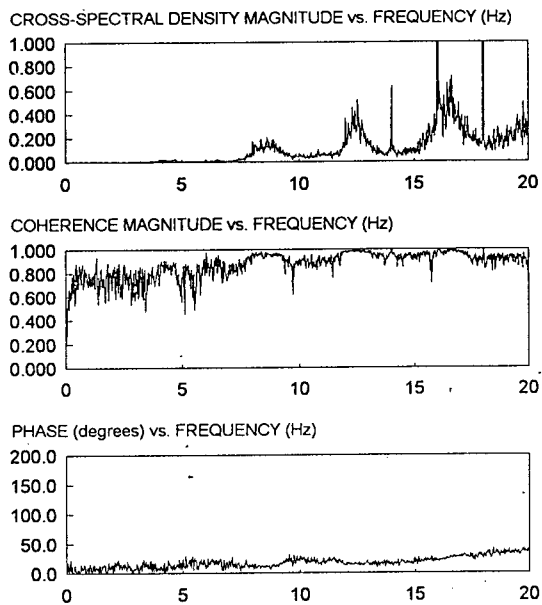
1. All plots completed with high resolution frequency (0.0195 Hz) and with 16 segments

FIGURE D23

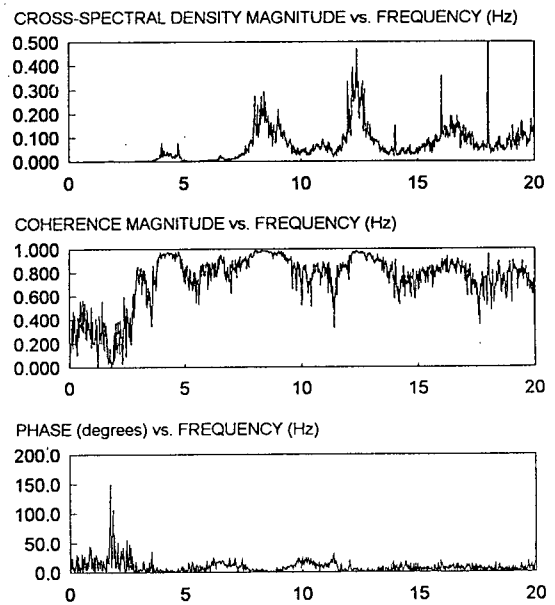
CROSS-SPECTRAL DENSITY, COHERENCE and PHASE FACTOR FUNCTIONS
Bedrock, Upstream-Downstream Direction

RUSKIN DAM AMBIENT VIBRATION FIELD TEST, HIGH RESERVOIR, 7 & 8 May 1994

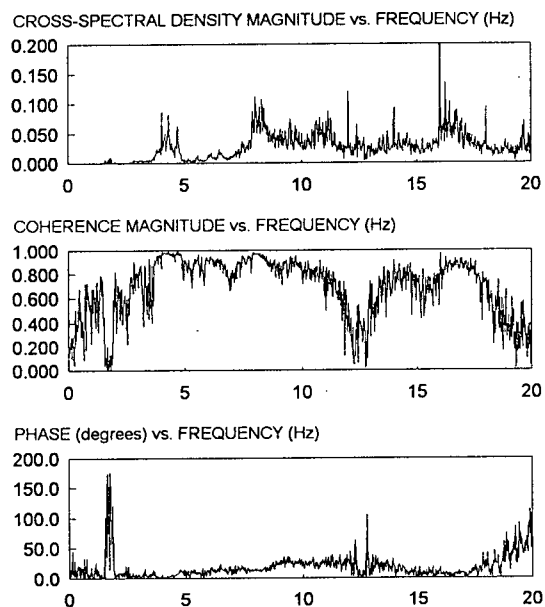
NODES 31 and 33



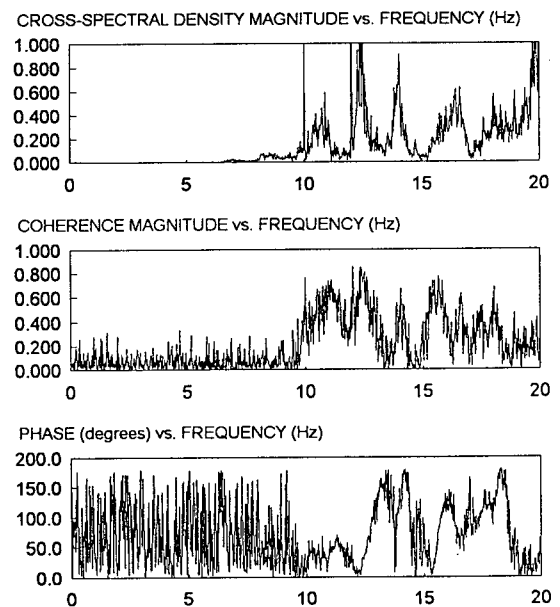
NODES 32 and 34



NODES 35 and 37



NODES 36 and 37

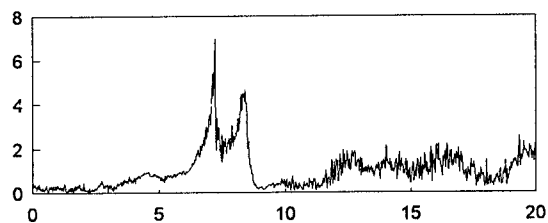


NOTES:

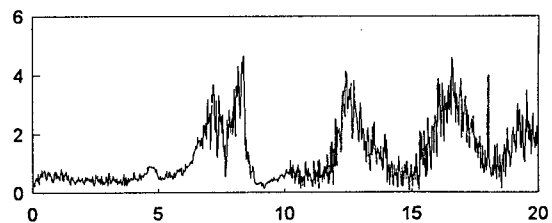
1. All plots completed with high resolution frequency (0.0195 Hz) and with 16 segments

FIGURE D24	CROSS-SPECTRAL DENSITY, COHERENCE and PHASE FACTOR FUNCTIONS Bedrock, Vertical Direction RUSKIN DAM AMBIENT VIBRATION FIELD TEST, HIGH RESERVOIR, 7 & 8 May 1994
------------	--

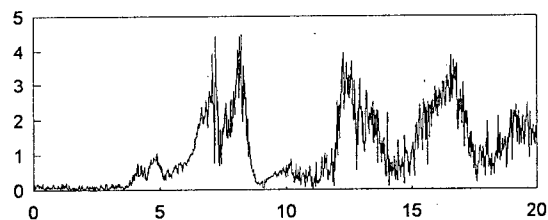
NODE 19



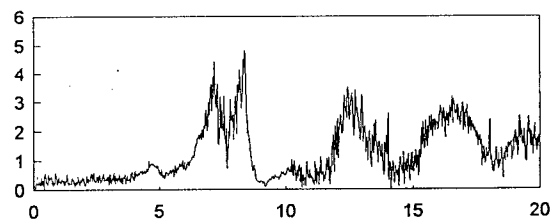
NODE 31



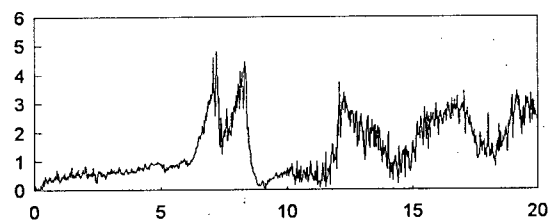
NODE 32



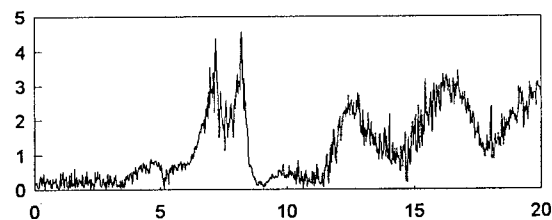
NODE 33



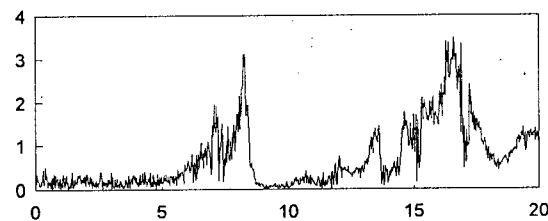
NODE 34



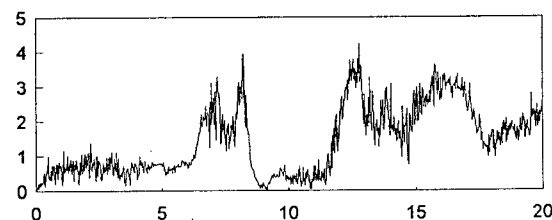
NODE 35



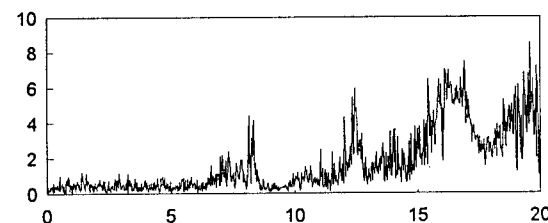
NODE 36



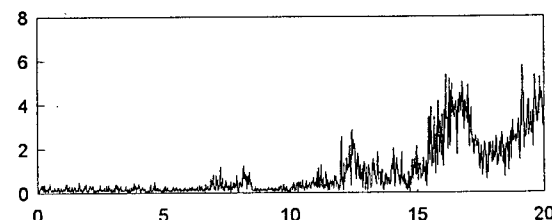
NODE 37



NODE 38



NODE 39



NOTES:

1. All plots completed with high resolution (0.0195 Hz) and 16 segments
2. Abscissa: frequency (Hz), ordinate: transfer function gain magnitude

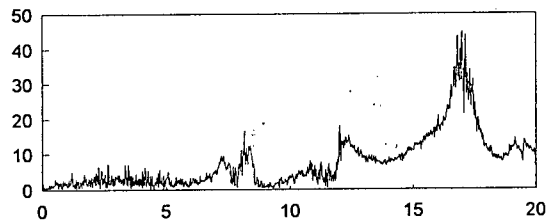
FIGURE D25

TRANSFER FUNCTION GAIN

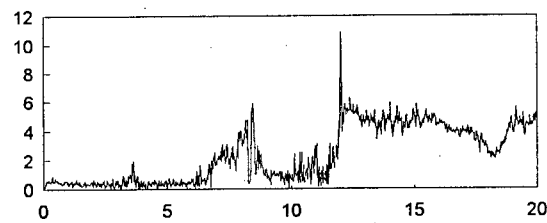
East Bedrock and Reference Sensor, Upstream-Downstream Direction

RUSKIN DAM AMBIENT VIBRATION FIELD TEST, HIGH RESERVOIR, 7 & 8 May 1994

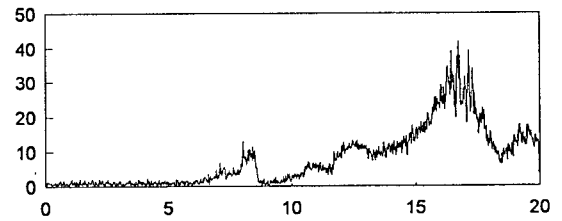
NODE 27



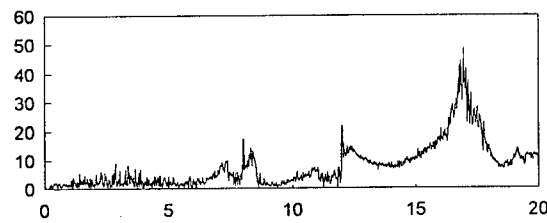
NODE 28



NODE 29



NODE 30



NOTES:

1. All plots completed with high resolution (0.0195 Hz) and 16 segments
2. Abscissa: frequency (Hz), ordinate: transfer function gain magnitude

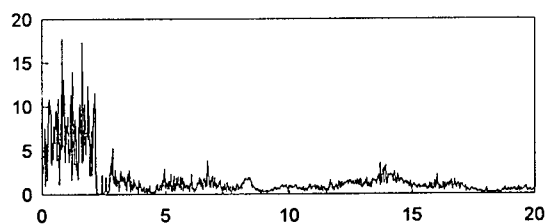
FIGURE D26

TRANSFER FUNCTION GAIN

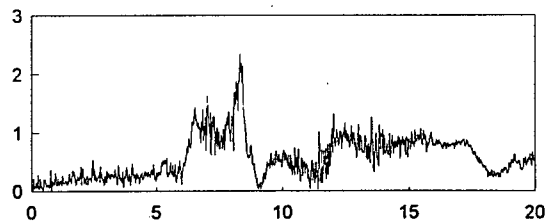
East Bedrock and Reference Sensor, Upstream-Downstream Direction

RUSKIN DAM AMBIENT VIBRATION FIELD TEST, HIGH RESERVOIR, 7 & 8 May 1994

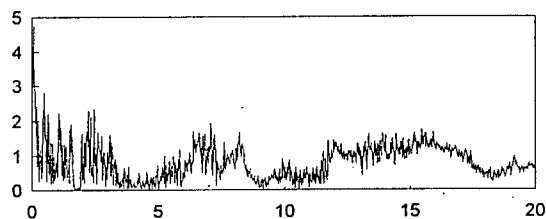
NODE 19



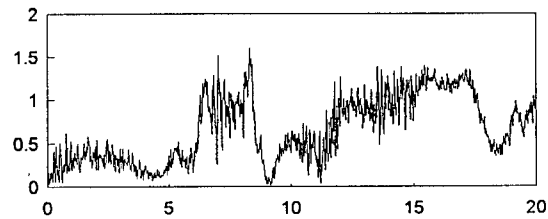
NODE 31



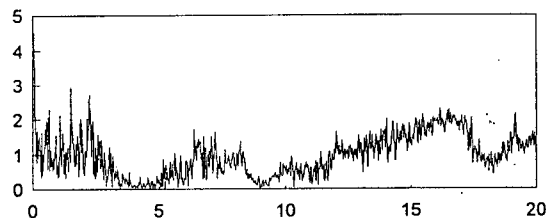
NODE 32



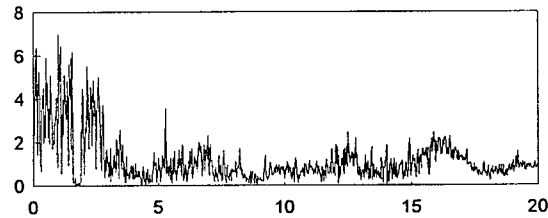
NODE 33



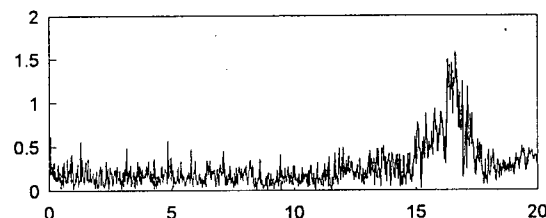
NODE 34



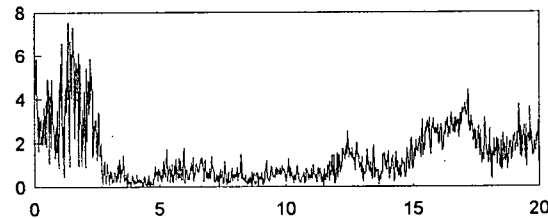
NODE 35



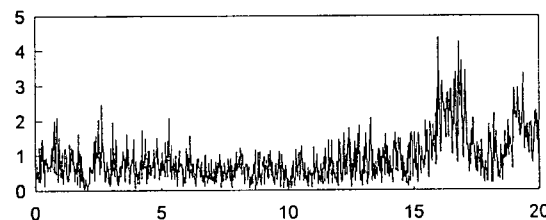
NODE 36



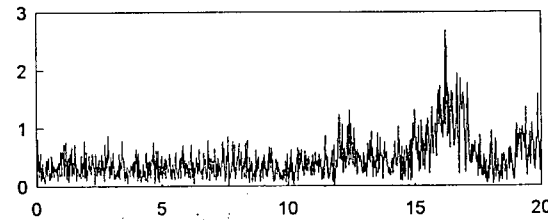
NODE 37



NODE 38



NODE 39



NOTES:

1. All plots completed with high resolution (0.0195 Hz) and 16 segments
2. Abscissa: frequency (Hz), ordinate: transfer function gain magnitude

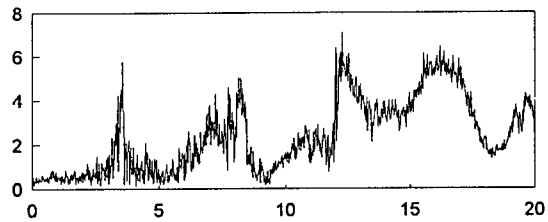
FIGURE D27

TRANSFER FUNCTION GAIN

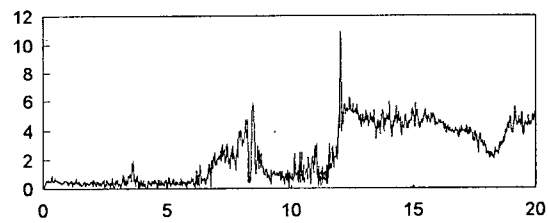
East Bedrock and Reference Sensor, Vertical Direction

RUSKIN DAM AMBIENT VIBRATION FIELD TEST, HIGH RESERVOIR, 7 & 8 May 1994

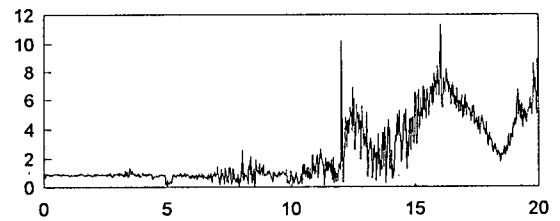
NODE 27



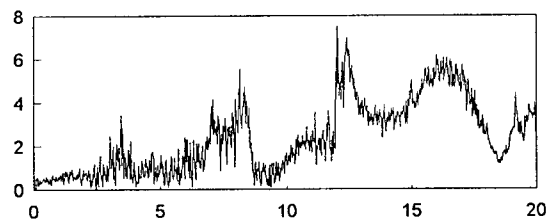
NODE 28



NODE 29



NODE 30



NOTES:

1. All plots completed with high resolution (0.0195 Hz) and 16 segments
2. Abscissa: frequency (Hz), ordinate: transfer function gain magnitude

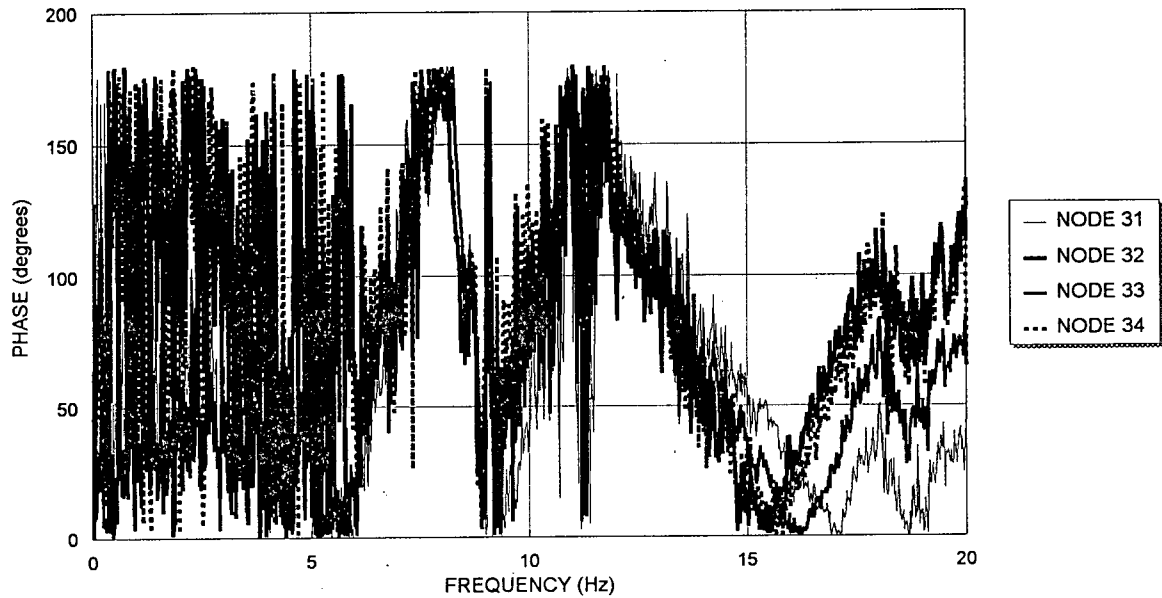
FIGURE D28

TRANSFER FUNCTION GAIN

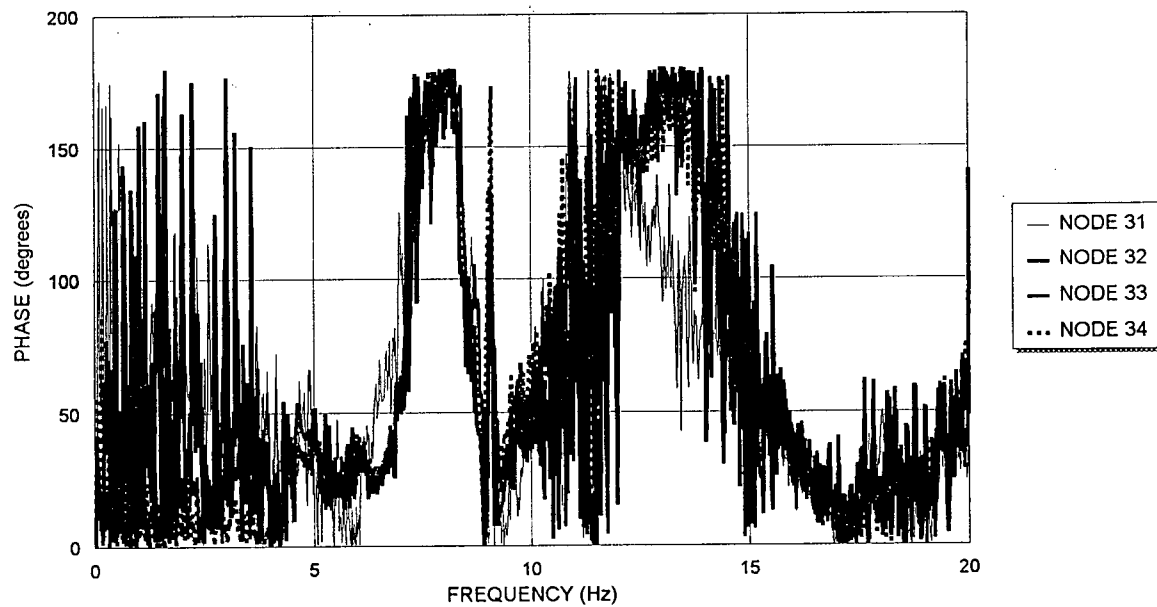
East Bedrock and Reference Sensor, Vertical Direction

RUSKIN DAM AMBIENT VIBRATION FIELD TEST, HIGH RESERVOIR, 7 & 8 May 1994

VERTICAL



UPSTREAM-DOWNSTREAM



NOTES:

1. All plots completed with high resolution frequency (0.0195 Hz) and with 16 segments

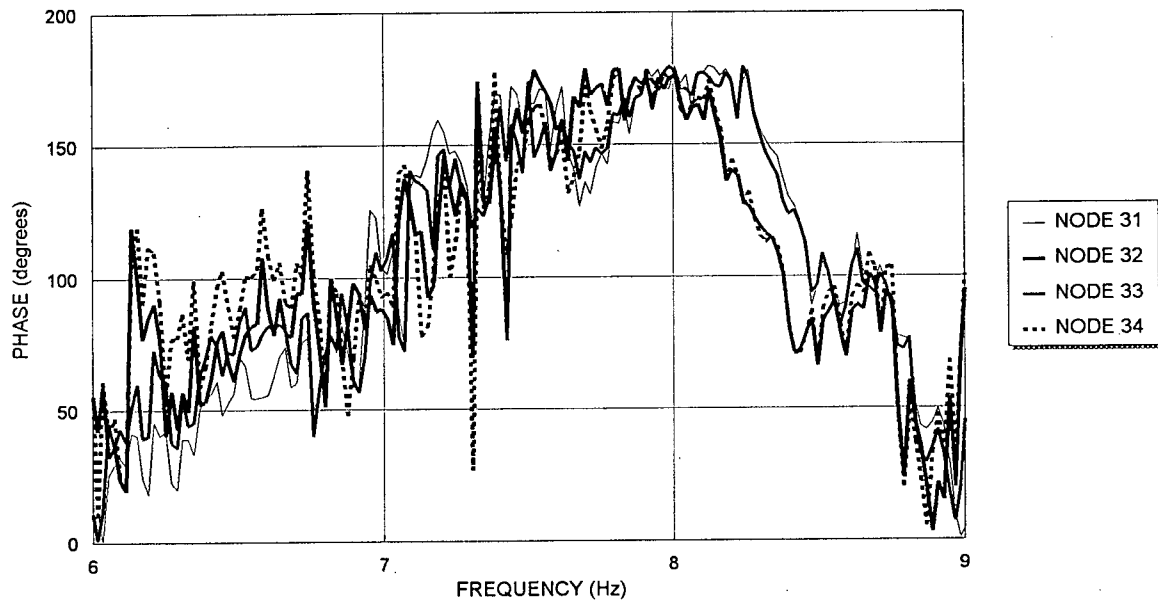
FIGURE D29

PHASE FACTOR FUNCTION, 0-20 Hz

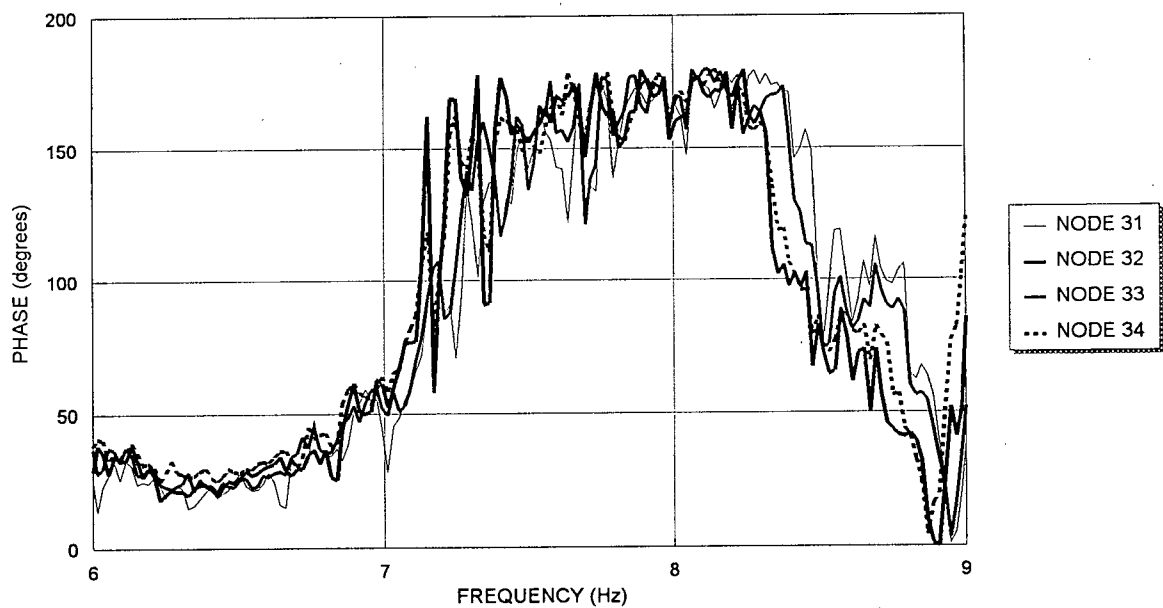
U/S & Vert., Input: Nodes 32-34 (E. Bed.) & Node 31 (PI), Output: Node 13 (Ogee)

RUSKIN DAM AMBIENT VIBRATION FIELD TEST, HIGH RESERVOIR, 7 & 8 May 1994

VERTICAL



UPSTREAM-DOWNSTREAM



NOTES:

1. All plots completed with high resolution frequency (0.0195 Hz) and with 16 segments

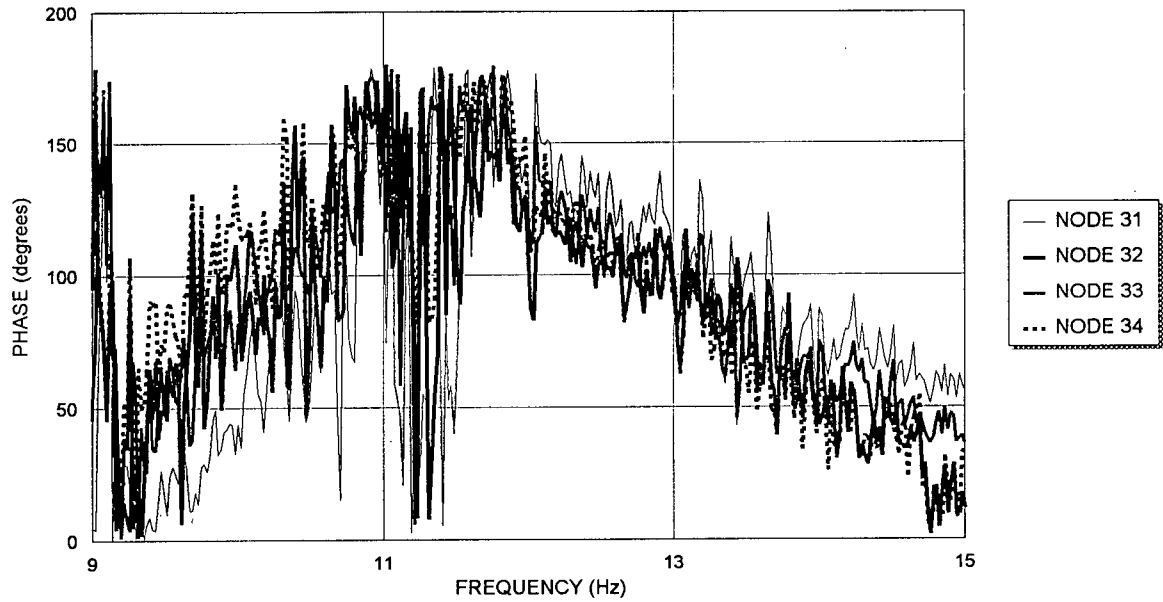
FIGURE D30

PHASE FACTOR FUNCTION, 6-9 Hz

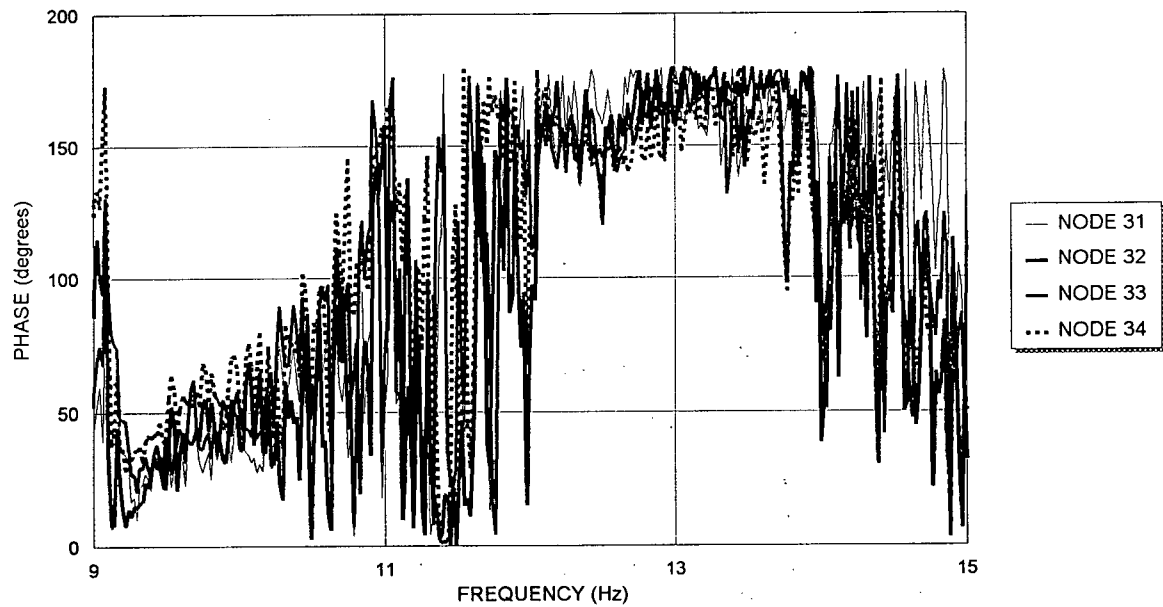
U/S & Vert., Input: Nodes 32-34 (E. Bed.) & Node 31 (PI), Output: Node 13 (Ogee)

RUSKIN DAM AMBIENT VIBRATION FIELD TEST, HIGH RESERVOIR, 7 & 8 May 1994

VERTICAL



UPSTREAM-DOWNSTREAM



NOTES:

1. All plots completed with high resolution frequency (0.0195 Hz) and with 16 segments

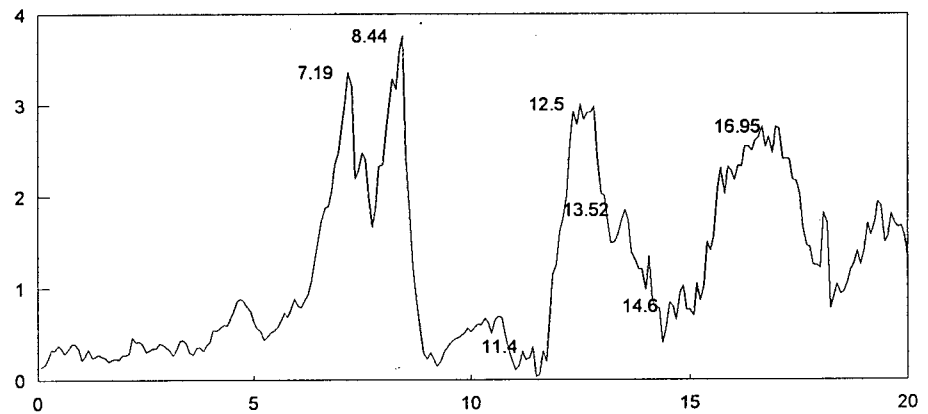
FIGURE D31

PHASE FACTOR FUNCTION, 9-15 Hz

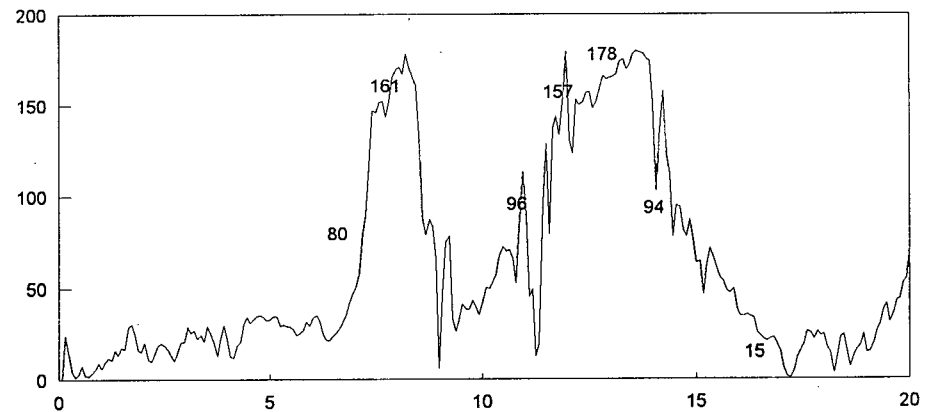
U/S & Vert., Input: Nodes 32-34 (E. Bed.) & Node 31 (PI), Output: Node 13 (Ogee)

RUSKIN DAM AMBIENT VIBRATION FIELD TEST, HIGH RESERVOIR, 7 & 8 May 1994

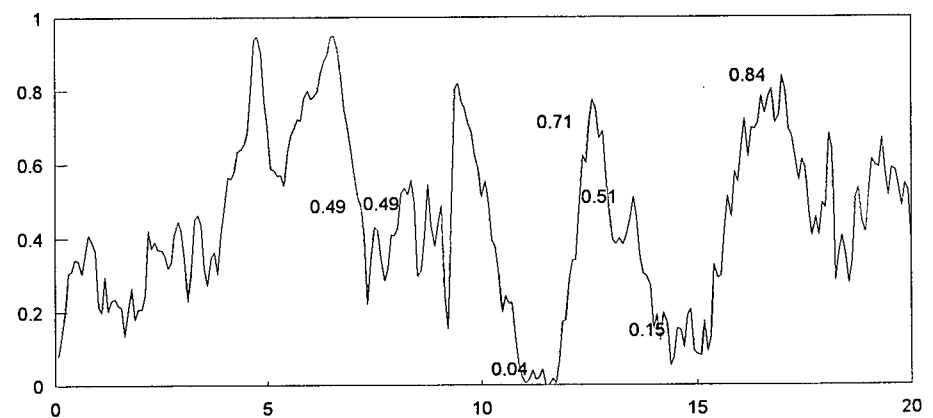
TRANSFER
FUNCTION GAIN
MAGNITUDE
vs.
FREQUENCY (Hz)



PHASE
(degrees)
vs
FREQUENCY (Hz)



COHERENCE
MAGNITUDE
vs
FREQUENCY (Hz)



NOTES:

1. All plots at low resolution (0.0781 Hz) and with 64 segments
2. Transfer function gain local maxima frequencies are indicated, as are the corresponding phase factor and coherence values

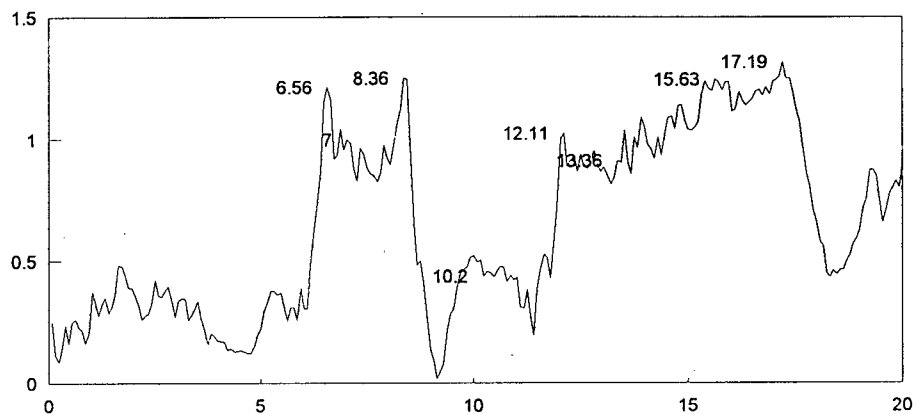
FIGURE D32

TRANSFER FUNCTION GAIN, PHASE FACTOR AND COHERENCE

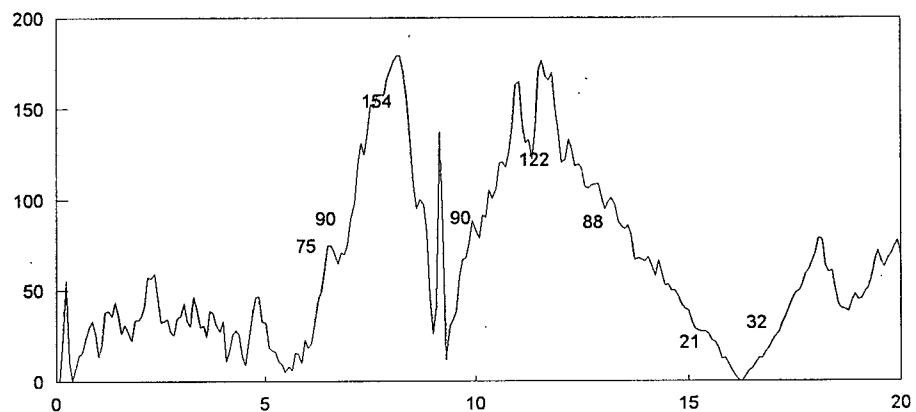
Upstream-Downstream Direction, Input: Node 33 (Bedrock), Output: Node 13 (Ogee)

RUSKIN DAM AMBIENT VIBRATION FIELD TEST, HIGH RESERVOIR, 7 & 8 May 1994

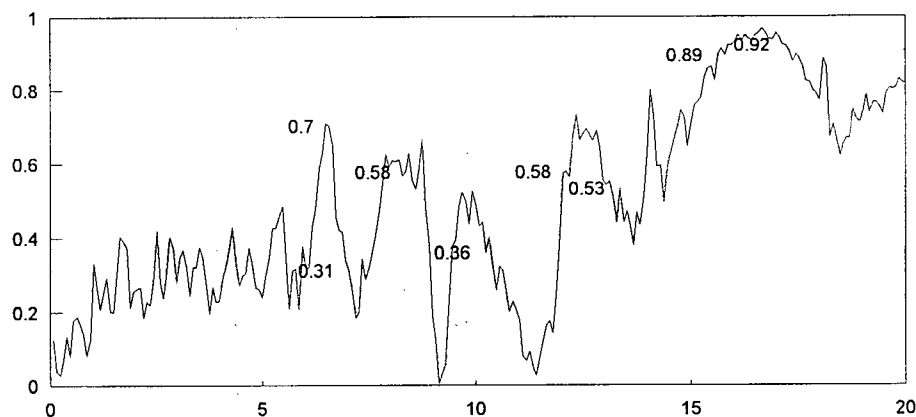
TRANSFER
FUNCTION GAIN
MAGNITUDE
vs.
FREQUENCY (Hz)



PHASE
(degrees)
vs
FREQUENCY (Hz)



COHERENCE
MAGNITUDE
vs
FREQUENCY (Hz)



NOTES:

1. All plots at low resolution (0.0781 Hz.) and with 64 time histories.
2. Local transfer function peak frequencies are indicated, as are the corresponding phase and coherence factors.

FIGURE D33

TRANSFER, PHASE AND COHERENCE FUNCTIONS

Vertical Direction, Input: Node 33 (Bedrock), Output: Node 13 (Ogee)

RUSKIN DAM AMBIENT VIBRATION FIELD TEST, HIGH RESERVOIR, 7 & 8 May 1994

**AMBIENT VIBRATION ASSESSMENT OF RUSKIN DAM
DYNAMIC PROPERTIES**

APPENDIX E

NUMERICAL MODELLING STUDIES

CONTENTS

<u>Section</u>	<u>Subject</u>	<u>Page</u>
E.1	General	315
E.2	Calibration Study	316
E.3	Parametric Studies	316
Figures (E1 through E18)		321-338

E.1 GENERAL

A summary of all models and their significant parameters is contained in Table E1.

Table E1
Summary of Model Parameters

SUMMARY OF BASE MODEL PARAMETERS						
		RESERVOIR ELEVATION (ft)	FOUNDATION DYNAMIC MODULUS (psf x 10 ⁶)	CONCRETE DYNAMIC MODULUS (psf x 10 ⁶)	MODIFIED BOUNDARY CONDITIONS	ENLARGED FOUNDATION
		211.0	1.04-6.27	7.2	NONE	NO
SUMMARY OF MODIFICATIONS FROM BASE MODEL PARAMETERS						
STUDY	MODEL NO.	RESERVOIR ELEVATION (ft)	FOUNDATION DYNAMIC MODULUS (psf x 10 ⁶)	CONCRETE DYNAMIC MODULUS (psf x 10 ⁶)	MODIFIED BOUNDARY CONDITIONS	ENLARGED FOUNDATION
Calibration	1	0				
	2	188.5				
	3					
Parametric	4		2.09			
	5		4.18			
	6		6.27			
	7			10.8		
	8				At power intake	
	9					Additional 40 ft to each abutment

To perform the calibration and parametric studies, a basis for comparison of the mode shapes was required. The ambient measurement locations on the ogee and gallery defined the points with which comparison was to be drawn. As well, the cross-canyon direction was considered insignificant in relation to the upstream-downstream and vertical directions and so the latter two were chosen as the directions to form comparisons. The ambient measurement locations are shown on the base numerical model in Figure E1.

The attached Figures E1-E5 depict the first six significant operating deflected shapes identified with the ambient work, for each of the low and high reservoir tests, as defined along the ogee and gallery in the upstream-downstream and vertical directions.

The attached Figures E6-E11 depict the first five mode shapes for the base model analyzed with; no reservoir, at the low reservoir elevation matching that during the low reservoir ambient test, at the high reservoir elevation matching that during the high reservoir ambient test. The mode shapes are defined along the ogee and gallery in the upstream-downstream and vertical directions.

Figures E13-E18 depict the first five mode shapes for each of the parametric study models, as defined along the ogee and gallery in the upstream-downstream and vertical directions.

E.2 CALIBRATION STUDY

The calibration study is discussed in the main text.

Figure E12 contains the results of a MAC analysis performed to study the correlation between the ambient mode shapes and the numerical model mode shapes. The MAC values are between 0 and 1 and were calculated using the aggregate of points on the ogee and gallery. The deck was not included.

E.3 PARAMETRIC STUDIES

One feature noted from the ambient analyses detailed in Appendices C and D was that the operating deflected shapes viewed with VISUAL seemed to indicate a "marching" across the ogee and gallery, from east to west, of inflection points with increasing frequency. This effect is noted in Figures E2-E5, where if one discounts the first operating deflected shape at 4.5-4.6 Hz (which corresponds to a natural frequency of the bedrock), the remaining operating deflected shapes exhibit this effect. It is more clearly witnessed when actually using VISUAL. The base model did not show this behaviour. Inspection of Figures E8 and E10 shows that the mode shape corresponding to the third natural frequency is a single curvature, as defined along the ogee, the amplitude of which is highest where the tallest section of the dam is located. Therefore, one feature of the improved model sought after was an ordered progression of mode shapes with zero, one and then two inflection points (possibly near realizing single, double and triple curvatures).

The calibration study had shown that at the high reservoir elevation, the difference between the first and second natural frequencies was not great enough. Therefore, the second feature for an improved model was selected to be a greater difference between those natural frequency magnitudes.

The following aspects of the numerical model were not considered for parametric study:

Element type and Mesh Density: These are important considerations for stress analysis. However, the detail in the model suggested that the mesh density was more

than adequate. In fact, a much coarser model would have been preferred for the calibration/parametric study. The elements chosen did not include rotation degrees of freedom. This was not considered significant.

Mass Density Of Concrete and Water: These parameters are not considered to vary significantly enough to warrant parametric study.

Spatial Variation Of Concrete Modulus: It is postulated that there could be a variation in concrete modulus. The reservoir acting against the upstream face of the dam would enhance curing and compressive strength development. The modulus varies with the compressive strength and so may be higher on the upstream face. However, there is no in-situ test data or literature to support this postulation and so it was not pursued.

The items selected for parametric study are as follows:

Foundation Dynamic Modulus: BCH engineering had suggested that the foundation bedrock below the dam was of variable quality and had therefore identified ranges of foundation dynamic modulus which would allow parametric studies. Firstly, the basic impact of varying the foundation dynamic modulus was required. So in order to enhance understanding, models would be analyzed with foundations of uniform foundation dynamic modulus. Using the ranges given in the BCH engineering recommendations, models with uniform foundation dynamic modulus of 2.09×10^8 , 4.18×10^8 and 6.27×10^8 psf were analyzed (Models 4, 5 and 6).

Concrete Dynamic Modulus: The concrete dynamic modulus was felt to be of significant influence and so was selected for study. An arbitrary increase of 50% was made (Model 7).

Modified Boundary Conditions: The power intake had not been represented in the base model. Where the power intake was located, the base model had restraints in the upstream-downstream direction. It was felt that the power intake structure would not provide this severe a restraint. In addition, careful examination of the mode shapes corresponding to the second natural frequency suggested that at the east end of the dam, where the power intake was located, that there was a significant difference between the ambient and base model results. On the ogee, the base model showed an almost complete double curvature whereas the ambient mode shape was closer to a curvature and a half. This did not extend to the gallery where the shapes were similar. Refer to Figures E2 through E11 for the mode shapes. Therefore, a model was analyzed which released the upstream-downstream restraints on the upstream face of the abutment where the power intake was located (Model 8).

Enlarged Foundation: The foundation size was arbitrarily enlarged by adding a 40 foot width to each abutment (Model 9).

Shown in Table E2 is a summary of the first and second natural frequency magnitudes, along with the difference between these.

Table E2
Summary of First/Second Natural Frequency Magnitudes

STUDY		MODEL NO.	NATURAL FREQUENCY (Hz)		
			FIRST	SECOND	DIFFERENCE BETWEEN FIRST AND SECOND
Ambient	Low		8.2-9.0	13.3-13.9	4.3-5.7
	High		6.9-7.3	13.0-13.6	5.7-6.7
Calibration	No	1	10.0	15.3	5.3
	Low	2	8.6	13.9	5.3
	High	3	7.5	11.6	4.1
Parametric	Foundation Dynamic Modulus	4	6.8	10.5	3.7
		5	7.7	11.4	3.7
		6	8.1	11.7	3.6
	Concrete Dynamic Modulus	7	8.6	13.7	5.1
	Modified Boundary Conditions	8	7.5	11.5	4.0
	Enlarged Foundation	9	7.5	11.6	4.1

Shown in Table E3 is a summary of the number of inflection points along the ogee, in both the vertical and upstream-downstream directions. This table will be referred to when describing the mode shape ordering. This is a very simplistic appraisal of mode shape order, as it does not consider vertical sections through the dam, however, the ambient measurements were restricted to only the ogee and gallery.

Results of the parametric studies were as follows:

Foundation Dynamic Modulus

Referring to Table E2, the frequencies are found to increase as the foundation dynamic modulus is increased, as is to be expected. The difference between the first and second natural frequency magnitudes does not change significantly. In fact, the difference shows a slight decrease.

Reviewing Figures E13-E15 shows that the ordering of mode shapes, by number of inflection points along the ogee, does change somewhat with increasing foundation dynamic modulus. Model 4, with the lowest foundation dynamic modulus exhibits an

ordering of shapes similar to the base model (Figure E10). Increasing the foundation dynamic modulus yields an order wherein the first three mode shapes are single, double and triple curvature of the ogee, with 0, 1 and 2 inflection points respectively, as noted in Table E3.

Table E3
Number Of Inflection Points Along Ogee

STUDY		MODEL NO.	NUMBER OF INFLECTION POINTS ALONG OGEE		
			FIRST NATURAL FREQUENCY	SECOND NATURAL FREQUENCY	THIRD NATURAL FREQUENCY
Ambient	Low		0	1	2
	High		0	1	2
Calibration	No	1	0	1	2
	Low	2	0	1	0
	High	3	0	1	0
Parametric	Foundation Dynamic Modulus	4	0	1	0
		5	0	1	2
		6	0	1	2
	Concrete Dynamic Modulus	7	0	1	0
	Foundation Density	8	0	1	0
	Modified Boundary Conditions	9	0	1	0
	Enlarged Foundation	10	0	1	0

Increasing the foundation dynamic modulus yields a better model, as far as mode shape ordering is concerned. Unfortunately, the magnitude of the foundation dynamic modulus for the models producing the acceptable ordering is a minimum of 4.18×10^8 psf, which is higher than the bounds given by BCH engineering study for the central portion of the foundation.

Concrete Dynamic Modulus

Table E2 shows that increasing the concrete dynamic modulus increases the difference between the first and second natural frequencies, a desirable result. Unfortunately, the

magnitudes of the first and second natural frequencies also increase, which is an undesirable result.

Reviewing Figures E16 and E10 shows that the first three mode shapes are similar to the base model. A mode shape with two inflection points (in both upstream-downstream and vertical directions) does not occur until the fifth mode shape.

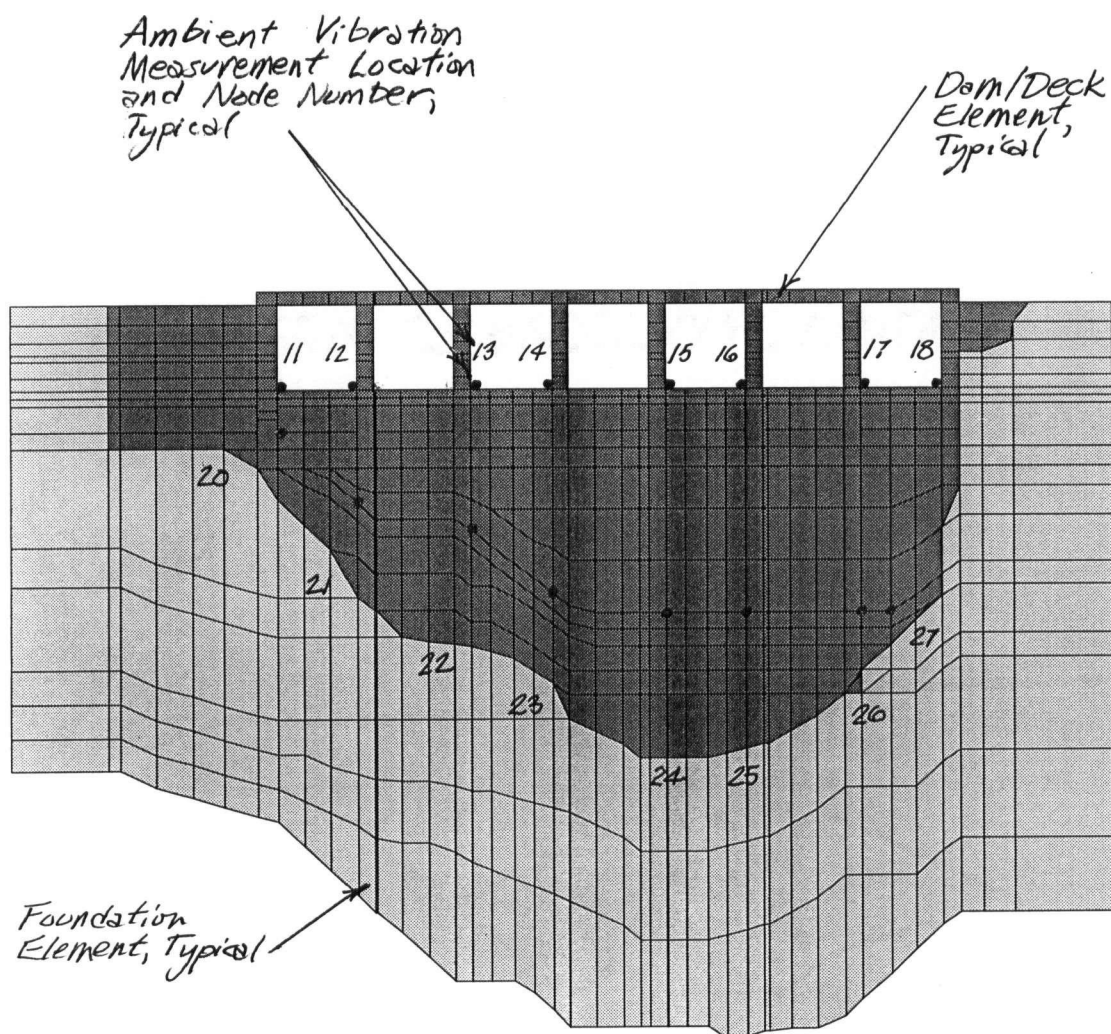
Increasing the concrete dynamic modulus results in a better difference between the first and second natural frequencies, however, the magnitudes become too high and the mode shape ordering becomes more inaccurate.

Modified Boundary Conditions

Results shown in Tables E2, E3 and Figures E17 and E4 indicate that very little difference resulted, by releasing the node restraints. The overall model stiffness was reduced slightly, which does reflect itself in a very small drop in magnitude for each natural frequency, not always evident as the values quoted in Figure E17 are to one decimal place.

Enlarged Foundation

Results shown in Tables E2, E3 and Figures E18 and E4 indicate very little difference with the enlarged foundation. The magnitude of natural frequencies for this model did drop slightly, which is not always shown as the frequency values shown are only to one decimal place. This indicates that the foundation size in the base model has been taken far enough away from the dam, at least on the abutments, so that it does not impact the modal analysis of the dam.



The Measurement Locations Corresponding To Node Numbers 20-27 Are Located In The Drainage Gallery and Are Shown Above Projected Onto The Downstream Face Of The Dam

NOTES:

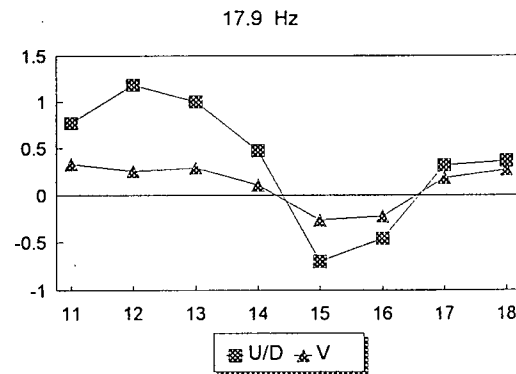
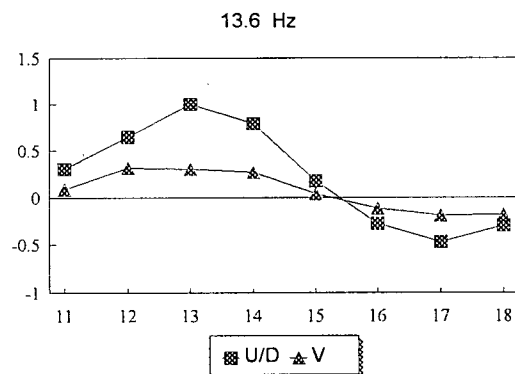
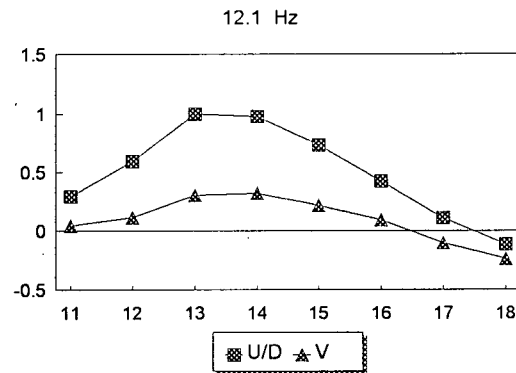
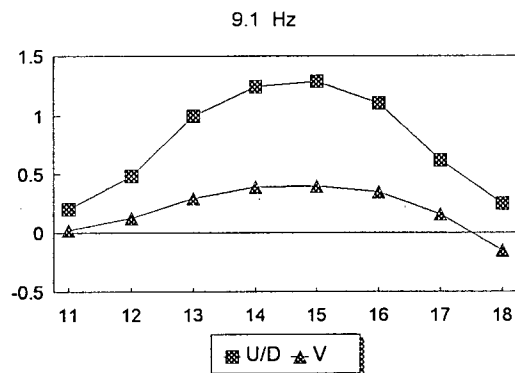
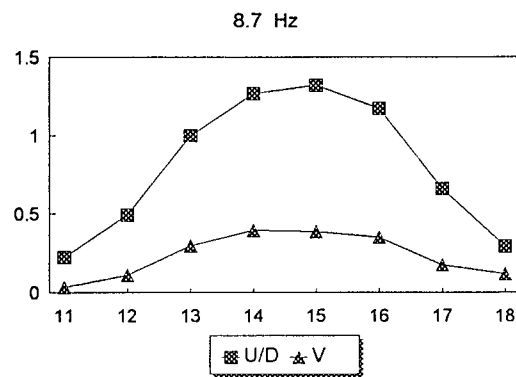
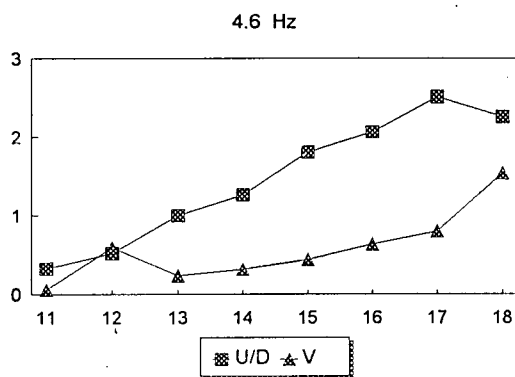
1. Shown above is a view of the numerical FEM base model of the dam from downstream side.

FIGURE E1

MODE SHAPES/OPERATING DEFLECTED SHAPES

Locations of Nodes/Measurement Locations Used

RUSKIN DAM NUMERICAL MODELLING STUDIES

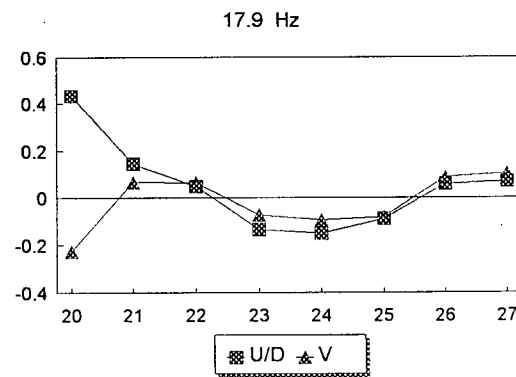
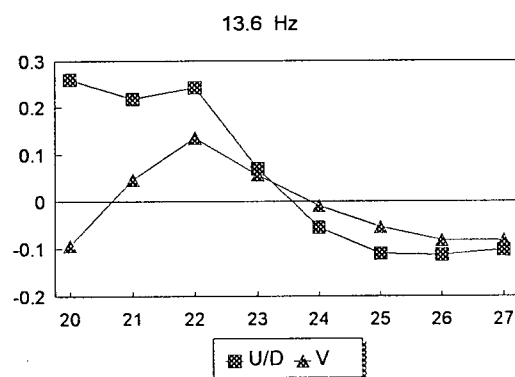
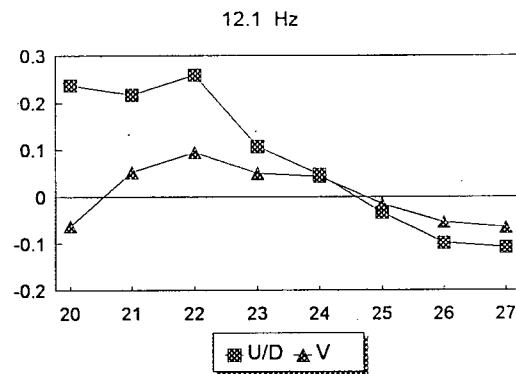
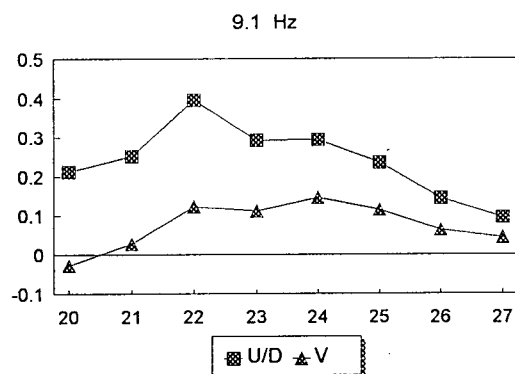
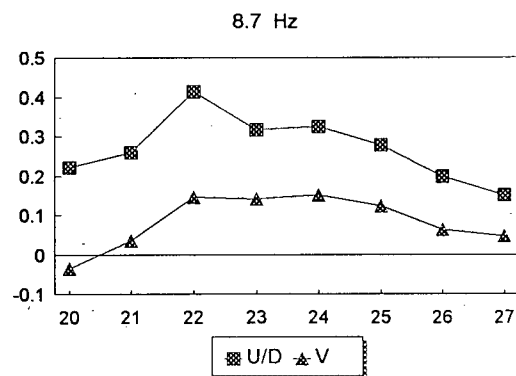
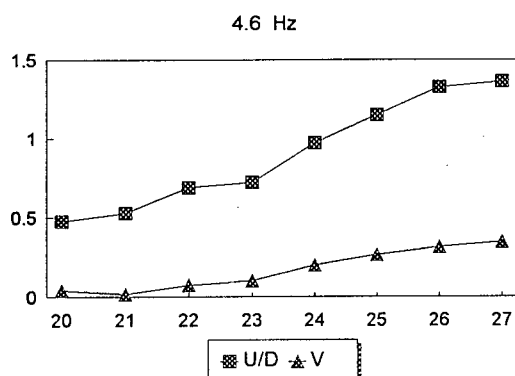


NOTES:

1. Abscissa: amplitude normalized to the reference sensor location (measurement location #13)
2. Ordinate: ambient vibration measurement locations along ogee, see Figures A4 and E1 for their locations
3. Ambient : completed with high resolution frequency (0.0195 Hz) and 16 segments
4. Ambient : coherence window: 0-1, phase window: 0-90 degrees
5. In legend, U/D=upstream-downstream direction, V=vertical direction
7. Positive sense: downstream in upstream-downstream direction, up in vertical direction

FIGURE E2 FIRST SIX AMBIENT OPERATING DEFLECTED SHAPES (defined along ogee)

RUSKIN DAM AMBIENT VIBRATION FIELD TEST, LOW RESERVOIR, 31 April & 1 May 1994

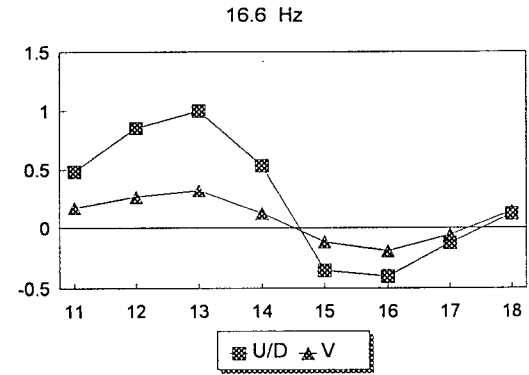
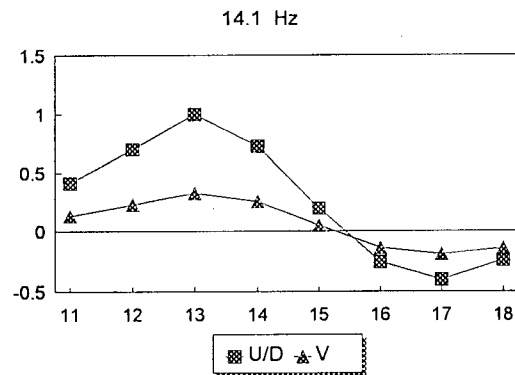
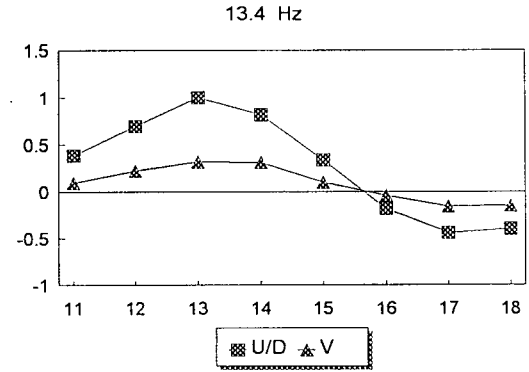
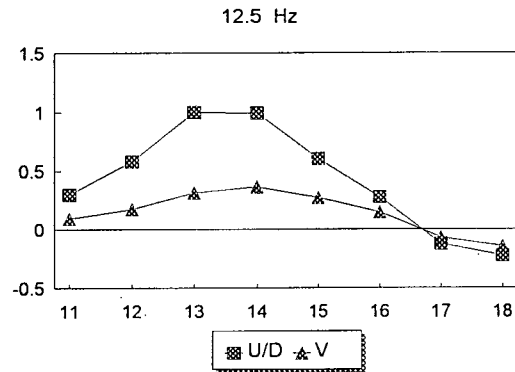
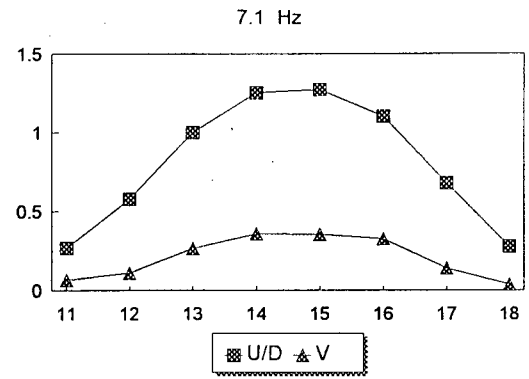
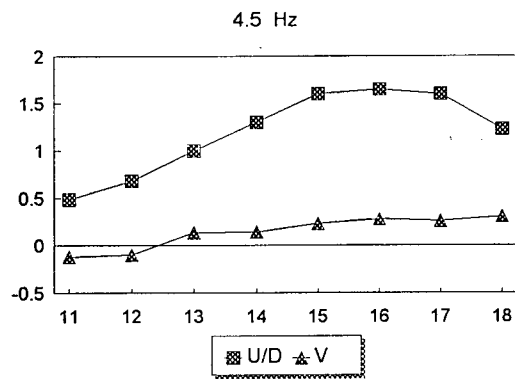


NOTES:

1. Abscissa: amplitude normalized to the reference sensor location (measurement location #13)
2. Ordinate: ambient vibration measurement locations along ogee, see Figures A4 and E1 for their locations
3. Ambient : completed with high resolution frequency (0.0195 Hz) and 16 segments
4. Ambient : coherence window: 0-1, phase window: 0-90 degrees
5. In legend, U/D=upstream-downstream direction, V=vertical direction
7. Positive sense: downstream in upstream-downstream direction, up in vertical direction

FIGURE E3 FIRST SIX AMBIENT OPERATING DEFLECTED SHAPES (defined along gallery)

RUSKIN DAM AMBIENT VIBRATION FIELD TEST, LOW RESERVOIR, 31 April & 1 May 1994

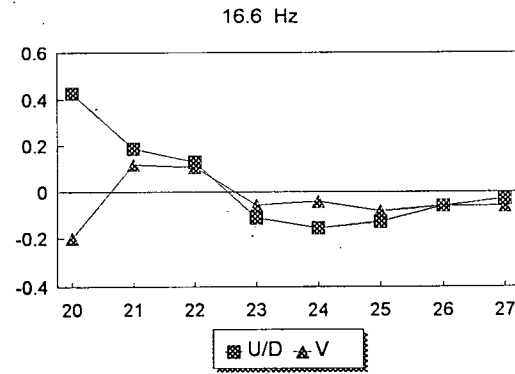
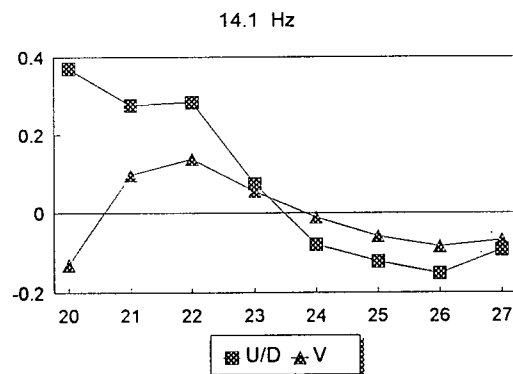
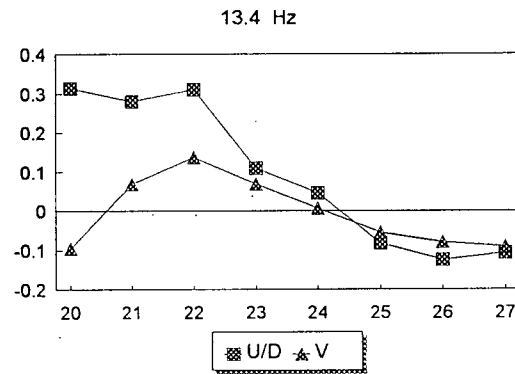
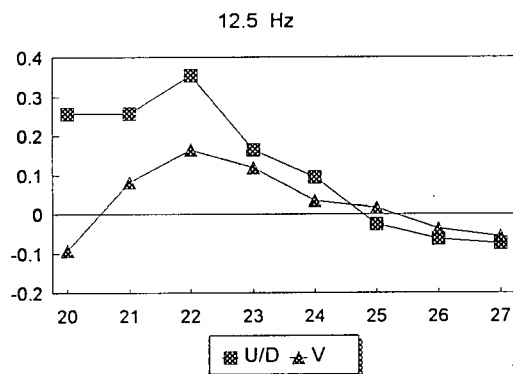
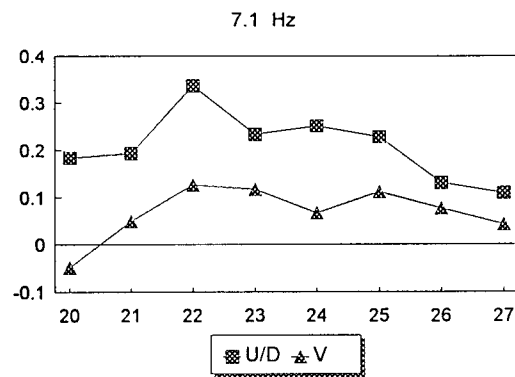
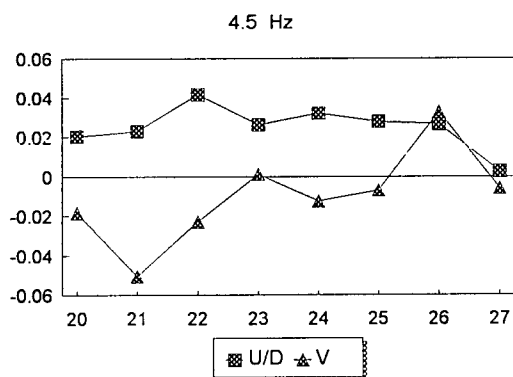


NOTES:

1. Abscissa: amplitude normalized to the reference sensor location (measurement location #13)
2. Ordinate: ambient vibration measurement locations along ogee, see Figures A4 and E1 for their locations
3. Ambient plots completed with high resolution frequency (0.0195 Hz) and 16 segments
4. Ambient plots: coherence window: 0-1, phase window: 0-90 degrees
5. In legend, U/D=upstream-downstream direction, V=vertical direction
7. Positive sense: downstream in upstream-downstream direction, up in vertical direction

FIGURE E4 FIRST SIX AMBIENT OPERATING DEFLECTED SHAPES (defined along ogee)

RUSKIN DAM AMBIENT VIBRATION FIELD TEST, HIGH RESERVOIR, 7 & 8 May 1994



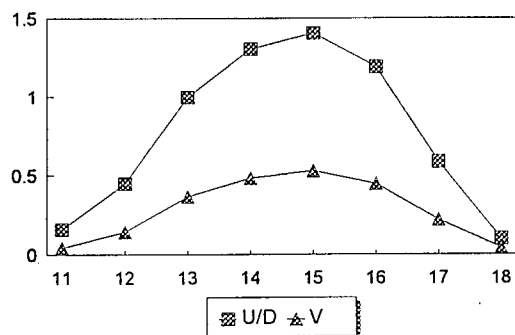
NOTES:

1. Abscissa: amplitude normalized to the reference sensor location (measurement location #13)
2. Ordinate: ambient vibration measurement locations along ogee, see Figures A4 and E1 for their locations
3. Ambient plots completed with high resolution frequency (0.0195 Hz) and 16 segments
4. Ambient plots: coherence window: 0-1, phase window: 0-90 degrees
5. In legend, U/D=upstream-downstream direction, V=vertical direction
7. Positive sense: downstream in upstream-downstream direction, up in vertical direction

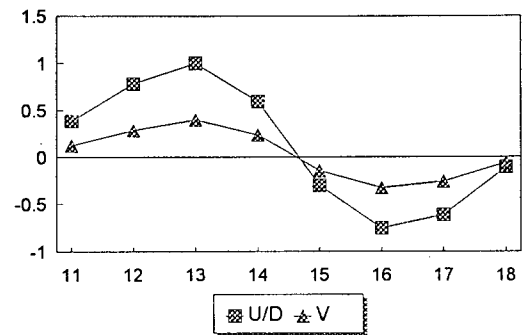
FIGURE E5 FIRST SIX AMBIENT OPERATING DEFLECTED SHAPES (defined along gallery)

RUSKIN DAM AMBIENT VIBRATION FIELD TEST, HIGH RESERVOIR, 7 & 8 May 1994

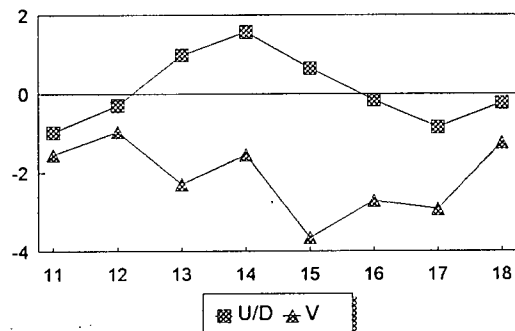
MODE 1: 10.0 Hz



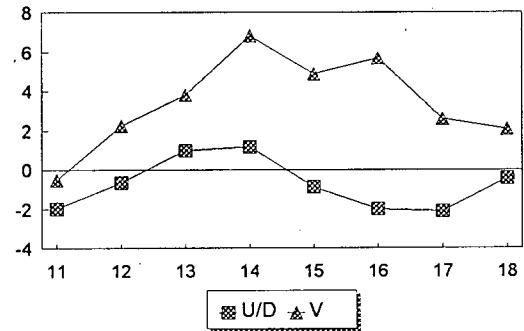
MODE 2: 15.3 Hz



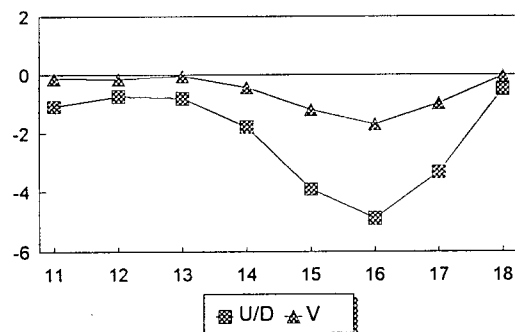
MODE 3: 15.9 Hz



MODE 4: 16.8 Hz



MODE 5: 17.6 Hz



NOTES:

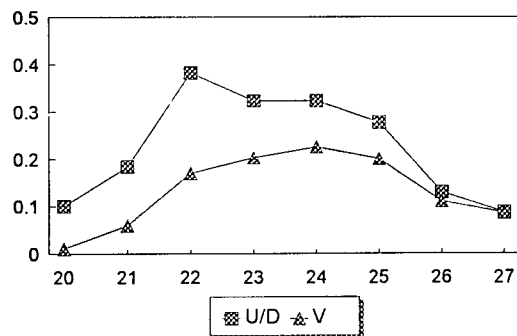
1. Abscissa: amplitude normalized to the reference sensor location (measurement location #13)
2. Ordinate: ambient vibration measurement locations along ogee, see Figures A4 and E1 for their locations
3. In legend, U/D=upstream-downstream direction, V=vertical direction
4. Positive sense: downstream in upstream-downstream direction, up in vertical direction

FIGURE E6 FIRST FIVE NUMERICAL MODEL MODE SHAPES (defined along ogee)

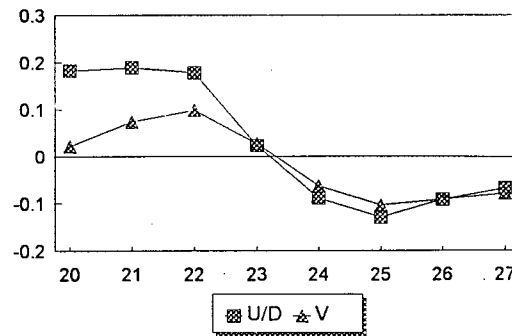
MODEL 1: No Reservoir

RUSKIN DAM NUMERICAL MODEL: ANSYS 5.1

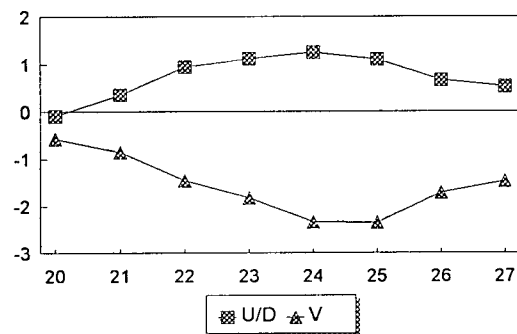
MODE 1: 10.0 Hz



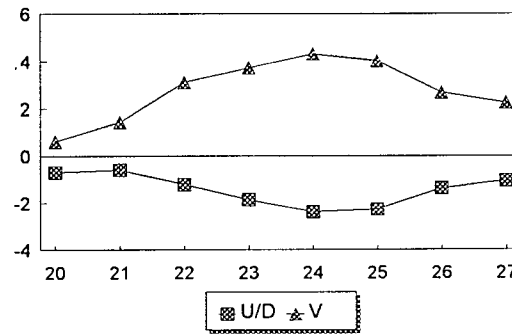
MODE 2: 15.3 Hz



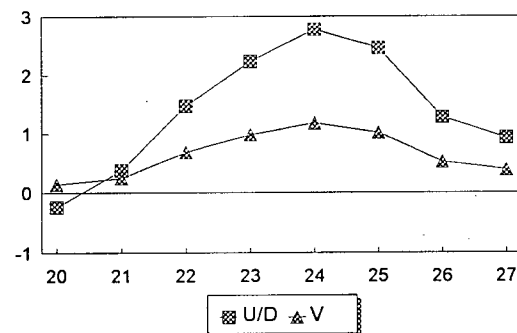
MODE 3: 15.9 Hz



MODE 4: 16.8 Hz



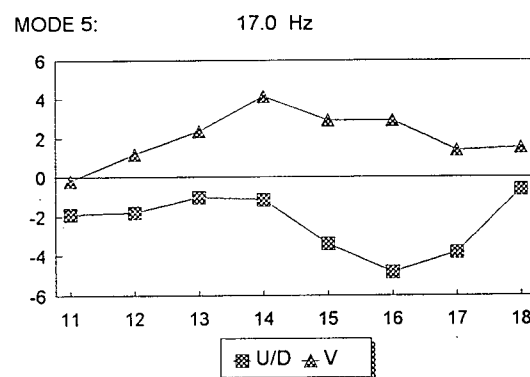
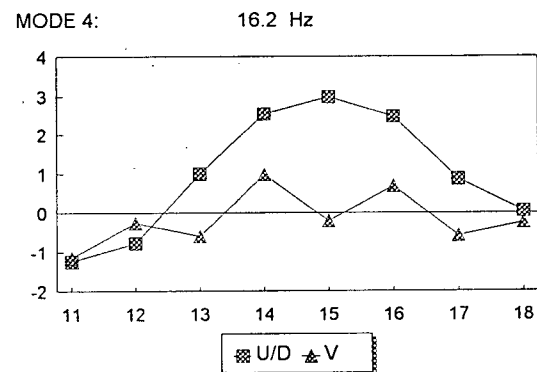
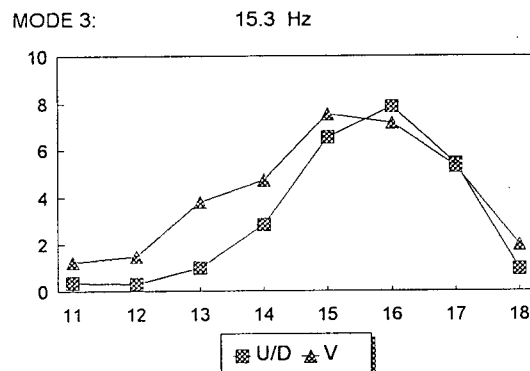
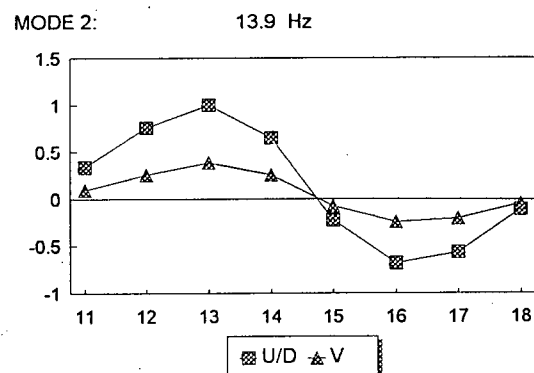
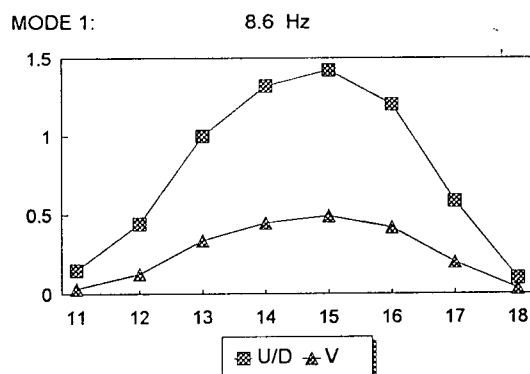
MODE 5: 17.6 Hz



NOTES:

1. Abscissa: amplitude normalized to the reference sensor location (measurement location #13)
2. Ordinate: ambient vibration measurement locations along ogee, see Figures A4 and E1 for their locations
3. In legend, U/D=upstream-downstream direction, V=vertical direction
4. Positive sense: downstream in upstream-downstream direction, up in vertical direction

FIGURE E7 FIRST FIVE NUMERICAL MODEL MODE SHAPES (defined along gallery)
MODEL 1: No Reservoir
RUSKIN DAM NUMERICAL MODEL: ANSYS 5.1



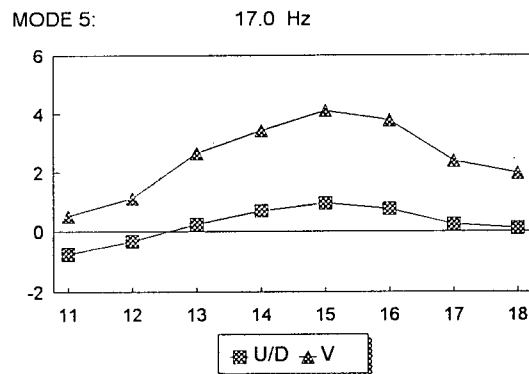
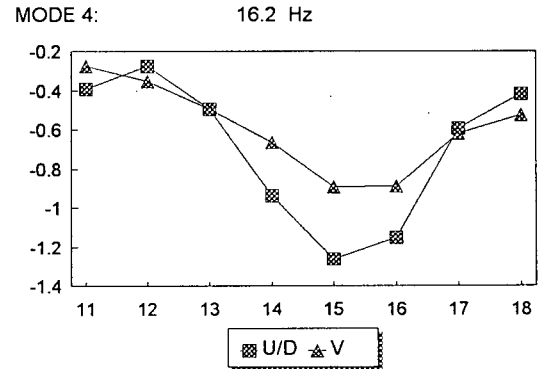
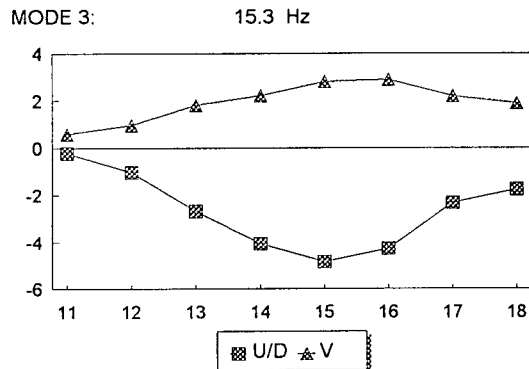
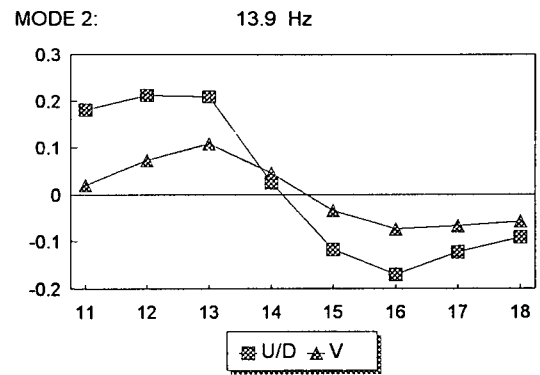
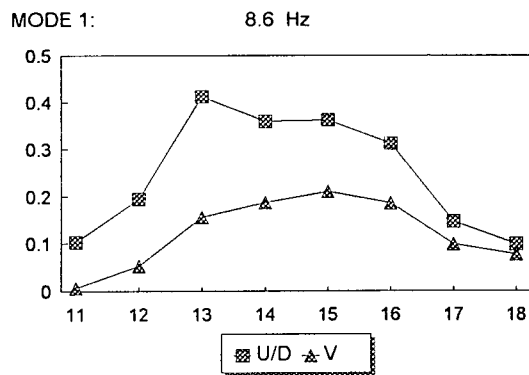
NOTES:

1. Abscissa: amplitude normalized to the reference sensor location (measurement location #13)
2. Ordinate: ambient vibration measurement locations along ogee, see Figures A4 and E1 for their locations
3. In legend, U/D=upstream-downstream direction, V=vertical direction
4. Positive sense: downstream in upstream-downstream direction, up in vertical direction

FIGURE E8 FIRST FIVE NUMERICAL MODEL MODE SHAPES (defined along ogee)

MODEL 2: Low Reservoir

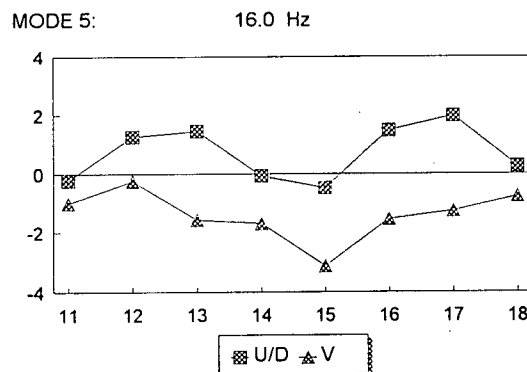
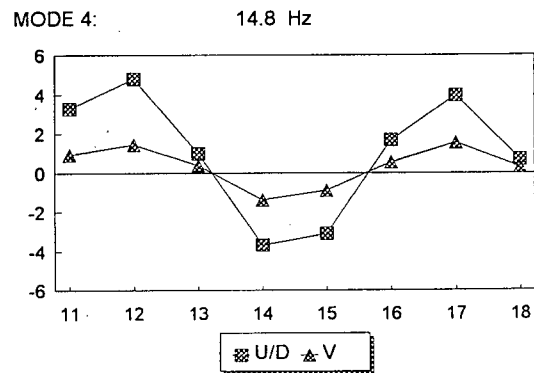
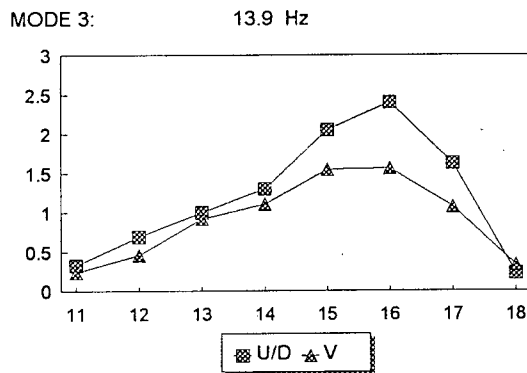
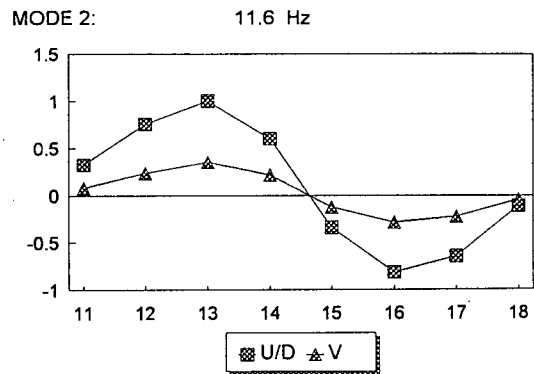
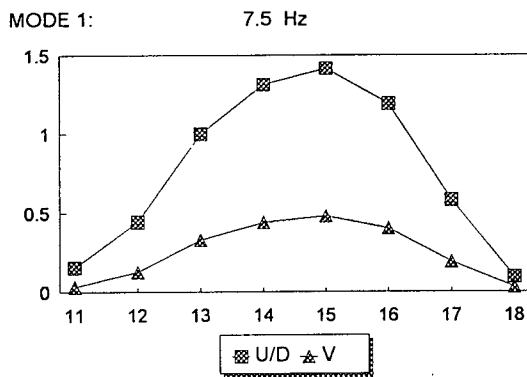
RUSKIN DAM NUMERICAL MODEL: ANSYS 5.1



NOTES:

1. Abscissa: amplitude normalized to the reference sensor location (measurement location #13)
2. Ordinate: ambient vibration measurement locations along ogee, see Figures A4 and E1 for their locations
3. In legend, U/D=upstream-downstream direction, V=vertical direction
4. Positive sense: downstream in upstream-downstream direction, up in vertical direction

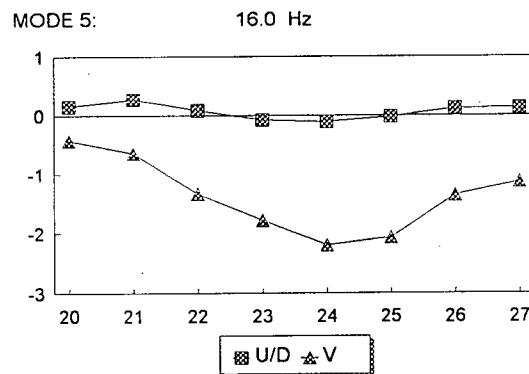
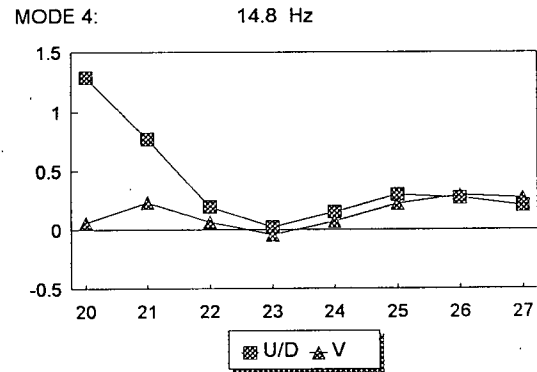
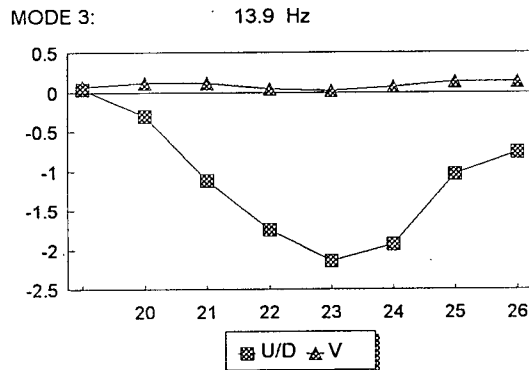
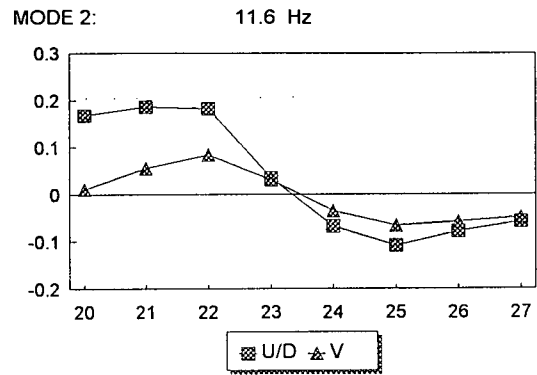
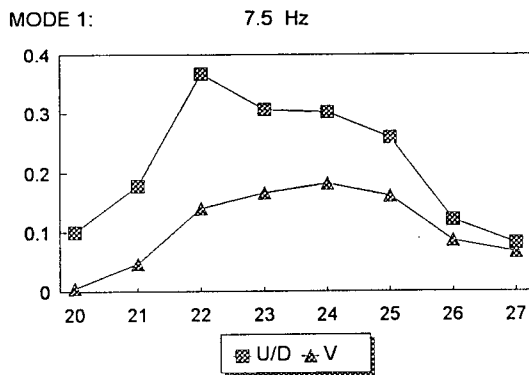
FIGURE E9 FIRST FIVE NUMERICAL MODEL MODE SHAPES (defined along gallery)
 MODEL 2: Low Reservoir
 RUSKIN DAM NUMERICAL MODEL: ANSYS 5.1



NOTES:

1. Abscissa: amplitude normalized to the reference sensor location (measurement location #13)
2. Ordinate: ambient vibration measurement locations along ogee, see Figures A4 and E1 for their locations
3. In legend, U/D=upstream-downstream direction, V=vertical direction
4. Positive sense: downstream in upstream-downstream direction, up in vertical direction

FIGURE E10 FIRST FIVE NUMERICAL MODEL MODE SHAPES (defined along ogee)
 MODEL 3, High Reservoir
 RUSKIN DAM NUMERICAL MODEL: ANSYS 5.1



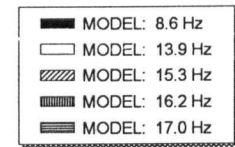
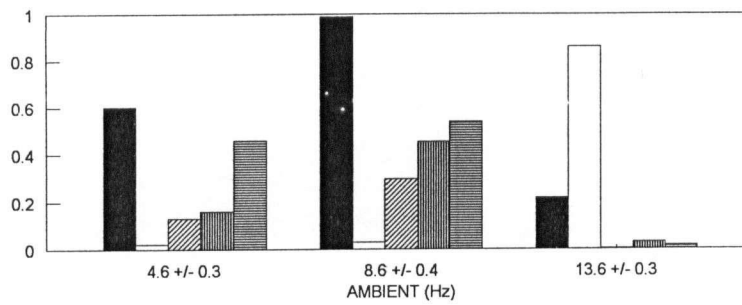
NOTES:

1. Abscissa: amplitude normalized to the reference sensor location (measurement location #13)
2. Ordinate: ambient vibration measurement locations along ogee, see Figures A4 and E1 for their locations
3. In legend, U/D=upstream-downstream direction, V=vertical direction
4. Positive sense: downstream in upstream-downstream direction, up in vertical direction

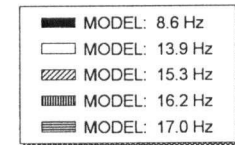
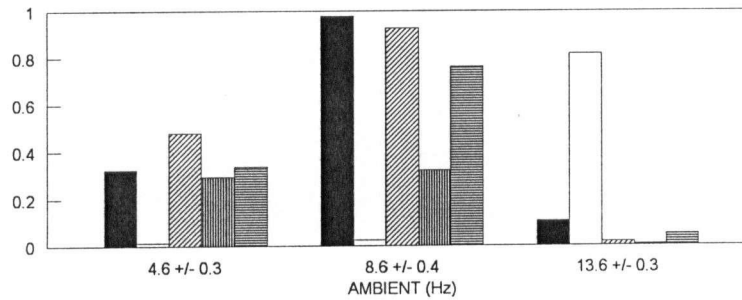
FIGURE E11 FIRST FIVE NUMERICAL MODEL MODE SHAPES (along gallery)
 MODEL 3, High Reservoir
 RUSKIN DAM NUMERICAL MODEL: ANSYS 5.1

LOW
RESERVOIR

U/D-D/S

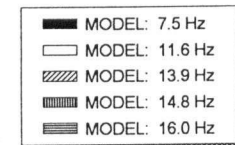
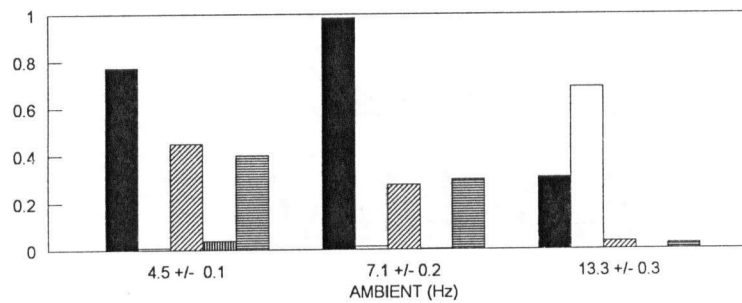


VERTICAL

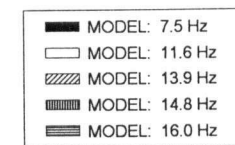
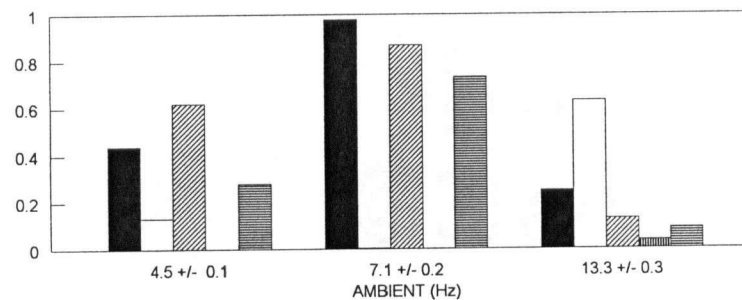


HIGH
RESERVOIR

U/D-D/S



VERTICAL



NOTES:

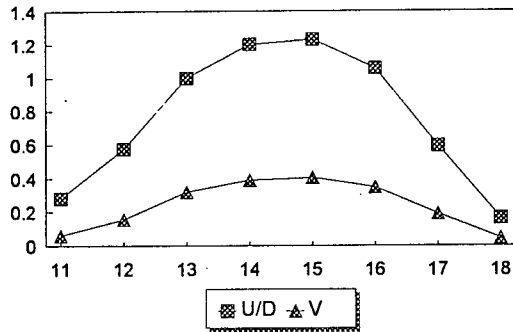
1. Abscissa: MAC value between 0 and 1
2. Ordinate: experimental frequency values in Hz

FIGURE E12 MAC ANALYSES

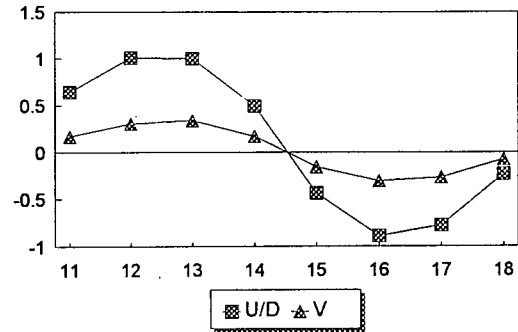
Comparison Between Reservoir Levels

RUSKIN DAM AMBIENT VIBRATION FIELD TEST, LOW/HIGH RESERVOIR TESTS

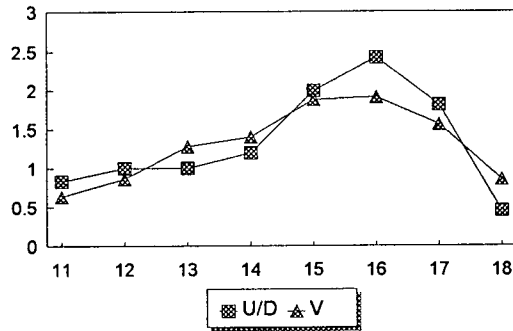
MODE 1: 6.8 Hz



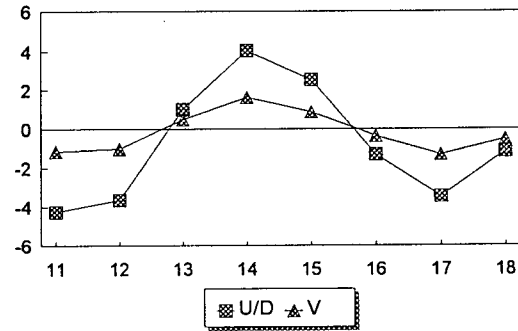
MODE 2: 10.5 Hz



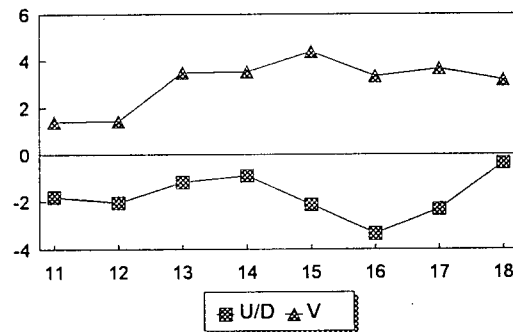
MODE 3: 13.3 Hz



MODE 4: 13.7 Hz



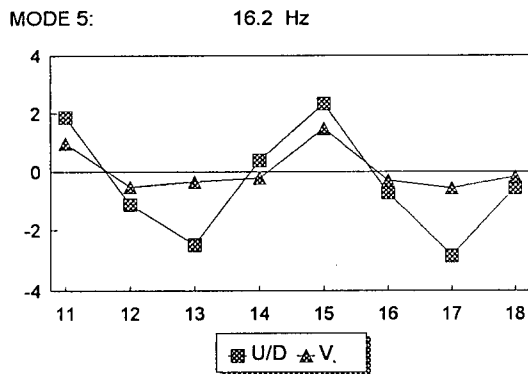
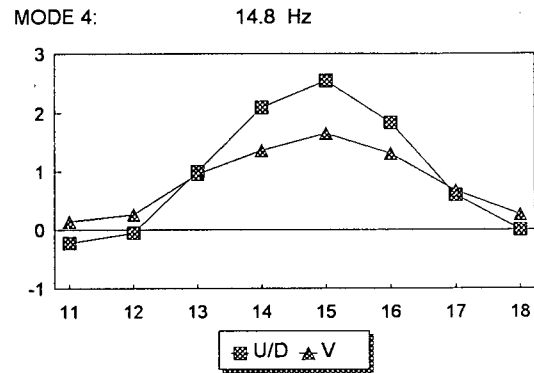
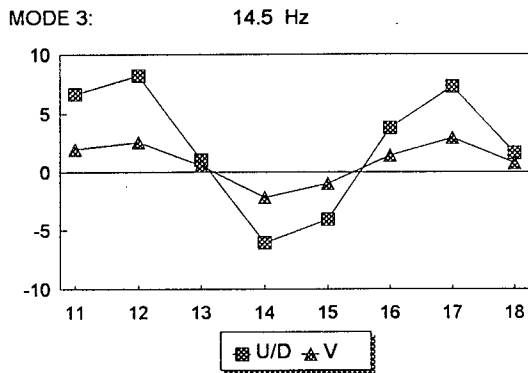
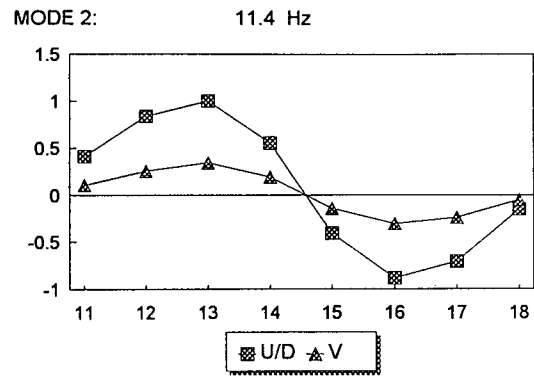
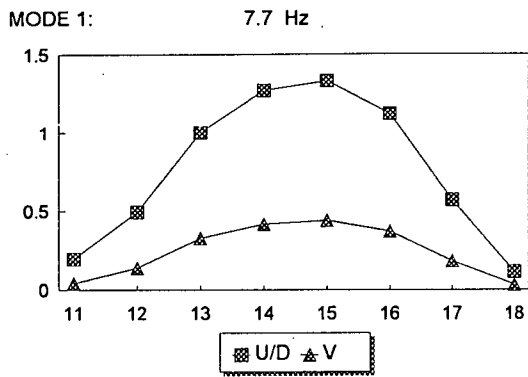
MODE 5: 14.9 Hz



NOTES:

1. Abscissa: amplitude normalized to the reference sensor location (measurement location #13)
2. Ordinate: ambient vibration measurement locations along ogee, see Figures E1 and A4 for their locations
3. In legend, U/D=upstream-downstream direction, V=vertical direction
4. Positive sense: downstream in upstream-downstream direction, up in vertical direction

FIGURE E13 FIRST FIVE NUMERICAL MODEL MODE SHAPES (defined along ogee)
 MODEL 4, High Reservoir, Foundation Dynamic Modulus: 2.09E8 psf
 RUSKIN DAM NUMERICAL MODEL: ANSYS 5.1

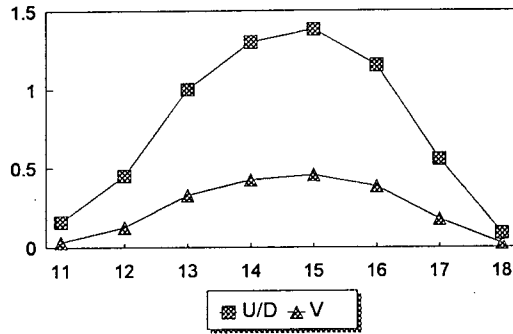


NOTES:

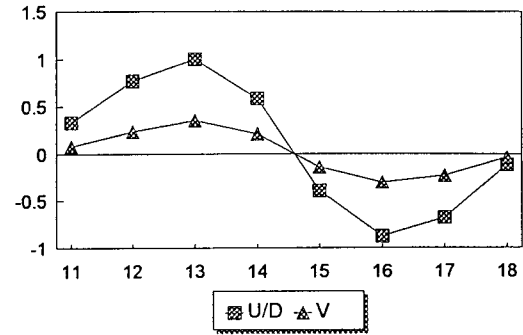
1. Abscissa: amplitude normalized to the reference sensor location (measurement location #13)
2. Ordinate: ambient vibration measurement locations along ogee, see Figures E1 and A4 for their locations
3. In legend, U/D=upstream-downstream direction, V=vertical direction
4. Positive sense: downstream in upstream-downstream direction, up in vertical direction

FIGURE E14 FIRST FIVE NUMERICAL MODEL MODE SHAPES (defined along ogee)
 MODEL 5: High Reservoir, Foundation Dynamic Modulus: 4.189E8 psf
 RUSKIN DAM NUMERICAL MODEL: ANSYS 5.1

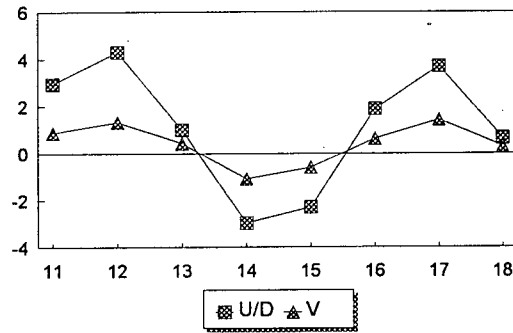
MODE 1: 8.1 Hz



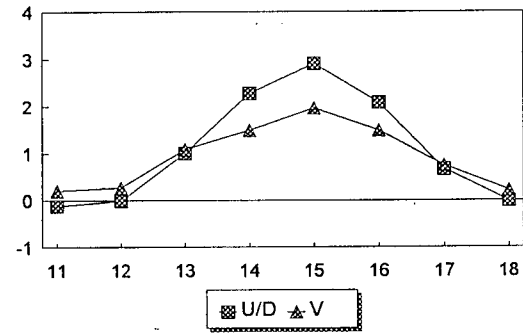
MODE 2: 11.7 Hz



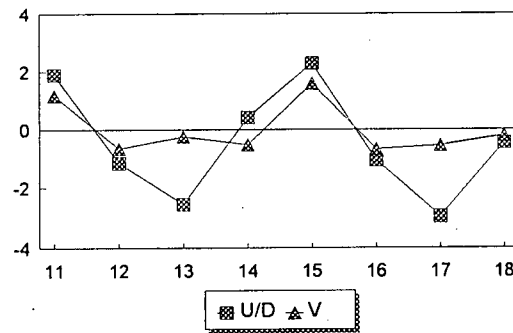
MODE 3: 14.8 Hz



MODE 4: 15.5 Hz



MODE 5: 16.3 Hz

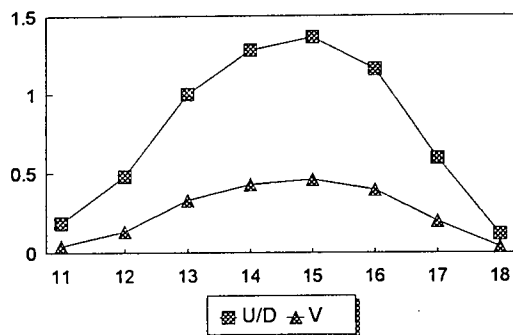


NOTES:

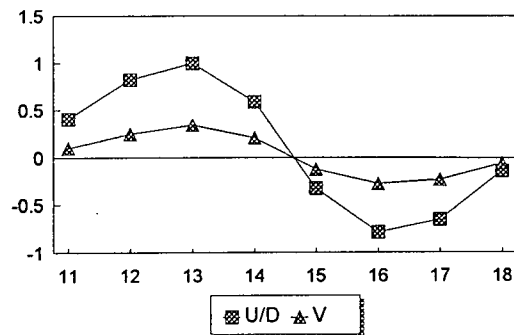
1. Abscissa: amplitude normalized to the reference sensor location (measurement location #13)
2. Ordinate: ambient vibration measurement locations along ogee, see Figures E1 and A4 for their locations
3. In legend, U/D=upstream-downstream direction, V=vertical direction
4. Positive sense: downstream in upstream-downstream direction, up in vertical direction

FIGURE E15 FIRST FIVE NUMERICAL MODEL MODE SHAPES (defined along ogee)
 MODEL 6: High Reservoir, Foundation Dynamic Modulus: 6.27E8 psf
 RUSKIN DAM NUMERICAL MODEL: ANSYS 5.1

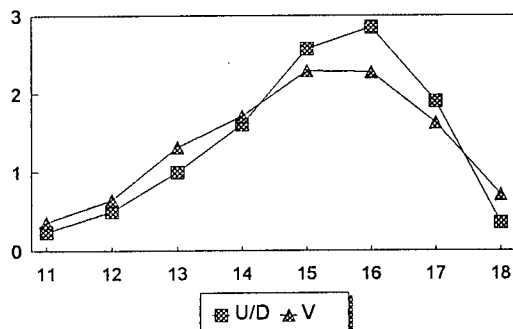
MODE 1: 8.6 Hz



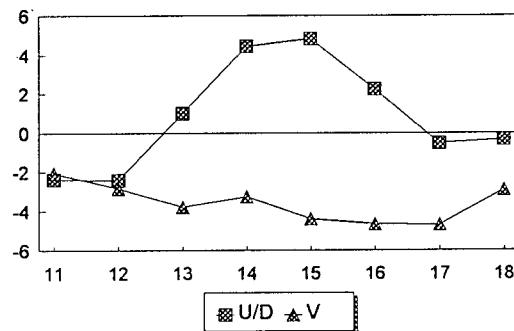
MODE 2: 13.7 Hz



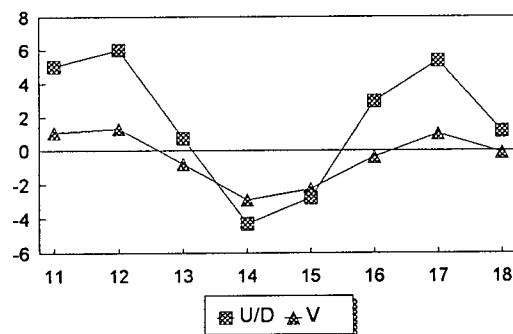
MODE 3: 15.8 Hz



MODE 4: 17.4 Hz



MODE 5: 17.7 Hz

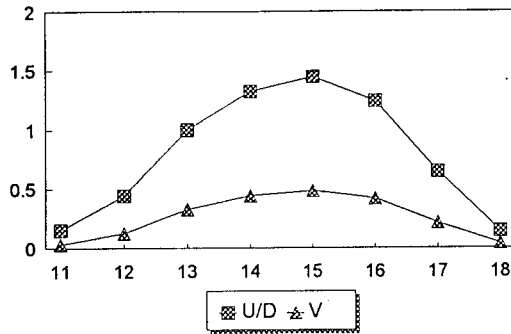


NOTES:

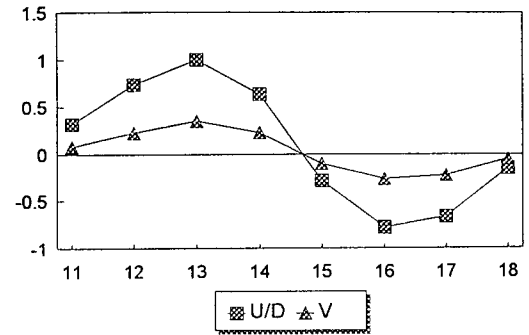
1. Abscissa: amplitude normalized to the reference sensor location (measurement location #13)
2. Ordinate: ambient vibration measurement locations along ogee, see Figures A4 and E1 for their locations
3. In legend, U/D=upstream-downstream direction, V=vertical direction
4. Positive sense: downstream in upstream-downstream direction, up in vertical direction

FIGURE E16 FIRST FIVE NUMERICAL MODEL MODE SHAPES (defined along ogee)
 MODEL 7: High Reservoir, Concrete Dynamic Modulus: 10.8E8 psf
 RUSKIN DAM NUMERICAL MODEL: ANSYS 5.1

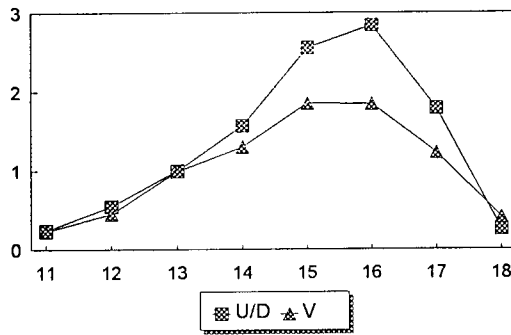
MODE 1: 7.5 Hz



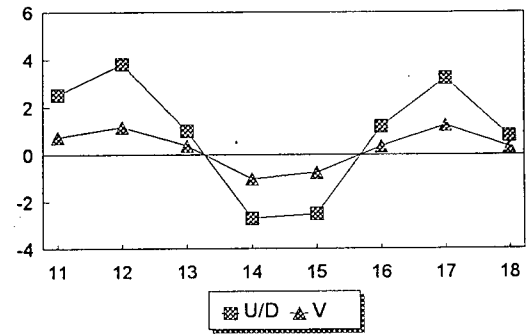
MODE 2: 11.5 Hz



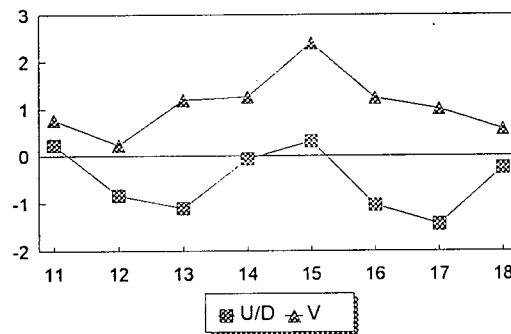
MODE 3: 13.9 Hz



MODE 4: 14.7 Hz



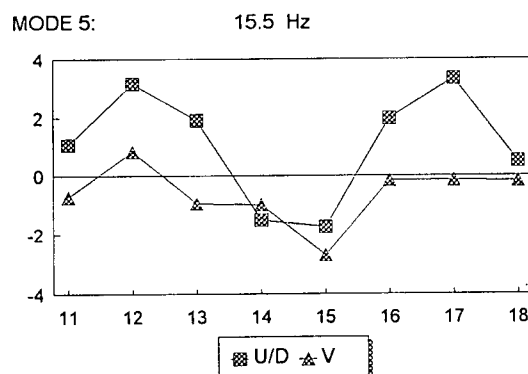
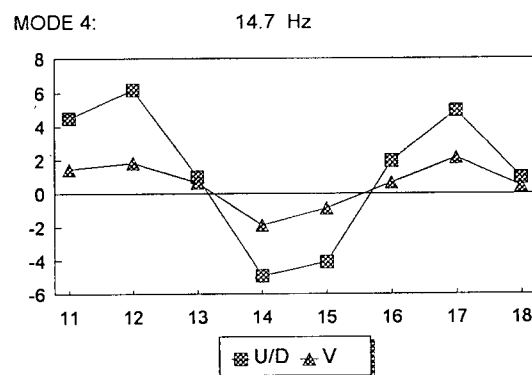
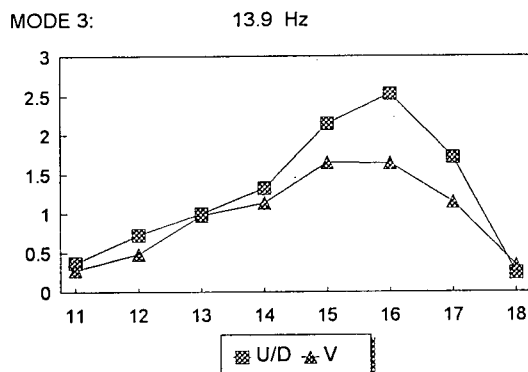
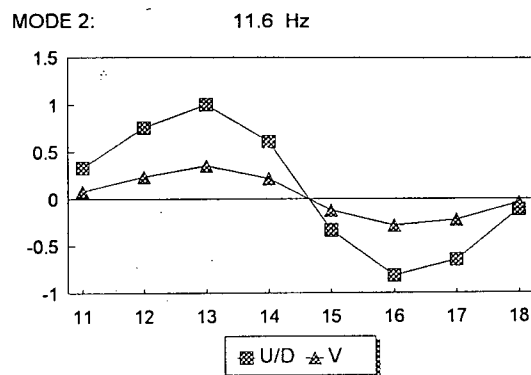
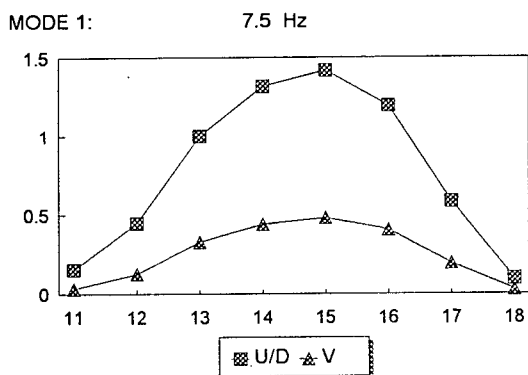
MODE 5: 16.0 Hz



NOTES:

1. Abscissa: amplitude normalized to the reference sensor location (measurement location #13)
2. Ordinate: ambient vibration measurement locations along ogee, see Figures E1 and A4 for their locations
3. In legend, U/D=upstream-downstream direction, V=vertical direction
4. Positive sense: downstream in upstream-downstream direction, up in vertical direction

FIGURE E17 FIRST FIVE NUMERICAL MODEL MODE SHAPES (defined along ogee)
MODEL 8, High Reservoir, Modified Intake Boundary Condition
RUSKIN DAM NUMERICAL MODEL: ANSYS 5.1



NOTES:

1. Abscissa: amplitude normalized to the reference sensor location (measurement location #13)
2. Ordinate: ambient vibration measurement locations along ogee, see Figures A4 and E1 for their locations
3. In legend, U/D=upstream-downstream direction, V=vertical direction
4. Positive sense: downstream in upstream-downstream direction, up in vertical direction

FIGURE E18 FIRST FIVE NUMERICAL MODEL MODE SHAPES (defined along ogee)
 MODEL 9, High Reservoir, Enlarged Foundation
 RUSKIN DAM NUMERICAL MODEL: ANSYS 5.1